

BLDSC no :- DX 172245

LOUGHBOROUGH
UNIVERSITY OF TECHNOLOGY
LIBRARY

AUTHOR/FILING TITLE

WORRAL, D R

ACCESSION/COPY NO.

036000343

VOL. NO.

CLASS MARK

LWBW COPY

~~10 DEC 1993~~

30 JUN 1995

~~28 JUN 1996~~

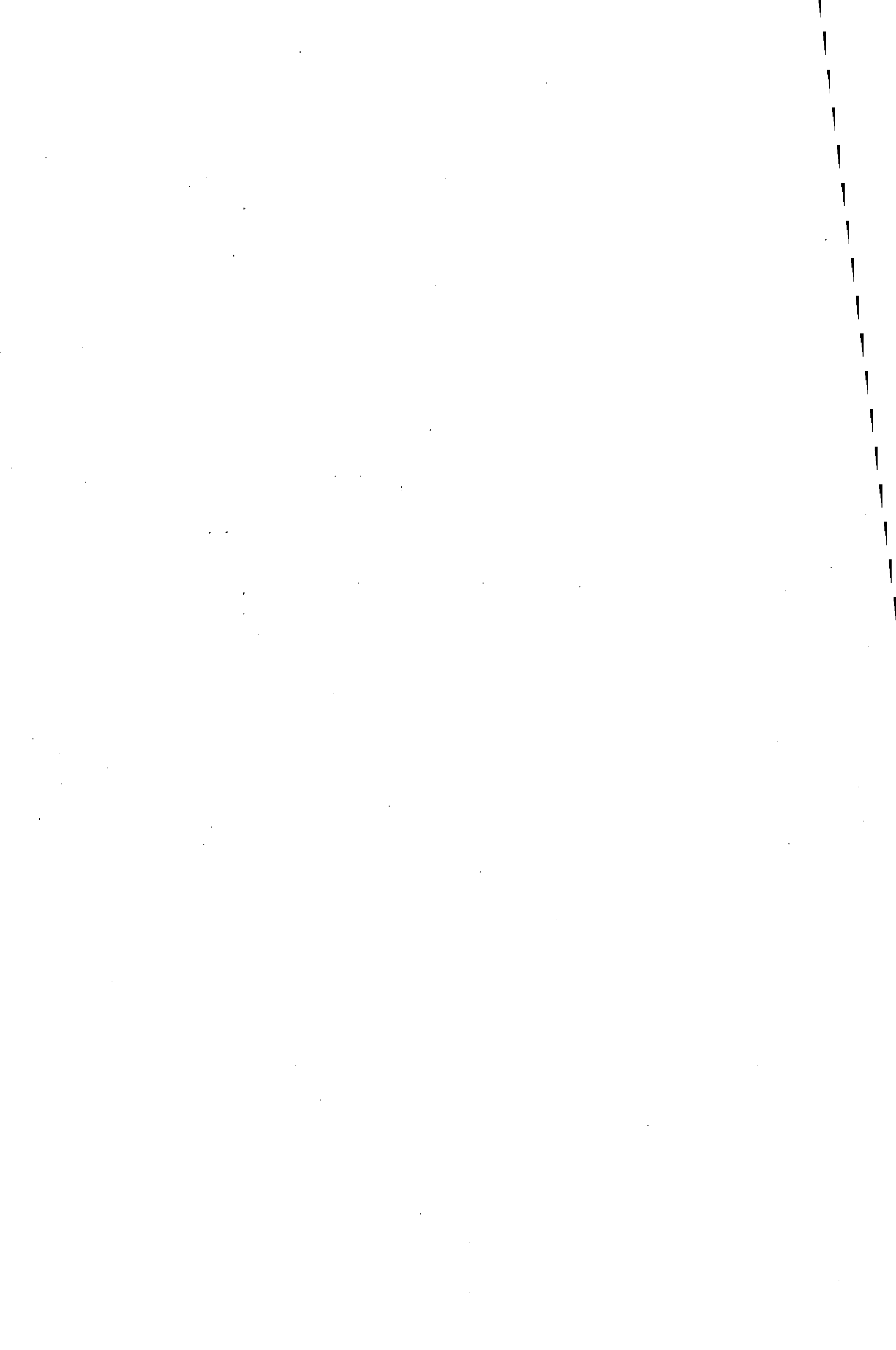
13 FEB 1996

27 JUN 1997

036000343 5



BADMINTON PRESS
18, THE HALFORPT
SYSTON
LEICESTER LE7 8LD
ENGLAND
TEL: 0533 602917
FAX: 0533 696639



LASER PHOTOLYSIS OF PHOTOGRAPHIC IMAGE DYES

BY

DAVID ROBERT WORRALL BSc CChem MRSC

A Doctoral thesis submitted in partial fulfilment of the
requirements for the award of Doctor of Philosophy of
the Loughborough University of Technology

February 17, 1992

(c) by David Robert Worrall February 17, 1992

Loughborough University of Technology Library	
Date	Sept 92
Ref	
Call No	036000343

W9923172

To Pat and Don Worrall and Barbara and Mike Pilbeam, for
their support throughout my endeavours in higher education.

"Programming computers is a little like shopping in Brent Cross; its very easy to get something interesting, but getting what you want is a different matter entirely"

PCW, paraphrased by DRW

Table of Contents

Table of Tables	iii
Table of Figures	v
Abstract	1
1 Introduction	3
1.1 Photochemical principles	3
1.2 Transitions between states	9
1.3 Energy Transfer	19
1.3.1 Collisional (exchange) mechanism	20
1.3.2 Coulombic (induced dipole) mechanism ...	22
1.3.3 Radiative ("trivial") energy transfer ..	24
1.4 Spectroscopy of excited states	24
1.4.1 Emission Techniques	25
1.4.2 Absorption Techniques	31
1.5 Light sources	35
1.5.1 Laser light sources	35
1.5.2 Xenon Arc Lamps	44
1.6 Singlet oxygen	44
1.6.1 Introduction	44
1.6.2 Production of singlet oxygen	46
1.6.3 Methods of studying singlet oxygen	48
1.6.3.1 Phosphorescence Emission	48
1.6.3.2 Thermal lensing	49
1.6.3.3 Time dependent disappearance of an acceptor	50
1.6.4 Singlet oxygen quenching mechanisms	50
1.6.4.1 Chemical quenching processes	50
1.6.4.2 Physical quenching processes	51
1.7 Isomerisation in flexible dye systems	53
1.8 Photochemistry and Photophysics of Azomethine Dyes	57
2 The Colour Photographic Development Process	67
2.1 Introduction	67
2.2 Colour Development Chemistry	68
2.3 Formation of the latent image	72
2.4 The mechanism of dye formation	72
3 Experimental	75
3.1 Ground state absorbance spectra	75
3.2 Nanosecond Laser Flash Photolysis	75
3.2.1 Data Collection	75
3.2.2 Data Analysis	78
3.2.3 Experimental Details	79
3.3 Picosecond Laser Flash Photolysis	80
3.3.1 Mode-Locked laser system	80
3.3.2 Pulse Amplification	82
3.3.3 Characterisation of picosecond pulses ..	82
3.3.4 Generation of probe wavelengths	85

3.3.5	Coherent Coupling Artefact	86
3.3.6	Pump-Probe laser flash photolysis	87
3.3.7	Experimental Layout	88
3.3.8	Data collection	91
3.3.9	Data Processing	94
3.3.10	Experimental Details	95
3.4	Singlet Oxygen Luminescence detection	95
3.5	Photographically formed coatings	96
3.5.1	Introduction	96
3.5.2	Coating making methodology	96
3.5.3	Dispersion Manufacture	98
3.5.4	Coating manufacture	98
3.5.5	Exposing and Developing	98
3.5.6	Fading experiments	99
3.6	Manufacture of hand coatings	99
3.7	Materials	101
4	Fitting of Experimental Data	104
4.1	Introduction	104
4.2	Modified sequential simplex approach	107
4.3	Analytical solution	110
4.4	Selection of convergence criteria	111
4.5	Numerical solution of differential equations using fourth-order Runge-Kutta integration	113
5	Nanosecond Flash Photolysis Studies	116
5.1	Introduction - summary of previous work	116
5.2	Laser flash photolysis of pyrazolotriazole azomethine dyes	121
5.3	Isomerisation yield from the triplet state ..	122
5.4	Estimation of isomer molar decadic absorption coefficients	129
5.5	Isomerisation yield from direct excitation ..	135
5.6	Effect of dissolved oxygen and β -carotene concentration on isomerisation yields	141
5.7	Anti isomer relaxation rates	143
5.8	Flash photolysis studies of azine dyes	149
6	Picosecond pump-probe laser flash photolysis	154
6.1	Introduction	154
6.2	Kinetic Data	160
6.3	Kinetic Model	162
6.4	Modelling of data	168
7	Dye fading in photographic coatings	190
7.1	Introduction	190
7.2	Results of fading experiments	195
Appendix 1:	Dye ground state absorbance spectra ...	209
Acknowledgements	218
References	219

Table of Tables

Relationships between autocorrelation and pulse full width half maxima	84
Wavenumber shifts in a range of solvents	86
Minimum isomerisation efficiencies from the triplet states of PT azomethine dyes	129
Anti isomer molar absorption coefficients from triplet sensitisation	130
Anti isomer molar absorption coefficients from ground state depletion measurements in benzene solution	133
Anti isomer molar absorption coefficients from ground state depletion measurements in acetonitrile solution	133
Isomerisation efficiencies from direct excitation for the 6-CO ₂ Et substituted PT dye in benzene solution	139
Isomerisation efficiencies from direct excitation for the 6-CO ₂ Et substituted PT dye in acetonitrile solution	140
Calculated 6-CO ₂ Et substituted PT dye isomerisation quantum yields in benzene and acetonitrile solutions	141
Anti isomer lifetimes in a range of solvents	144
Physical properties of solvents	145
6-CO ₂ Et substituted PT dye anti isomer relaxation times in glycerol/methanol mixes	145
Molar absorption coefficients for the 6-CO ₂ Et substituted PT dye in methanol	169
Molar absorption coefficients for the 6-CO ₂ Et substituted PT dye in di-n-butylphthalate	169
Molar absorption coefficients for the 6-CO ₂ Et substituted PT dye in benzene	169
Molar absorption coefficients for the 6-CO ₂ Et substituted PT dye in acetonitrile	170
Isomerisation quantum yields used in the modelling of picosecond data.....	170
Dye concentrations used in the picosecond pump-probe experiments.....	170
Best fits to data for the 6-CO ₂ Et substituted PT dye in methanol	174
best fits to data for the 6-CO ₂ Et substituted PT dye in di-n-butylphthalate	174

best fits to data for the 6-CO ₂ Et substituted PT dye in benzene	174
best fits to data for the 6-CO ₂ Et substituted PT dye in acetonitrile	174
best fits to data for dyes A2 and B2 in acetonitrile	175
best fits to data for dye E1 in Toluene	175
best fits to data for dyes B1 and B2 in toluene ...	175
best fits to data for dyes A2 and B2 in acetonitrile	175
best fits to data for the 6-CO ₂ Et substituted PT dye in a hand coating	175
Molar absorption coefficients for the 6-CO ₂ Et substituted PT dye in benzene	176
Molar absorption coefficients for the 6-CO ₂ Et substituted PT dye in acetonitrile	182
state C lifetime as a function of solvent	185
Quantum yields of dye fade in photographic images .	198
dye laydowns in faded coatings	200

Table of Figures

Potential energy surface showing Franck-Condon factors	14
Schematic representation of collisional energy transfer	21
Schematic of a single photon timing apparatus	28
Schematic of a streak camera	30
3- and 4- level laser systems	38
Transverse modes of oscillation in a resonant cavity	40
Frequency distribution for an axial mode of oscillation	41
Molecular orbital representation of ground state molecular oxygen	45
Dye sensitisation of singlet oxygen	47
Potential surfaces for activated and barrierless isomerisation	55
syn and anti isomeric configurations of PT dyes ...	58
Torsional mechanism for isomerisation	60
inversion mechanism for isomerisation	60
Transition state for torsional isomerisation mechanism	61
Transition state for inversion isomerisation mechanism	61
Torsional transition state with electron withdrawing substituents	62
Structure of colour product material	70
Dyes formed from various coupler classes	71
Oxidation of a p-phenyldiamine to the corresponding semiquinone	73
Resonance stabilisation of the semiquinone cation .	73
Quinonediimine cation structure	73
Coupling of the quinonediimine with the coupler anion	74
Schematic of a nanosecond flash photolysis system .	77
Schematic diagram of the picosecond laser system at the Rutherford-Appleton laboratory	83
Pump-probe laser flash photolysis system experimental layout	89
Schematic of beamsplitter assembly	91

Schematic of picosecond flash photolysis apparatus electronic system	93
High Intensity Daylight (HID) spectral profile	100
Structures of pyrazolotriazole azomethine dyes	102
Structures of pyrazolotriazole azomethine dyes	103
Transient difference spectrum of 6-CO ₂ Et PT in benzene	123
Transient difference spectrum of 6-CO ₂ Et PT dye in acetonitrile	124
Representative kinetic traces for the relaxation of the 6-CO ₂ Et PT dye anti isomer in acetonitrile solution	125
Ground state spectra of 6-CO ₂ Et PT dye in benzene and acetonitrile solutions	126
Anti isomer absorption spectra calculated assuming a range of isomerisation yields from the triplet state	132
Anti isomer absorption spectra in benzene and acetonitrile	134
Energy level model used to calculate isomerisation yield	137
General structure of PT dyes	146
resonance delocalisation in pyrazolotriazole azomethine dyes	147
General structure of azine dyes	149
Triplet-triplet absorption spectrum of azine in acetonitrile	151
Singlet oxygen luminescence intensity as a function of laser energy for azine dye and phenazine in acetonitrile	152
Singlet oxygen lifetime as a function of azine concentration in acetonitrile solution	152
Polymethine dye potential energy surface	157
Picosecond transient absorption data for the 6-CO ₂ Et substituted PT dye in d-n-butylphthalate solution	161
Potential energy surface used to explain the photophysical behaviour of pyrazolotriazole azomethine dyes	163
Illustrating the effect on an absorbance profile of convolution with the probing pulse	172

Best fits to picosecond transient difference data for dyes A2 and B2 in acetonitrile solution probing at 640nm	177
Best fits to picosecond transient difference data for the 6-CO ₂ Et substituted PT dye in acetonitrile solution probing at 630nm and 640nm	178
Best fits to picosecond transient difference data for the 6-CO ₂ Et substituted T dye in benzene solution probing at 650nm and for dye E1 in toluene solution probing at 650nm	179
Best fits to picosecond transient difference data for the 6-CO ₂ Et substituted PT dye in methanol solution probing at 640nm	180
Best fits to picosecond transient difference data for the 6-CO ₂ Et substituted PT dye in ethyl acetate solution probing at 630nm	181
Picosecond transient absorption change for the 6-CO ₂ Et dye in a hand coating probing at 640nm	182
Reaction of singlet oxygen with dialkyamino groups	201
Singlet oxygen quenching constant for dye K1 in acetonitrile	206
6-CO ₂ Et substituted PT dye in acetonitrile solution. Concentration 1.68×10^{-5} mol dm ⁻³	209
6-CO ₂ Et substituted PT dye in di-n-butylphthalate solution. Concentration 2×10^{-5} mol dm ⁻³	210
6-CO ₂ Et substituted PT dye in methanol solution. Concentration 2×10^{-5} mol dm ⁻³	211
Dye B2 in acetonitrile solution. Concentration 4×10^{-5} mol dm ⁻³	212
Dye A2 in acetonitrile solution. Concentration 4×10^{-5} mol dm ⁻³	213
Dye E1 in acetonitrile solution. Concentration 4×10^{-5} mol dm ⁻³	214
Dye B2 in methanol solution. Concentration 4×10^{-5} mol dm ⁻³	215
Dye A2 in methanol solution. Concentration 4×10^{-5} mol dm ⁻³	216
Dye E1 in methanol solution. Concentration 4×10^{-5} mol dm ⁻³	217

Abstract

Studies have been carried out investigating the photochemical and photophysical properties of pyrazolo-triazole azomethine dyes. Such compounds can be used as magenta images in the subtractive colour photographic process. This work has been carried out both in dilute fluid solution and in high concentration, high viscosity systems designed to mimic the photographic product.

Picosecond pump-probe laser flash photolysis studies have provided the first observation of photoinduced transient absorption changes attributable to the excited states of this class of dyes, and have allowed assignment of the excited singlet state lifetime as being in the range 1 to 3ps at room temperature, with little dependence upon solvent properties or the pattern of substituents on the dye skeleton. Using picosecond laser flash photolysis it has also been possible to observe evolution of the population along the ground state potential surface to the two isomeric forms, the rate of this process showing some solvent dependence.

Nanosecond and picosecond laser flash photolysis studies have been used to investigate the process of syn-anti and anti-syn isomerisation about the azomethine linkage. The syn-anti photoisomerisation occurs on picosecond timescales, the anti isomer so produced relaxing thermally back to the syn form on timescales ranging from microseconds to milliseconds. The rate constant for this process is a complex function of solvent properties as well as being dependent upon steric factors within the molecule, and the reasons for this are discussed. Triplet energy sensitisation studies have demonstrated that a pathway exists for this isomerisation process via the triplet manifold, and has allowed determination of minimum isomerisation quantum yields from the triplet state. Such studies have also allowed estimation of limits for the molar decadic absorption coefficients of

the anti isomer.

The photographic product dyes have been demonstrated to be efficient quenchers of singlet molecular oxygen, the quenching mechanism being predominantly physical in nature. The quantum yields of singlet oxygen production are too small to be measured using time resolved techniques. These factors are used to explain in part the resistance of such compounds to oxidative photodegradation.

Steady state irradiation of azomethine dyes in systems designed to simulate the photographic product by a high intensity source of known spectral profile has allowed determination of the quantum yields of photodegradation, which in combination with the results obtained in fluid solution provide a basis for explaining the behaviour of image dyes in the photographic product environment.

Chapter 1

Introduction

1 Introduction

1.1 Photochemical principles

In a primary photochemical process, light must be absorbed by the system for a photochemically induced reaction to take place; absorption of ultra-violet or visible light produces an electronically excited state of generally a molecule or atom in the system, although in for example solid state semiconductors to describe excitation of discrete particles may be misleading since excitation involves promotion of an electron from the valence band to the conduction band in the system, the threshold wavelength for such an excitation being determined by the bandgap in the semiconductor in question. Taking the example of discrete molecules in solution, the amount of light absorbed by such a solution at a given wavelength is described by the Beer-Lambert law

$$A = \log_{10} \frac{I_0}{I_t} = \epsilon lc \quad (1.1)$$

where A is termed the absorbance at a given wavelength, ϵ is the molar decadic absorption coefficient (also termed the molar decadic extinction coefficient or simply extinction coefficient) at that wavelength, l is the pathlength and c the concentration of absorbing species. It is evident that the absorbance by a species at a given wavelength is proportional to the concentration of that species.

A commonly used parameter in photochemical investigations is the quantum yield of a process, given the symbol ϕ . The quantum yield of a photochemical or photophysical process undergone by a molecule may be defined in one of two ways:

$$\phi = \frac{\text{number of molecules undergoing a process}}{\text{number of quanta absorbed}} \quad (1.2)$$

or

$$\phi = \frac{\text{rate of a process}}{\text{rate of absorption of quanta}} \quad (1.3)$$

The quantum yield of a given process in a molecule depends upon what other competing processes are occurring, and the relative rates thereof. Hence for a process such as fluorescence, which involves a radiative transition between states of the same spin multiplicity (see later), if there are no competing processes which allow relaxation from the fluorescent state, then fluorescence will occur with a quantum yield of one. Any other competing process will have the effect of decreasing the quantum yield, the extent to which they do being determined by the relative rates of the competing processes. Obviously the lifetime of the state involved will be determined by the rate of the fastest occurring process. Hence a process occurring with a rate greater than that of the fluorescence has the effect of not only reducing the quantum yield, but also of decreasing the lifetime of the state from which fluorescence is occurring which is generally, although not exclusively, the first excited singlet state.

Photochemistry involves the use of light to generate populations of electronically excited states of molecules, and often also to probe their subsequent fate. These electronically excited states may then undergo reactions, such as electron transfer, which are not possible from the ground state giving rise to the phenomenon of light induced reactions. The probe used may be a second light source, measuring how the transmittance of a sample (or the reflectance of a diffusely scattering

sample) changes with time, or it may be convenient to use either fluorescence or phosphorescence from the excited states themselves to monitor the excited states produced. A variety of other techniques may also be used to monitor excited state processes, and these include nuclear magnetic resonance (NMR), electron spin resonance (ESR), thermal lensing, photoacoustic spectroscopy and analysis of either the rate of consumption of a reactant or of production of a product. In many light-induced reactions, analysis of the products of reaction also provides valuable clues regarding mechanistic pathways. Photochemical investigational methodology falls broadly into two categories; time resolved techniques and steady state techniques. Time resolved techniques involve the use of a short pulse of light, often from a Q-switched or mode-locked laser but on occasions from a flashlamp discharge, to produce a population of excited states, the time evolution of these states being monitored, while steady state investigations involve the use of a continuous light source to produce a population of excited states, the fate of which may then be monitored. In any given experiment, it may be possible to directly observe the excited states of interest using one or several of the aforementioned techniques, or it may be necessary to monitor the reactions of other molecules in the system in order to extract the information of interest.

Electrons in molecules are usually referred to as residing in molecular orbitals, which may for simplicity be imagined as being derived from combination of the atomic orbitals on the individual atoms from which the molecule was formed, although this picture has no real physical significance. Such molecular orbitals may be classified according to symmetry type with respect to the wavefunction which describes them, and may also be of bonding, antibonding or non-bonding character

depending upon the level of electron density between the bonded nuclei. Antibonding orbitals take the same symmetry designations as bonding orbitals. Taking the example of a diatomic molecule for simplicity, in a sigma (σ) type orbital the sign of the wavefunction remains unchanged with respect to rotation about the molecular axis. A pi (π) type orbital has positive and negative lobes separated by a single nodal plane, and a change in sign of the wavefunction results from rotation of half a turn about the bond axis. A delta (δ) type orbital is characterised by a change in the sign of the wavefunction on rotation of one quarter of a turn about the bond axis. Bonding and antibonding are differentiated in the notation by the use of a '*' superscript on the symbols describing antibonding orbitals. For unconjugated molecules the $\sigma \rightarrow \sigma^*$ transition will be of highest energy, followed by the $\pi \rightarrow \pi^*$, with the $n \rightarrow \pi^*$ (non-bonding to π^*) transition being of lowest energy. However, a high degree of conjugation may raise the energy of the π -orbital sufficiently that in such systems the $\pi \rightarrow \pi^*$ transition will be of lowest energy. The energy of $\sigma \rightarrow \sigma^*$ transitions are generally such that these may only be excited with radiation of wavelength shorter than 200nm, and consequently most photochemical processes involve initial excitation of either an $n \rightarrow \pi^*$ or $\pi \rightarrow \pi^*$ transition.

Electronic states of molecules, whether they be ground or excited states, are characterised by certain properties. The orbital configuration is one parameter, and for any orbital configuration there will be what is termed a spin multiplicity. This is calculated as $2S+1$, where S is the sum of the spin angular momentum quantum numbers s describing the individual electrons of the molecule in question. Hence when all of the electrons are spin paired, the total spin angular momentum is zero and the multiplicity of the state is 1 and termed a singlet. Similarly,

if there are two spin-unpaired electrons in the molecule, the total spin angular momentum is $1/2 + 1/2 = 1$, the multiplicity is 3 and the state is termed a triplet. Hund's rules^[1] state that for degenerate orbitals

(i) Electrons tend to avoid being in the same orbital as far as possible and

(ii) two electrons, each singly occupying a pair of degenerate orbitals, tend to have their spins parallel in the lowest energy state.

It is therefore empirically predicted on the basis of these rules that triplet states will be of lower energy than the corresponding singlets, and this is indeed found experimentally. It should be noted that if we are allocating electrons to residence in molecular orbitals, then if we place two electrons in the same orbital they are necessarily spin paired; a triplet state may only arise when we have two single electrons allocated to different orbitals. This is a part of the Pauli exclusion principle, the whole being also referred to as the antisymmetry principle. It arises since for particles such as electrons having half integer spin ($n + 1/2$, where n is an integer), only antisymmetric wavefunctions are allowed, and if the both electrons in a given MO were to have the same spin the wavefunction would be symmetrical with respect to interchange of electrons. Generally the antisymmetry principle allows not more than one electron to possess a given set of quantum numbers, including s . A more detailed discussion of the antisymmetry principle may be found in the text by McWeeny^[2]. Terms are applied to radiative and non-radiative transitions which describe the multiplicities of the states involved. Where the initial and final states have the same spin multiplicity, radiationless transitions between these are termed internal conversion, while the corresponding radiative process is referred to as fluorescence. The corresponding

processes between states of differing spin multiplicities are termed intersystem crossing and phosphorescence, respectively. Transitions between states where there is no change in spin multiplicity are said to be allowed and generally proceed at an appreciable rate. Those which involve a change in spin multiplicity, e.g. singlet to triplet transitions, are spin forbidden and consequently proceed at a much slower rate. This is discussed further in section 1.2.

Ground and excited states of molecules are often described by what are termed potential energy surfaces, which are at their simplest plots of total molecular potential energy as a function of some molecular co-ordinate, for diatomic molecules (or systems which may be approximated as such) this co-ordinate is typically internuclear distance. For more complex molecules, the potential energy will be a function of probably several molecular co-ordinates, and as such its determination and representation are matters of some approximation. It is common to represent such surfaces as one-dimensional, with the displayed co-ordinate encompassing all the relevant molecular motion affecting the potential; or else each possible co-ordinate of motion is made the subject of an individual potential curve. Obviously from the point of view of attempting to explain the observed molecular photophysics the former approach has more merit, although it must still be appreciated that it is simply an approximation. Also, external influences such as solvent may have a profound effect upon the shapes and potentials of the surfaces involved, and as such it is often difficult to make meaningful comparisons of the behaviour of molecules in vastly differing solvent systems in terms of potential surfaces without an at least qualitative knowledge of the types of state involved in terms of dipole moments, steric factors, hydrogen bonding

etc. It is worth noting that the fact that potential energy surfaces may be used at all in this manner is a direct result of the validity of the Born-Oppenheimer approximation, which states that since transitions between orbitals take place on timescales much shorter than nuclear motion, such transitions may be described as taking place relative to a fixed molecular geometry.

1.2 Transitions between states

The probabilities of transitions between states depend upon the orbital configurations of the initial and final states; if for a fully allowed electronic transition (i.e. one in which energy and momentum are conserved, and small displacements are involved (good overlap)) nuclear and spin configurations remain constant, the transition rate is determined only by electronic motion. Changes in orbital, vibrational or spin configuration on making the transition between initial and final states serve to decrease the overall rate. For example, a transition between states in a linear diatomic molecule where the initial and final states have identical equilibrium internuclear separations can proceed with no restriction due to nuclear motion; however, if the internuclear separations at equilibrium are different, the transition rate will depend on the ability of the molecule to undergo changes in nuclear motion, since motion of this kind occurs much slower (10^{-13} to 10^{-12} s) than electron "jumps" between orbitals (10^{-14} to 10^{-16} s), and so is rate determining. This is formulated in the Franck-Condon principle:^[3]

Since electronic transitions are much faster than nuclear motion, electronic transitions occur most favourably when the nuclear structure of the initial and final states are most similar.

In quantum mechanical terms, the initial and final states may be described in terms of wavefunctions, which are solutions to the three dimensional Schrodinger wave equation^[2], given acceptable boundary conditions. The solutions will then be finite, single valued, and continuous, all differentials of which are also continuous. Using standard notation, the energy of a given state may be determined from its wavefunction by

$$\langle E \rangle = \frac{\int \Psi^* \hat{H} \Psi d\tau}{\int \Psi^* \Psi d\tau} \quad (1.4)$$

where $\langle E \rangle$ indicates an average or "expectation" value of the energy and \hat{H} is the Hamiltonian operator, derived from the classical expression for energy as a function of position and momentum. The "hat" signifies that it is a quantum mechanical operator. The integral with respect to $d\tau$ indicates that the integral is evaluated with respect to all coordinates contained within the integrand, and Ψ^* is the complex conjugate of Ψ , the wavefunction describing the state. Note that if Ψ is real, then $\Psi = \Psi^*$. Following the abbreviations of Hanna^[4]

$$\int_{\text{allspace}} \Psi^* \hat{H} \Psi d\tau \equiv \langle \Psi^* | \hat{H} | \Psi \rangle \quad (1.5)$$

and

$$\int_{\text{allspace}} \Psi^* \Psi d\tau \equiv \langle \Psi^* | \Psi \rangle \quad (1.6)$$

and all wavefunctions subsequently used, unless otherwise stated, are normalised such that $\langle \Psi^* | \Psi \rangle$ is equal to one. Generally, the average value of an observable quantity of a system can be calculated from an equation of the type given above for the energy, the difference being the choice of operator used in the numerator. The

probability of transitions between initial and final states i and f , due to weak perturbations, can be formulated in terms of a "Golden Rule",

$$\text{probability} = \frac{2\pi}{h} \rho \langle \Psi_f | \hat{\alpha} | \Psi_i \rangle^2 \quad (1.7)$$

where ρ is the density of initial and final states capable of coupling and $\hat{\alpha}$ is the operator coupling the states. $\langle \Psi_f | \hat{\alpha} | \Psi_i \rangle$ is often referred to as the "matrix element" coupling states i and f . Obviously from the standard notation

$$\langle \Psi_f | \hat{\alpha} | \Psi_i \rangle = \int \Psi_f \hat{\alpha} \Psi_i d\tau \quad (1.8)$$

It was noted in the classical description of transitions that the observed rate constant may be reduced by the need for changes in electronic, nuclear or spin configuration. Expressions for these rate limiting factors can be derived using perturbation theory^[5]. The zero order energy eigenvalue equation may be defined as

$$\hat{H}_0 \Psi_m^0 = E_m^0 \Psi_m^0 \quad (1.9)$$

where the zero superscripts indicate that the wavefunctions and energies are zero order i.e. single electron values unperturbed by the influence of other electrons. If the interaction with other electrons is small, then the wavefunction and the energy will only be slightly modified. Defining the perturbed operator \hat{H} as

$$\hat{H} = \hat{H}_0 + \lambda \hat{H}' \quad (1.10)$$

where $\lambda \hat{H}'$ represents a small perturbation on \hat{H}_0 , and λ is an arbitrary multiplier. The new eigenvalue equation taking account of the state perturbation is

$$\hat{H} \Psi_m^n = E_m^n \Psi_m^n \quad (1.11)$$

where here the wavefunction is termed the n th order corrected wavefunction, the correction to the zero order function including powers of λ up to and including λ^n . The first order corrected wavefunction is then given by

$$\Psi_m^1 = \Psi_m^0 + \frac{\langle \Psi_k^0 | \hat{H}' | \Psi_m^0 \rangle}{E_m^0 - E_k^0} \Psi_k^0 \quad (1.12)$$

since provided \hat{H}' is small λ is usually set to one. The mixing coefficient a_{km} between states k and m is

$$a_{km} = \frac{\langle \Psi_k^0 | \hat{H}' | \Psi_m^0 \rangle}{E_m^0 - E_k^0} \quad (1.13)$$

and the probability of the transition from state m to state k is a_{km}^2 , i.e.

$$a_{km}^2 = \left| \frac{\langle \Psi_k^0 | \hat{H}' | \Psi_m^0 \rangle}{E_m^0 - E_k^0} \right|^2 \quad (1.14)$$

The factors, then, reducing the transition probability between states i and f may be approximated by

$$P \approx \left| \frac{\langle \Psi_f^0 | \hat{\alpha} | \Psi_i^0 \rangle}{E_i^0 - E_f^0} \right|^2 \quad (1.15)$$

which are modifications to the overall transition probability arising from first order perturbations to the zero order wavefunctions due to coupling of the states via the appropriate operators. The overall observed rate constant is then

$$k_{obs} = k_{max} \left| \frac{\langle \Psi_f^0 | \hat{H}_e | \Psi_i^0 \rangle}{E_i^0 - E_f^0} \right|^2 \left| \frac{\langle \Psi_f^0 | \hat{H}_{so} | \Psi_i^0 \rangle}{E_i^0 - E_f^0} \right|^2 \langle \chi_i | \chi_f \rangle^2 \quad (1.16)$$

where \hat{H}_e and \hat{H}_{so} are operators describing orbital and spin-orbit interactions, respectively, and $\langle \chi_i | \chi_f \rangle$ is the Franck-Condon factor, also termed the vibrational overlap

integral, analogous to the electronic overlap integral, and is related to the probability of transition between two vibrational states. The vibrational wavefunctions and electronic wavefunctions are analogous, and just as Ψ^2 gives the probability of finding an electron at a point in space, so χ_v^2 represents the probability of finding the nuclei at a given internuclear distance during vibration in a given level v . Thus we have a quantum mechanical interpretation of the Franck-Condon principle. The vibrational wave function χ describes the momentum of the nuclei and their position in space relative to the electron cloud, and the probability of an electronic transition is related, as indicated in equation 1.16, to the square of the vibrational overlap integral. The function $\langle \chi_i | \chi_f \rangle$ is related to the probability that state χ_i will have the same configuration and momentum as state χ_f , a condition set out in the statement of the Franck-Condon principle as being required. This is illustrated schematically in figure 1.1.

It is worth noting that, while changes in orbital, vibrational or spin configurations occurring with an electronic transition may serve to decrease its rate, coupling between electronic and nuclear motions may actually serve to allow a transition where from purely electronic considerations it may be strictly forbidden (i.e. $\langle \Psi_f | \hat{H} | \Psi_i \rangle = 0$). Provided the nuclear motion only causes a small change in electronic energy relative to the pure electronic states, we can again use perturbation theory to evaluate the splitting energy associated with coupling to the nuclear motion. The splitting energy E_v is then

$$E_v = \pm \frac{\langle \Psi_f | \hat{H}_v | \Psi_i \rangle}{E_f - E_i} \quad (1.17)$$

which is the energy difference between the electronic states and what are termed the vibronic states. E_v is generally very small since nuclear motion provides only a small perturbation to the electronic energy. However, provided $\langle \Psi_f | \hat{H}_v | \Psi_i \rangle \neq 0$ then even when the transition is strictly forbidden on purely electronic grounds, there will still be a finite rate for the transition since the golden rule may now be formulated as

$$\text{probability} = \frac{2\pi}{h} \rho \langle \Psi_f | \hat{H}_v | \Psi_i \rangle^2 \quad (1.18)$$

and consequently vibronic coupling provides a mechanism for transition between states i and f .

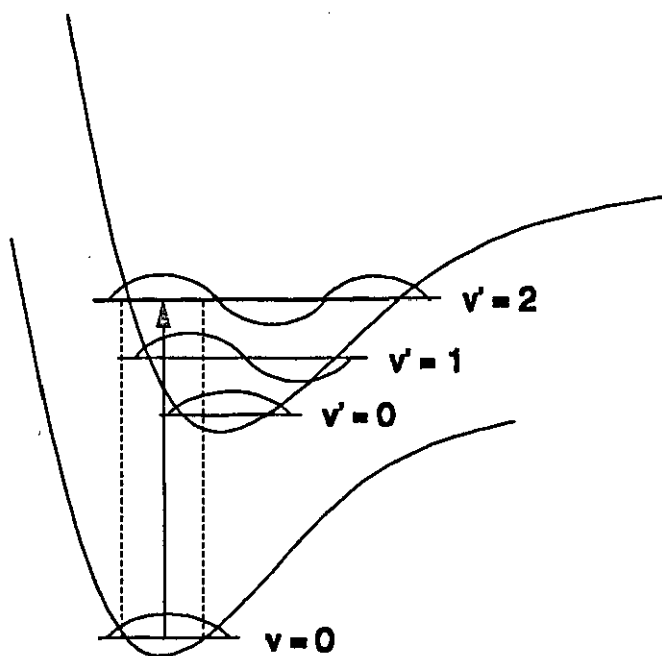


Figure 1.1: Schematic illustration of the Franck-Condon principle. Here the $v=0$ to $v'=2$ transition has the best overlap.

Up to this point transitions between states have only been considered for isolated molecules in the absence of an external field. It is now necessary to consider the effect of an external field, such as a light wave, on the probabilities of transitions between states. The

intensity of radiation absorbed, emitted or scattered by a sample as a result of a transition between states i and f is related to the state wavefunctions Ψ_i and Ψ_f , associated with energy levels E_i and E_f . The frequency ν of the radiation emitted or absorbed is related to the energy difference between states. The intensity of light absorbed as a function of frequency is expressed in the molar decadic absorption coefficient ϵ . It is related to the theoretical absorption strength of the spectral line in question, which is calculable provided the wavefunctions describing the states involved are known. The absorption strength of a spectral line of a molecule will depend on

- (a) the magnitude of the interaction with the light wave
- (b) the population difference between the states in question

A light wave consists of orthogonal electric and magnetic vectors propagating in space, and when considering the absorption of light it is the interaction of the molecule with the electric field which is of interest. Magnetic resonance techniques, where interaction with the magnetic vector is important, will not be discussed here. The oscillating electric field of the light wave may be described by an equation of the form

$$E = E_0 \cos(2\pi\nu t) \quad (1.19)$$

A molecule can be viewed as an assembly of charged particles, and as a consequence will, at any given time, have an instantaneous dipole moment μ which will be related to the number of moving particles and their positions relative to a fixed point of reference. The energy of interaction between a dipole moment and an electric field is the vector dot product of the field strength and the

dipole moment. (A vector dot product, also termed a scalar product, is the product of the magnitude of two vectors multiplied by the cosine of the angle between them).

$$E = -\mu \cdot E \quad (1.20)$$

thus the presence of the electric field will add a term to the Hamiltonian operator which is dependent upon the instantaneous dipole moment of the system. In this instance the perturbing Hamiltonian will be (cf. equation 1.10)

$$\mathcal{H}' = -\mu E_0 \cos(2\pi\nu t) \quad (1.21)$$

and if the system begins in state i , the probability of finding the system in state f at some later time t will be a_{fi}^2 , where again a_{fi} is a mixing coefficient. The integrals in the expression for the mixing coefficient (cf. equation 1.13) are of the form

$$\langle \Psi_f | \mu | \Psi_i \rangle \quad (1.22)$$

where this integral is called the transition moment and is given the symbol R^{fi} . Note here that μ in the above is not an operator (as signified by the absence of a "hat") but serves here to indicate an operator involving the dipole moment. Also, time dependent perturbation theory shows that a_{fi} will be small unless ν in equation 1.19 is equal to the energy difference between states i and f [4]. Hence the transition probability will be proportional to $|R^{fi}|^2$ and to the density of radiation at a frequency corresponding to the energy difference between the states, ν_{fi} . The probability that the system in state i will absorb a photon of this frequency and make a transition to state f in unit time is then

$$P_{fi} = B_{fi} \rho(\nu_{fi}) \quad (1.23)$$

where

$$B_{fi} = \frac{8\pi^3}{3h^2} |R^{fi}|^2 \quad (1.24)$$

and B_{fi} is the Einstein coefficient for induced absorption (or induced emission). Electronic transitions do not simply occur at a single frequency but over a range of frequencies, so the energy density absorbed at a single frequency must be replaced by that over the whole range. If the Beer-Lambert law is also taken into account^[6] we can re-write the Einstein coefficient as

$$B_{fi} = \frac{2.303c}{h\nu_{fi}\eta N_0} \int_{\text{band}} \epsilon(\nu) d\nu \quad (1.25)$$

which provides a link between calculated absorption intensities (equation 1.24) and experiment through measurement of integrated absorption intensities.

As indicated above, the Einstein coefficient for stimulated emission is the same as that for stimulated absorption; hence the net absorption or emission of energy by the sample will depend on the population difference between the states involved. If the populations of the states are equal, no net emission or absorption will be observed.

As noted previously, the probability of radiationless transition between two states is proportional to the square of the expectation value of the perturbing operator connecting the states between which transition is occurring. For transitions between states of differing spin multiplicity, spin-orbit perturbation is required. To the first order approximation, spin-orbit coupling is forbidden between states of the same orbital configuration^[7]. The orbital configurations generally encountered in organic molecules are n, π^* , arising from the promotion of an electron from a non-bonding orbital

to a π^* antibonding orbital, and π, π^* arising from a $\pi^* \leftarrow \pi$ transition. To the first order approximation, then, the singlet-triplet radiationless selection rules may be formulated as

$$\langle S_{n, \pi^*} | \hat{H}_{so} | T_{n, \pi^*} \rangle \approx \langle S_{\pi, \pi^*} | \hat{H}_{so} | T_{\pi, \pi^*} \rangle \approx 0$$

and

$$\langle S_{n, \pi^*} | \hat{H}_{so} | T_{\pi, \pi^*} \rangle \neq 0$$

or, put more simply, the transition $n, \pi^* \leftrightarrow \pi, \pi^*$ is allowed while $n, \pi^* \leftrightarrow n, \pi^*$ and $\pi, \pi^* \leftrightarrow \pi, \pi^*$ are forbidden. In order to assess the overall transition probability it is necessary to take account of vibrational overlap integrals between singlet and triplet states^[8], i.e. $\langle \chi_{S,i} | \chi_{T,j} \rangle$, where i and j represent vibrational levels in the singlet and triplet states respectively. To rationalise the forbiddenness of transitions between states of the same orbital configuration but differing spin configuration we need to take account of the fact that total angular momentum in the system is conserved. Motion of electrons in orbitals, being moving charges, generates a magnetic field which can act locally on another electron, providing a magnetic torque capable of "flipping" the spin of that electron. This flip will obviously lead to a change in total spin angular momentum in the system, so a compensating jump of the electron to another orbital with a corresponding change in orbital angular momentum acts to conserve total angular momentum. This phenomenon is termed spin-orbit coupling and facilitates intersystem crossing between states with differing total spin. Classically, The magnitude of the spin-orbit coupling energy is the vector dot product of the magnetic field generated by electronic motion and the electron spin magnetic moment.

$$E_{so} = -\mathbf{H}_e \cdot \boldsymbol{\mu}_s \quad (1.26)$$

The magnitude of the magnetic field, and consequently the coupling energy, increases with increasing atomic number. Thus spin flips should be most probable for systems containing a heavy atom accessible to the electron whose spin is to be flipped. Another possible mechanism for enhanced intersystem crossing in a solute in a heavy atom solvent involves the singlet of the solute molecule mixing with that of the solvent, while the triplet of the solute also mixes with that of the solvent. The solvent contains a heavy atom and therefore its singlet and triplet states are strongly mixed and transition between them is not strongly forbidden. Therefore, mixing of the solute and solvent triplet and singlet states relaxes the spin-forbiddleness of the solute singlet-triplet transition^[9]. This may be expressed as

$$\langle T | \hat{H}' | S \rangle = \frac{\langle T | \hat{H}^I | {}^3\Psi_{\text{solv}}^a \rangle \langle {}^3\Psi_{\text{solv}}^b | \hat{H}_{so} | {}^1\Psi_{\text{solv}}^a \rangle \langle {}^1\Psi_{\text{solv}}^a | \hat{H}^{II} | S \rangle}{\Delta E_b \Delta E_a} \quad (1.27)$$

where \hat{H}_{so} is an operator relating to the spin-orbit coupling in the solvent, and \hat{H}^I and \hat{H}^{II} are operators describing the specific interactions coupling the states in the solute and solvent.

1.3 Energy Transfer

Analogous to intramolecular transitions between states, the probability of radiationless energy transfer between a donor D^* and an acceptor A may be formulated in terms of a "Golden Rule",

$$\text{Probability}(D^*A \rightarrow DA^*) \propto \rho \langle \Psi_f | \hat{H} | \Psi_i \rangle^2 \quad (1.28)$$

where Ψ_f and Ψ_i are the composite wavefunctions describing the final and initial states, and are the products of the wavefunctions appropriate for the states of the donor and acceptor after and before energy transfer. This probability is related to the rate constant for energy transfer, k_{et} . There are two possible mechanisms for radiationless energy transfer, namely exchange (collisional) and coulombic (dipole-dipole) transfer, which will be dealt with in turn in sections 1.3.1 and 1.3.2. It is convenient, therefore, to separate the operator into two components, one for the coulombic interaction and one for exchange. The probability of energy transfer is then

$$k_{et} = \underbrace{\langle \Psi_f | \hat{H}_e | \Psi_i \rangle^2}_{\text{exchange}} + \underbrace{\langle \Psi_f | \hat{H}_c | \Psi_i \rangle^2}_{\text{coulombic}} \quad (1.29)$$

given that the correct coefficients are included within the above operators.

1.3.1 Collisional (exchange) mechanism

Collisional energy transfer may be visualised as an exchange of electrons between donor and acceptor molecules; an electron from the LUMO of the donor "jumps" to the LUMO of the acceptor, and one from the acceptor HOMO "jumps" to the HOMO of the donor (figure 1.2). For this process to occur there must be overlap of the electronic charge clouds between donor and acceptor molecules in space (i.e. collisions between molecules). Exchange energy transfer may occur in a single step or in several steps; there may be concerted exchange of electrons, electrons may be exchanged in a stepwise manner via charge transfer exchange involving a radical ion pair, or covalent bonding electron exchange may take place where donor and acceptor form a chemically bound intermediate such as a diradical.

In the former, a donor LUMO to acceptor LUMO jump is the first stage, while in the latter the acceptor HOMO to donor HOMO jump occurs first.

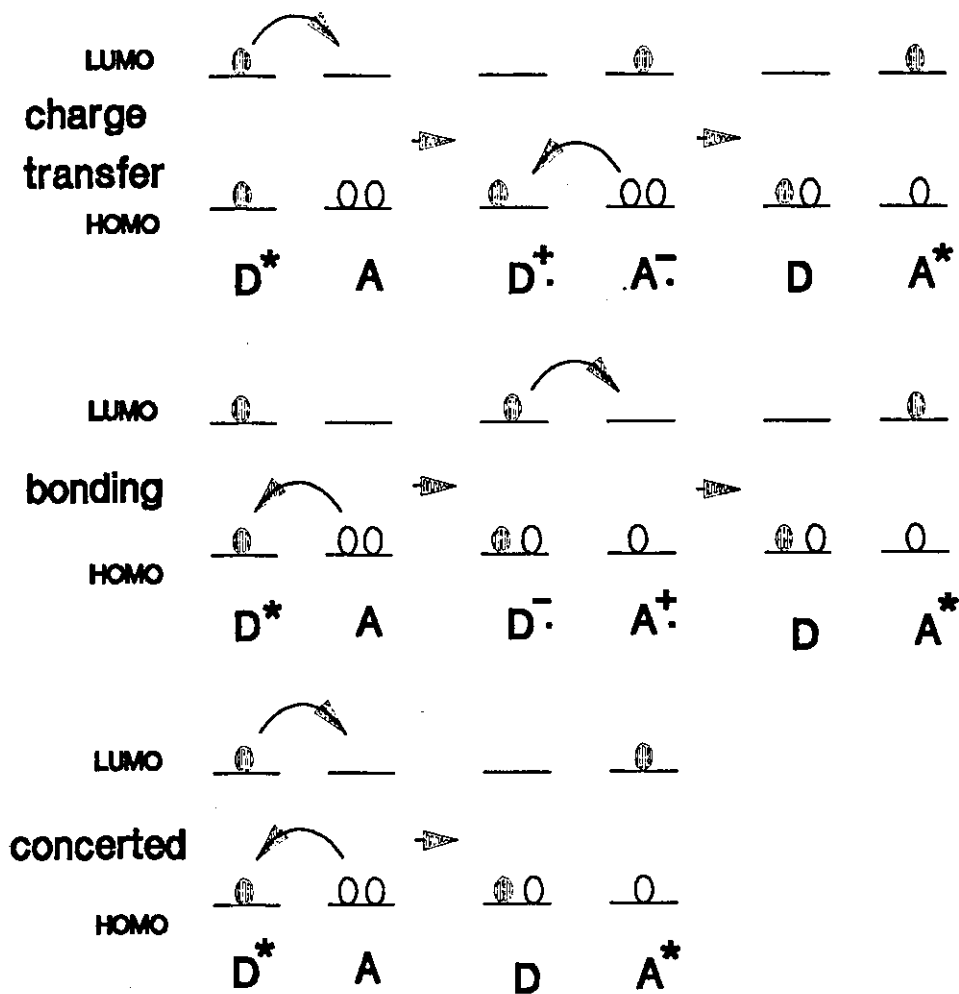


Figure 1.2: Schematic representation of the possible mechanisms of exchange energy transfer
 A theory for energy transfer by electron exchange was derived by Dexter^[10]

$$k_{\text{ET}}(\text{exchange}) = K J e^{-\frac{2R_{DA}}{L}} \quad (1.30)$$

where K is related to the specific orbital interactions, J is a spectral overlap integral normalised for the acceptor molar decadic absorption coefficient and R_{DA} is the donor-acceptor separation relative to their Van der Waals radii L . By normalising J to ϵ_A k_{ET} is independent of the magnitude of ϵ_A , in contrast to the prediction for $k_{et,coulombic}$ (see section 1.3.2). As a consequence, processes such as triplet-triplet energy transfer proceed in fluid solution via exclusively an exchange mechanism since ϵ_A , corresponding in this instance to the molar absorption coefficient for the $T_n \leftarrow S_0$ transition, will be very small. The rate of exchange energy transfer decreases very rapidly with distance as $e^{-2R/L}$ (equation 1.30), while the dipole-induced energy transfer rate decreases much more slowly as R^{-6} (equation 1.33), and may proceed at an appreciable rate at distances of several tens of angstrom. This exponential fall-off of the rate of exchange energy transfer with distance may be rationalised as a consequence of the requirement for overlap of the electronic charge clouds; the rate of energy transfer will decrease as the rate at which charge density decreases with increasing distance from the nuclei, which may in most cases be approximated to an exponential function.

1.3.2 Coulombic (induced dipole) mechanism

While in collisional exchange energy transfer the probability of energy transfer depends on the electronic interactions of the charge clouds of the two molecules, coulombic energy transfer depends on electrostatic interactions. Oscillatory motion of an electron in the LUMO of, say, D^* may perturb the motion of an electron in the HOMO of A . If resonance results, energy transfer occurs whereby the electron in the LUMO of D^* relaxes to the HOMO, while the electron in the HOMO of A is

excited to its LUMO. Hence we have coupling between an oscillating dipole on D^* and the electrons on A, which is analogous to absorption of light where there is coupling between the electrons of A and the oscillating electric field of the light wave.

According to classical theory, the interaction energy between two electric dipoles is related directly to the magnitude of the two transition dipoles and the distance between them. Forster^[11] identified the magnitude of the dipole moments with the oscillator strengths for the radiative transitions in donor and acceptor, and quantified dipole-dipole interaction energy in terms of the measured oscillator strengths, which are proportional to the integrated absorption coefficient and to the square of the transition dipole moment. Forster showed that the rate of energy transfer k_{ET} could be related to E , the coulombic interaction energy, by

$$k_{ET}(\text{Coulombic}) \propto E^2 \approx \frac{\mu_D^2 \mu_A^2}{R_{DA}^6} \quad (1.31)$$

hence k_{ET} is proportional to the squares of the transition dipole moments and to the inverse sixth power of the molecular separation. The transition moments are related to experimentally measured quantities by

$$\mu_D^2(D^* \leftrightarrow D) \propto \int \epsilon_D \quad \text{or} \quad k_D^0 \quad (1.32)$$

and similarly for $A \leftrightarrow A^*$, where $\int \epsilon$ is the integrated molar decadic absorption coefficient and k^0 is the pure radiative lifetime^[12]. Since we are considering $D \leftarrow D^*$ and $A^* \leftarrow A$, we select $\int \epsilon_A$ and k_D^0 to replace the squares of the transition dipoles. Taking account of the spectral overlap between donor emission and acceptor absorption spectra, then

$$k_{\text{ET}}(\text{Coulombic}) = k \frac{\kappa^2 k_D^0}{R_{DA}^6} J(\epsilon_A) \quad (1.33)$$

where κ^2 takes account of the fact that interaction of the dipoles depends on their relative orientation in space, and for a random distribution is 2/3, k is a constant determined by such things as solvent refractive index, and $J(\epsilon_A)$ is the spectral overlap integral.

Experimentally, it is often the efficiency of energy transfer which is measured. It is convenient to define an efficiency for which the rate of energy transfer equals the sum of the other rates of deactivation of D^* . This will occur at a molecular separation $R=R_0$, termed the "critical separation".

1.3.3 Radiative ("trivial") energy transfer

This is, as the name implies, the simplest of the energy transfer processes. It involves absorption of emission (fluorescence or phosphorescence) from a donor molecule by an acceptor molecule, producing excitation of the acceptor molecule. Hence the efficiency with which this process occurs will depend on the degree of overlap between the emission spectrum of the donor and absorption spectrum of the acceptor, the emission quantum yield of the donor, the concentration of quencher molecules and the strength of the absorption transition therein.

1.4 Spectroscopy of excited states

There are several possible means of monitoring the production and decay of excited state species. In this section only optical methods, monitoring either absorption by or emission from the states of interest, will be considered, although it must be borne in mind that there are several non-optical monitoring techniques which may be of use in some circumstances. Both emission

and absorption techniques may be either steady state or time resolved, and the application of each will be considered.

1.4.1 Emission Techniques

(a) Steady State Techniques

Steady state emission methods involve the use of an appropriate excitation source, generally a xenon lamp, to produce a steady state population of excited states. Emission from these excited states is then detected using a photomultiplier. Both exciting beams and the detected fluorescence are usually passed through monochromators, so that the sample is excited with only a narrow band of wavelengths, and emission in only a narrow band is detected from the sample. This allows emission spectra (emission intensity as a function of emission wavelength) and excitation spectra (emission intensity at a fixed wavelength as a function of excitation wavelength) to be determined. Also, the use of monochromators on both exciting and emitted beams allows good rejection of scattered excitation light to be achieved. However, it must be borne in mind that the intensity of emission from a sample increases with increasing excitation intensity and hence the use of narrow monochromator bandwidths may not be possible with weakly emitting samples. It is for this reason that intense light sources are usually employed in emission spectroscopy. When investigating dilute solutions the emission is usually collected perpendicular to the exciting light beam; when detecting emission from opaque, highly concentrated or highly scattering samples, it is common to have the excitation beam at a grazing incidence to the surface, and to detect the fluorescence nearly normal to the surface ensuring that the specular reflectance of the exciting beam does not enter the detection system.

Similar instrumental arrangements may be employed for determining phosphorescence spectra of materials, typically at low temperatures. Here the arrangement differs in that there are choppers interposed between excitation source and sample, and sample and detection system, rotating out of phase with one another such that no light can reach the detection system while the sample is being excited. Hence any prompt fluorescence will not be detected, and only the longer lived phosphorescence will produce a signal.

(b) Single Photon Timing

Single photon timing (SPT), also less correctly termed single photon counting, is a sensitive technique for determining emission lifetimes. The excitation source in this instance is a short pulse light source, typically a nanosecond flash lamp or a picosecond laser. The flashlamps are generally filled with either nitrogen or hydrogen, depending upon the wavelength of excitation required. The pulsewidth from such a lamp may be adjusted by varying such parameters as gas pressure, repetition rate, discharge voltage and electrode spark gap, the shortest pulse available being about 1ns. However, there is a trade-off between lamp intensity and pulse width, and as a consequence it is often necessary to optimise these two parameters for a given system depending on emission quantum yield and lifetime. Picosecond sources are typically dye lasers synchronously pumped by mode-locked Nd:YAG or gas lasers. The excitation pulses are then either the amplified pulses from such a dye laser, or are the direct output from a cavity dumped dye laser.

The mode of operation of the instrumentation is then as follows. A photomultiplier located near the excitation source detects the emission of an excitation pulse, and starts a counter. This excitation pulse then

excites the sample to an upper electronic state. There then may follow various non-radiative processes until the state from which emission will occur is reached. Emission from this state will then occur, the probability of emission at a given time being related to the population of the state, and consequently to the length of time after the excitation pulse that emission occurs. A second photomultiplier then detects one of the emitted photons and generates a pulse which stops the counter. The time between start and stop pulses is converted to a pulse whose amplitude is proportional to that time by a time to amplitude converter (TAC). This pulse is digitised by a multichannel analyser, and a memory channel therein corresponding to this digital value is incremented by one. In so doing, therefore, a histogram is constructed where the pulse height corresponds to the probability of a photon being emitted by the sample at a given time after excitation, which in turn as indicated above is related to the population of the state and therefore to its lifetime. In practice the intensity of emitted light is cut down to such an extent that only about two percent of start pulses are met by a corresponding stop pulse, to ensure that the probability of a stop pulse being detected at a specific time is proportional to the probability of a photon being emitted by the sample at that time. The instrumentation is shown schematically in figure 1.3. It is common for exciting and emitted wavelengths to both be isolated using monochromators or suitable filters. For good precision, then, in the analysis of the emission decay it is necessary to collect a large number of start and stop events, typically at least 10000 counts in the channel with the largest number of counts. As a consequence single photon timing experiments often require a long counting time, even

with high repetition rate sources, and particularly where the sample emits with a very low quantum yield or a long lifetime. This can present experimental difficulties with samples which photochemically degrade under the conditions of excitation.

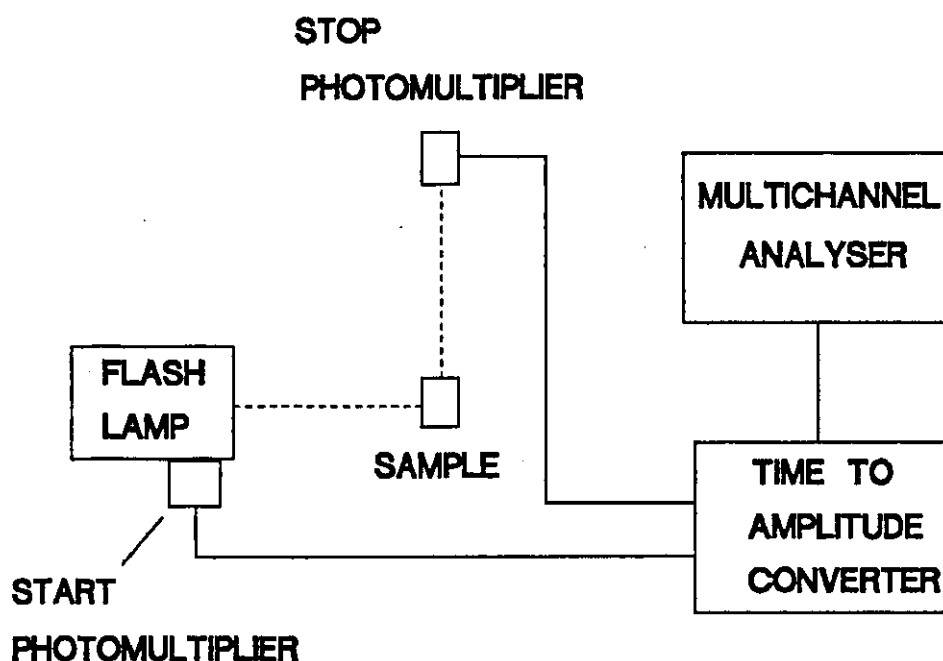


Figure 1.3: Schematic of a single photon timing apparatus

It must be noted that here it is necessary to obtain from the instrumentation a reference signal termed an instrument response function. As the name suggests, this reflects the intrinsic response of the instrumentation to the sequence of events described above,

and originates in part from the pulse width of the excitation source, and also in the response times of the photomultipliers and electronics, these latter points taking on a greater significance at very short pulse widths. As a consequence, if a diffuse scatterer is placed in the instrumentation, the scattered photons will not be sharply at one point in time but will have a characteristic time function termed the instrument response. This instrument response function will consequently be convolved with any emission decay recorded, and must be taken account of when attempting to fit kinetic models to the data.

(c) Streak Camera Methods

These involve the use of a streak camera to provide a real time profile of the emission decay. As an excitation source it is common to use a picosecond source in the form of a synchronously pumped dye laser, either amplified or operating in cavity dumped mode. A schematic diagram of a streak camera is shown in figure 1.4, and its mode of operation is as follows. When the sample is excited, it emits light with a time dependent intensity profile which follows the excited state lifetime. This emitted light hits a screen from which it ejects electrons, which are then accelerated by an electric field. Across another pair of plates is applied a voltage which is ramped from zero up to a given level in a certain time. Hence the image of the emitted light in electrons is spread out at 90 degrees to the original light. These electrons then hit a phosphor screen and the electron image is converted back to a light image. This light image is then captured using a CCD camera or some similar device. Hence the rate at which the voltage is swept between the plates determines the timebase of the streak camera.

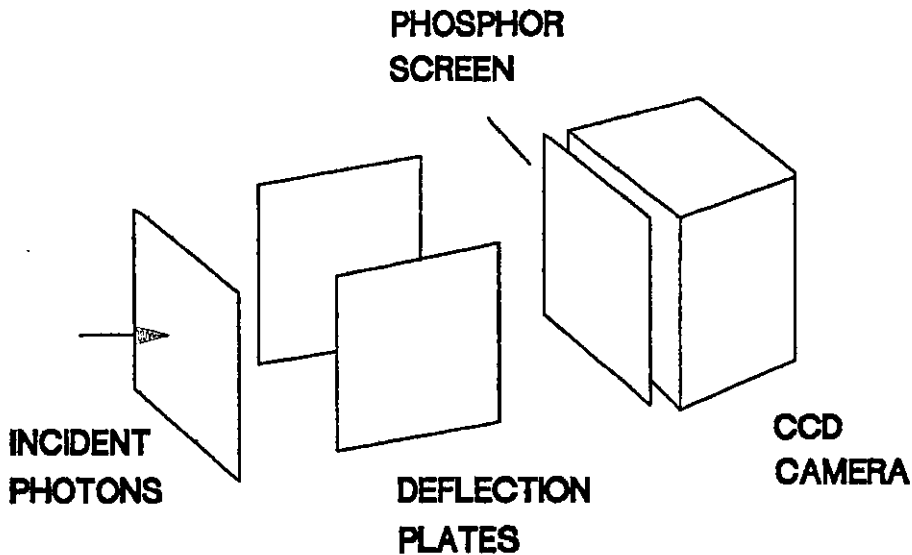


Figure 1.4: Schematic of a streak camera

In practice it is often the case that this voltage sweep provides a slightly non-linear timebase, but this can be corrected for by providing the streak camera with calibration light pulses separated by a known time, generated by sending the pulses slightly different distances. Streak cameras therefore have the advantage over SPT instruments in that data acquisition can be much more rapid, in that all of the information may be collected essentially in a single shot or average of several shots. Also, they generally have streak speeds

which allow the reliable determination of lifetimes shorter than the instrument response function of many SPT instruments. However, they have the disadvantage of being less sensitive and giving data of less accuracy and precision than SPT.

(d) Phase shift methods

The previously described techniques (SPT, streak camera) provide a record of the decay of the luminescence signal as a function of time. Quite different in principle is the phase shift method. Here the sample is excited by a sinusoidally varying source; the emission from the sample will also vary sinusoidally, but will lag behind the excitation waveform. The longer the sample emission lifetime, the greater the phase shift between the two waveforms. For an emission decay described by a single exponential function, the phase shift δ is given by^[13]

$$\delta = \tan^{-1}(2\pi f\tau) \quad (1.34)$$

where f is the modulation frequency. The major disadvantage of such methods are that they are difficult to use when analysing complex kinetics, since only one phase shift is measured regardless of the kinetic complexity. This problem may be overcome in part by measuring phase shifts at a number of modulation frequencies.

1.4.2 Absorption Techniques

(a) Steady State Absorption

In this technique we usually measure the probability of the ground state of a molecule, usually the S_0 state, absorbing a photon and being promoted to a higher electronic state as a function of excitation wavelength. Hence this is a technique principally used for investigating the light absorbing properties of the

ground state of a molecule rather than electronically excited states, since using steady state light sources it is usually not possible to produce sufficiently large excited state populations to allow their absorption spectra to be recorded. To determine the absorption spectra of electronically excited states it is usually necessary to employ pulsed techniques as described later in this section. The instrumentation for recording steady state absorption spectra consists of an excitation source in the form of generally a tungsten lamp for use in the visible region and a deuterium lamp for use in the ultra-violet region of the spectrum. The wavelength of interest from the source is selected using a monochromator, and in many instruments the beam is split into two. One beam is passed through the sample, and one through a reference, which in solution spectrophotometry is usually pure solvent contained in a cell identical to that containing the sample. This is done so that it is possible to correct for absorption of the light by the solvent or the cell, and also to correct for variation in lamp intensity with wavelength. There is in general no monochromator interposed between the sample and the detection system, but the instrument geometry is usually arranged so that very little emission is detected by having the samples located some distance from the detection system. Detection of the light transmitted by the sample and reference usually consists of a photomultiplier, although in some instruments this is replaced by a photodiode array. In this circumstance a range of wavelengths are passed through the sample simultaneously, and are then dispersed and are incident upon the photodiode array. This has the advantage over instruments which need to scan a monochromator in order to achieve wavelength resolution that spectra can be

gathered very quickly, allowing one to follow chemical reactions where absorbing reactants are consumed or absorbing products formed. Often the ability to obtain complete spectra of the course of a reaction rather than simply obtaining the absorbance change as function of time at only one wavelength provides valuable insight into the mechanisms involved, since they may allow identification of intermediate species.

(b) micro- and nanosecond flash photolysis

The technique of flash photolysis is a very powerful one for investigating photochemical processes, since it does not have the inherent limitation of some other techniques that the states of interest must be emissive. It is possible using this technique to monitor the production and decay of excited states which do not emit. The technique employs an intense pulse of light, originally from a flashlamp discharge^{[14][15][16]} or more commonly nowadays from a Q-switched laser^[17], to produce a high population of excited states. This population of excited states is monitored using a second light source, commonly a xenon arc lamp but sometimes continuous wave lasers are employed. The time evolution of the excited states is monitored as the difference in absorption between the system at equilibrium and the system at a time t after the arrival of the excitation pulse. Monitoring of events occurring on micro and nanosecond timescales is possible in real time using fast photomultipliers and transient digitisers or digital oscilloscopes. It must be borne in mind that if kinetic events in the system of interest are occurring on a timescale comparable with the exciting pulsewidth, then the excited states produced will be decaying as the sample is being excited and this must be taken account of in the analysis of kinetic data.

(c) Picosecond pump-probe laser flash photolysis

In principle, flash photolysis on picosecond timescales is similar to that performed on nanosecond timescales, in that an intense excitation pulse is employed to produce a population of excited states, the time evolution of which is monitored by detecting the difference in absorbance between the system at equilibrium and at a time t after the arrival of the excitation pulse. However, due to the very fast timescales involved it is not possible to capture the transient events in real time. Instead, the time evolution of the transients is monitored as follows. The excitation source employed in such experiments is a mode-locked laser, and the analysing source is also a mode-locked laser, often the same laser providing both beams. The sample is then excited by a pulse of light from the laser, and the second pulse (the analysing pulse) arrives at the sample a given time t after the exciting pulse. The time delay between the pulses is generated by sending pumping and probing beams through slightly differing pathlengths. The parameter of interest is then the amount of the probe pulse absorbed by the sample at a given time after the arrival of the pumping pulse, relative to the amount absorbed before the arrival of the pumping pulse. Here again there is a slight complication introduced where the events of interest occur on a timescale comparable with the pulsewidth, not only due to the pumping pulse as is the case with nanosecond and microsecond flash photolysis, but also due to the finite width of the probing pulse. This is since if the absorbance of the sample changes during the probing pulse duration, the amount of probe absorbed will reflect only the average absorbance during the pulsewidth. Hence in interpreting

such data it is necessary to deconvolute both the pumping and probing pulse profiles from the measured absorbance changes.

1.5 Light sources

1.5.1 Laser light sources

The term 'laser' is an acronym derived from the term Light Amplification by Stimulated Emission of Radiation. Before describing in detail the mechanism of laser action, it is useful to describe some of the properties of laser sources which contribute to their suitability for a wide range of applications including as excitation and probing sources in photochemical investigations.

(a) Coherence

Laser light sources have the property of coherence, which is essentially preservation of relative phase within the propagating light beam; the phases of the light waves are correlated in both space and time.

(b) Directionality

Laser sources are highly directional sources which have very low divergence; usually the divergence is close to the diffraction angle for the laser aperture^[18].

(c) Monochromaticity

Laser sources are generally operated such as to have a very narrow frequency bandwidth, either by tuning the cavity length so as to cause laser action from only one transition within the lasing medium, or by placing wavelength selection devices such as gratings within the cavity to allow amplification of only a narrow band of wavelengths within the cavity. The properties of laser cavities will be dealt with in more detail later.

Laser action depends on two factors; light amplification by stimulated emission and optical oscillation in a resonant cavity. Each of these will be dealt with in turn.

(a) Light amplification by stimulated emission

Consider a simple atomic system consisting of two energy levels, an upper level n and lower level m , of energies E_n and E_m and populations N_n and N_m .

E_n ----- population N_n

E_m ----- population N_m

One possible process which can take place in this system is absorption of a photon of light of energy $E_{nm} = E_n - E_m$, which promotes an atom from level m to level n . The power absorbed from a beam of photons of energy E_{nm} is

$$P_{\text{absorbed}} = h\nu_{nm} B_{nm} N_m \rho(\nu_{nm}) \quad (1.35)$$

where $\rho(\nu_{nm})$ is the power density of the incident photons and B_{nm} is the Einstein coefficient representing the strength of the upward transition (section 1.2). Following absorption of radiation, there are two possible radiative processes which can occur; spontaneous emission and stimulated emission. The power radiated as a result of spontaneous emission is

$$P_{\text{spontaneous}} = h\nu_{nm} A_{nm} N_n \quad (1.36)$$

where A_{nm} represents the probability of spontaneous emission for the transition from state n to state m . The second possibility is stimulated emission, where an excited atom is stimulated to emit by the incidence of a photon of light whose energy matches the energy

gap in the excited moiety. Important properties of the photon so produced are that it is emitted in the same direction as and in phase with the stimulating photon, and has the same energy, giving rise to the coherence of a laser beam. The power radiated by stimulated emission is then

$$P_{\text{stimulated}} = h\nu_{nm} B_{nm} N_n \rho(\nu_{nm}) \quad (1.37)$$

where B_{nm} is the Einstein coefficient representing the strength of the downward transition from level n to level m , which is in fact equal to B_{mn} , the strength of the upward transition. The issue as to whether the beam of emitted photons grows or dies depends in part upon whether photon absorption or stimulated emission dominates in the system. From equations 1.35 and 1.37 this can be expressed as

$$\frac{P_{\text{stimulated}}}{P_{\text{absorbed}}} = \frac{h\nu_{nm} N_n B_{nm} \rho(\nu_{nm})}{h\nu_{nm} N_m B_{mn} \rho(\nu_{nm})} = \frac{N_n}{N_m} \quad (1.38)$$

so for the emitted power to exceed losses by absorption we require that the ratio

$$\frac{N_n}{N_m} > 1 \quad (1.39)$$

i.e. that there is a "population inversion" (a greater population in the upper state than in the lower state) between states m and n . In order to obtain a population inversion, two principle techniques are used; optical pumping, where the lasing medium is surrounded by a flash tube emitting light at a frequency appropriate to excite the lasing material, and the use of an electrical discharge to cause ionisation with subsequent acceleration of charged particles in an electric field. The accelerated particles collide with particles of the lasing medium thus causing excitation. Optical

pumping is commonly used in solid state lasers such as Nd:YAG (neodymium doped yttrium aluminium garnet) lasers, while electrical discharge excitation is often used in gas lasers such as helium-neon (He-Ne) lasers to produce population inversion.

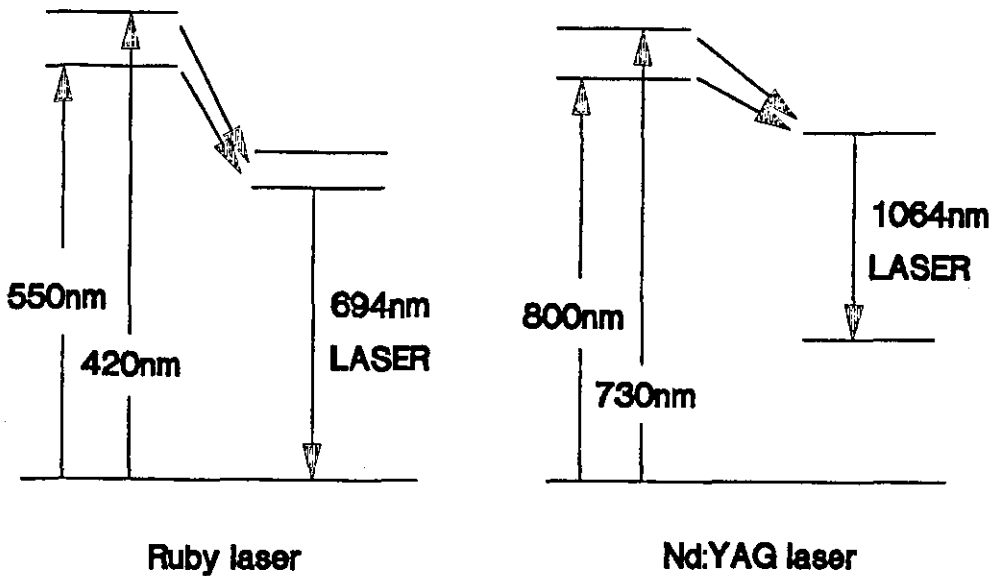


Figure 1.5: Four- and Three-level laser systems

The drawback in the use of a two level system such as described above is that both absorption and stimulated emission may be triggered by the same photon. As a result, population inversion is difficult to achieve and generally 3-level or 4-level systems are used. Examples of 3-level and 4-level systems, as present in ruby lasers and Nd:YAG lasers respectively, are shown in figure 1.5. 4-level systems have the advantage over three level systems in that there is a smaller population in the lower level of the lasing transition to invert.

(b) Optical oscillation in a resonant cavity

An optical cavity is required to give a directional beam, to give the beam phase coherence, and to sustain laser action. To sustain lasing, we require gain in intensity due to stimulated emission to be greater than the loss due to absorption and other losses in the cavity such as scattering. This requires an adequate population inversion, as discussed above, and an adequate pathlength through the lasing medium. There are many reflections back and forth in a laser cavity to give a long pathlength.

It is necessary at this point to consider the modes of oscillation (standing wave patterns) in an optical cavity. There are two cases to consider; transverse modes and axial modes.

(i) Transverse modes

These reflect the intensity distribution across the output mirror, and arise due to beams following off-axis paths between the two cavity mirrors, resulting in interference and cancellation. Transverse modes are often described by the notation TEM_{pq} , where TEM stands for Transverse Electric and Magnetic fields. Examples of transverse modes and their corresponding value of p and q are given in figure 1.6. Ideally we operate the laser in TEM_{00} , where there is a gaussian intensity profile across the beam; this is termed uniphase operation, and may be achieved by placing an iris concentric with the optical axis of the cavity to suppress all but this mode.

(ii) Axial modes

These describe the standing wave patterns along the axis of the beam (axis of the cavity), and are analogous to the modes of oscillation in e.g. a taut string. Each standing wave pattern, corresponding to a wavelength $\lambda = 2l/n$, where n is the number of half-wavelengths

contained within length l , is a mode of oscillation and has associated with it a frequency distribution (figure 1.7). Note that here we can define a quality factor or Q-factor for the cavity as

$$Q = \frac{\nu_n}{\Delta\nu} \quad (1.40)$$

For an active optical cavity, Q-factors may be as high as 10^{11} , as a consequence of the very narrow output bandwidth.

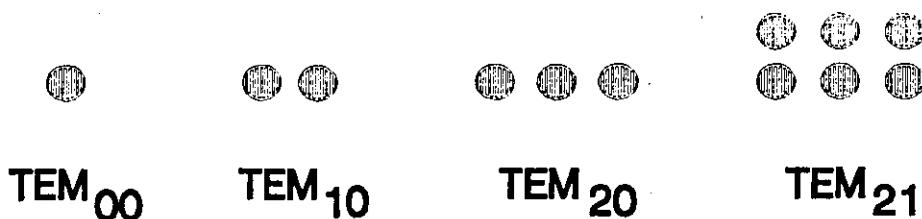


Figure 1.6: Transverse laser modes

In fact, modes of oscillation in a resonant cavity are usually described in terms of both transverse and longitudinal modes simultaneously, by notation of the kind TEM_{pqn} , where p and q describe the transverse mode and n describes the axial mode in question.

So far, all of the comments about laser action have been made for lasers in general, but lasers may be divided broadly into two categories; continuous wave (CW) lasers, where the output power level is maintained for periods of time greater than 0.25 seconds^[19] and often for considerably longer, and pulsed lasers where the energy is delivered as a single pulse or a train of pulses, the pulse duration being less than 0.25s. Two methods may be applied in producing pulsed laser operation; Q-switching and mode locking.

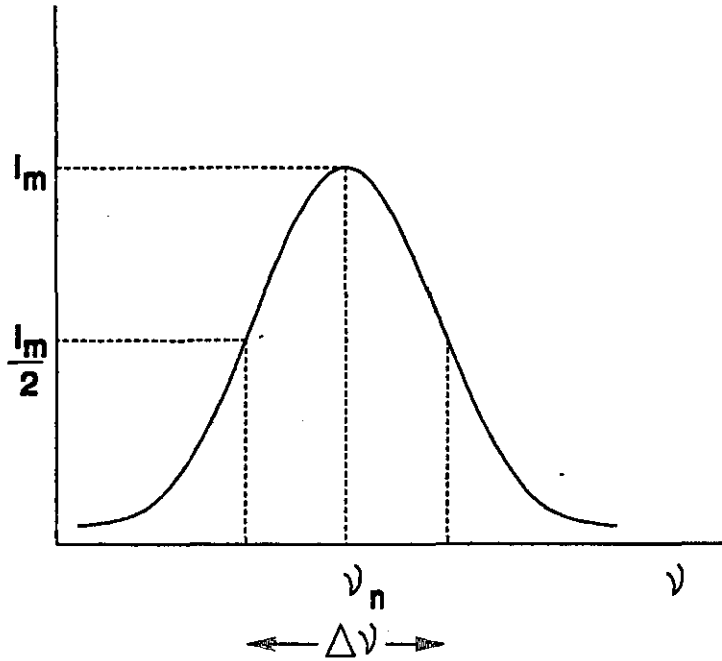


Figure 1.7: Frequency distribution for an axial mode of oscillation

(a) Q-switching

We met one definition of the Q-factor or quality factor of an optical cavity in equation 1.40. The Q-factor may also be defined as

$$Q = \frac{2\pi\nu_0 \cdot (\text{energy stored in mode})}{(\text{energy lost per second from mode})} \quad (1.41)$$

Q-switching, then, involves moving from a high loss, low Q situation to a low loss, high Q situation. This is often achieved in modern lasers by the technique of active Q-switching, where an electro-optical shutter is placed within the cavity. The shutter employed is often a Pockels cell, which is based upon voltage-induced birefringence in a suitable material. In the presence of an applied field (in the form of a high voltage across the crystal), no light is passed through

a pair of crossed polarisers. When the high voltage is briefly switched off, the material between the filters ceases being birefringent and light passes through the cell. With such a shutter closed, laser action does not occur and the gain of the cavity is low as is the Q-factor (high loss from all modes); this provides an opportunity to pump the lasing medium to produce a high population inversion. On opening the shutter, the gain of the cavity increases and laser action can occur, resulting in a high Q-factor for the output mode and rapid depopulation of the upper lasing level. This results in the output of the laser being a single, high intensity pulse. Obviously, repetitive pumping and shutter operation will result in the output being a train of pulses.

(b) Mode locking

Mode-locking is achieved by modulating the gain of the laser with a period equivalent to the round trip time of the laser cavity^[20]. Lasers used for short pulse generation have a large number of oscillating longitudinal modes (section 1.5.1), and locking together the phases of these modes results in laser output which is a series of discrete pulses separated by the cavity round trip time. This phase locking is generally achieved in continuous wave Nd:YAG and ion lasers by the technique of active mode locking, where the gain of the cavity is modulated by Bragg diffraction in a quartz prism. A radio frequency source is applied through a transducer to the prism, and an acoustic standing wave is set up therein. The loss, proportional to the acoustic intensity, is thus modulated at twice the radio frequency. The output from the laser is then a series of pulses the separation of which is determined by the inverse modulation frequency rather than the cavity length.

Active mode-locking may also be achieved by the technique of synchronous pumping. In a synchronously pumped dye laser, the cavity length corresponds with the interpulse spacing of a mode-locked pump laser, or a multiple thereof. The gain is thus modulated at the round trip frequency, and mode-locking occurs. When the dye laser cavity is correctly set, the resulting pulses may be up to 100 times shorter than the pumping laser pulse, due to increasing gain on the rising edge of the dye pulse followed by gain saturation at the peak; these processes produce greater amplification in the centre of the pulse intensity profile, shortening the pulse with successive round trips. This process continues until dispersive forces in the laser become significant, and a steady state is reached between compressive and dispersive forces.

Another important feature of many laser systems concerns not the laser action itself, but the generation of wavelengths other than the laser fundamental. An important method of achieving this is second harmonic generation, where double the laser fundamental frequency (half the wavelength) is produced. Franken first observed this phenomenon when passing light from a ruby laser through a quartz crystal^[22]. This phenomenon arises since the incident electromagnetic field produces a polarisation in the matter concerned. This polarisation consists of linear and non-linear terms, the coefficients corresponding to these non-linear terms being generally less than one. These non-linear terms in the polarisation are the origin of the generation of second and higher harmonics. Since second harmonic generation is second order with respect to the amplitude of the electromagnetic field representing the optical radiation, this only occurs with high

efficiency for intense optical pulses. Systems possessing macroscopic inversion symmetry (e.g. liquids and gases) have vanishingly small non-linear coefficients, and consequently second harmonic generation is limited to principally single crystals of certain classes and to surfaces^[22]. However, this phenomenon is not limited to doubling of the frequency of a single pulse of light, but is also applicable to the mixing of two frequencies of light incident upon the medium simultaneously^[23].

1.5.2 Xenon Arc Lamps^[24]

Xenon arc lamps used as analysing sources in photochemistry are operated at pressures of approximately 20 atmospheres to give an output which is a continuum; if operated at lower pressures the lamps produce an output composed of discrete wavelengths corresponding to the emissive transitions in the excited atoms. Such lamps are operated with DC power supplies, and are mounted vertically with the larger anode above the smaller cathode, with typical anode-cathode separations in the range 2 to 4mm. The output is a smooth continuum with some weak lines superimposed in the visible region and some stronger lines in the near infra-red. As analysing sources in photochemical investigations, lamps with input powers ranging from 150 to 1000 watts are typically used.

1.6 Singlet oxygen

1.6.1 Introduction

Oxygen is unique among homonuclear diatomic molecules having an even number of electrons in that it is paramagnetic in its ground state. Taking the simplest representation of the oxygen molecule derived using the linear combination of atomic orbitals (LCAO) approach (figure 1.8), it is clear that in the ground

state the lowest energy configuration corresponds to the presence of two spin parallel electrons in the two degenerate π_g (antibonding) molecular orbitals derived from the P_x and P_y atomic orbitals on the discrete oxygen atoms.

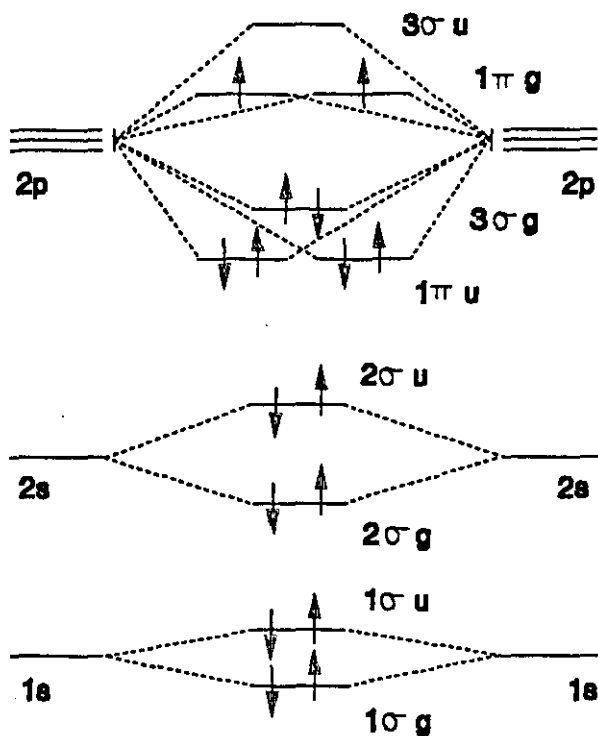


Figure 1.8: Molecular orbital diagram for ground state molecular oxygen

Consequently, the ground state has triplet multiplicity and is described by the spectroscopic state symbol ${}^3\Sigma_g^-$. There are two other possible configurations of these two electrons; one involving the electrons with spins paired in separate orbitals, and one with the two electrons spin paired but both in the same orbital, which may be described by the state symbols ${}^1\Sigma_g^+$ and ${}^1\Delta_g$, respectively. Clearly in the simple molecular orbital picture this latter arrangement is doubly degenerate, there being the possibility of the electrons being localised in either of the two π_g orbitals. Since these two orbitals are isoenergetic in the absence of a suitable perturbing field, distinction between them

is generally not made. The two states described above, the $^1\Sigma_g^+$ and $^1\Delta_g$, lie 158 kJ mol^{-1} and 95 kJ mol^{-1} respectively above the ground state. The $^1\Delta_g$ state is the state from which reactivity of singlet oxygen is almost exclusively observed as a consequence of its appreciable lifetime; even when excitation is initially to $^1\Sigma_g^+$, this rapidly relaxes to $^1\Delta_g$ and it is from here that reaction may occur. It is this latter state which is usually referred to as singlet oxygen, and where the term singlet oxygen is used here it will refer to the $^1\Delta_g$ state.

1.6.2 Production of singlet oxygen

Probably the most common method of producing singlet oxygen is through dye sensitised energy transfer to ground state molecular oxygen. In such a method, the interactions between ground state oxygen and the excited singlet and triplet states of the sensitising dye must be taken into account. The overall quantum yield of production of singlet oxygen will be the sum of the yields of production from oxygen quenching of both the first excited singlet and triplet states

$$\phi_{\Delta} = \phi_{\Delta}(S_1) + \phi_{\Delta}(T_1) \quad (1.42)$$

However, account must be taken of the fact that not all the quenchings of T_1 and S_1 will result in production of singlet oxygen; also, quenching of S_1 by ground state molecular oxygen may give rise to the first triplet state T_1 , which may then itself be quenched by ground state oxygen and produce singlet oxygen. This quenching of the singlet state to produce the triplet may be accompanied by production of singlet oxygen if the $S_1 \rightarrow T_1$ energy gap exceeds 95 kJ mol^{-1} . A scheme describing the possible interactions of sensitiser triplet and singlet states with ground state oxygen is shown as figure 1.9.

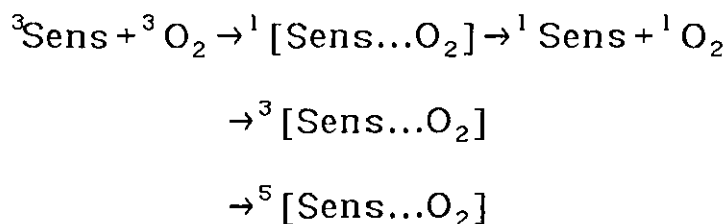
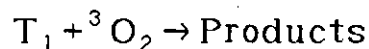
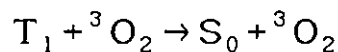
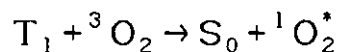
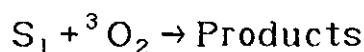
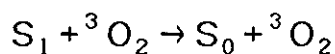
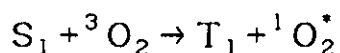
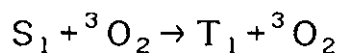


Figure 1.9: Singlet oxygen sensitisation scheme

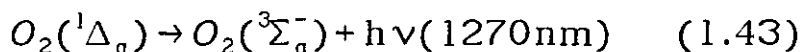
As illustrated at the bottom of figure 1.9, there are three possible spin multiplicities for the encounter complex between the sensitiser triplet state and the triplet ground state of molecular oxygen. These have singlet, triplet and quintet degeneracies. The process shown, i.e. the coming together of ground state oxygen and sensitiser triplet state to produce singlet molecular oxygen and the singlet ground state of the sensitiser, is only spin allowed if the reactants, products and transition state have common resultant spins. Clearly this is only the case for the singlet encounter complex, which is only formed with a probability of 1/9. The other complexes, however, generally break down to give back the sensitiser triplet state and ground state oxygen, so there exists the possibility

of further encounters and possibly singlet oxygen production. In addition, the triplet complex may intersystem cross to the singlet, which may then break down to produce singlet oxygen.

1.6.3 Methods of studying singlet oxygen

1.6.3.1 Phosphorescence Emission

Isolated molecules of oxygen in the $^1\Delta_g$ state may spontaneously undergo a radiative transition to the ground state through



for which process the rate constant is approximately 0.93 h^{-1} ^[25]. Collisions with other molecules may induce radiative and non-radiative transitions to the ground state, reducing both the lifetime of the state and the quantum yield of phosphorescence therefrom. However, even given that the quantum yield of near-infrared emission is only of the order of 10^{-6} , it is possible to quite readily detect singlet oxygen phosphorescence following excitation of oxygen-containing solutions of suitable sensitising dyes. There are two approaches taken to the use of the phosphorescence emission as an analytical tool; pulsed excitation of the solution of interest^{[26][27]}, and steady state illumination and detection. Following pulsed excitation, the decay of the singlet oxygen phosphorescence signal gives a direct measure of its lifetime in the system under investigation. The measured rate constant will be the sum of the intrinsic rate constant for deactivation in the particular solvent, and any bimolecular quenching rate constants and quencher concentrations. Hence not only can the lifetime of singlet oxygen in a particular solvent be directly measured, but also

bimolecular singlet oxygen quenching constants determined. Steady state phosphorescence measurements have also been employed determine quenching constants using the Stern-Volmer equation^[28]

$$\frac{I_0}{I} = 1 + \frac{k_q[Q]}{k_d} \quad (1.46)$$

by measuring the steady state phosphorescence intensity I as a function of quencher concentration.

1.6.3.2 Thermal lensing

Local temperature changes in gases and liquids cause changes in refractive index and density and these lead to the system acting as a diverging lens. Non-radiative transitions from excited states in solution release energy which can cause these local heating effects, which are then probed by a laser source which is deflected by the thermal lens. Thermal lensing is ideal therefore for probing the decay rates of excited states not having favourable spectroscopic properties for using conventional absorption or emission techniques. The dynamic range of time resolved thermal lensing is determined by two factors; the acoustic transit time of the heat across the laser beam, determined by the velocity of sound in the medium, and the thermal recovery time of the medium. In practice in solution the dynamic range is approximately 0.1-500 microseconds, making the technique ideal for investigating the relaxation of singlet oxygen^[29]. Time resolved thermal lensing can be used to measure quantum yields of singlet oxygen formation^[30] and in addition the time profile of heat generation can be used to yield the lifetime of the singlet oxygen.

1.6.3.3 Time dependent disappearance of an acceptor^{[31][32][33]}

Probably the best known example of a chemical quenching reaction of an organic compound with singlet oxygen is that of diphenylisobenzofuran (DPBF), which reacts to form either the monomeric peroxide or o-dibenzoylbenzene, dependent upon reaction conditions. This is an example of a molecule for which the chemical quenching constant is very much larger than that for physical quenching and as such reaction of singlet oxygen with DPBF may be approximated as quantitative. This has been made use of in chemical methods for detecting and monitoring singlet oxygen in a variety of systems. Under certain conditions, a plot of the first order rate constant for DPBF bleaching against quencher concentration gives as its slope the bimolecular quenching constant.

1.6.4 Singlet oxygen quenching mechanisms

The deactivation of singlet oxygen can involve a route whereby the quencher undergoes no ultimate chemical change (physical quenching), having rate constant k_{pq} , or may be the result of a chemical reaction forming a product (chemical quenching) proceeding with rate constant k_{cq} . In both cases similar intermediates may be involved, and commonly both processes are, to an extent, at work in a given system.

1.6.4.1 Chemical quenching processes

Chemical quenching of singlet oxygen involves reaction of singlet oxygen with a substrate molecule to form an oxidised chemical species. This process may be autooxidation, where the compound sensitising singlet oxygen is itself attacked, or may be dye-sensitised photooxidation of a substrate, as is

the case in using DPBF as an oxidisable acceptor to investigate singlet oxygen in solution (section (1.6.3.3)).

1.6.4.2 Physical quenching processes

A number of mechanisms for the physical (i.e. the absence of ultimate chemical reaction) deactivation of singlet molecular oxygen have been proposed, and several or all of these may be at work in a given system. The principal mechanisms will be dealt with individually.

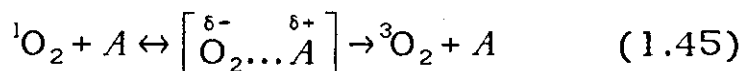
(a) Quenching by solvents

The lifetime of singlet molecular oxygen varies considerably with solvent. There is some correlation between the infra-red properties of the solvent in question and the singlet oxygen lifetime; the greater the solvent absorption at 7880 cm^{-1} (1270nm), the shorter the singlet oxygen lifetime. This implies that direct conversion of the singlet oxygen electronic excitation energy into vibrational energy in the solvent is dominant in determining the rate of decay. As a consequence, in solvents such as water, hydrocarbons and alcohols which possess overtone and combination bands having appreciable absorption in this region, the singlet oxygen lifetime is very short, being at most only a few tens of microseconds. In solvents such as freons and perdeuterated solvents, the positions of the infra-red absorption frequencies are such as not to facilitate such energy transfer and singlet oxygen lifetimes are often from several hundreds of microseconds to several milliseconds. Theories simply taking account of solvent infra-red properties are not, however, very successful in predicting the singlet oxygen lifetime in a given solvent. Taking account of other solvent properties

can result in more successful theories; inclusion of a term relating to polarity has been shown to work quite well for alcohols.

(b) Charge transfer quenching

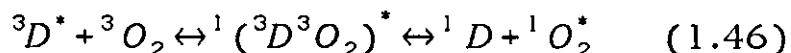
Various compounds have been suggested to quench singlet oxygen by a mechanism involving charge transfer mediated spin-orbit coupling, such as sulphides^[34], phenols^[35] and amines, where there have been shown to be correlations between the rate constants for physical quenching of singlet oxygen and the ionisation potential of a number of aliphatic and aromatic amines, giving support to this partial charge transfer proposal^[36]. From work on the physical quenching of singlet oxygen by amines, there appear to be two factors at work in determining the quenching rate constant; one is the ionisation potential, the quenching rate increasing with decreasing ionisation potential supporting the partial charge transfer mechanism, but in addition the quenching rate is seen to decrease with increasing steric hindrance α to the amino nitrogen^[37]. This implies close approach of the oxygen to the amino nitrogen is required for quenching to occur. The mechanism proposed may be represented as



Azomethine dyes^[38] have also been proposed to quench singlet oxygen at least in part via a mechanism of this kind. Clearly the amino group on the p-phenylenediamine moiety of the azomethine is the region of the molecule which may be expected to participate in such a mechanism.

(c) Quenching by energy transfer

A number of compounds have been reported as efficient quenchers of singlet oxygen in solution via the mechanism of energy transfer. One of the most effective of these is β -carotene. Singlet molecular oxygen lies only 95 kJ mol⁻¹ above its ground state, and the triplet states of magenta pyrazolotriazole azomethine dyes have energies only slightly above this. Azomethine dyes have been demonstrated to be efficient quenchers of singlet oxygen, and certainly for the magenta series it appears that electronic energy transfer from the singlet oxygen to the dye may well make a contribution to the quenching mechanism.



Reverse energy transfer of this kind has been observed for molecules whose triplet energy approaches that of singlet oxygen^[39]. β -carotene and certain nickel complexes having low lying triplet states have been demonstrated to quench singlet oxygen via electronic energy transfer^[40].

1.7 Isomerisation in flexible dye systems

The isomerisation reaction in general, being a relatively simple unimolecular process, has attracted attention as a model reaction through which to study solvent effects on reaction rates, and as such there have been a number of models and theories proposed to explain experimental data. The simplest models with which to describe isomerisation taking place via an excited state involve only two stable conformations and may be formulated in terms of two extreme cases; each involves initial excitation of one isomeric form to its first excited singlet state, the population of which then evolves along an appropriate molecular co-ordinate to a

conformation approximately mid-way between the two extreme isomeric forms. From this "perp" conformation internal conversion to the ground state surface takes place followed by rapid partitioning between the two possible isomers. The shapes of the excited state surfaces corresponding to these two extremes are illustrated in figure 1.10; here we have either the initial and final states on the excited state potential surface separated by a barrier of height greater than kT , such that thermal quasi-equilibrium is reached in the first potential well before the changes in conformation proceed, or there is what may be described as an all-downhill potential leading to isomerisation in the excited state and the population evolves very rapidly to the perp conformation.

Once the perp conformation has been reached, there are two possible descriptions of the process of internal conversion to the ground state potential surface; a so-called "pinhole" sink function, where internal conversion occurs only from one well-defined position on the excited state surface, and a position dependent sink function where the internal conversion probability varies smoothly with position as e.g. a gaussian function. A detailed theoretical treatment of both pinhole and position dependent sink functions has been presented by Bagchi, Fleming and Oxtoby^[41]. In the case of a pinhole sink the internal conversion rate should be characterised by a single exponential function and have a linear viscosity dependence, whilst a position-dependent sink should display non-exponential excited state relaxation kinetics with a non-linear viscosity dependence. However, it has been suggested that relaxation via a gaussian sink should show a single exponential decay at all practical values of viscosity in fluid solution^[42]. The rate at which the population evolves to the sink position depends on the steepness of the potential; the steeper the

potential, the greater the accelerating force on the molecule and the higher the rate (the higher the frequency, ω , of the motion). It should be noted that barrier heights and potential surface shapes may be profoundly affected by solvent parameters, and hence changes in solvent parameters may induce variations in ω which in turn cause variations in the rates of internal processes which are not the direct result of viscosity changes.

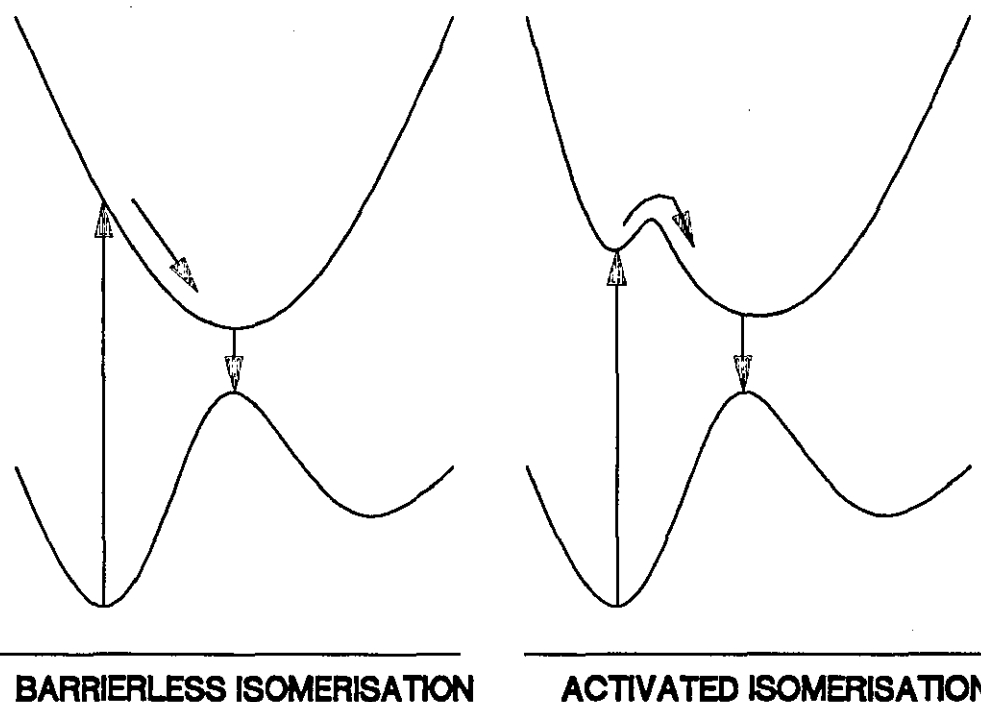


Figure 1.10: Potential surfaces for barrierless and activated isomerisation

Results obtained for 1,1'-diethyl-4,4'-cyanine and pinacyanol yield values of ω of $5.2 \times 10^{12} \text{ s}^{-1}$ and $1.5 \times 10^{12} \text{ s}^{-1}$ respectively, suggesting a much shallower excited state potential surface in the sink region for pinacyanol. Also, the sink itself is calculated as small relative to the molecular dimensions for 1,1'-diethyl-4,4'-cyanine, so justifying the use of the pinhole sink approximation in this circumstance. For pinacyanol, however, the sink is calculated as being much larger, suggesting a somewhat

flat potential surface as concluded from the low frequency of the motion. Also, the relaxation rate of 1,1'-diethyl-4,4'-cyanine has been shown to have a wavelength dependence, the rate decreasing by a factor of two in changing the wavelength of excitation from 620nm to 560nm^[43]. Such a wavelength dependence suggests the absence of a barrier to isomerisation in the excited state, since in this circumstance it is anticipated that the time taken to reach the sink will depend on the position upon the excited state surface to which excitation takes place. It should of course be noted that the particular mode excited in the molecule by the absorption of light is most likely not the one involved in the isomerisation process. After excitation the energy is redistributed and part of it will enter the isomerisation pathway via coupling between the modes. It is therefore difficult to gain a quantitative relationship between excitation wavelength and the precise position on the excited state surface that constitutes the initial state as a result of excitation by this wavelength without a detailed knowledge of the potentials and couplings. However, it may be anticipated that the higher the excitation energy relative to the 0-0 transition, the higher will be the position on the potential surface to which excitation takes place.

An alternative scenario to explain the wavelength dependence of the relaxation rate would be to invoke the presence of two isomeric forms in the ground state having slightly differing absorption spectra and relaxation times; this should give a non-linear dependence of relaxation time on excitation wavelength, since the relaxation time should level off at the short and long wavelength extremes of excitation corresponding to the lifetimes of each isomeric form. Also, deviations from a single exponential relaxation scheme should be observed.

Since neither of these cases were observed for 1,1'-diethyl-4,4'-cyanine, in this instance the explanation of essentially a "negative" potential barrier in the excited state seems most likely.

1.8 Photochemistry and Photophysics of Azomethine Dyes

Azomethine dyes belong to the general class of imines, which contain in the simplest case the nitrogen analogue of a carbonyl functionality. Primary imines are unstable to hydrolysis even in aqueous solution, hydrolysing rapidly to yield the corresponding carbonyl. Substituted imines, or Schiff bases as they are often termed, are also unstable to hydrolysis when the substituents are aliphatic; when the substituent on either carbon or nitrogen is a phenyl group or a substituted phenyl, the resulting imine is generally quite stable. All of the azomethine dyes studied here have a phenyl group attached directly to the imine nitrogen, and as a consequence of this and the functionality on the carbon atom, they are quite stable to hydrolysis.

Pyrazolone and pyrazolotriazole (PT) azomethine dyes are well known as magenta image formers in the subtractive colour development process. They are formed during development by the oxidative coupling of a p-phenylenediamine and the appropriate coupler (pyrazolone or PT) (section 2.4). These dyes exhibit two maxima in their visible absorption spectra; a high intensity band typically in the green region ($\epsilon > 10^4 \text{ dm}^3 \text{ mol}^{-1} \text{ cm}^{-1}$, $\lambda_{\text{max}} \approx 530 \text{ nm}$, although the precise wavelength may be shifted by substituents) and a lower intensity band ($\epsilon < 10^4 \text{ dm}^3 \text{ mol}^{-1} \text{ s}^{-1}$) in the blue region. The band in the blue region is of considerably lower intensity for the PT dyes than for the pyrazolones, and consequently the former are capable of giving a purer hue. These two bands respond differently to solvent and substituent effects, and consequently are assigned as being two distinct

electronic transitions rather than vibronic structure of the lowest singlet-singlet transition.

Unsymmetrical azomethine dyes can exist as two distinct isomeric configurations about the azomethine linkage, referred to as the syn and anti configurations, shown for a general PT dye structure in figure 1.11.

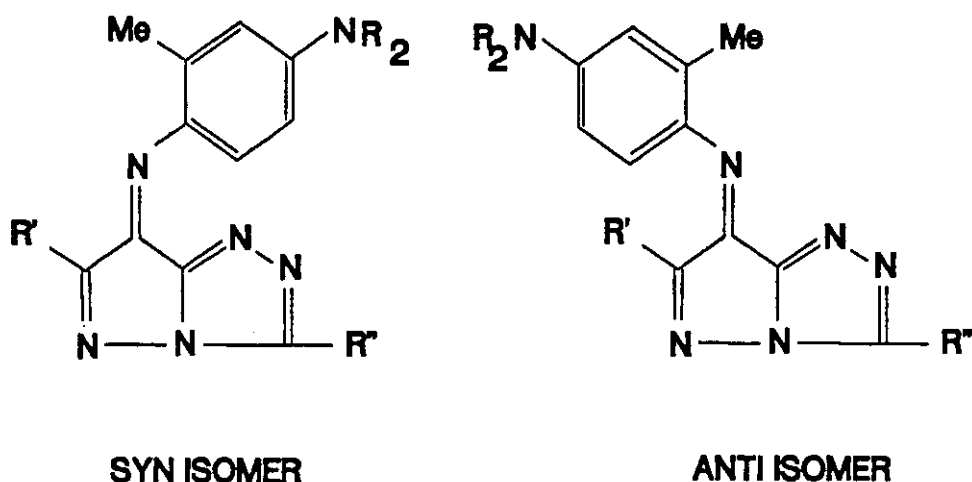


Figure 1.11: Syn and anti isomeric configurations for a PT dye

NMR measurements have shown that the 6-H substituted PT dye exists as exclusively the syn isomer at room temperature in CDCl₃ solution^[44]. NMR studies involving pyrazolone dyes have demonstrated that they exist also either as exclusively or predominantly syn isomers, depending on steric effects^[45]. X-ray crystallographic data suggests that this is also the case in single crystals, and that here the pyrazolone and the phenylenediamine rings are not co-planar, but that the dihedral angle between the ring systems varies from a minimum of some 14°, increasing with increasing steric crowding ortho to the azomethine bond on the p-phenylenediamine ring^[46].

This increase in dihedral angle is assigned to twisting mostly of the N-phenyl bond, but with some contribution from twisting of the N-pyrazolonyl double bond. This twisting results in a bathochromic shift of the dye λ_{\max} from about 500nm to 630nm, resulting in a hue shift from magenta to cyan, by reducing the bond order of the azomethine linkage and allowing more resonance delocalisation and charge transfer character in the dye ground state. Similar conclusions about the non-coplanarity of these two ring systems in pyrazolone azomethine dyes have been reached from NMR observations in fluid solution^[47].

The syn-anti isomerisation process about the carbon-nitrogen double bond may proceed via two distinct mechanisms; torsion about the double bond, or linear inversion over the nitrogen atom^[48], although it is probable that for a given dye isomerisation may proceed via a path whereby both mechanisms make a contribution^[49]. The torsional mechanism involves rotation about the carbon-nitrogen double bond, and for such rotation to occur there must be a reduction of bond order in the transition state. During the isomerisation process the C-N-C bond angle will remain constant at 120°, as will the sp² hybridisation of the nitrogen atom. A change in charge distribution in the bond will, however, obviously occur, as illustrated in figure 1.12. Inversion over the nitrogen atom occurs with a change of both bond angle at the nitrogen, from 120° to 180°, and hybridisation, from sp² to sp, in the transition state. Here, though, the double bond remains intact throughout the isomerisation process and again a change in charge distribution may occur as the non-bonding electrons on the azomethine nitrogen atom may become involved in conjugation with other π -electron systems attached thereto, thus stabilising the transition state (figure 1.13).

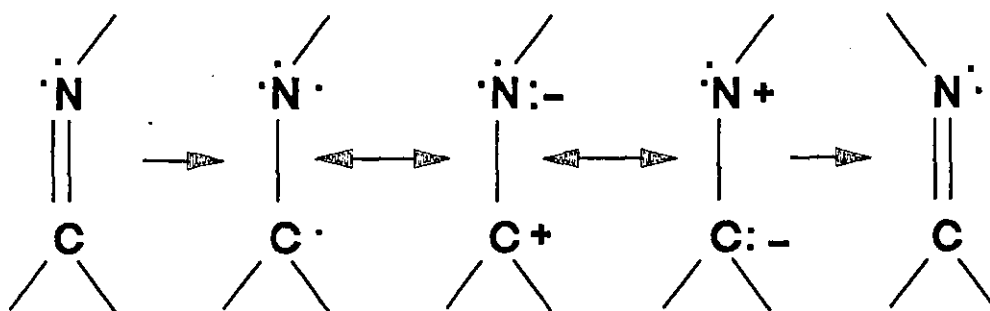


Figure 1.12: Torsional isomerisation mechanism

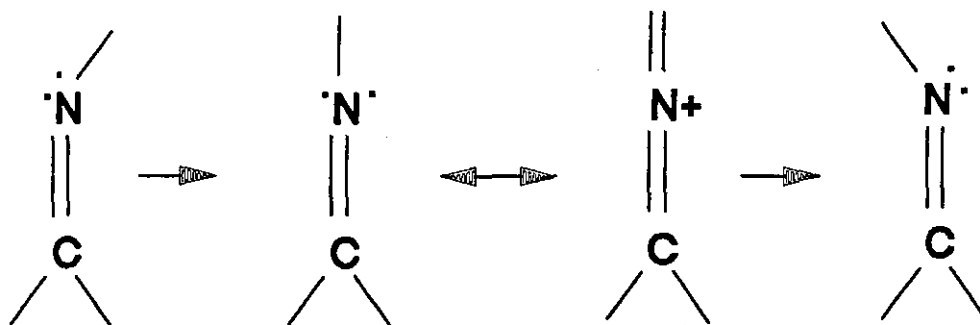


Figure 1.13: Inversion isomerisation mechanism

It should be possible, then, to make inferences about the major isomerisation mechanism operative in a particular dye from considering how the nature of the substituents about the azomethine bond will affect the stability of the transition states for the two mechanisms, and thus the activation energies for the processes. Considering the nature of the substituent in the para position of the aromatic ring attached to the nitrogen atom of the bond, it is clear that strongly electron-donating substituents will favour a torsional mechanism, via a transition state of the kind shown in figure 1.14, while electron withdrawing substituents will favour inversion by involving the nitrogen non-bonding pair of electrons in the conjugated system (figure 1.15).

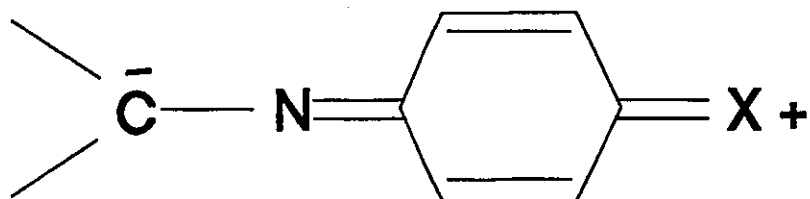


Figure 1.14: Transition state for torsional isomerisation mechanism

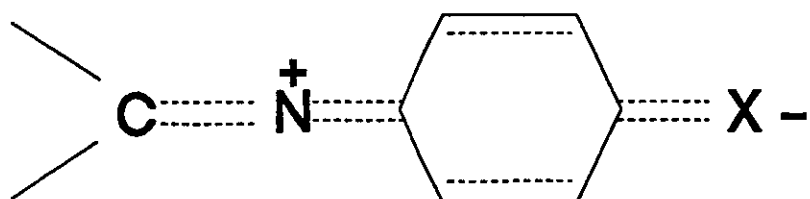


Figure 1.15: Transition state for inversion isomerisation mechanism

Attention must also be given to the nature of the substituents on the azomethine carbon atom, and how these will affect transition state stabilisation. If these substituents are electron withdrawing, then in the presence of an electron donating para substituent on the aromatic system attached to the nitrogen this will further act to stabilise the transition state for torsion (figure 1.16) and this will undoubtedly be the favoured mechanism; if the para substituent is electron withdrawing, then inversion may be favoured through the intermediate shown previously in figure 1.15.

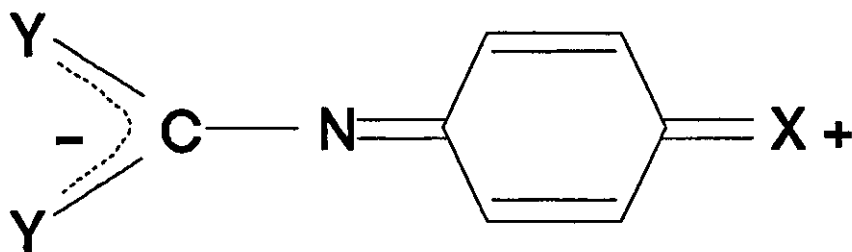


Figure 1.16: Torsional isomerisation transition state with electron withdrawing substituents

If the groups attached to the azomethine carbon are electron donating, however, both torsion and inversion may occur, although inversion may be favoured due to greater electron density in the azomethine bond. Both mechanisms will undergo an increase in activation energy as the para substituent becomes more electron donating. Herkstroeter has used Hammett plots to investigate the isomerisation mechanism in pyrazolone and benzoylacetanilide azomethine dyes^[50]. These plots are based upon the Hammett equation^[51]

$$\log \frac{k_i}{k_H} = \rho \sigma_i \quad (1.47)$$

where k_i is the rate constant for the process with substituent i and k_H is that for the unsubstituted (H-substituted) reactant. ρ is a parameter characteristic of a particular reaction in a particular solvent, and is indicative of the sensitivity of a reaction to the nature of the substituent of interest. σ_i is characteristic of the substituent, and is defined as

$$\sigma_i = pK_a(\text{benzoic acid}) - pK_a(\text{substituted benzoic acid}) \quad (1.48)$$

and the pK_a of benzoic acid in water at 25°C is taken as 1 on this scale. Hence a negative sigma corresponds to greater acidity in the substituted acid and consequently to an electron releasing group, while a positive sigma is indicative of lesser acidity and hence an electron withdrawing substituent. The greater the effect of the substituent, the larger the value of sigma. By plotting the sigma constants for the para substituents on the phenyl ring against the logarithm of the ground state isomerisation rate constants, Herkstroeter found that such plots go through a minimum at $\sigma=0$, which he interprets as indicating a change in isomerisation mechanism in going from positive sigma (electron withdrawing) to negative sigma (electron donating). The presence of the methyl group ortho to the azomethine nitrogen accelerates the isomerisation process but does not alter the shape of the Hammett plots; thus the implication is that such substitution accelerates both inversion and rotation.

The isomerisation process has been demonstrated to be brought about by electronic excitation, and is complete on timescales of less than a few tens of nanoseconds, the time resolution of our nanosecond flash photolysis apparatus. In dyes not symmetrical about the carbon-nitrogen double bond isomerisation is readily observed as a bathochromic shift in the dye absorption spectrum. The less stable anti isomer so produced relaxes thermally to the syn form on timescales ranging from microseconds to milliseconds depending on temperature, solvent properties and dye substitution patterns.

Triplet energy transfer to these dyes results in production of the isomer, indicating the existence of an isomerisation pathway involving the triplet state. However, the rise of the absorption due to the isomer follows precisely the decay of the sensitiser triplet state, indicating that the triplet state of the dye must

have a lifetime shorter than a few hundred nanoseconds. Picosecond transient absorption studies conducted by us on pyrazolotriazole azomethine dyes^[52] has demonstrated that two intermediate states are produced, having solvent-dependent deactivation times of 1 to 3 picoseconds and 5 to 12 picoseconds. Following deactivation of these intermediates there remains a species which does not decay on the timescale accessible with the picosecond apparatus (3ns) and having the same spectral characteristics and being produced with a yield consistent with the isomer produced by flash excitation in the nanosecond time domain.

We have demonstrated that in solutions of PT azomethine dyes both in solvents containing heavy atoms and those not, using nanosecond excitation pulses to directly induce isomerisation, there is no effect on isomer yield of dissolved oxygen concentration, or of the concentration of β -carotene. This observation is independent of solvent and dye substitution patterns. There has been observed for pyrazolone azomethine dyes^[53] in solvents containing a heavy atom, e.g. chlorobenzene, bromobenzene and iodobenzene, and for a 6-methyl substituted PT azomethine dye in benzene solution^[54], a very small effect of oxygen concentration on isomer yield, these results being obtained using flashlamp excitation. Thus in these experiments there is produced an intermediate with sufficient lifetime to be intercepted by dissolved oxygen, from which isomerisation can occur. The implication from the experiments with pyrazolone dyes is that the heavy atom through increased spin-orbit coupling increases the yield of triplet state, and isomerisation from the triplet manifold then makes a significant contribution to the overall isomer yield. Heavy atoms such as bromine may only be expected to have an influence on rates of

intersystem crossing and internal conversion corresponding to 10^8 to 10^9 s^{-1} ^[53], and it is known from nanosecond flash photolysis studies (section 5.3) that the rate constant for triplet deactivation is at least 10^7 s^{-1} , and from picosecond studies (chapter 6) the deactivation rate of the state assigned as the first excited singlet of the syn isomer is of the order of 10^{11} s^{-1} , so while there is the implication that the presence of a heavy atom has an influence on the rate of intersystem crossing, its effect on the overall triplet yield may be expected to be very small, although the singlet state of the anti isomer may be longer lived and therefore more amenable to heavy atom perturbation. A greater isomer quantum yield is measured in heavy atom solvents, suggesting that the yield of isomer from the triplet state is greater than from the singlet. The lack of sensitivity of pyrazolone azomethine dye isomer yields to oxygen concentration in solvents containing no heavy atoms suggests then that triplet states are not formed with a high quantum yield under such conditions and isomerisation is predominantly via the singlet state. This also shows that the singlet state(s) of these dyes are not quenched by oxygen, and as such it is possible to place an upper limit on the singlet lifetime, since oxygen would be expected to quench at the diffusion controlled rate, in benzene the diffusion controlled bimolecular rate constant being 3×10^{10} $dm^3 mol^{-1} s^{-1}$ ^[55]. Assuming the concentration of oxygen in oxygen saturated benzene to be 7.25×10^{-3} $mol dm^{-3}$ ^[56], then if it were possible to detect a 2% reduction in isomer yield due to oxygen quenching this puts an upper limit on the singlet lifetime of 10^{-10} s. We have observed the precursor to the isomer in pyrazolotriazole azomethine dyes, tentatively assigned as the singlet state, to have a lifetime an order of magnitude shorter than this. The

interpretation of the results of the studies with pyrazolone dyes, and with the 6-Me substituted PT, has been that interception of the triplet state by oxygen results in "unsymmetrical" quenching of the triplet state resulting in a different ratio of syn to anti isomer yield from the triplet manifold than prevails from triplet state decay in the absence of quenching. However, in view of the results gathered here alternative interpretations may be advanced. One involves production of a long-lived triplet state following from excitation of the anti isomer only, the triplet state being produced from the syn isomer only in small yield or having a very short lifetime. The excitation wavelength available for this work, 532nm from an Nd:YAG laser, gives very little excitation of the anti isomer due to its bathochromically shifted absorbance spectrum and hence very little of this effect will be seen in these experiments. A second possible explanation is that as a consequence of the larger excitation bandwidth associated with a flashlamp discharge excitation into the shorter wavelength absorption band of the dye can take place, populating the second excited singlet state. Intersystem crossing from S_2 may then be more efficient than from S_1 , leading to greater triplet state population.

Chapter 2

The Colour Photographic Development Process

2 The Colour Photographic Development Process

2.1 Introduction

The photographic process is a technology which has had a profound effect upon the way in which we perceive and relate to the world. Before the advent of television, photographs, whether as stills in newspapers or as films or newsreels, provided the only visual images of events outside the immediate experience of the individual, and as such shaped the way in which such events were perceived and interpreted. Even today, with a wide range of electronic storage and retrieval systems available, photographs still play an important role in the media. Additionally, photography is a relatively cheap technology readily accessible to the general public, and the combined professional and consumer market is a multimillion pound industry. There can be few people in the developed world whose lives have not been influenced by photography, whether through the media by films, magazines and newspapers, or simply through capturing personal events on film. However, in part as a consequence of photographs generally being used for recording images of the world with which we are all familiar, consumers very rapidly notice when the end product is less than perfect. Where the end product is a colour slide, a negative or a film for projection, then deterioration is caused by the storage conditions in terms of heat, humidity and exposure to chemicals. In the case of a colour negative, however, many people will not notice the degradation since fading can often very successfully be compensated for in the printing process. Where the end product is a colour print, if as is often the case this is put on display then it is photochemical degradation which is largely responsible for the deterioration. In each instance the various dyes used to produce the colour image, the yellow, magenta and cyan image dyes, will show

different susceptibilities to degradation with the result that the balance of colour in the image will change. The degradation pathway which concerns us here is the light induced fading of colour photographic prints, and in this respect the magenta image dyes are by far the most susceptible, which is unfortunate since we are most sensitive to loss of the magenta dye and least to the loss of yellow dye. The consequence of this is that on prolonged exposure to light, generally the first noticeable change in the colour balance is that flesh tones become "colder" and take on a bluish tinge; this is particularly noticed since we are all familiar with flesh tones in everyday life and as such are clear as to what constitutes an "acceptable" hue. Subtle changes in other aspects of a photograph, such as the colour of a dress or a building, may go unnoticed for much longer periods of time^[57].

As a consequence of the nature of the chemistry involved in the photographic process, which will be described later in this chapter, there are severe restrictions on the general classes of dyes which can be employed. Also, the precise mechanisms by which the dyes degrade under various conditions are little understood. As a consequence, attempts to improve photochemical dye stability have been limited to largely ad-hoc peripheral structural modifications to the basic dye nucleus.

2.2 Colour Development Chemistry^{[58][59]}

This account is intended to give an introduction to the chemistry involved in the development of a colour photographic image and to the microscopic and macroscopic structure of the photographic product, reference to which will be made later in chapter 7. A detailed description of the process of sensitisation of silver halides to wavelengths throughout the visible spectrum is beyond the scope of this account, and for a description of this

process the reader is referred elsewhere^[58]. Also, only those processes leading to colour prints will be considered; the development methodology for producing colour positives for e.g. colour slides will not be considered.

The colour photographic image is subtractive in nature, i.e. the dyes in the product absorb various wavelengths, effectively subtracting them from a white light source, and in so doing the transmitted light will contain the unabsorbed wavelengths. There are three dyes used in the subtractive colour process, each absorbing ideally approximately one third of the visible spectrum and transmitting the other two thirds. These three dyes, termed subtractive primaries, are in colour yellow (minus blue), magenta (minus green) and cyan (minus red). Hence if cyan and magenta dyes are placed over a white light source, the resulting transmitted colour will be blue. If all three dyes at equal density are placed over such a source, the result is a neutral density from white through grey to black, depending upon the densities.

The first step in the photographic process is the recording of the blue, green and red components of the scene of interest in spectrally sensitised emulsions; these emulsions consist of silver halide grains and contain dyes sensitive in the spectral region of interest since silver halides are only sensitive to wavelengths in the blue to ultraviolet region of the spectrum. The spectrally sensitised emulsions are arranged as a multilayer package. The blue sensitive layer is placed on top, and this is consequently the first layer to be exposed. Since as mentioned above the silver halide in the red and green sensitive layers will also respond to blue and ultra-violet wavelengths, a yellow filter is placed after the blue sensitive layer and before the red and green sensitive layers to remove these wavelengths (figure 2.1).

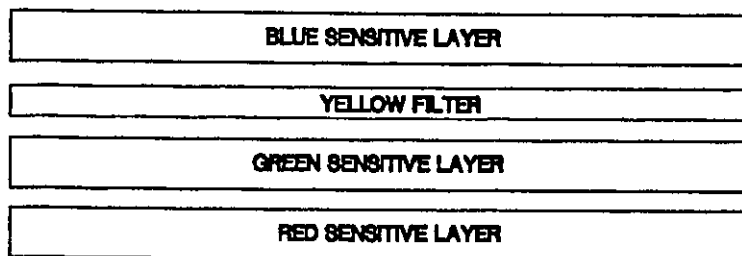


Figure 2.1: Layer structure of colour photographic material

Latent images of the blue, red and green components of a scene are thereby formed in the blue, red and green sensitive layers. In addition to the silver halide and the sensitising dyes, compound known as colour couplers are also incorporated within the layers. These react with compounds known as developers to produce an image in colour complementary to those in the scene photographed. When this negative is printed onto material similar in structure, we obtain after processing a positive image.

The basic chemistry of dye formation in the development process was developed in 1912 by Fischer^[60], but was not applied commercially until the 1930s. Developing agents of the p-phenylenediamine or p-aminophenol types are oxidised by reaction with exposed silver halide, although in modern dye-forming chemistry developing agents are almost exclusively of the p-phenylenediamine class. The oxidised developer then reacts with the coupler to form the dye, the dye hue depending upon the nature of the coupler in question. Couplers containing open-chain active methylene groups generally form yellow dyes; those with active methylene groups contained within heterocyclic rings, such as those in the pyrazolone and pyrazolotriazole class, form magenta dyes. The products of reaction of developer with both of these classes of coupler leads to dyes belonging to the azomethine class. Couplers containing an active methine group (i.e. the

para position of a phenol or naphthol) form cyan dyes, and these belong to the indoaniline class. Representative structures of the couplers and the dyes to which they lead are shown in figure 2.2.

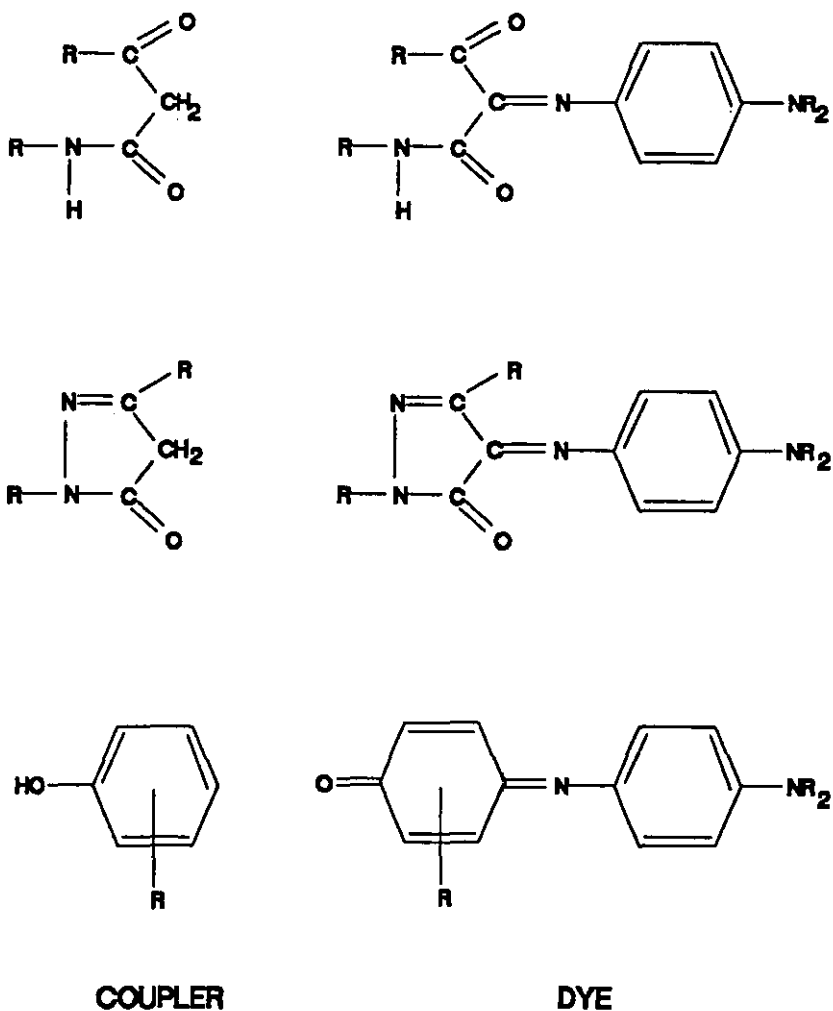


Figure 2.2: Dyes formed from various coupler classes

These general dye types are those typically found in modern colour photographic products. Other classes of dyes, such as azine and azo dyes, have been experimented with but the indoaniline and azomethine systems have been found to be the most suitable for reasons amongst others of simplicity of development chemistry and purity of hue.

2.3 Formation of the latent image

In photography, the sensitive material is exposed to a very small quantity of light, so small in fact that it is not possible to detect a change in the material by conventional means. The developer contains an agent which reduces an exposure-dependent fraction of the silver halide to silver metal, and is itself oxidised. This oxidised form of the developer then goes on to form the image dye, as detailed in section 2.4. Much of the theory of latent image formation was developed by Gurney and Mott^[61]. The chemically active product of the exposure of a silver halide emulsion to light is a silver aggregate. The primary act in photolysis is the formation of a photoelectron, which subsequently combines with a silver ion to form a silver atom. A single silver atomic centre is capable of trapping a free electron and capturing a second mobile silver ion, which forms a two-atom silver centre which has enhanced thermal stability over a one-atom centre. Growth of the silver aggregate may then continue until it reaches such a size as to become catalytic and the silver halide grain in which it resides then becomes developable. The silver aggregate, however, can still continue to grow after this catalytic stage has been reached provided photoelectrons continue to be supplied.

2.4 The mechanism of dye formation

Dye formation begins with the oxidation of a p-phenylenediamine developer molecule by the silver halide, with reduction of a silver ion; this is generally the slowest step in the development process, and is illustrated in figure 2.3. Here the product of the oxidation of the developer is the corresponding semiquinone.

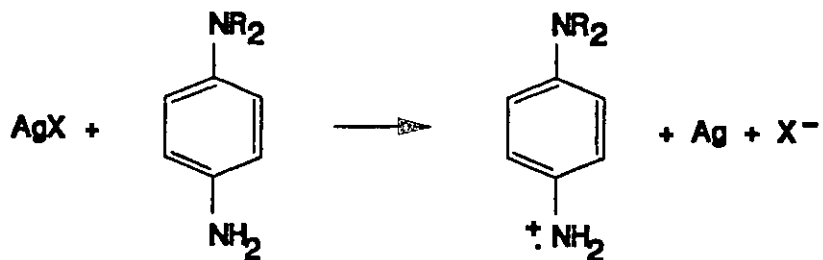


Figure 2.3: Oxidation of the p-phenylenediamine developer to the semiquinone
This semiquinone is stabilised by resonance

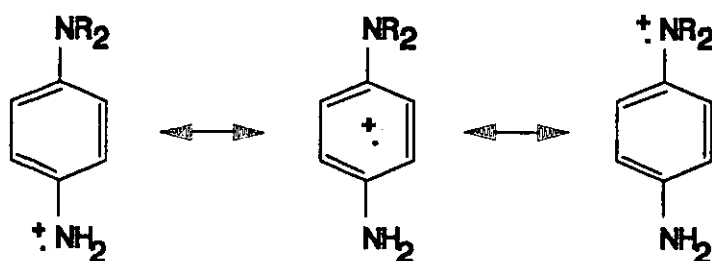


Figure 2.4: Resonance stabilisation of semiquinone cation

Formation of the semiquinone is followed by deprotonation, either involving reaction with further silver halide^[62] or by reaction of two semiquinones to give the quinonediimine cation (figure 2.5) and the p-phenylenediamine^[63]

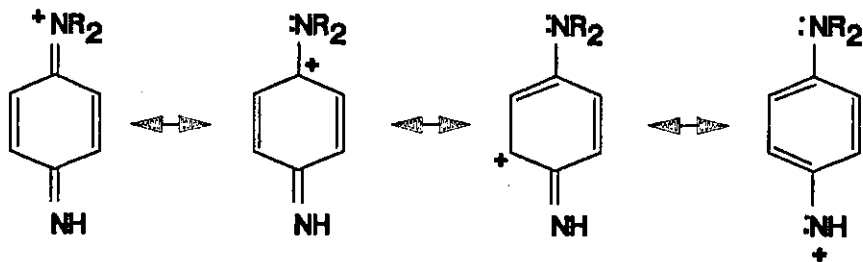


Figure 2.5: Quinonediimine cation structure

As indicated, the quinonediimine is also resonance stabilised. Following formation of the quinonediimine cation, the next stage in the development process involves reaction between the oxidised developing agent and the anion of the coupler to form a leuco dye. This is illustrated in figure 2.6.

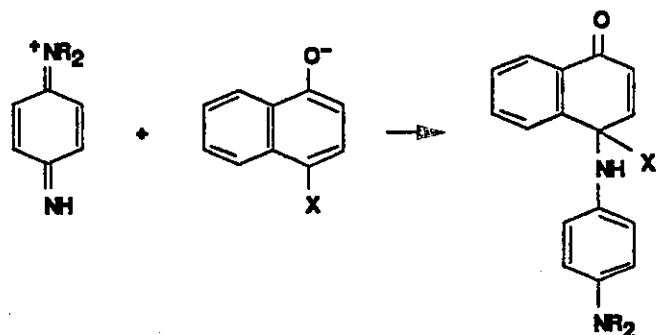


Figure 2.6: Coupling of quinonediimine cation with the coupler anion forming the leuco dye. Couplers are classified as being either 4- or 2-equivalent, depending upon whether or not oxidation of the leuco dye is necessary for the formation of the dye. The equivalency is defined as the number of moles of silver required for the formation of one mole of dye. Whether a coupler is 4- or 2-equivalent depends upon the nature of the groups which needs to be eliminated in the dye forming process. In figure 2.6, if the group X is simply H, then the dye formation involves the two-electron oxidation of the leuco dye and consequently the H-substituted coupler is 4-equivalent. If on the other hand the group X were Cl, dye formation would involve elimination of HCl and the Cl-substituted coupler would therefore be 2-equivalent.

Chapter 3

Experimental

3 Experimental

3.1 Ground state absorbance spectra

All ground state absorbance spectra were recorded using either a Pye-Unicam SP8-250 or a Phillips PU-8800 UV-Visible spectrophotometer. Emission spectra were recorded using either a Perkin-Elmer 3000 fluorescence spectrometer, or the home built fluorescence spectrometer in the laboratory of Dr L.F. Vieira-Ferreira at the Technical University of Lisbon in Portugal, full details of which have been published^[64]. The software controlling all of these instruments has been specially written for these applications jointly by myself and Mr. P.A. Leicester, formerly of Loughborough University chemistry department.

3.2 Nanosecond Laser Flash Photolysis

3.2.1 Data Collection

There are two nanosecond laser flash photolysis apparatus in use at Loughborough; one built around a Lumonics hyperYAG HY200 Q-switched Nd:YAG laser, and the other around a JK Lasers (now Lumonics) JK2000 Q-switched Nd:YAG laser, the latter having a two stage (oscillator/amplifier) dye laser associated with it. The wavelengths available from these lasers which are routinely used for photochemical investigations are the second, third and fourth harmonics of the Nd:YAG laser fundamental wavelength at 1064nm. These are located at 532nm, 354nm and 266nm, respectively. The excitation wavelengths used throughout have been 532nm and 354nm. The analysing source used on both systems is a 275W xenon arc lamp (Optical Radiation Corporation), with suitable filters interposed between it and the sample to cut off unwanted wavelengths. It is possible to provide an extra pulse of voltage to the arc lamp to increase its intensity by approximately a factor of 10 for a period of about 1 ms by the use of

an arc lamp pulsing unit (Applied Photophysics). The detection system comprises an f3.4 grating monochromator (Applied Photophysics Ltd) and an R928 side window photomultiplier tube (Hamamatsu). The accelerating voltage is applied to the photomultiplier using a 412B high voltage power supply (Fluke). The output voltage from the photomultiplier tube is directed to the input of one of two digitising devices; a 2432A digital oscilloscope (Tektronix) or a 7912d transient digitiser (Tektronix) with a 7A13 differential comparator plug-in (Tektronix). These devices have maximum single-shot digitisation speeds of 4ns and 5ns per point, respectively, with 8 bit vertical resolution and a programmable number of pre-trigger points. Both, however, are linear to 10 bit resolution, thus allowing greater than 8 bit resolution to be achieved by averaging. Both instruments are interfaced to 80286 based IBM compatible computers running MS-DOS version 3.3 operating systems via a general purpose interface bus (GPIB), which allows setting of the instrument parameters and the passing of digital data from the instrument direct to the computer for analysis. The GPIB interface card in the computer is a model PC2A (National Instruments), the driver software being provided by National Instruments and Tektronix. Shutters are placed between the arc lamp and the sample, and also between laser and sample, allowing irradiation of the sample by both, either or neither beams. Control of these shutters is achieved using the computer via a DT2808 digital/analogue analogue/digital (D/A A/D) card (Data Translation Ltd.). All of the software used to control the operation of and data acquisition from the flash photolysis system has been written in Loughborough by myself, Mr. P.A. Leicester and Dr. G.P. Kelly.

The operation of the flash photolysis system is as follows. A schematic of the apparatus is shown in figure 3.1. Overall control of the timing of the various events involved in the operation of the system is performed by a quartz oscillator and a series of analogue delay modules, designed and built in-house at Loughborough.

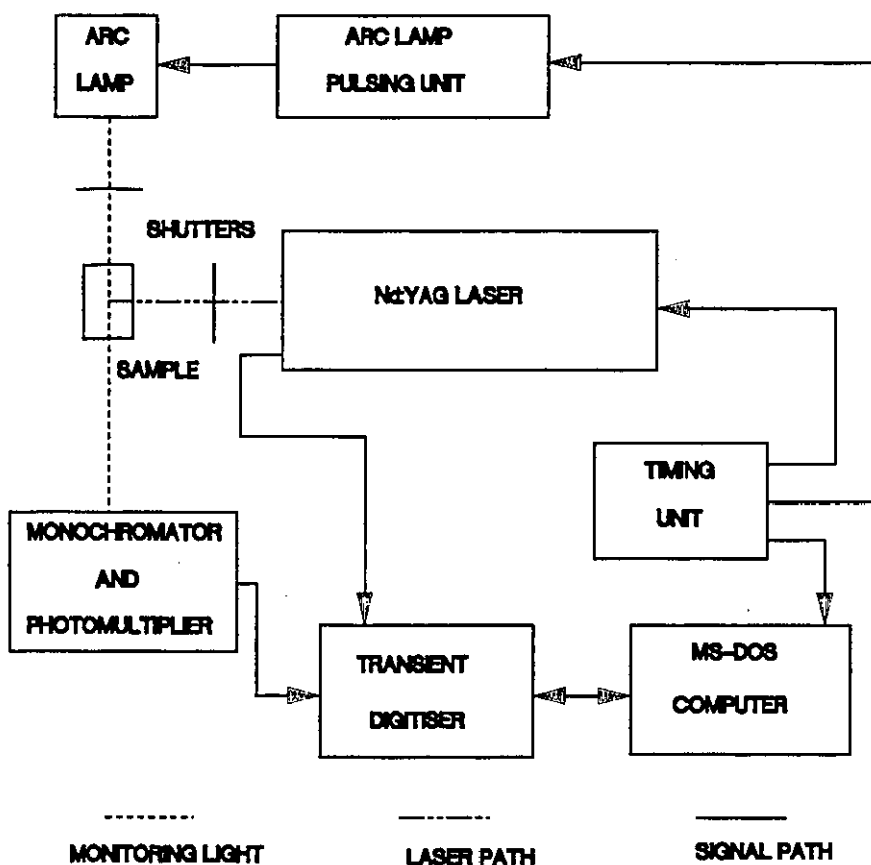


Figure 3.1: Schematic of nanosecond flash photolysis apparatus

The first action in the sequence is the triggering of the computer. On receiving a trigger, the computer instructs the digitiser via the GPIB interface to arm its timebase and to digitise a signal upon receipt of

the next trigger. The computer then waits for the digitiser to acknowledge that the digitising sequence has completed. The next action is the opening of the appropriate shutters. As mentioned above there are two shutters in the system, one between the arc lamp and the sample and one between the laser and sample. These allow the recording of topline (neither shutter open), baseline (arc lamp shutter only), transient (both shutters) and emission (laser shutter only open). The use of these various traces in the analysis of the data is described fully in section 3.2.2. If the arc lamp is to be pulsed to increase its intensity, the pulsing unit is the next device to be triggered. Following this, after sufficient time for the shutters to open and the arc lamp intensity to reach its plateau, the laser is triggered to fire. The firing of the laser triggers the digitiser in one of two ways. On the JK2000 system, a part of the laser beam is reflected off a glass plate into a fibre optic, from where it is incident upon a photodiode. In the HY200 system, leakage of 1064nm light from the end cavity mirror is incident upon a photodiode and provides the trigger. On receiving the trigger, the digitiser digitises the signal appearing at the input. When the digitising is complete, the data is transferred to the computer, displayed on the screen, and stored on disk as a random access file to make analysis more convenient. This is the completion of the collection cycle, and following storing of the data the computer waits for the next trigger from the timing unit.

3.2.2 Data Analysis

The four traces obtained from the flash photolysis apparatus, namely the baseline, topline, absorption and emission traces, are manipulated to obtain the required data as follows. An array corresponding to

corrected transmission change is generated by subtracting the emission trace from the transient absorption trace. It should be noted at this point that emission correction in this manner is only effective provided the emission trace stays on screen; if the emission is so strong as to go off screen or to overload the photomultiplier, then the corrected region where this occurred cannot be treated with any reliability. Next the range of the screen is calculated by subtracting the topline from the baseline; this ensures that the calculated transmission change is independent of the relative positions of baseline and topline. The change in transmission is then calculated as

$$\Delta T = 1 - \frac{\text{transmission}_c}{\text{baseline}_c} \quad (3.1)$$

where the subscripts *c* denote that baseline and transmission are corrected for topline and emission, respectively. The required analytical parameter in solution flash photolysis is the absorbance change, and this is calculated as

$$\Delta A = \log_{10} \left(\frac{1}{1 - \Delta T} \right) \quad (3.2)$$

using the Beer-Lambert law, since ΔT is always a number between 0 and 1.

3.2.3 Experimental Details

All experiments were carried out with solutions contained within 1cm x 1cm quartz cuvettes. Where solutions were degassed, this was performed using three freeze-pump-thaw cycles to a pressure of approximately 5×10^{-5} mbar on the vacuum apparatus at Loughborough. Excitation wavelengths used were 532nm and 354nm, with maximum pulse energies of 90mJ and 36mJ respectively. The laser light was defocussed onto the sample using

a -120mm focal length lens, giving maximum energy densities at the sample of 30mJ cm^{-2} and 12mJ cm^{-2} , respectively. Where a smaller energy density than this was required, the pulse energy was reduced by partial absorption in a solution of sodium nitrite in deionised water. All experiments were carried out at room temperature (18 to 23 °C).

3.3 Picosecond Laser Flash Photolysis

The picosecond laser system at the Rutherford-Appleton laboratory (RAL) consists of a frequency doubled mode-locked Nd:YAG laser, synchronous pumping a Rhodamine 6G dye laser. The pulses from this dye laser are amplified at 10Hz in a 3-stage Nd:YAG pumped dye amplifier to give pulse energies of approximately $500\mu\text{J}$.

3.3.1 Mode-Locked laser system

The mode-locked laser consists of formerly a Spectra-Physics series 3000 and latterly a Spectron Nd:YAG laser, acoustooptically mode-locked, the frequency doubled output of which is used to synchronously pump Rhodamine 6G in a Spectra-Physics model 375B dye laser. The minimum output pulse width from this laser system is typically about 4 picoseconds if satellite pulses are eliminated. In the synchronously pumped dye laser, however, the limiting factor on the width of the pulse available is not dispersion within the dye laser cavity, but the pulse width of the pump laser. To overcome this limitation on the pulse width available, the present solution is to employ a saturable absorber in the gain jet, which shortens the dye pulse by effectively truncating the edges of the pulse. Saturable absorbers, therefore, are wavelength dependent since they act by absorbing part of the dye pulse; this causes some inconvenience in their use since each has only a small operating wavelength range, much smaller than that of the gain dye, and hence

changing wavelength and keeping a short pulse also means changing saturable absorber. Also, adding saturable absorber to the gain jet can significantly reduce the power output from the laser, and there is therefore a trade-off between pulse length and gain in the synchronously pumped laser. This may be carried through the amplification system and may result in a drop in amplified output, although the dye laser and amplifier are usually operated such that gain in the amplifier is saturated. A proposed development of the picosecond laser system to overcome this problem is to shorten the pumping Nd:YAG laser pulse using grating compression, this shorter pumping pulse negating the need for a saturable absorber. Grating compression is achieved by first passing the beam through a short fibre optic, which broadens the bandwidth of the pulse by the process of self phase modulation^{[65][66]} where an intense optical pulse sees an intensity dependent refractive index as it travels through a medium. This intensity dependence modulates the phase of the pulse as the intensity rises and falls, so altering the frequency distribution. Redder components arise from the rising edge of the pulse, while bluer arise from the trailing edge. The process of group velocity dispersion "chirps" the pulse, that is separates out the frequency components in time and consequently in space. A pair of gratings is then used to compress the pulse in space and consequently in time, the result being a pulse shorter than before the compression but with a larger bandwidth, there being a trade-off here between bandwidth and pulsewidth for transform-limited pulses (section 3.3.3). This technique does result in some reduction in power available from the pumping

laser in the compressor, but has the advantage that a short pulse can be maintained over the tuning range of the dye laser.

3.3.2 Pulse Amplification

Typical powers obtainable from the synchronously pumped dye laser are of the order of 50mW, corresponding to a pulse energy of the order of 1nJ. These low energy pulses are amplified in a three-stage dye amplifier pumped at 10Hz by a Quanta-Ray DCR-3 injection seeded Nd:YAG laser; injection seeding increases the stability of the laser output pulse by causing operation in a single axial mode. The timing of the firing of the DCR-3 relative to the mode-locker pulse train is variable, so that this can be made coincident with the arrival of a pulse from the dye laser, which can then stimulate emission from the dye cells at the point of maximum population inversion. This gives a gain of approximately 5×10^5 resulting in pulse energies of 300-500 μ J. A schematic diagram of the laser system is given in figure 3.2.

3.3.3 Characterisation of picosecond pulses

The diagnostic available at RAL for the characterisation of picosecond pulses is located only on the output from the synchronously pumped dye laser, and consists of a second harmonic generation autocorrelator. The basis of autocorrelation measurements is in the use of non-linear optical phenomena which produce a signal (or enhance a signal) only when two pulses are present in the non-linear medium at the same time. In the second harmonic generation autocorrelation technique, a non-linear crystal is used to convert part of the laser pulse to its second harmonic, the intensity of which as a function of delay between two identical pulses overlapping in space in the crystal being the measured parameter. It is possible to suppress the

second harmonic generated by a single pulse and to directly measure the signal due to the addition of two photons, one from each pulse.

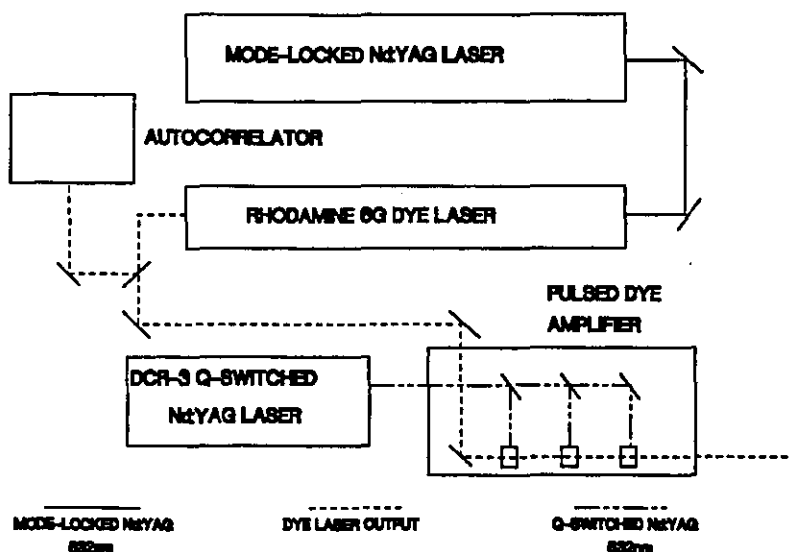


Figure 3.2: Schematic of Rutherford-Appleton Laboratory picosecond laser system

One way to achieve this is to polarise the two beams orthogonally, and to orient the crystal for type II frequency doubling, where for mixing to occur the two waves must travel as the ordinary and extraordinary waves in the crystal^[67].

The application of the above technique to mode-locked lasers yields information about the average behaviour of the laser, rather than giving shot to shot diagnostics, and this should be borne in mind when interpreting autocorrelation data. The display of the oscilloscope monitoring the detected second harmonic resulting from the mixing of the two pulses is the convolution of the two pulse shapes, and obtaining the actual pulse duration from such a convolution depends upon knowing accurately certain properties of the pulse.

This is since the second order autocorrelation function is intrinsically symmetrical and cannot be used to obtain the pulse shape unless it is known, by other means, also to be symmetrical. If the pulse is transform limited (that is, the time-bandwidth product for the pulse shape is fulfilled, and the pulse is smooth) then the full-width-half-maximum (FWHM) of the pulse itself is related by a simple numerical factor to the FWHM of the second harmonic autocorrelation. Such relations for typical pulse shapes are shown in table 3.1^[68]. In situations where the pulse is far from transform limited, the presence of a coherence spike on the trace clearly indicates this; However, for pulses only a little broader than the transform limit a smooth trace may still be obtained and great care must be exercised in interpretation.

Pulse shape	$\Delta\tau / \Delta t$
Square	1
Gaussian	1.414
Lorentzian	1.55

Table 3.1 : Relationships between FWHM of autocorrelation functions and FWHM of actual pulse shapes

While these techniques for characterising very short pulses are applicable to the output of, say, a synchronously pumped dye laser, they are clearly inappropriate for measuring essentially single shot pulse widths from the pulsed dye amplifier, which operates at the much slower repetition rate of 10Hz. Here, the only reliable way of measuring pulse widths is by using standard samples in a pump-probe experiment for which the rise of the observed signal is known to be prompt, so that the measured rise time is in fact simply a convolution of pump and probe pulses. Here again, as

in the case of autocorrelation functions described above, certain assumptions about pulse shapes must be made in order for pump and probe pulse widths to be obtained from such experiments. Suitable dyes for this purpose have been found to be the saturable absorber 3,3'-dimethyloxatricarbocyanine iodide (MeDOTC)^[69], and the mode-locking dye 2-(p-dimethylaminostyryl)-benzothiazolyethyl iodide (DASBTI)^[69], which have been used for pulse characterisation with excitation at 600nm and 300nm respectively, in each case a prompt bleach of ground state absorbance being monitored in the 600nm to 650nm wavelength region.

3.3.4 Generation of probe wavelengths

There are two techniques which have been used for generating probe wavelengths shifted from the laser fundamental frequency; one of these has been stimulated Raman emission from a range of solvents. A list of typical solvents used along with their wavenumber shifts are given in table 3.2. A second method employed to generate probe wavelengths has been white light continuum generation^[70] by self phase modulation (section 3.3.1) achieved by focussing the laser fundamental wavelength into a water/D₂O mixture. It should be noted that the direct photoionisation of water via a two photon process is not possible under the conditions which prevail here, since the ionisation threshold of water is 6.5 eV^[71] and hence pulses shorter than 380nm are required for the two-photon process. During the course of the picosecond flash photolysis experiments conducted during this work, the shortest wavelengths used from which to produce continuum were 585nm.

Solvent	Frequency Shift /cm ⁻¹
Carbon Tetrachloride	460
Chloroform	667
Cumene	990
Furan	1180
Bromocyclohexane	1438
Isoprene	1792
1-Hexyne	2116
Acetonitrile	2250
Methanol	2831
Ethanol	2921

Table 3.2: Wavenumber shifts from a range of solvents

Each of these techniques has advantages and disadvantages; Raman generation can give narrow wavelength distributions but is limited in the main to Stokes shifts from the laser wavelength, while continuum generation gives access to wavelengths shorter than the fundamental.

3.3.5 Coherent Coupling Artefact

Pump-probe experiments performed using identical pulses (i.e. derived from the same laser source) may be subject to non-linear interactions between pump and probe pulses which generate additional features in the observed signals at delays close to zero, an effect observed by several authors^{[72][73][74]}. However, the reported coherent coupling has been between pulses of the same frequency, while we have observed^[75] a coupling artefact for pump and probe pulses of differing fundamental frequencies, the probe being generated by continuum in water/D₂O. One rationale which can be put forward to explain this observation is that of a noise burst in the dye laser producing, on occasions, a sufficient increase in bandwidth of the laser for pump

and probe pulses to overlap in frequency. The fact that the coherence peak is present for only a very short time suggests that both pulses have an appreciable bandwidth^[76]. A second possibility is the generation of a weak continuum in the sample which effectively broadens the bandwidth of the pumping pulse, although the power density at the sample is estimated as being only 10^8 W cm^{-2} , which is considerably less than has been routinely used to generate continuum although that is not to say that it is necessarily below the continuum generation threshold. The coherence artefact occurs by diffraction of the pump pulse off a population grating produced by interference of pump and probe beams resulting in spatial modulation of the pump intensity^[77]. If the excitation process produces a decrease in absorption in the sample at the wavelength of interest, the scattered signal travels in precisely the same direction as the probe beam. If, however, the excitation produces an increase in absorption, the grating is produced out of phase with the interference pattern and the result is a further decrease in probe intensity. In general, the coherence spike will have the same sign as the observed signal^[20]. Obviously, for coupling of this nature to occur, coherence must be carried through the continuum generation to the continuum pulse, a not unlikely situation given the processes responsible for continuum production (section 3.3.4).

3.3.6 Pump-Probe laser flash photolysis

Pump-probe laser flash photolysis^[78] in the picosecond time domain involves excitation (pumping) of the sample at one wavelength and analysing for changes in transmission (probing) using either the same wavelength^[79], or a different wavelength derived either from a different laser source or by frequency

shifting techniques as described in section 3.3.4^{[10][11]}. Time resolution is achieved by varying the time delay between the arrival of pump and probe pulses at the sample, thus allowing probing of events occurring picoseconds to nanoseconds after the pumping pulse.

3.3.7 Experimental Layout

The experimental pump-probe system is illustrated in figure 3.3. The major components worthy of further comment are:

(a) Continuum cell

The continuum cell and associated optics are used to generate probe wavelengths away from the laser fundamental by the processes described in section 3.3.4. The continuum or Raman produced in the cell is re-collimated by the second lens, and then may be passed through a pin-hole to effect spatial filtering and produce a beam approaching diffraction-limited (effectively the pulse is convoluted with the shape of the pin-hole, and this "cleans up" the energy profile across the beam). Experiments have demonstrated that under most circumstances this pin-hole can be dispensed with without degrading the quality of the collected data, since the spatial filtering, provided the collimation is good, is effected by the pin-hole adjacent to the sample chamber.

(b) Variable slide delay and corner cube

A corner cube mounted on a worm-gear driven platform is used to vary the time delay between pump and probe pulses. The platform is driven by a stepping motor which is computer controlled via an RS232 interface. A corner cube (or retroreflector) is used in this instance in preference to a mirror, since provided the incoming beam is parallel to the axis of the slide, the reflected beam will also be parallel.

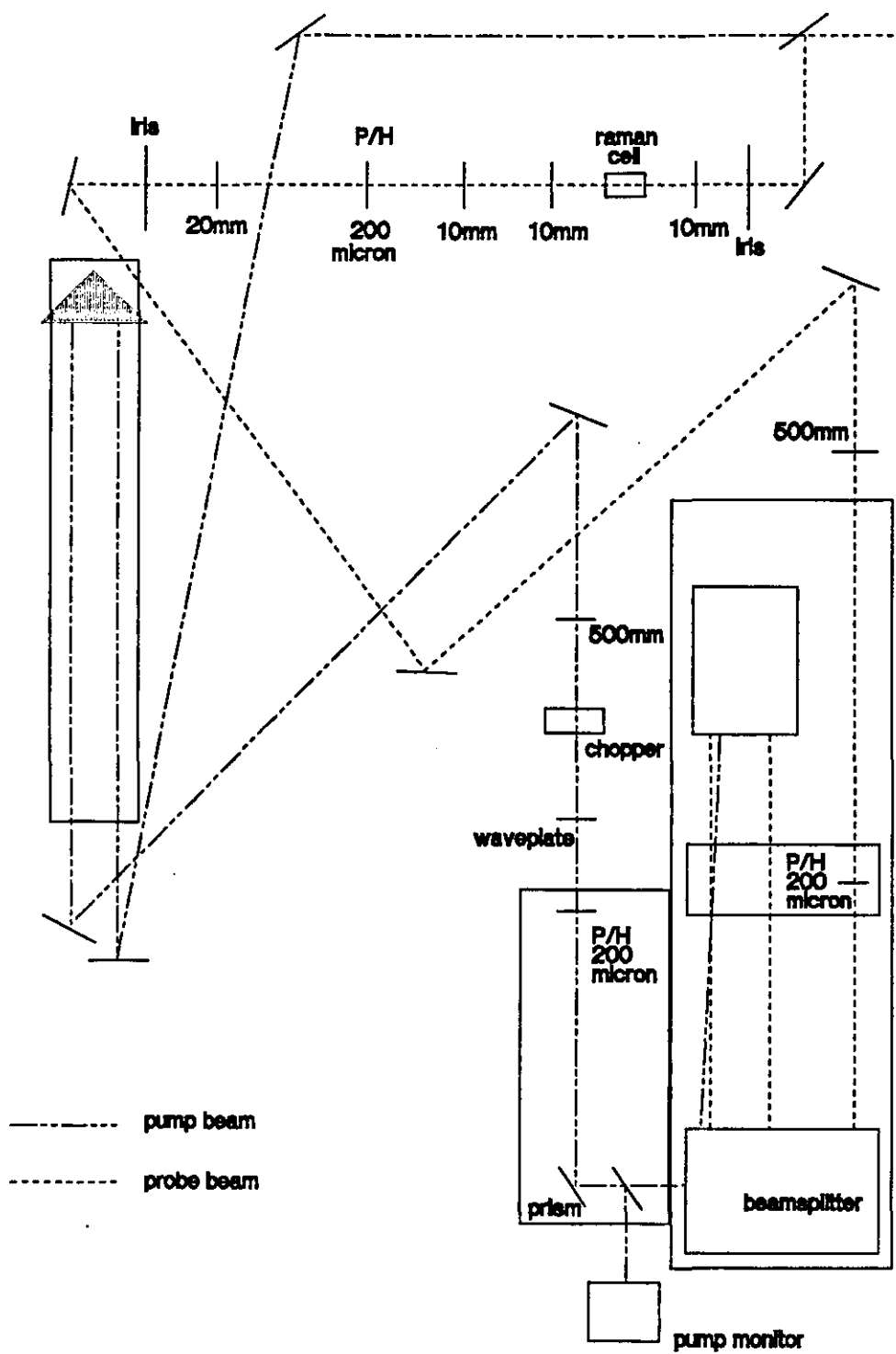


Figure 3.3: Picosecond pump-probe laser photolysis optical arrangement

This alleviates problems which may arise through slight deviations of the mount as it travels along the slide, since the path of the beam after the corner cube will remain constant.

(c) Fresnel rhomb and Glan-Thompson polariser

The purpose of the combination of the Fresnel rhomb and the polariser is to enable the relative polarisations of the pump and probe beams to be accurately set. On emerging from the corner cube, the pump beam is elliptically polarised, and the Glan-Thompson polariser is used to plane polarise the light by allowing through only those components aligned with a particular axis. The rhomb then acts as a half-wave retarder, thus allowing the plane of the polarised light to be rotated to the desired angle.

(d) Frequency programmable chopper

A frequency programmable chopper is placed in the pump beam path to chop out every other pump shot; this is achieved by operating the chopper at 35Hz, this 35Hz signal being derived from the same oscillator providing the 10Hz signal triggering the DCR-3 laser pumping the dye amplifier. This interleaving of pump on and pump off shots allows accurate assessment of the pump induced changes.

(e) Beamsplitter

A schematic of the beamsplitter assembly is shown in figure 3.4. The design is such as to attempt to limit random differences between the sample and reference probe beams, since each undergoes two transmissions and two reflections through the cube beamsplitters and prisms before passing through two Glan-Thompson polarisers. The polarisers allow adjustment of the relative intensities of sample and reference beams to facilitate balancing of the difference detector, since the probe beam is plane

polarised on entering the beamsplitter assembly by a third polariser; adjustment is by rotating the polariser on the reference beam since the polarisation of this beam is not critical in the context of the experiment. Two 50cm focal length lenses are located at the exit of the beamsplitter, and focus the probe beam into the sample; this means that the beams are diverging as they approach the detectors, placing a limitation on how far from the samples the detectors can be located. It may be desirable, certainly in circumstances where there is considerable emission from the sample around the analysing wavelength, to place the detectors as far from the samples as possible.

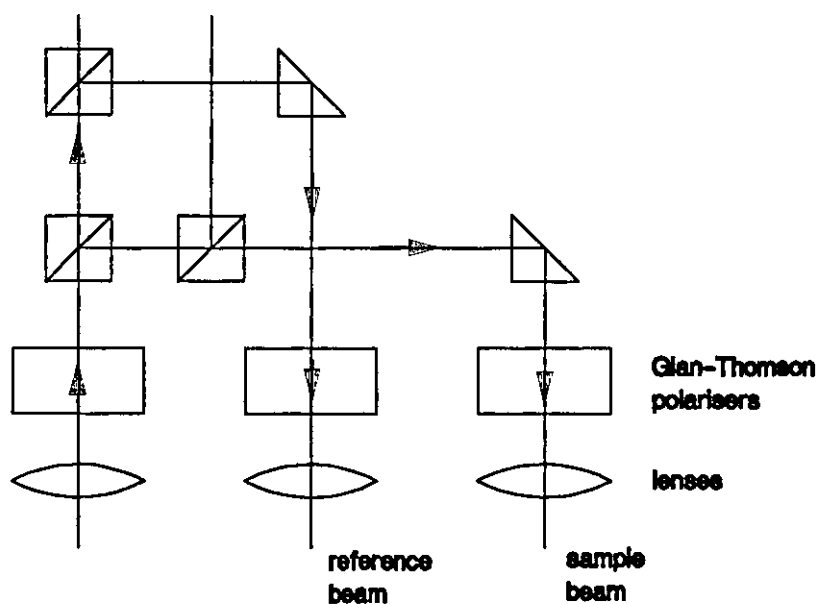


Figure 3.4: Schematic of beamsplitter assembly

3.3.8 Data collection

The detectors used to monitor the pump and probe signals are based on the design of Pollard and Zenith^[82], utilising 1 x 1 cm UV sensitive PIN diodes

from Hamamatsu (S1723-05). The pump signal detector is a single diode and amplifier circuit, an integrating sphere being placed in front of the diode to ensure even illumination of the surface. The probe detector consists of two diodes connected across a differential amplifier circuit, the output from this amplifier being the difference between the two diode outputs, a separate amplification stage providing a signal proportional to the sum of the signals from the two diodes to allow normalisation to probe intensity. The output from each diode is maintained below 250mV by the use of neutral density filters to preserve linearity.

The signals from each diode/amplifier combination are fed into SR250 gated integrators (Stanford Research Ltd), which integrate the signals in a gate typically 300ns wide, the gate width and position being optimised to give the best signal linearity and lowest noise. The integrated signal is output as an analogue voltage between 0 and 10V, this use of analogue amplifiers up to this stage negating the errors which would be introduced by digitising a very small signal. The integrated output is then fed to an SR245 analogue to digital/ digital to analogue (A/D D/A) converter and computer interface, and the data fed to a microcomputer via a GPIB (General Purpose Interface Bus) interface. A schematic diagram of the electronic interconnections in the picosecond data acquisition system is shown in figure 3.5. All data acquisition and subsequent processing is controlled by the microcomputer using software written in-house at Loughborough University jointly by myself, Mr P.A. Leicester and Dr. G.P. Kelly.

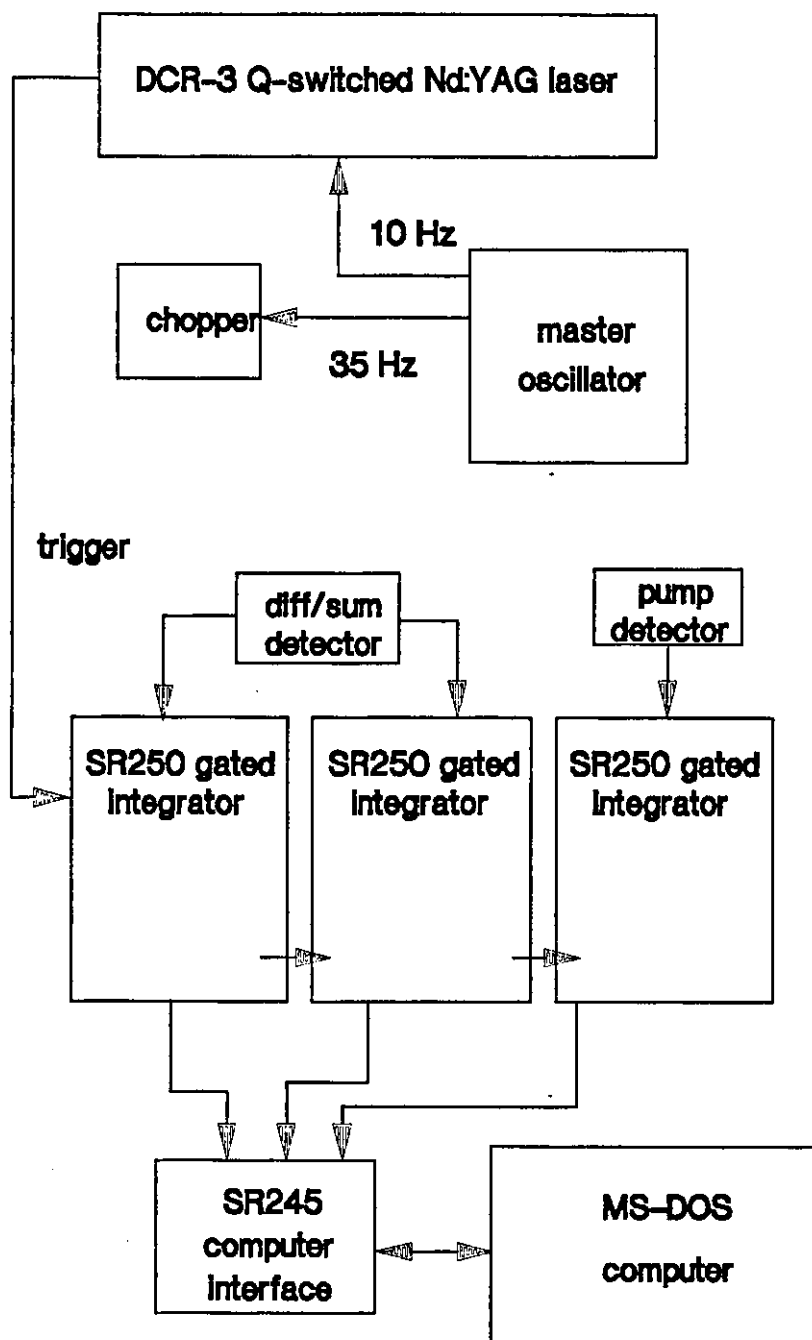


Figure 3.5: Electronic control diagram relating to the picosecond pump-probe apparatus

3.3.9 Data Processing

The analytical parameter required from these experiments is the change in transmission induced by the pumping pulse at a particular time after its arrival. The normalised probe intensity change induced by the pumping pulse at a time delay t after arrival of the pump pulse of energy P is

$$\left[\frac{\Delta I(P)}{I} \right]_{t,u} = \frac{\bar{D}_{on} - \bar{D}_{off}}{\bar{N} - \bar{N}_{baseline}} \quad (3.3)$$

where D and N are proportional to the sum and difference signals, respectively, \bar{D}_{on} is the mean difference signal with the pump on, \bar{D}_{off} is the mean difference signal with no pump (background signal), $\bar{N}_{baseline}$ is the mean sum signal in the absence of incident probe and the subscript u indicates that the value of $\Delta I(P)/I$ is uncorrected and at this stage only proportional to percentage transmission change. No correction for emission is necessary with the samples investigated here since the emission quantum yield at ambient temperatures is too low for this system to be detected. The value of $\Delta I(P)/I$ is then normalised to pump intensity using

$$\left[\frac{\Delta I}{I} \right]_{t,u} = \frac{\left[\frac{\Delta I(P)}{I} \right]_{t,u} \bar{P}_{series}}{\bar{P} - \bar{P}_{baseline}} \quad (3.4)$$

where \bar{P}_{series} is the mean pump intensity for the whole kinetic run. This value of $\Delta I/I$ thus obtained is then corrected to actual percentage transmission change by multiplication by a factor f , obtained from a measurement of the difference signal obtained when an 8% reflecting glass slide is placed in the sample beam. The factor f is then calculated as

$$f = \frac{0.08(\bar{N} - \bar{N}_{baseline})}{(\bar{D}_{in} - \bar{D}_{out})} \quad (3.5)$$

where \bar{D}_{in} and \bar{D}_{out} relate to the difference signal with the glass slide in and out of the beam, respectively. The analytical parameter most useful in the interpretation of such data, that is the absorbance change, is calculated from

$$\Delta A = -\log_{10} \left(1 - \left(\left(\frac{\Delta I}{I} \right)_t, f \right) \right) \quad (3.6)$$

3.3.10 Experimental Details

All experiments were carried out with solutions contained within 1cm x 1cm quartz cuvettes. All solutions were air equilibrated. The excitation wavelength used throughout this work was 585nm, and pulse energies at the sample ranged from 3 μ J to 12 μ J per pulse. All results presented were recorded using "magic angle" relative polarisations between pumping and probing beams unless otherwise stated (chapter 5). Neutral density filters were placed in the pumping beam to reduce its intensity when determining the dependence of signal size on pump energy. All experiments were carried out at room temperature (17 to 21 °C).

3.4 Singlet Oxygen Luminescence detection

The singlet oxygen luminescence detector, used to detect the phosphorescence at 1270nm resulting from radiative relaxation of the $^1\Delta_g$ state of molecular oxygen (chapter 7), is based on that previously described in the literature^{[83][84]}. It consists of reverse biased germanium photodiode (Judson J16-8SP-1205M) coupled to 55dB gain pre-amplifier (Judson PA100). A silicon filter (CVI laser corporation 31023-83602101-0TT, anti-reflection coated with PP-1012SI) is placed in front of the photodiode in order to filter out wavelengths below

1100nm. Samples are placed in a quartz cuvette and excited with 308nm pulses from a nitrogen laser, the pulse energy being less than 2 millijoules in all cases. The diode and filter are placed close to a face of the sample cell so as to detect emission perpendicular to the exciting pulse. The signal from the detector is digitised and fed to a computer for analysis.

3.5 Photographically formed coatings

3.5.1 Introduction

Much of the work concerning the fading of photographic product dyes has been conducted using specially formulated photographically formed coatings containing only one product dye, either yellow, magenta or cyan, in one layer rather than the usual multilayer product (section 2.1). These particular samples are then subjected to steady state irradiation by a high intensity source of known spectral profile, so that the rate of absorption of photons can be accurately calculated, and from the rate of loss of dye density with time a quantum yield of dye fade can be calculated in the coating.

3.5.2 Coating making methodology

The manufacture of the coating consists of mixing a dispersion, consisting of coupler, gelatin, and surfactant, with a silver halide emulsion, the whole then being coated on either photographic paper base, or on a transparent acetate base (Note here that the terms "dispersion" and "emulsion" are used as they are in the photographic industry, and in chemical terms a "dispersion" may more properly be referred to as an oil-in-water emulsion, and an emulsion as a dispersion of silver halide crystals). The base is "subbed" on one (or, in the case of the transparent base, sometimes two) sides with a thin layer of gelatin. This layer of

gelatin is bound to the base and causes the coating to adhere to the base; without this subbing the coating would peel off the base when it dried.

Dispersion Formulation

The dispersion is formulated in two parts; one part containing the coupler and coupler solvent, and the other containing the gelatin, surfactant etc. These two are then mixed together and homogenised to form the dispersion. The compositions of the two parts are as follows.

Part 1 Composition:

Coupler	44 wt %
Di-n-butylphthalate	44 wt %
2(2-butoxyethoxy)ethyl acetate	7 wt %
Dioctylhydroquinone	5 wt %

Here, the coupler is one part of the final product dye, formed by reaction with the developer in the development process (chapter 3). Here, the coupler solvent is di-n-butylphthalate, although this solvent is not used in the commercial product material. The dioctylhydroquinone is added to act as a scavenger for unreacted developer in the processing stage.

Part 2 Composition:

Gelatin (Rouselott 31745)	8.7 wt %
Diphenylnaphthosulphonic acid	9.6 wt %
Sodium Propionate	.8 wt %
Propionic acid	1.2 wt %
Water	79.7 wt %

Here, the gelatin is the matrix in which the droplets of coupler solvent containing the coupler and the other components are contained; the droplets are stabilised in the matrix by a surfactant, in this instance diphenylnaphthosulphonic acid.

3.5.3 Dispersion Manufacture

The gelatin, sodium propionate, propionic acid and water are mixed together and allowed to stand for two hours in order to allow the gelatin to absorb water and swell. Once swelled, the mixture is heated at 60°C in a water bath to melt the gelatin. The part 1 mixtures are pre-heated in a water bath to 60°C, then transferred to a hotplate at 170°C and heated until the whole mixture has melted. Surfactant is added to the part 2 mixtures and the whole stirred to allow re-equilibration at 60°C. Each part 1 mixture is then made up to 500g with part 2 mixture, and the whole homogenised at 20000 rpm for five minutes.

3.5.4 Coating manufacture

Having made the dispersions, it is then necessary to calculate the amount of dispersion relative to emulsion which is necessary to achieve the required dye density in the final exposed coating. This will depend in part on whether or not the coupler is a two-equivalent or a four-equivalent coupler, since a four-equivalent requires four moles of silver per mole of dye formed, while a two-equivalent requires only two (section 2.4). This done, the required dispersion and emulsion compositions are taken to the coating tracks, where they are coated onto the base of choice using a coating block of the design of Kobayashi, Morita and Uchida^[85].

3.5.5 Exposing and Developing

The coating produced by the method described above is cut into small (15cm x 3cm) strips, and these are exposed individually. The visible light source used to expose the light sensitive coatings is filtered through a Wratten 2B filter and a granularity wedge (a variable neutral density filter, the optical density of which

varies in steps across it), which gives a range of dye optical densities across the strip. The exposed strips are then developed using the C-41 process^[86].

3.5.6 Fading experiments

The exposed coatings containing the dye at a range of concentrations in terms of moles per square metre are then subjected to a high intensity source of visible light to cause photochemical degradation at a measurable rate. The source used was the high intensity daylight (HID) source at Kodak Ltd.'s research laboratories in Harrow, Middlesex. The spectral irradiance profile of this source is reproduced in figure 3.6. The dye laydown in moles per square metre before irradiation was determined using high performance liquid chromatography (HPLC), and the laydown after irradiation determined spectrophotometrically using the optical density prior to fade to determine a molar decadic absorption coefficient for the coating in question (chapter 7).

3.6 Manufacture of hand coatings

The hand coatings are designed to mimic as far as possible the photographically formed coatings, but are made with pre-formed dyes and consequently dyes that cannot be formed using the photographic process can be investigated in the product environment. The formulation of the hand coatings is as follows for a dye with a molecular weight of about 1000 g mol^{-1} and a molar absorption coefficient of $10^4 \text{ dm}^3 \text{ mol}^{-1} \text{ cm}^{-1}$, with which parameters an absorbance of approximately 1.5 is obtained at the dye λ_{max} with a dry coating thickness of about 10 micrometres.

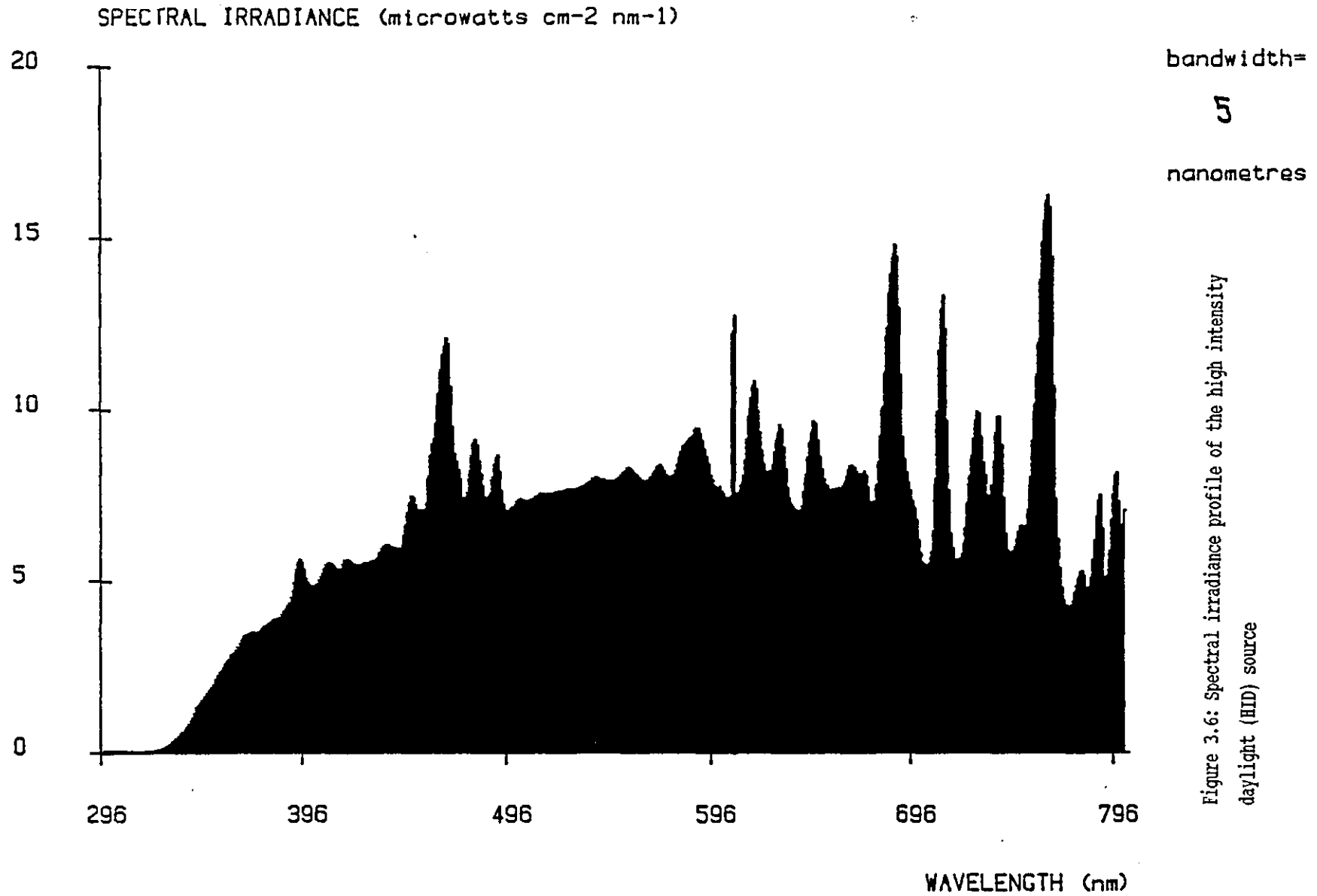


Figure 3.6: Spectral irradiance profile of the high intensity daylight (HID) source

2.5g of a 50% gelatin / 50% water solid is added to 22.5g of a 1.388g dm^{-3} solution of sodium dodecyl sulphate, and the whole heated to dissolve the gelatin. To 20g of the resulting solution is added a solution of 35mg of dye and 105mg of di-n-butylphthalate in 2cm^3 of ethyl acetate, and the whole homogenised using a soniprobe for 5 minutes. The resulting mixture is then spread onto an acetate base "subbed" with gelatin, and dried flat. The mixture is spread at an appropriate thickness given that shrinking of the gelatin causes the dry coating to have a thickness about a tenth that of the wet coating.

3.7 Materials

All solvents were spectrophotometric grade (Aldrich) except methanol, which was HPLC grade (Aldrich) and di-n-butylphthalate which was gold label (Aldrich). Benzophenone was 99+ % gold label (Aldrich). 2'-acetonaphthone was reagent grade (Aldrich) recrystallised three times from ethanol. All dyes were supplied by Kodak Ltd, Harrow, Middlesex, and were used as supplied. The structures of the dyes corresponding to the designations used in the text are shown in figures 3.7 and 3.8.

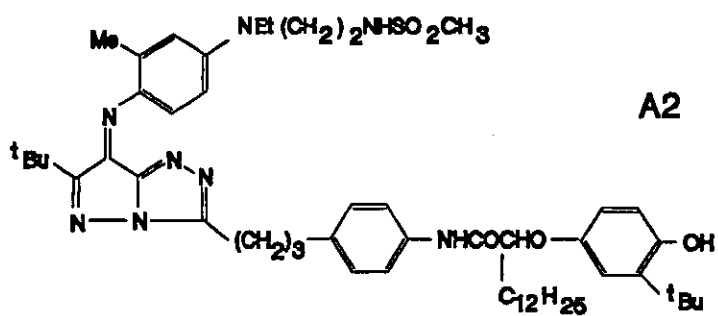
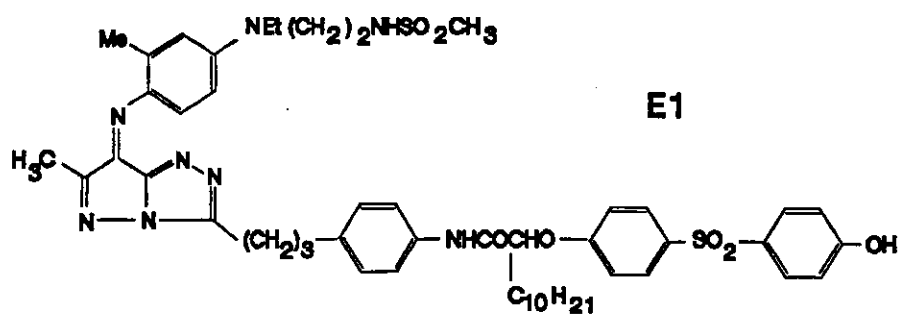
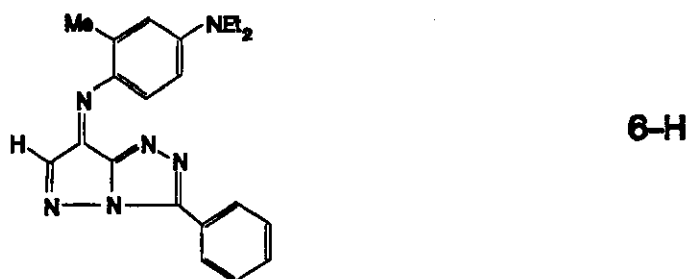
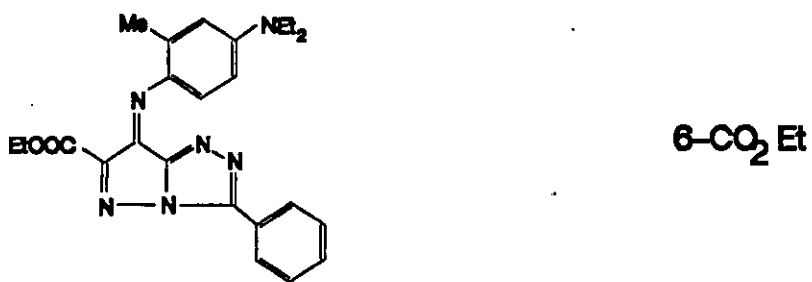


Figure 3.7: azomethine dye structures

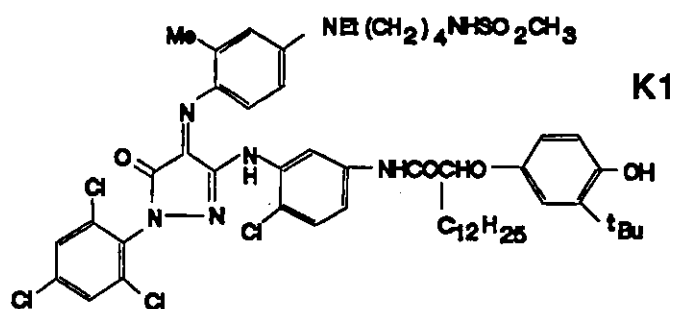
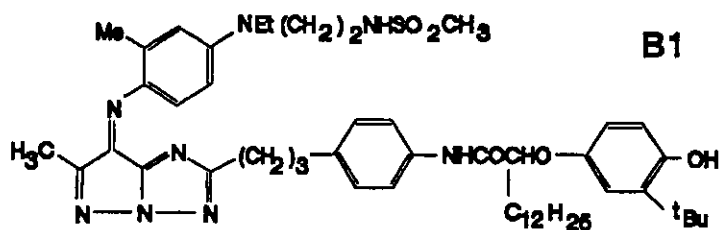
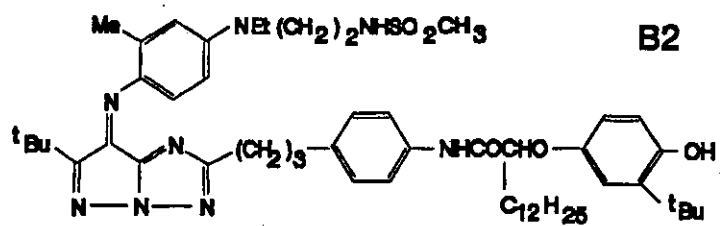


Figure 3.8: azomethine dye structures

Chapter 4

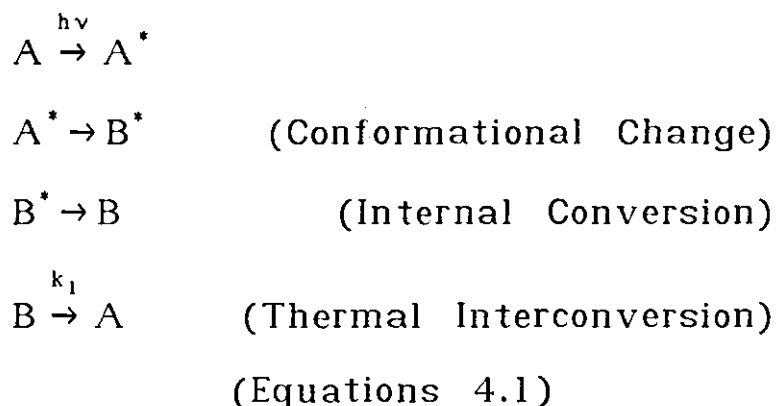
Fitting of Experimental Data

4 Fitting of Experimental Data

4.1 Introduction

A major part of the interpretation of data obtained from flash kinetic experiments, both absorption and emission studies, revolves around the fitting of appropriate kinetic models to the experimental data. Here there are two major problems to be solved; firstly, it is necessary to select a kinetic model which may reasonably be used to interpret the data set, and secondly a method of fitting the model to the data must be found.

The first of these problems may be solved very easily for certain simple systems, for example the unimolecular relaxation of an isomeric form of a dye back to the stable ground state conformation. This reaction may be described by the scheme detailed in equations 4.1.



The assumptions made here are that all of the processes except the relaxation of state B back to state A along the ground state potential surface are very fast, and that the timescale upon which this relaxation occurs is long relative to the length of the pulse which perturbed the system. In this instance, both the exciting pulse and the excited state interconversion process can be ignored and the data may be fitted using a simple single exponential decaying function;

$$B_t = B_0 e^{-k_1 t} \quad (4.2)$$

where B_t and B_0 are the concentrations of species B, produced by the excitation pulse, at times $t=t$ and $t=0$ (immediately following flash excitation), respectively, and k_1 is the first order rate constant. The second problem, that of fitting the model to the data, may also be solved very simply in this instance since it is possible to linearise a single exponential function simply by taking natural logarithms; this yields an equation of the form

$$\ln B_t = \ln B_0 - k_1 t \quad (4.3)$$

hence a plot of $\ln B$ against t will yield a straight line of slope $-k_1$ and intercept $\ln B_0$, thus giving the two parameters which we require, namely the instantaneous population produced by the exciting pulse and the rate at which this population relaxes back to equilibrium. The slope and intercept of such a plot can be determined analytically by the use of a linear least squares optimisation procedure^[87]. This approach is not, however, the best to take to a problem of this kind, since taking logarithms decreases the signal to noise ratio of the linearised data set relative to the raw data, an effect very pronounced at small signal intensities; hence there is often a large uncertainty in the parameters obtained via this method. A better method therefore of fitting non-linear kinetic models to experimental data is to use a non-linear fitting routine, to fit the function itself rather than a linearised form. There are of course only a limited number of situations where the option of a linear least squares optimisation procedure exists, such as for simple first or second order kinetics, and most more complex models are not amenable to linearisation and thus non-linear routines are essential. Such methods are necessarily iterative, taking an initial guess to the parameters in the model and successively improving

on these estimates with successive iterations; the two non-linear fitting methods employed for the data presented here, namely the modified sequential simplex routine^{[88][89][90]} and the use of a Taylor series expansion to approximate the equations, are described in detail in sections 4.2 and 4.3. Each approach has its merits, and it is necessary to select the most appropriate method for the problem in hand. The use of a Taylor series expansion to linearise the equation and the subsequent solving of the n linear equations corresponding to the n parameters being fitted is a very fast procedure which usually converges (reaches a stable solution where further iteration does not improve the quality of the result to within a pre-determined level of tolerance) within ten iterations for most models (for a discussion of convergence criteria, see section 4.4). However, it is clear from section 4.3 that to use such a procedure requires solution of the differential equations describing the system and the derivation of the partial differential equations with respect to each variable parameter within the model. If an analytical solution to the differential equations cannot be obtained, as is the case here with the kinetic scheme used to model the picosecond transient absorption data due to the presence of the gaussian pulse function, or as can arise for certain radical combination or triplet-triplet heteroannihilation reactions, then not only the function itself but also the partial differentials must be approximated numerically. The modified sequential simplex approach, however, although like all so-called "hill-climbing" techniques being somewhat slow, taking generally more iterations to converge than the Taylor series method, requires only the solution to the differential equations and not the partial differential equations; this means that for equations having no analytical solution we require only one approximation,

that to the solution itself. The simplex approach also has the advantage of being much more robust than the Taylor series, being able to converge to a solution even when the initial guesses to the parameters are not good. Hence latterly for fitting of kinetic models having analytical solutions we have adopted the Taylor series approximation method, while for other situations the sequential simplex is the method of choice. Fitting of models to the data obtained from nanosecond flash photolysis presented in chapter 5, although such models have analytical solutions, was however for the most part achieved using the sequential simplex method. The software for performing the sequential simplex method of fitting models to experimental data was written in Loughborough by myself; that for fitting using an analytical solution based around a Taylor series expansion was written in Loughborough by Dr. I.V. Khemilinski.

4.2 Modified sequential simplex approach^[91]

The simplex fitting method involves an empirical search through the parameter space, all parameters being varied simultaneously. A simplex is a geometrical figure. If the model being fitted has n parameters, the simplex will have $n+1$ vertices and the parameter space through which the search proceeds is n dimensional. To perform fitting using the simplex approach, it is necessary to begin with a reasonable set of initial approximations to the parameters, P_i . The model is evaluated using these parameters and compared with the data we are trying to fit the model to by using an appropriate mathematical test, for example χ^2 (section 4.4). This value of χ^2 then corresponds to this particular combination of parameters and hence to one vertex of the simplex. It is then necessary to calculate further guesses to the parameters to make up the other n vertices of the simplex, and to calculate

a χ^2 value for each one. This is done by multiplying each parameter in turn by 1.1, i.e. designating each point on the simplex by V_i

$$V_2 = f(1.1P_1, P_2, \dots, P_{n+1})$$

$$V_{n+1} = f(P_1, P_2, \dots, 1.1P_{n+1}) \quad (4.4)$$

Having evaluated χ^2 for each point on the simplex, we then select three of them; that with the highest χ^2 which we designate V_h , that with the next highest V_{nh} and that with the lowest, V_l . The simplex is then moved through the parameter space seeking to minimise the value of χ^2 . There are three operations available with which to do this; reflection, expansion and contraction. Having evaluated V_h , the point of the simplex having the highest value of χ^2 , the assumption is made that this point lies furthest away from the real solution, and that this solution therefore lies on the far side of all the other points of the simplex relative to V_h . Hence the simplex is moved in this direction by reflecting it through the centroid of all of the points excluding V_h to generate the new point V_r . This is performed by first calculating the centroid C as

$$C = \frac{1}{n} \sum_{i=1, i \neq h}^{n+1} V_i \quad (4.5)$$

The reflected point V_r is then calculated as

$$V_r = (1 - \alpha)C - \alpha P_h \quad (4.6)$$

where α is generally not set to one to avoid the simplex oscillating back and forth between two points. There are three possible results of such a reflection, which will

be dealt with in turn.

(a) V_r is better than V_h but worse than V_l

In this instance a new simplex is formed by replacing V_h with V_r , and the process of reflection is repeated.

(b) V_r is better than V_l

If this is the case then the reflection was very successful, and it appears that this is the correct direction for the parameters to be varied in. The search is continued in this direction by expanding the simplex to form a new point V_e .

$$V_e = \gamma V_r + (1 - \gamma)C \quad (4.7)$$

Here γ is the expansion coefficient, which again is set to a non-integer value to avoid instability. If this expansion is successful, that is V_e is better than V_r , then V_h is replaced by V_e and the process of reflection repeated.

(c) V_r is worse than or the same as V_h

If this is the case, then the minimum may be on the same side of C as V_h , so the simplex is contracted and the point V_c is generated

$$V_c = (1 - \beta)C + \beta V_h \quad (4.8)$$

where β is the contraction coefficient. Oscillations may occur for $\beta = 0.5$, so it is usually set slightly different to this value. If V_c is better than V_h , V_h is replaced by V_c and the process of reflection repeated. Contraction of the simplex rarely fails, unless it is very close to the minimum. If this is the case, it is necessary to re-define the simplex and start again.

In summary, then, the simplex moves around in the parameter space, expands along directions which minimise χ^2 , and contracts as it approaches a minimum on the χ^2 surface.

4.3 Analytical solution^[91]

A detailed discussion of the mathematical basis behind this method is not appropriate here, and so only an overview of the methodology will be presented. For a rigorous treatment, the reader is referred to the accounts of Wentworth^{[92][93]} and Bevington^[94]. The method may be summarised as follows. Again, we begin with a reasonable set of guesses to the parameters in the model, P_j . The actual values of the parameters we will designate P_j^0 such that

$$\begin{aligned} P_1^0 &= P_1 + \delta P_1^0 \\ &\cdot \\ &\cdot \\ P_n^0 &= P_n + \delta P_n^0 \end{aligned} \quad (4.9)$$

where δP_j^0 are corrections to P_j and are small enough (i.e. the initial guesses are sufficiently close to the real solution) for the function in question to be expanded in a Taylor series and the series truncated after the first term. Hence

$$F(x_i, P_1^0, P_2^0, \dots, P_n^0) = F(x_i, P_1, P_2, \dots, P_n) + \sum_{j=1}^n \left(\frac{dF}{dP_j} \right)_i \delta P_j^0 \quad (4.10)$$

and every parameter in equation 4.10 is known except the values of δP_j^0 . Hence we can solve the equations, there being n equations for n parameters in the model, to yield values of δP_j^0 and use these as corrections to our initial guesses as in equation 4.9. If the series expansion in equation 4.10 were exact, the corrected initial guesses would correspond with the correct values; in practice because of the approximation in 4.10 the new values are generally only better approximations than the originals.

Hence the procedure is to take these new initial guesses and to repeat the procedure, thus iterating closer to the true solution with each cycle. Note that in this method we are solving for corrections to the values of the parameters in the model, rather than for the parameters themselves.

4.4 Selection of convergence criteria

Having decided upon the model with which to fit the experimental data and a method by which to perform this, it is necessary to judge the quality of a particular fit to assess whether or not successive iterations are in fact making any significant improvement. If the improvements are not significant, the solution is said to have converged. The most common numerical test used to judge the quality of a fit to experimental data is the χ^2 (chi squared) value. χ^2 is defined as^[95]

$$\chi^2 = \sum_{i=1}^n W_i [y(t_i) - Y(t_i)]^2 \quad (4.11)$$

where $y(t_i)$ is the measured and $Y(t_i)$ the calculated value of the i th data point, and W_i is the weighting factor of the i th data point. This factor is included so that those points which are determined with most reliability can be made to make the greatest contribution to the χ^2 value. It has been found for the flash photolysis data presented here that applying the same weight to each point yields the best fits. Thus the value of χ^2 reflects the sum of the squares of the differences between the calculated and experimental data points, and obviously the smaller χ^2 the less the difference between calculation and experiment and the better the fit. Convergence of the model is usually deemed to have occurred when successive iterations do not result in a reduction in χ^2 of more than a given amount. In the fitting of the data performed here this is set as one part in 10^5 . Thus the value of

χ^2 gives an objective comparison between fits of different models to the same data set, provided of course that the data range over which fitting is performed is the same in each case. χ^2 then is obviously a function of the parameters in the model, and we can construct what we term a χ^2 surface, by plotting the value of χ^2 as a function of the model parameters. If we have only two parameters, it is very easy to visualise such a surface, which will be characterised by peaks and troughs the precise shape of which depending upon the model in question. For more than two parameters, it is not possible to visualise such a surface. However, it is clear that certainly for a large number of parameters there exists the possibility of more than one minimum on the surface, although one will almost certainly be deeper than the others. This therefore is one of the problems associated with fitting mathematical models to data; although a minimum may be found, it is not possible to tell whether or not this is the global minimum (that is, the deepest minimum on the surface) or simply a local minimum. The only way to be certain that the global minimum has been reached is to fit the data several times starting with different initial guesses to see whether the system always converges to the same solution.

There are two graphical methods of judging the quality of the fit which are commonly employed. These are a plot of the weighted residuals between the actual and fitted data, where the residuals are defined as

$$R_i = W_i[y(t_i) - Y(t_i)] \quad (4.12)$$

The residuals should be randomly distributed around zero for a good fit. Also employed is the autocorrelation function of the weighted residuals, which is a good

diagnostic tool for the randomness of the scatter of the weighted residuals^[96]. The autocorrelation function $C(t)$ is defined as

$$C(t_j) = \frac{\frac{1}{m} \sum_{i=1}^m W_i^{\frac{1}{2}} R_i W_{i+j}^{\frac{1}{2}} R_{i+j}}{\frac{1}{n} \sum_{i=1}^n W_i R_i^2} \quad (4.13)$$

where n is the number of data points and m is the number of terms evaluated. It is the normal practice to evaluate $C(t)$ only for values of j ranging from 0 to $n/2$, so that m is always at least $n/2$. This is done since at small values of m improper averaging of $C(t)$ may result and give misleading values for the autocorrelation function. For a good fit (random distribution of residuals) $C(t)$ shows high frequency, low amplitude fluctuations about the zero line. For a poor fit (residuals not randomly distributed) $C(t)$ exhibits pronounced low frequency oscillations about the zero line. Inspection of the residuals and autocorrelation plots gives much more information about the quality of the fit than simple inspection of the actual and fitted data.

4.5 Numerical solution of differential equations using fourth-order Runge-Kutta integration^[97]

The general expression for the Runge-Kutta algorithms is

$$Y_{i+1} \approx Y_i + Q(x, y, h) \quad (5.14)$$

where $Q(x, y, h)$ is an approximation to the integral

$$\int_{x_i}^{x_{i+1}} F(x, y) dx \quad (5.15)$$

The fourth-order Runge-Kutta algorithm is used in preference to the second- or third-order due to the improved accuracy of the approximation, and in preference

to using Euler's method for the same purpose due to their greater efficiency of computation to achieve a given level of accuracy. The fourth order Runge-Kutta algorithm, however, as the name suggests, requires four function evaluations per step. The equations for evaluating the fourth order Runge-Kutta approximation are as follows.

$$y_{i+1} \approx y_i + \frac{1}{6}(k_1 + 2k_2 + 2k_3 + k_4) \quad (5.16)$$

where

$$k_1 = hF(x_i, y_i)$$

$$k_2 = hF\left(x_i + \frac{h}{2}, y_i + \frac{k_1}{2}\right)$$

$$k_3 = hF\left(x_i + \frac{h}{2}, y_i + \frac{k_2}{2}\right)$$

$$k_4 = hF(x_i + h, y_i + k_3)$$

(Equations 5.17)

Here, h is the interval over which the function is evaluated.

The method may be extended to evaluate the solution to a system of differential equations by application of the modified set of equations shown as equations 5.18 and 5.19, where here the subscript i indicates the particular differential equation in the system, and obviously takes values up to and including n where n is the number of equations in the system.

$$y_{x_0+h} \approx y_{i_0} + \frac{1}{6}(k_{i_1} + 2k_{i_2} + 2k_{i_3} + k_{i_4}) \quad (5.18)$$

where

$$k_{i1} = hF_i(x_0, y_{i0})$$

$$k_{i2} = hF_i\left(x_0 + \frac{h}{2}, y_{i0} + \frac{k_{i1}}{2}\right)$$

$$k_{i3} = hF_i\left(x_0 + \frac{h}{2}, y_{i0} + \frac{k_{i2}}{2}\right)$$

$$k_{i4} = hF_i(x_0 + h, y_{i0} + k_{i3})$$

(Equations 5.19)

Chapter 5

Nanosecond Flash Photolysis Studies

5 Nanosecond Flash Photolysis Studies

5.1 Introduction - summary of previous work

Much of the work attempting to characterise the excited states of PT azomethine dyes and related compounds has to date been conducted in fluid solution at room temperature using microsecond and, more recently, nanosecond emission and absorption techniques, and has met with limited success. This may in part be attributed to the fact that the fluorescence quantum yields of these compounds under such conditions are very low, of the order of 10^{-4} , and as a consequence the emission in many solvents is masked by solvent Raman bands. This factor has limited the determination of emission spectra to solvents such as tetrachloromethane, where the Stokes Raman shift is very small^[98]. Fluorescence quantum yields and fluorescence lifetimes are observed to increase rapidly as the temperature is decreased^[99], although even at liquid nitrogen temperatures no phosphorescence emission can be detected. In addition, no transient signal attributable to triplet-triplet absorption can be observed using nanosecond flash photolysis techniques, leading to the conclusion that either the triplet states are not populated in appreciable amounts (i.e. that the intersystem crossing yields are small), or the triplet state lifetime is too short for it to be resolved using our apparatus. Characterisation of the triplet states is a matter of interest, however, since they may play an important role in light-fading reactions; they are the longest lived electronically excited state in many organic molecules, and as such are the state most available for bimolecular reactions with, for example, oxygen.

Determination of the triplet energy levels of azomethine dyes has been achieved with some success^[100]. The rate of triplet energy transfer to a triplet energy acceptor reaches a limiting value when the energy of the

sensitiser triplet state exceeds that of the quencher by 12 kJ mol^{-1} ^[101]. In solvents whose viscosity η exceeds 3 centipoises, the energy transfer rate approaches the diffusion controlled limit. In less viscous media, the limiting rate constant is less than the diffusion controlled limit, which may be attributed to the energy transfer process being somewhat inefficient, and hence in low viscosity solvents diffusion apart of donor and acceptor can compete with energy transfer^{[102][103]}. This rate limiting factor in the energy transfer process has been assigned as being due to orientational requirements between donor and acceptor, and indeed evidence from low temperature phosphorescence studies has revealed the presence of such a requirement in the energy transfer between benzophenone and phenanthrene d_{10} ^[104]. In a plot of the logarithm of the rate of energy transfer against the difference in triplet energy between sensitiser and quencher, the final slope is predicted by the Arrhenius equation^[105]

$$\ln k = \ln A - \frac{E_a}{RT} \quad (5.1)$$

provided the quencher does not undergo any change in geometry upon accepting excitation energy. When such changes of geometry do occur, then if these changes lower the acceptor triplet state energy the slopes of the plots will be shallower than predicted by the Arrhenius equation. Such a phenomenon has historically often been referred to as "non-vertical" energy transfer^[106], but since this terminology infers concomitant electronic transitions and nuclear rearrangement, it will not be used here. Rather, it is probably more accurate to state that energy changes due to modification of the molecular geometry in going from ground to triplet state can contribute to the overall energy. Such shallow slopes in

Arrhenius plots have been observed in triplet energy transfer to yellow azomethine dyes derived from benzoylacetanilide.

Flash kinetic spectroscopy has been applied to determine the rate of energy transfer to azomethine dyes from a range of sensitiser having a graded range of triplet energies. The rate of relaxation of the sensitiser triplet state is monitored in the presence and absence of quencher, where the decay is described by

$$-\frac{d[{}^3S^*]}{dt} = k_d[{}^3S^*] + k_q[{}^3S^*][Q] + k_2[{}^3S^*]^2 \quad (5.2)$$

In practice, it may be possible to arrange the experimental conditions (choice of sensitiser, laser pulse intensity) such that the second order term may be neglected and the sensitiser triplet decay in the absence of quencher may be described by an equation of the type

$$[{}^3S^*]_t = [{}^3S^*]_o e^{-k_d t} \quad (5.3)$$

However, if the second order term makes a significant contribution to the overall relaxation mechanism, the triplet state decay will be described by a more complex equation

$$[{}^3S^*]_t = \frac{k_d [{}^3S^*]_o}{(k_d + k_2 [{}^3S^*]_o) e^{k_d t} - k_2 [{}^3S^*]_o} \quad (5.4)$$

In the presence of quencher, the concentration thereof is usually arranged to be such that the second order term makes an insignificant contribution to the overall decay mechanism and the sensitiser triplet state decay may then be described as a simple first order:

$$[{}^3S^*]_t = [{}^3S^*]_o e^{-(k_d + k_q [Q])t} \quad (5.5)$$

hence k_q can be calculated from the rate of triplet decay in the presence and absence of quencher, and a knowledge of the quencher concentration. In these experiments the only transient absorptions seen are due to either the sensitiser triplet state or, in cases where the dye in question is unsymmetrical about the azomethine bond, to syn-anti isomerisation. Isomerisation occurs on time-scales much shorter than the sensitiser triplet decay, as evidenced by the fact that the rise of absorption by the isomeric form follows exactly the decay of the sensitiser triplet. Consequently, back energy transfer from the azomethine dye to the sensitiser can be neglected as a consequence of the very short triplet state lifetime of the dye. This very rapid isomerisation process does however mean that where isomerisation occurs energy transfer to both isomeric forms is possible, and a composite rate constant for energy transfer only can be measured, since neither the configurations present nor the rates of energy transfer to these configurations are known. Hence where the dye is not symmetrical about the azomethine bond, if there are large changes in triplet energy as a result of intramolecular geometrical rearrangement there will be observed a very shallow slope to the Arrhenius plot and consequently considerable uncertainty in the measurement of the triplet energy. Arrhenius plots for many azomethine dyes having triplet energies sufficiently high to be determined by this means are shallower than predicted by the Arrhenius equation, which may be interpreted as indicating that the triplet energy does indeed change upon isomerisation; this is not to say that there is necessarily a large difference between the triplet energies of the syn and anti isomeric forms, since there may be a deep minimum in the triplet energy potential surface at some intermediate conformation.

From experiments such as these with magenta pyrazolone dyes, it was found that an upper limit only could be placed on their triplet energies since energy transfer from violanthrene, the lowest energy suitable donor available, proceeded at the limiting rate. Hence since E_{e} for violanthrene is 105 kJ mol^{-1} [107] an upper limit for the magenta pyrazolone dye triplet energy is 93 kJ mol^{-1} . Similar experiments conducted using pyrazolo-triazole (PT) azomethine dyes demonstrate that these have slightly higher triplet energies, that for a 6-methyl substituted PT dye being determined as $100 - 118 \text{ kJ mol}^{-1}$ [54]. It has been concluded for pyrazolone dyes that their triplet energies show a dependence upon the electron donating or electron withdrawing nature of the substituent in the para position on the phenylenediamine ring relative to the azomethine nitrogen. Maximum triplet energies are seen in those dyes for which the Hammett sigma constant of the para substituent is approximately zero; both positive or negative sigma values (corresponding to electron withdrawing and electron donating character, respectively) have the effect of decreasing the triplet energy. Electron donating substituents have a greater effect on the triplet energy than do electron accepting substituents [108].

It is worthwhile contrasting these results with those obtained for azine dyes, which differ from the azomethine dyes only in that there is an extra bond preventing isomerisation about the C=N linkage. These compounds, which have structural similarities with yellow azomethine dyes derived from pyvaloylacetanilide, benzoylacetanilide, dibenzoylmethane and diacetylmethane, have triplet energies of about 190 kJ mol^{-1} , approximately the same as for the similar yellow azomethine dyes.

However, their triplet states are readily observed, having lifetimes in degassed methanol of some 70 μ s, and being readily quenched by dissolved oxygen and β - carotene.

5.2 Laser flash photolysis of pyrazolotriazole azomethine dyes

Studies were conducted to investigate the effects of direct photolysis of pyrazolotriazole azomethine dyes in dilute fluid solution. The second harmonic of an Nd:YAG laser proved to be an appropriate excitation wavelength for these experiments. As mentioned previously (section 1.7), following nanosecond pulsed laser excitation no transient absorption attributable to an electronically excited state of the dye may be detected; however, in unsymmetrical dyes it is possible to detect the syn-anti isomerisation about the azomethine linkage. This is manifested as a change in the absorbance spectrum of the compounds giving rise to a transient difference spectrum displaying a depletion in the region where the stable syn form has greatest absorbance, and an absorption where the molar absorption coefficient of the anti form is the greater. The isosbestic point (where both syn and anti isomers have equal molar absorption coefficient) occurs at a wavelength dependent upon both the nature of the dye and the particular solvent used. The transient difference spectrum obtained immediately following excitation of a benzene solution of the 6-CO₂Et PT dye with 20 mJ cm⁻² 532nm radiation is reproduced in figure 5.1, while that under similar conditions in acetonitrile solution is reproduced in figure 5.2 with the time evolution of the transient spectrum also shown. It is readily discerned that there is no dependence of the relaxation kinetics on the analysing wavelength, suggesting the presence of only one decaying species. Representative kinetic traces at analysing wavelengths of 550nm and 700nm, together with plots of residuals and

autocorrelation of residuals functions (chapter 4) are shown in figure 5.3. The function fitted to the data is a simple falling exponential (i.e. first order kinetics). The ground state absorption spectra of the dye in the two solvents are shown reproduced for comparison in figure 5.4.

5.3 Isomerisation yield from the triplet state

As described in section 1.7, it is possible to produce isomerisation about the carbon-nitrogen double bond both by direct excitation and from triplet energy transfer. In populating the anti isomer via triplet energy transfer it is clear that all isomerisation must come from the triplet manifold provided there is no appreciable direct excitation of the acceptor at the wavelength chosen to excite the donor. In practice it is possible to arrange both the absorbance of the azomethine dye at the exciting wavelength and the laser energy density to be sufficiently low that negligible ground state depletion (and consequent anti isomer production) results from direct excitation. This can be achieved while still producing a significant population of sensitiser triplet states and having a dye concentration great enough that quenching of the sensitiser triplet state by the dye dominates over unimolecular relaxation (or triplet-triplet annihilation) by careful choice of excitation wavelength and sensitising species. The triplet sensitisers chosen for this purpose were 2'-acetonaphthone and benzophenone, two different molecules being used to ensure that the results were independent of sensitiser. The triplet state of 2'-acetonaphthone has an appreciable lifetime in degassed benzene, and an energy of some 246 kJ mol^{-1} [109], well in excess of those determined for azomethine dyes. The benzophenone triplet state has a somewhat shorter lifetime in degassed benzene, being some $6 \mu\text{s}$, and hence a slightly lower fraction of the triplets will be intercepted by a

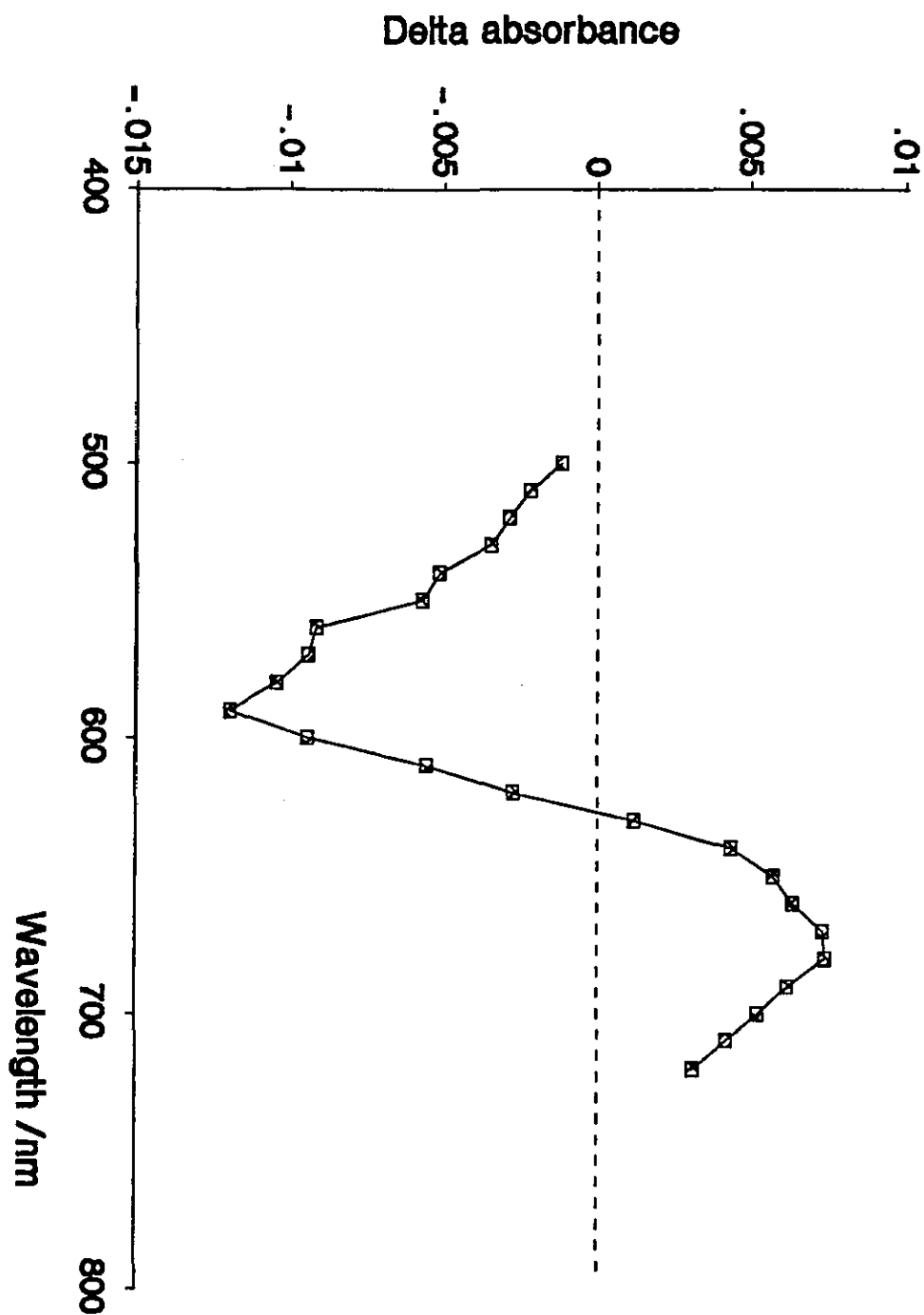


Figure 5.1: Transient difference spectrum of 6-CO₂Et substituted PT dye in air equilibrated benzene solution, dye concentration $1.48 \times 10^{-5} \text{ mol dm}^{-3}$

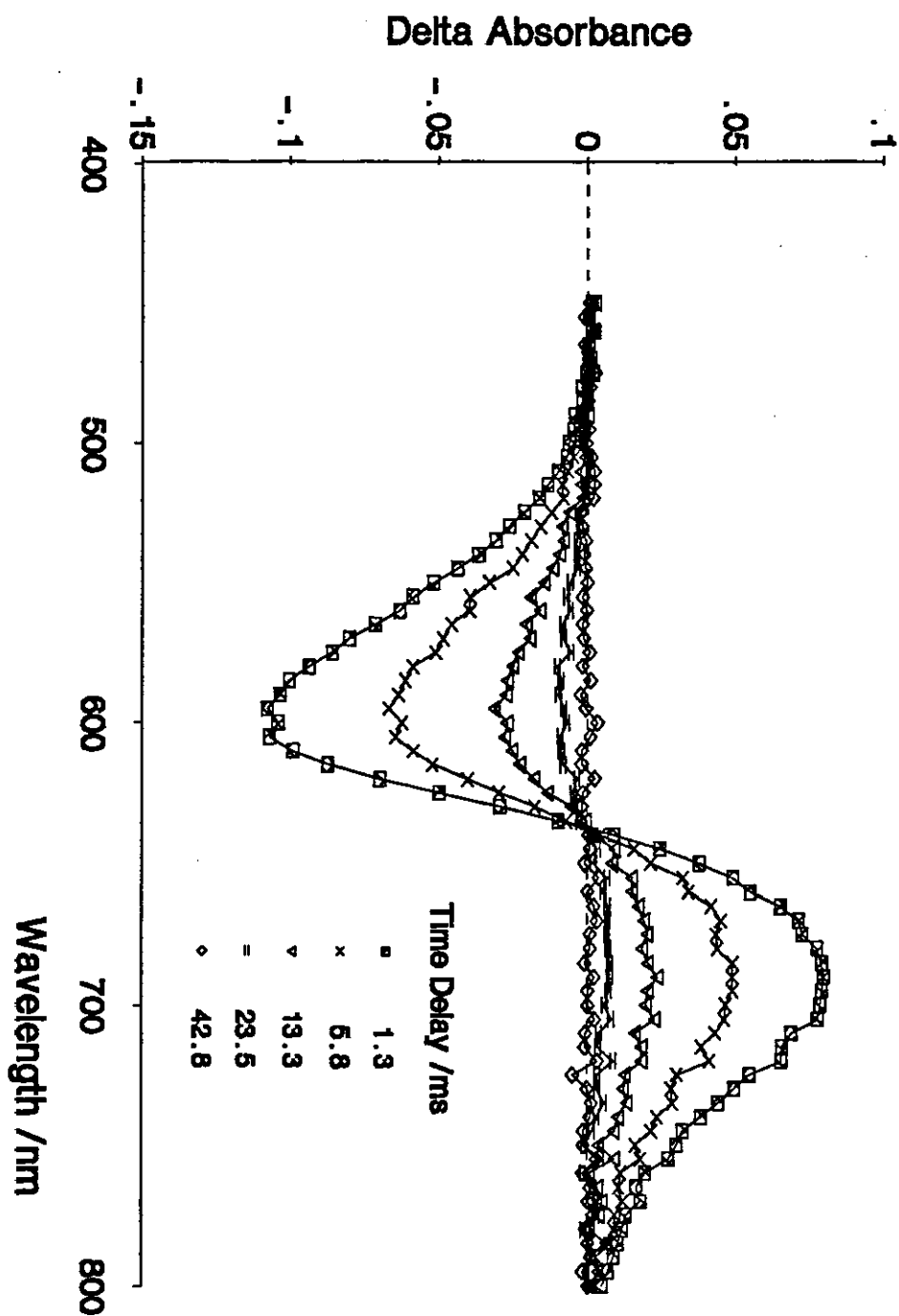


Figure 5.2: Transient difference spectrum of 6-CO₂Et substituted PT dye in air equilibrated acetonitrile solution, dye concentration $1.68 \times 10^{-5} \text{ mol dm}^{-3}$

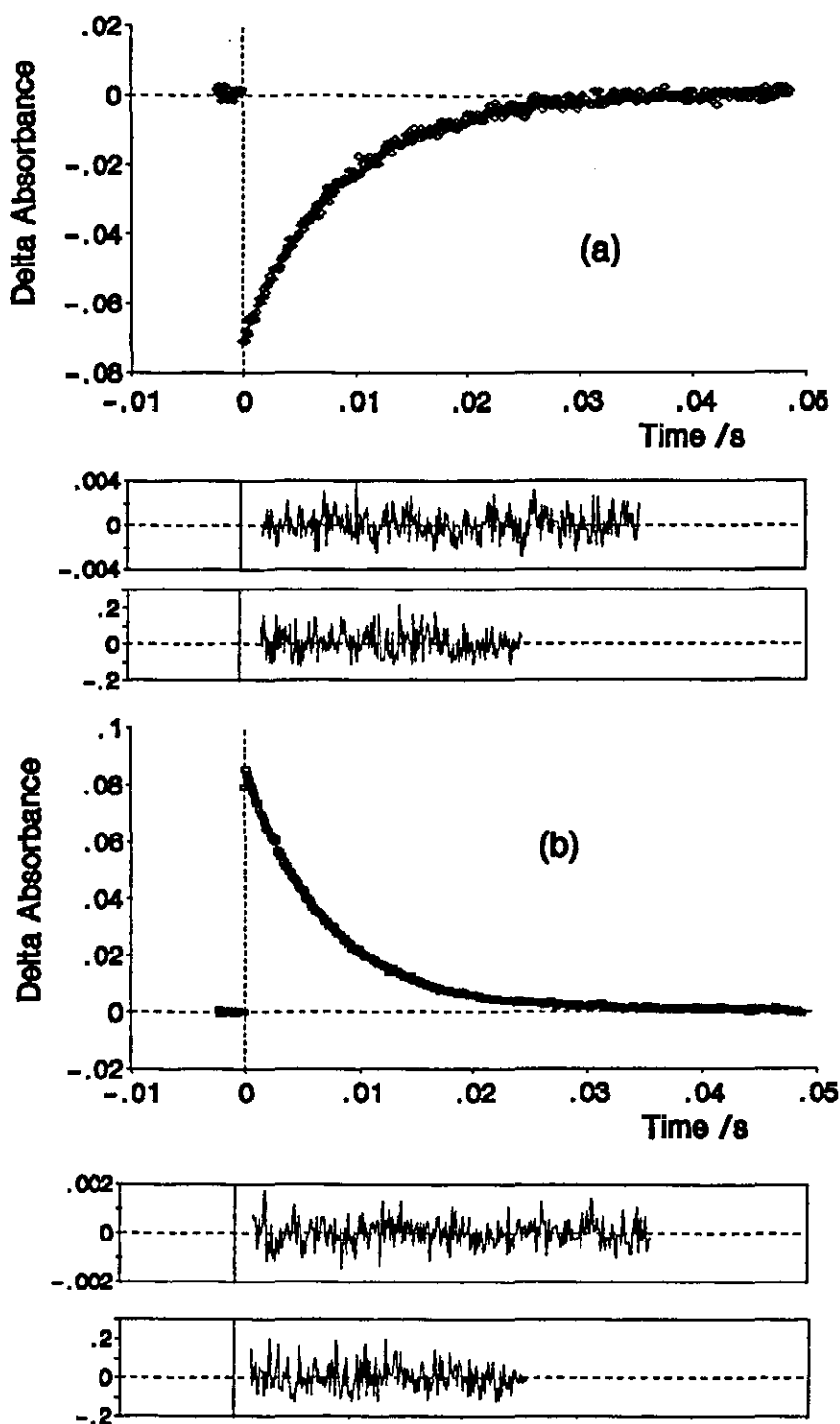


Figure 5.3: Kinetic traces showing thermal relaxation of 6-CO₂Et substituted PT dye in air equilibrated acetonitrile solution, dye concentration 1.68×10^{-5} mol dm⁻³, (a) analysing wavelength 550nm (b) analysing wavelength 700nm. Also shown are the plots of residuals (upper trace) and autocorrelation of residuals (lower trace) for each kinetic analysis. The traces are fitted with lifetimes of 8.3 and 7.6 milliseconds, respectively.

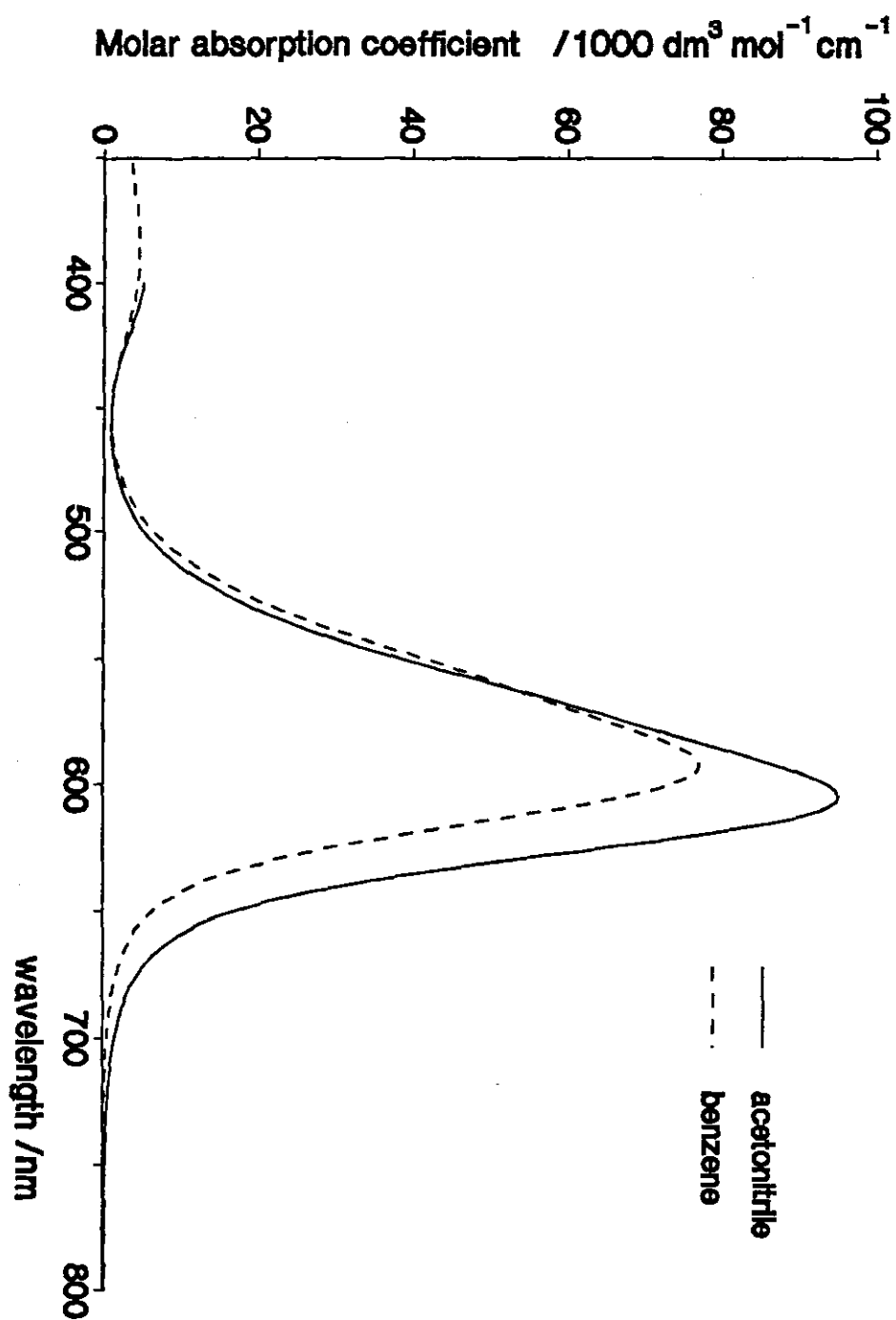


Figure 5.4: Ground state absorption spectra of 6-CO₂Et substituted PT dye in air equilibrated benzene and acetonitrile solutions

given dye concentration. Its triplet state energy, 287 kJ mol⁻¹ [110], is again well in excess of that observed for azomethine dyes. The concentrations of benzophenone and 2'-acetonaphthone used in the sensitisation experiments were 5x10⁻³ mol dm⁻³ and 2.5x10⁻³ mol dm⁻³, respectively. Azomethine dyes were added to the solutions at a concentration of 7x10⁻⁵ to 1x10⁻⁴ mol dm⁻³ in all cases. The principal dye chosen for this series of experiments was the 6-CO₂Et substituted PT, as a consequence of its ground state absorption spectrum being red-shifted relative to most magenta azomethine dyes, facilitating virtually independent observation of the sensitiser triplet states and the dye anti isomer. Taking the example of benzophenone triplet sensitized isomerisation of the 6-CO₂Et substituted PT dye, the experimental methodology was as follows. Flash excitation of a 5x10⁻³ mol dm⁻³ solution of benzophenone, degassed using three freeze-pump-thaw cycles to a final pressure of 5x10⁻⁵ mbar, with 3 mJ cm⁻² of 354nm radiation (the third harmonic of an Nd:YAG laser) yields the triplet state decaying by a predominantly first order process with a first order rate constant of 1.55±0.04x10⁵ s⁻¹. Adding dye at a concentration of 1x10⁻⁴ mol dm⁻³ to this solution increases the decay rate to 7.7±0.4x10⁵ s⁻¹, and here the decay is a clean first order. Therefore, the proportion of sensitiser triplets intercepted by dye can be determined since

$$-\frac{d[{}^3S]}{dt} = k_d[{}^3S] + k_q[{}^3S][Dye] \quad (5.6)$$

and

$$[{}^3S]_t = [{}^3S]_0 e^{-(k_d+k_q[Dye])t} \quad (5.7)$$

so since $k_d = 1.55 \pm 0.04 \times 10^5 \text{ s}^{-1}$ and in the presence of dye the observed rate constant is $7.7 \pm 0.4 \times 10^5 \text{ s}^{-1}$, then the fraction of benzophenone triplets intercepted is

$$\frac{k_q[Q]}{k_d + k_q[Q]} = 0.8 \pm 0.1$$

From the molar decadic absorption coefficient of the benzophenone triplet in degassed benzene at 525nm, $7870 \text{ dm}^3 \text{ mol}^{-1} \text{ cm}^{-1}$, the concentration of triplets produced instantaneously in the laser pulse is $2.7 \pm 0.2 \times 10^{-6} \text{ mol dm}^{-3}$. Thus the concentration of isomer triplets produced by sensitisation is $2.2 \pm 0.4 \times 10^{-6} \text{ mol dm}^{-3}$. From the level of ground state depletion observed between 500nm and 530nm, assuming zero isomer molar decadic absorption coefficient in this region, the minimum isomer concentration arising from this triplet concentration is $9.4 \pm 1.2 \times 10^{-7} \text{ mol dm}^{-3}$. Therefore the minimum isomer yield from the triplet state is

$$\frac{9.4 \pm 1.2 \times 10^{-7}}{2.2 \pm 0.4 \times 10^{-6}} = 0.43 \pm 0.13$$

and obviously the maximum yield from the triplet state will be 1 if the isomer had appreciable molar decadic absorption coefficient in the 500nm to 530nm region. However, since the calculated yield is independent of analysing wavelength in the 500nm to 530nm region, this suggests that if the anti isomer were produced quantitatively from the triplet state the isomer spectrum would have to follow exactly the ground state absorption spectrum at least up to 530nm. While this is a possibility which cannot be completely discounted, the fact that such a situation would have to prevail for every dye and solvent combination investigated leads to the conclusion that it is unlikely. This is therefore the first evidence that there is negligible absorbance by the anti isomer in the

short wavelength edge of the syn isomer spectrum, an idea which will be returned to and developed more fully in sections 5.4 and 5.5. Therefore, the calculated yields from the triplet state shown in table 5.1 may on this basis be interpreted as being, within the uncertainty of the experiment, those which actually prevail rather than minimum values where the actual value may be considerably higher.

Dye	Sensitiser	Solvent	$\phi_{\text{anti isomer, triplet}}^{\text{minimum}}$
Blue PT	2'-acetonaphthone	Benzene	0.4 ± 0.1
Blue PT	Benzophenone	Benzene	0.4 ± 0.1
Blue PT	Benzophenone	Acetonitrile	0.35 ± 0.1
E1	Benzophenone	Benzene	0.45 ± 0.1
H-PT	Benzophenone	Benzene	0.09 ± 0.02

Table 5.1: Calculated isomerisation efficiencies from the PT dye triplet state

5.4 Estimation of isomer molar decadic absorption coefficients

The results obtained from the above experiments allow the (at least approximate) determination of isomer molar decadic absorption coefficients, since the population of the triplet state can be calculated from the triplet energy transfer experiments and the concentration of isomer can therefore be calculated from the estimated isomerisation efficiencies from the triplet state. It can readily be shown for this system that

$$\epsilon_1 = \frac{\Delta A(\lambda) + \epsilon_{GS}[GS]_0 - \epsilon_{GS}[GS]_t}{[GS]_0 - [GS]_t} \quad (5.8)$$

where $[GS]_0$ and $[GS]_t$ are the ground state concentrations before and immediately following the accepting of triplet excitation energy; in this instance $[GS]_t$ is the ground state concentration immediately following isomerisation from the triplet state after energy transfer is complete.

The minimum value thereof may be estimated from the maximum decrease in absorbance in a spectral region corresponding to absorption by the syn isomer induced by energy transfer since thermal relaxation of the isomer back to the stable ground state conformation occurs on timescales sufficiently long for it to be neglected (section 5.7). Thus taking account of the triplet state population calculated from the energy transfer experiments and the calculated isomerisation efficiencies from the triplet state, it is possible to determine molar decadic absorption coefficients for the isomer. These are shown calculated for the 6-CO₂Et substituted PT dye in benzene solution assuming an isomerisation yield from the triplet state of 0.4 (i.e that the anti isomer does not absorb in the short wavelength edge of the syn absorption band) at several wavelengths below in table 5.2. Obviously the error in the molar absorption coefficient will be comparable with that in the determined isomerisation efficiency, i.e. of the order of $\pm 25\%$.

λ/nm	$\epsilon(\text{GS})$ / $\text{dm}^3\text{mol}^{-1}\text{cm}^{-1}$	ΔA	$\epsilon(\text{anti isomer})$ / $\text{dm}^3\text{mol}^{-1}\text{cm}^{-1}$
670	2200	0.0427	50700
680	1280	0.0412	48100
690	740	0.0382	44100
700	470	0.0320	36800

Table 5.2: Anti isomer molar decadic absorption coefficients in benzene solution. (Ground state concentration 9.8×10^{-5} M, triplet state concentration from energy transfer $2.2 \pm 0.4 \times 10^{-6}$ M)

Using these molar absorption coefficients as a point of reference, then, it is possible to calculate the anti isomer absorption spectrum which prevails on the basis that the yield for the triplet state is 0.4. This is shown together with the syn isomer absorption spectrum in benzene solution in figure 5.5. Also shown are the anti isomer spectra which are calculated for yields from

the triplet state of 0.7 and 1. As is evident, as we assume a greater yield from the triplet state, so there must be greater absorbance by the anti isomer in the short wavelength edge of the syn isomer absorption spectrum.

It may be noted that it is possible to calculate isomer molar decadic absorption coefficient from data obtained in a different experiment, that is by using the transient difference spectra presented in section 5.2. It is possible to calculate the minimum conversion of syn to anti isomer by assuming that in the short wavelength edge of the syn absorption band there is no absorption by the anti form. By substituting this value for the conversion to the isomer into the expression for the isomer molar decadic absorption coefficient as in equation 5.8, the maximum isomer molar decadic absorption coefficient at a given wavelength may be calculated. This then allows maximum isomer molar decadic absorption coefficients at all wavelengths to be determined. Molar decadic absorption coefficients at a number of wavelengths calculated using this method for benzene solution are shown in table 5.3., while those in acetonitrile solution are shown in table 5.4. Errors on the determination of the ground state molar absorption coefficients are estimated as $\pm 6\%$, while those on the isomer molar absorption coefficients are somewhat larger and are estimated as $\pm 15\%$. These molar decadic absorption coefficients allow us to plot the absorption spectra of the anti isomers in benzene and acetonitrile solution, and use is also made of them in the modelling of the picosecond data (chapter 6). The absorption spectra in the two solvents, plotted as molar decadic absorption coefficient against wavelength, are shown in figure 5.6.

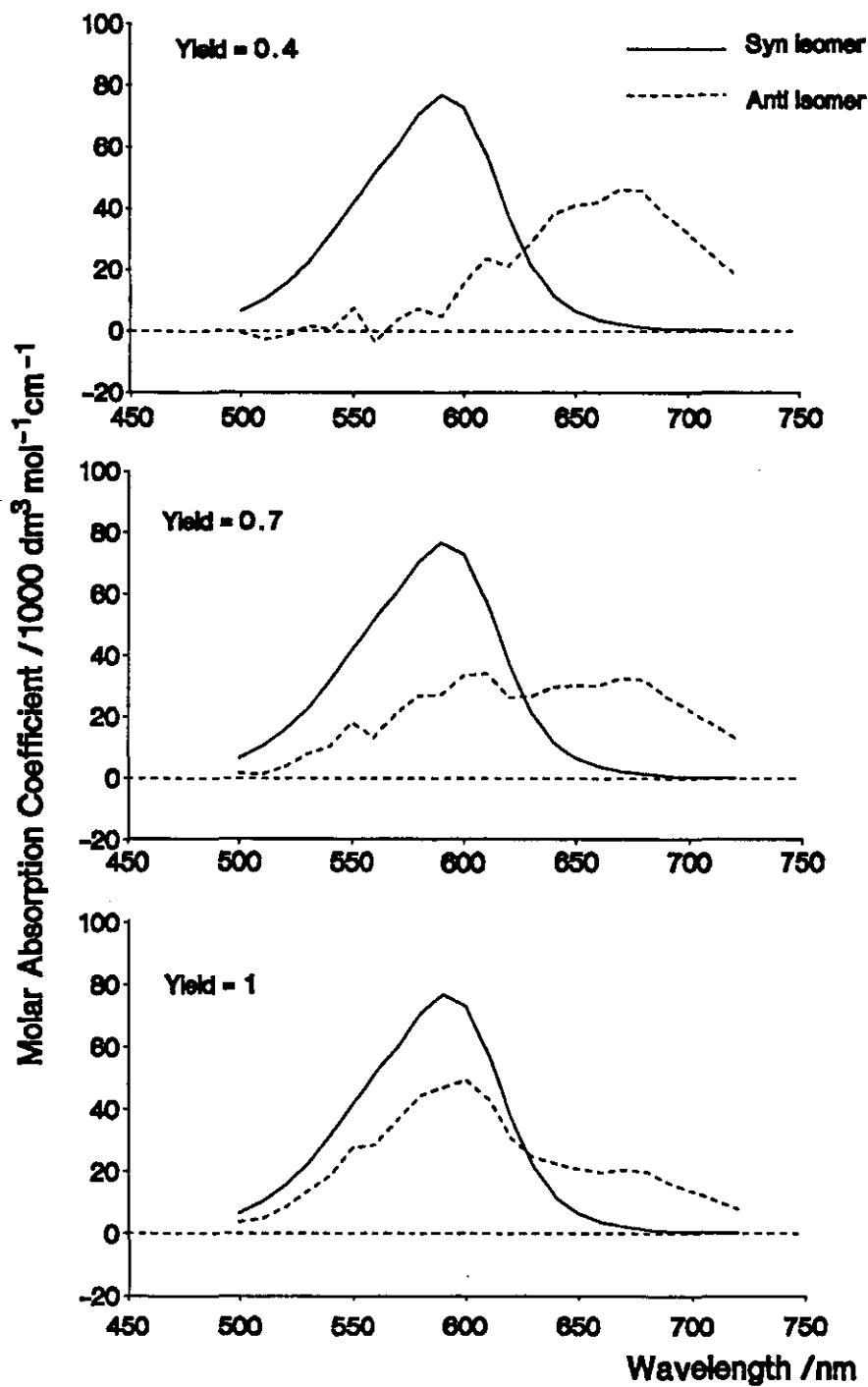


Figure 5.5. :6-CO₂Et substituted PT dye syn and anti isomer absorption spectra for various isomerisation yields from the triplet state

λ/nm	$\epsilon(\text{GS})$ $/\text{dm}^3\text{mol}^{-1}\text{cm}^{-1}$	ΔA	$\epsilon(\text{anti isomer})$ $/\text{dm}^3\text{mol}^{-1}\text{cm}^{-1}$
720	200	0.00312	18900
710	270	0.00419	25400
700	470	0.00524	31800
690	740	0.00620	37900
680	1280	0.00742	45700
670	2200	0.00735	46200
660	3700	0.00637	41800
650	6500	0.00573	40800
640	11690	0.00434	37700
630	21600	0.00119	28700
620	37800	-0.00274	21400
610	57300	-0.00556	24000
600	72840	-0.00943	16400
590	76800	-0.01195	5200
580	70300	-0.01045	7700
570	60600	-0.00941	4300
560	51500	-0.00916	-3300
550	41900	-0.00571	7700

Table 5.3: Anti isomer molar decadic absorption coefficients for the 6-CO2Et substituted dye calculated from direct excitation of a 1.48×10^{-5} mol dm^{-3} benzene solution

λ/nm	$\epsilon(\text{GS})$ $/\text{dm}^3\text{mol}^{-1}\text{cm}^{-1}$	ΔA	$\epsilon(\text{isomer})$ $/\text{dm}^3\text{mol}^{-1}\text{cm}^{-1}$
720	660	0.065	50660
710	950	0.069	54027
700	1490	0.079	62259
690	2260	0.08	63798
680	3511	0.078	63511
670	5654	0.071	60269
660	9580	0.055	51888
650	16900	0.038	46131
640	30600	0.009	37523
630	51800	-0.029	29492
620	76200	-0.069	23123
610	92500	-0.099	16346
600	94000	-0.1045	13615
590	85059	-0.103	5828
580	73600	-0.093	2062
570	62500	-0.08	962
560	50900	-0.063	2438
550	39000	-0.052	-1000

Table 5.4: Anti isomer molar decadic absorption coefficients 6-CO2Et substituted dye calculated from direct excitation of a 1.68×10^{-5} mol dm^{-3} acetonitrile solution

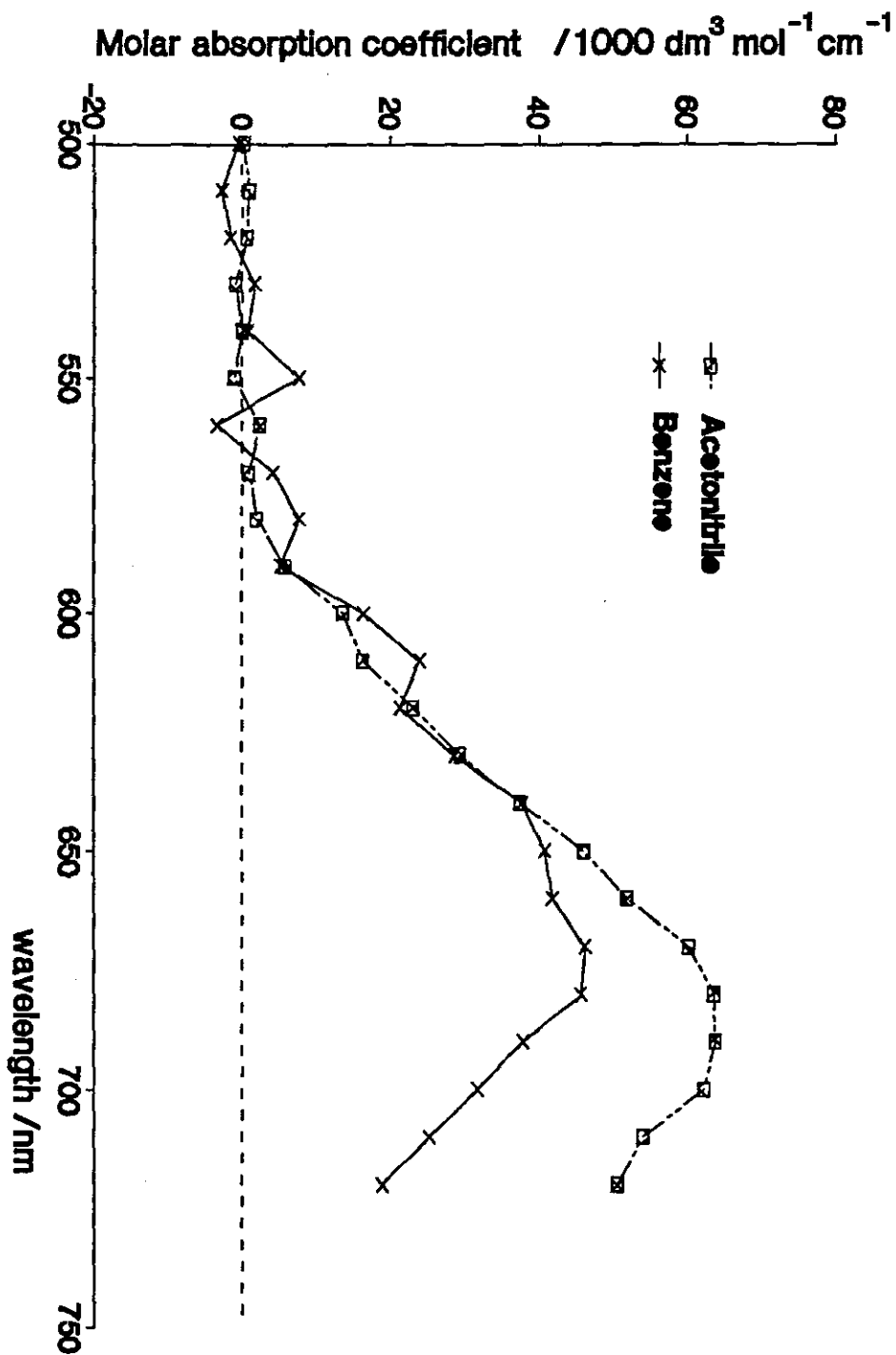


Figure 5.6: Absorbance spectra of 6-CO₂Et substituted PT dye anti isomers in benzene and acetonitrile solutions

It can clearly be seen, then, from these calculations that the same isomer absorption spectrum is calculated both from the triplet energy sensitisation experiments and as a consequence of direct excitation; this demonstrates that the same product is arrived at by both routes. However, the quantum yield of production of the isomer as a result of direct excitation (section 5.5) is substantially less than the yield of isomer from the triplet state. This fact may be interpreted in one of three ways:

(a) As a consequence of direct excitation isomerisation proceeds exclusively via the singlet state, and the difference simply reflects a difference in quantum yields between triplet and singlet states;

(b) Isomerisation proceeds exclusively via the triplet state and the lower yield from direct excitation is a result of a low intersystem crossing yield;

(c) From direct excitation, isomerisation proceeds through both the singlet and triplet manifolds, there being differing quantum yields from each state.

However, evidence from other experiments conducted (section 5.6) leads to the conclusion that the triplet state is not involved in the isomerisation process as a consequence of direct excitation, and therefore the implication is that the calculated differences in yield do indeed reflect differences in yield from triplet and singlet states.

5.5 Isomerisation yield from direct excitation

The calculation of the quantum yield of isomerisation as a result of direct photolysis of PT azomethine dyes is complicated to an extent by the fact that those molecules which are excited and do not isomerise return very rapidly to the ground state conformation on time-scales much shorter than the nanosecond excitation pulse. As such they are available to absorb further photons and

possibly isomerise, and hence this must be taken account of in calculating the quantum yield. Also, as ground state is converted to anti isomer, an appreciable lowering of absorbance at the excitation wavelength during the energy input may result, further complicating the calculation. The approach chosen to this problem, therefore, is to model the data obtained on the basis of the molar decadic absorption coefficients calculated above and the conversion efficiencies calculated in a similar manner (see later in this section), assuming in this instance that the laser pulse is a gaussian energy function with respect to time. This approximation is considered to be reasonable for a Q-switched Nd:YAG laser and is also simpler to handle mathematically than some of the other possible alternatives such as a sech^2 function, although it still means that an analytical solution to the differential equations used to describe the model is not possible since an analytical solution to the integral of a gaussian (referred to as an error function) cannot be evaluated. Therefore, the modelling is done by solving the differential equations numerically using fourth-order Runge-Kutta integration (section 4.5). The same four-level model as used for the picosecond data can be employed to calculate the conversion to the isomer for a given energy input, assuming as in the modelling of the picosecond data that only the singlet state is involved in isomerisation from direct excitation (chapter 6). The model used is illustrated in figure 5.7, and the differential equations describing this system are then as shown in equations 5.9.

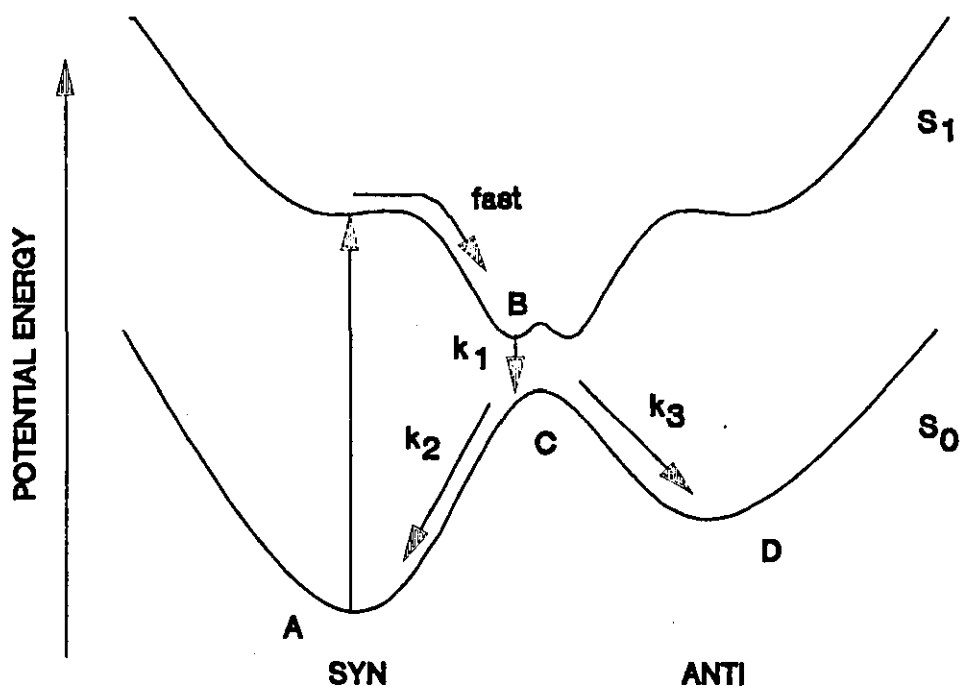


Figure 5.7: Schematic potential energy surface to describe the photophysical properties of pyrazolotriazole azomethine dyes

$$\frac{dA}{dt} = -\frac{P}{\sigma\sqrt{2\pi}} e^{-\frac{(t-t_0)^2}{2\sigma^2}} (1 - 10^{-\epsilon A}) + k_2 C$$

$$\frac{dB}{dt} = \frac{P}{\sigma\sqrt{2\pi}} e^{-\frac{(t-t_0)^2}{2\sigma^2}} (1 - 10^{-\epsilon A}) - k_1 B$$

$$\frac{dC}{dt} = k_1 B - (k_2 + k_3) C$$

$$\frac{dD}{dt} = k_3 C \quad (\text{equations 5.9})$$

The methodology behind the derivation of these equations is given fully in section 6.2. The value of P, the pump intensity, substituted into the equations is calculated as the total number of moles of photons (einstein) input per unit volume of solution, since when the gaussian function is integrated the total area under the curve is P. For a 30ns 532nm pulse, as obtained as

the second harmonic from the JK 2000 Nd:YAG laser used in these experiments, with an energy density of 20 mJ cm^{-2} , this corresponds to a value of P of 8.89×10^{-5} einstein dm^{-3} . The pulse energy density was calculated from the amount of tetraphenylporphine triplet state produced from flash excitation under identical conditions, the triplet state molar decadic absorption coefficient for TPP being known^[112]. Assuming that all of the energy in the pulse is contained within 3σ either side of the centre of the distribution (that is, that the total area under the curve of a gaussian function is contained from -3σ to $+3\sigma$. In fact, 99.7% of the energy is contained within this interval), this gives σ for the pulse of 5ns. The rate constants used are those obtained from fitting of the data obtained from the picosecond experiments conducted in the same solvents (section 6.3). The minimum conversion to isomer in benzene solution as a result of direct excitation is then calculated assuming no absorbance by the isomeric form at the probing wavelength. The minimum degree of conversion from direct excitation of a $1.48 \times 10^{-5} \text{ M}$ solution of the 6-CO₂Et PT dye in benzene solution by a 30ns 23 mJ cm^{-2} pulse are shown in table 5.5. As can readily be seen, this assumption gives a consistent conversion up to 590nm, after which there is an obvious deviation; this observation confirms that made in section 5.3, and lends more weight to the assumption that there is no absorption by the anti isomeric form in the short wavelength edge of the syn isomer absorption spectrum. In fact, on the basis of the data presented in table 5.5, it is possible to be more specific and state that there must be negligible absorption by the isomeric form of the 6-CO₂Et substituted PT dye at wavelengths shorter than 590nm. The same observation, i.e. that there is a consistent calculated conversion in the wavelength region up to approximately 590nm, is also

found for this same dye in methanol solution, and for the 6-H substituted PT dye in benzene solution, although this data is not presented here as the precise energy input used in these experiments was not determined and hence the data cannot be used in the computer simulations to determine the quantum yield.

λ/nm	$\epsilon(\text{GS})$	ΔA	$[\text{GS}]_t$	Conversion
500	6500	-0.00116	1.462E-05	0.012
510	10400	-0.00219	1.459E-05	0.014
520	15600	-0.00286	1.462E-05	0.012
530	22400	-0.00345	1.465E-05	0.010
540	31700	-0.00516	1.464E-05	0.011
550	41900	-0.00571	1.466E-05	0.009
560	51500	-0.00916	1.462E-05	0.012
570	60600	-0.00941	1.464E-05	0.010
580	70300	-0.01045	1.465E-05	0.010
590	76800	-0.01195	1.464E-05	0.011
600	72840	-0.00943	1.467E-05	0.009
610	57300	-0.00556	1.470E-05	0.007
620	37800	-0.00274	1.473E-05	0.005
630	21600	0.001199	1.486E-05	-0.004
640	11690	0.004346	1.517E-05	-0.025
650	6500	0.00573	1.568E-05	-0.060

table 5.5: Degree of isomerisation in benzene solution from direct excitation (molar absorption coefficient in units of $\text{dm}^3 \text{mol}^{-1} \text{cm}^{-1}$, concentration in mol dm^{-3})

Similar calculations performed for the same dye at 1.68×10^{-5} M in acetonitrile solution under the same conditions of excitation yield the results shown in table 5.6. It is obvious from this data that a similar trend is present to that seen in benzene solution, although the conversion to isomer is significantly higher in acetonitrile solution. Hence we may use the average values for the degree of isomerisation at wavelengths shorter than 590nm in both solvents as the required value in the modelling of the data.

λ/nm	$\epsilon(\text{GS})$	ΔA	$[\text{GS}]_t$	Conversion
500	5240	-0.0064	1.56E-05	0.073
510	8570	-0.0099	1.56E-05	0.069
520	13200	-0.0163	1.56E-05	0.074
530	19500	-0.0264	1.54E-05	0.081
540	28100	-0.0365	1.55E-05	0.077
550	39000	-0.052	1.55E-05	0.079
560	50900	-0.063	1.56E-05	0.074
570	62500	-0.08	1.55E-05	0.076
580	73600	-0.093	1.55E-05	0.075
590	85000	-0.103	1.56E-05	0.072
600	94000	-0.105	1.57E-05	0.066
610	92500	-0.099	1.57E-05	0.064
620	76200	-0.069	1.59E-05	0.054
630	51800	-0.029	1.62E-05	0.033
640	30600	0.009	1.71E-05	-0.018
650	16900	0.038	1.90E-05	-0.134

Table 5.6: Degree of isomerisation in acetonitrile solution from direct excitation (molar absorption coefficient in units of $\text{dm}^3 \text{mol}^{-1} \text{cm}^{-1}$, concentration in mol dm^{-3})

From the output of the modelling program, it is clear that the critical parameter, as would be anticipated, is the pulse energy; hence this is the major source of uncertainty in the calculated yields. In fact, the calculated yield changes in exact proportion with the pulse energy. Changing factors such as the state lifetimes has a much lesser effect on the final result. Hence the uncertainty in the final calculations will reflect the uncertainty with which the energy density is calculated, which compounding the error in the molar decadic absorption coefficient of the TPP triplet with that in determining the absorbance change leads to an overall error in the estimation of the energy input of approximately $\pm 10\%$. The overall error in the calculated quantum yields is thus quite large at around $\pm 25\%$. The calculated quantum yields for isomer production from the 6-CO₂Et substituted PT dye in acetonitrile and benzene solutions are shown in table 5.7.

Solvent	Conversion (measured)	Quantum yield (calculated)
Benzene	0.011 ± 0.001	0.0021 ± 0.0006
Acetonitrile	0.075 ± 0.006	0.014 ± 0.004

Table 5.7: Anti isomerisation quantum yields for the 6-CO₂Et substituted PT dye in benzene and acetonitrile solution calculated from the measured conversion

Hence it is obvious that the effects described above i.e. relaxation of the dye excited states during the pulse and subsequent re-excitation of the dye molecules has a significant effect on the observed conversion to anti isomer, and the calculated quantum yield of isomer production is consequently considerably less than the measured conversion.

5.6 Effect of dissolved oxygen and β -carotene concentration on isomerisation yields

As mentioned earlier (section 1.7), an effect of dissolved oxygen concentration on the quantum yield of anti isomer production has been reported both for pyrazolone azomethine dyes in solvents containing a heavy atom such as chlorobenzene and bromobenzene^[53], and for a 6-methyl substituted pyrazolotriazole (PT) dye in ethanol solution^[54]. The effect of oxygen concentration has been to reduce the observed degree of conversion to anti isomer. This implies the presence of an intermediate state, suggested by the investigators as a triplet state, in the pathway with sufficient lifetime to be quenched appreciably by oxygen. In addition, quenching of this state must result in a different ratio of syn to anti isomer production as compared with unimolecular relaxation of that state. Consequently, studies were conducted here using nanosecond laser flash photolysis involving a range of PT dyes and solvents to investigate this reported effect further. Using both oxygen and β -carotene

(having an estimated triplet energy of some 75kJ mol^{-1} ^[113] and as a consequence should be capable of quenching the dye triplets by energy transfer) as energy acceptors, no effect of their concentration on the observed isomerisation yield could be detected to within the error of the experiments. This error was determined as 4%, and hence any effect of oxygen or β -carotene concentration would have to have been somewhat less than this, while the effect reported in the literature is considerably larger. The particular PT dye used in the previous work^[54] where an effect was observed, the 6-methyl derivative, was not available for the studies presented here, but experiments with a 6-methyl substituted dye having a different ballast group and substitution on the nitrogen of the p-phenylenediamine group, dye E1, again yielded negative results. There is also no evidence from other sources which suggest the involvement of a triplet state in the isomerisation pathway from direct excitation. If the oxygen effect reported were indeed the result of quenching of a triplet state, then given the triplet energies of the PT dyes they would be anticipated to produce singlet oxygen. In fact, in experiments conducted using singlet oxygen luminescence detection, where a yield of 1% is detectable^[114], no singlet oxygen phosphorescence was detected following photolysis of any of the PT dyes in oxygenated solution. The fact that a 7% decrease in isomer yield on going from aerated to oxygenated solution was reported by Douglas^[54] suggests that the singlet oxygen so produced should be readily detected. A possible explanation for these observations is that appreciable population of the triplet state occurs only from the singlet state of the anti isomer. The experiments conducted here employed 532nm excitation using the second harmonic of a Q-switched Nd:YAG laser, and consequently very little excitation of the anti isomer would be

anticipated on the basis of the anti isomer absorption profiles calculated in section 5.4 and shown diagrammatically in figure 5.6. In the experiments performed by other authors^{[53][54]}, a flashlamp discharge was used as the excitation source. As a consequence a larger frequency bandwidth than in the laser photolysis experiments will have been used, allowing excitation of the anti isomer and hence triplet state production. If this explanation is indeed the case, it will have profound implications for the photofading of these compounds in the coating environment. If fading occurs predominantly from the triplet state, either by unimolecular photolysis or via a mechanism involving the production of singlet oxygen, then the steady state population of the anti isomer and its absorbance profile must be taken into account in the interpretation of fading data. This is discussed in more detail in chapter 7. However, a second explanation based on the large excitation frequency bandwidth used in the flashlamp excited experiments may be advanced, namely that there may be components of sufficiently short wavelength to excite the dye into the second excited singlet state, from where intersystem crossing (probably to the second or even a higher triplet state) may occur with greater efficiency than intersystem crossing from S_1 , possibly as a result of smaller S_2-T_n splitting. This again will have implications for photofading experiments, leading to a wavelength dependency of fading if, as is probable, dye fade occurs with differing quantum yields from the various triplet and singlet states which may be involved. This is also discussed in greater detail in chapter 7.

5.7 Anti isomer relaxation rates

Once the anti isomer has been populated, either as a result of direct excitation of the dye or by triplet energy transfer from a suitable donor, it thermally

relaxes back to the stable syn configuration via a unimolecular process. The rate of this process shows a temperature dependence, although activation energies for the process have not been determined here. The relaxation time is also strongly dependent upon both solvent and the nature of the substituent in the 6-position of the pyrazolotriazole ring system of the azomethine dye. Data for the relaxation of anti to syn isomers for a range of substituents and solvents is given in table 5.8. Here, $\bar{\tau}$ (mean \pm standard deviation of replicate determinations) is the lifetime of the anti isomer (i.e. the time taken for the magnitude of the absorbance change to fall to $1/e$ of its initial value). All determinations were performed at $21 \pm 1^\circ\text{C}$. Concentrations were in the range 1.5 to 4×10^{-5} mol dm^{-3} , and there was no effect of concentration on lifetime over the concentration range employed.

6-substituent	Solvent	$\bar{\tau}/\text{ms}$
-CO ₂ Et	Acetonitrile	7.89 \pm 1.33
	Di-n-butylphthalate	2.13 \pm 0.20
	Methanol	0.279 \pm 0.032
	Benzene	2.22 \pm 0.42
-H	Methanol	452 \pm 4
	Benzene	590 \pm 25
	Chlorobenzene	424 \pm 3
-CH ₃ (dye E1)	Methanol	3.4 \pm 0.5
	Acetonitrile	8.5 \pm 1.5

Table 5.8: Anti isomer relaxation rates

The dielectric constants and viscosities of the solvents used in performing the relaxation time experiments are shown tabulated in table 5.9. All parameters are at 20°C ^[115].

Solvent	Viscosity @ 20° C /cp	Dielectric Con- stant @ 20 °C
Acetonitrile	0.35	38.8
Benzene	0.65	2.28
Methanol	0.597	32.6
Chlorobenzene	0.799	5.71
Di-n-butylphthalate	20.0	6.44
Glycerol	1490	42.5

Table 5.9: Physical properties of solvents

There are several important points to note from this data. There is no correlation between isomer lifetime and solvent viscosity or dielectric constant; this is illustrated by data obtained for the relaxation times for the 6-CO₂Et substituted PT dye anti isomer in a range of methanol/glycerol mixtures, shown in table 5.10.

glycerol/methanol ratio	$\bar{\tau}/\mu\text{s}$	η/cp
Pure Methanol	279 ± 32	0.55
5:20	156 ± 18	0.88
12:13	164 ± 7	6.6
20:5	174 ± 12	133
24:1	385 ± 63	640

Table 5.10: 6-CO₂Et substituted PT anti isomer relaxation times in glycerol/methanol mixtures
Here, the tabulated viscosity is only approximate, being calculated using the equation given by Green^[116] calibrated using the data presented by Timmermans^[117]; at low viscosities there is good agreement between calculated and measured viscosities for such mixtures, but at the higher viscosities the error may be as large as ±15%. However, even allowing for such errors, it is clear that while there is a trend of increasing isomer

lifetime with increasing viscosity, this is not the only factor at work, as illustrated by the fact that even with 20 parts glycerol to 5 parts methanol, and consequently an appreciable viscosity, the isomer lifetime is still shorter than observed in pure methanol. The rate of the relaxation process will be determined in part by the free energy of solvation of the transition state through which the interconversion proceeds, since this will affect the activation energy. For a unimolecular pathway as considered here, if the transition state carries a charge greater than the reactant, it will be stabilised relative to that reactant by a polar solvent and the activation energy for the process will be lowered; the converse will be true in a non-polar solvent. It is therefore worthwhile considering the nature of the dyes investigated here and the sort of transition states we would expect for the ground state isomerisation process (see section 1.7 for a discussion of the factors influencing the isomerisation mechanism). The general structure of the dyes is shown in figure 5.8.

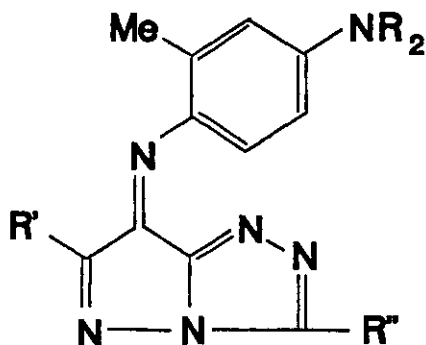


Figure 5.8: General PT dye structure

Clearly, the group in the para position on the aromatic ring attached to the azomethine nitrogen, NEt_2 , is strongly electron donating and as such would be expected to facilitate a torsional mechanism for isomerisation, involving rotation about the carbon-nitrogen double bond,

via the kind of transition state indicated in figure 5.9, where the negative charge will be delocalise over the pyrazolotriazole ring system. Note that the 6-substituent on the pyrazolotriazole ring system is not directly involved in this delocalisation, although undoubtedly it will influence the electron density in the PT ring system and hence the stability of the possible canonical structures. Therefore a degree of charge separation during the isomerisation process is anticipated to occur, and as such the energy of activation associated with the process may be expected to be lowered in highly polar or polarisable solvents. Inspection of the data of tables 5.7 and 5.9 clearly demonstrate that such a simple relationship between polarity and lifetime does not prevail. However, one of the possible canonical structures which may be drawn for the torsional mechanism transition state (figure 1.10) involves a biradical structure formed by homolytic rather than heterolytic cleavage of the azomethine double bond.

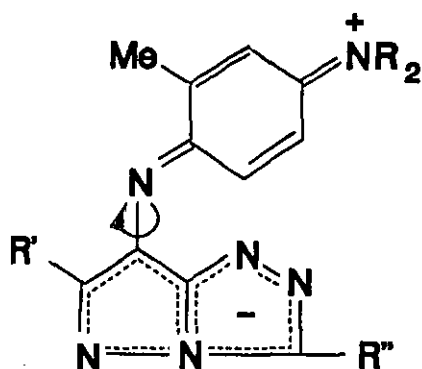


Figure 5.9: Schematic representation of a possible transition state in the PT dye torsional isomerisation mechanism

Indeed, data presented by Douglas suggests that the 6-CO₂Et substituted PT dye may isomerise via such a biradicaloid intermediate, this biradical having triplet character assigned on the basis of the pre-exponential

factor determined from Arrhenius plots^[118]. The difference in pre-exponential factor between, for example, the 6-Me and the 6-CO₂Et derivative is of the same order as that between those for stilbene and p-amino-p'-nitrostilbene where such a change in mechanism from a singlet dipolar to a triplet biradical mechanism has been proposed^[119]. The possibility of a triplet biradical mechanism for the isomerisation of these compounds is not unreasonable on the basis of the low lying triplet states, and the existence of a triplet state pathway to isomerisation is known. It is, however, difficult to rationalise the large solvent effects on the thermal back isomerisation rate in the 6-CO₂Et derivative on the basis of such a mechanism alone, and the implication therefore is that other processes must be at work in determining the isomer lifetime. One which must be considered is the relative solvation efficiencies of the two isomeric forms in the various solvents. Clearly if the anti isomer is stabilised in a particular solvent relative to the syn isomer as compared with some other solvent, then the isomer lifetime in the former may be anticipated to be longer. Such stabilisation effects may have their origin in differences in the degree of resonance delocalisation in the two forms and their relative dipole moments. There may also be entropy effects at work affecting the free energy of solvation, as a result of changes in hydrogen bonding in some solvents. In addition, it has been noted that the rate of back isomerisation is increased in protic solvents, as a consequence of protonation of the azomethine nitrogen atom^[120], which may explain the very large difference in isomer lifetime seen in comparing methanol and acetonitrile solutions where many of the physical solvent properties are similar. It is therefore anticipated that there may be other specific solvent-solute interactions such as this at work in determining

the stability of the states involved in any given solvent and hence the rates of anti-syn isomerisation. The thermal back isomerisation rates of the 6-H and 6-Me derivatives are much less sensitive to solvent changes than is the 6-CO₂Et. This factor may suggest that a different mechanism is dominant in these compounds, possibly one involving less of a change in charge distribution in the transition state relative to the stable conformations such as inversion over the azomethine nitrogen.

5.8 Flash photolysis studies of azine dyes

Azine dyes as a class are structurally very similar to the azomethine dyes, having a carbon-nitrogen double bond as a constituent of the chromophore, but the overall structure is held in a rigid geometry by the presence of an additional single bond (figure 5.10). These dyes exhibit a single peak in their ground state absorption spectrum with a λ_{max} at around 420nm, and consequently appear yellow in solution. However, aside from their triplet energies, which are similar to those of the corresponding dyes not possessing the extra bond, they display quite different photochemical and photophysical properties to the corresponding azomethine systems.

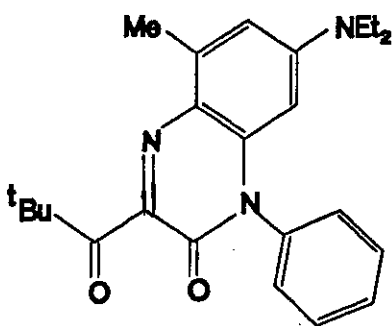


Figure 5.10: General structure of azine dyes

The most striking feature is that fluorescence from these compounds is readily observed, they emitting with a fluorescence quantum yield of 0.009 ± 0.002 relative to

fluorescein in glycerol as a standard (for which $\phi_f=1$ ^[122]). Their first excited singlet state lifetimes, as determined by single photon timing measurements, are approximately 600ps. Using nanosecond laser flash photolysis triplet-triplet absorption spectra are easily observed, assignment of the transient as being due to the triplet state is confirmed using oxygen quenching and beta-carotene sensitisation experiments. The triplet state lifetime is some 70 microseconds in degassed methanol. The triplet-triplet absorption spectrum is very broad, there being absorption throughout the visible region; the spectrum recorded in acetonitrile solution is reproduced in figure 5.11. In addition, azine dyes are efficient sensitisers of singlet oxygen. The quantum yield of singlet oxygen production from the azine dye shown in figure 5.10 in acetonitrile solution has been determined as 0.26 ± 0.02 from singlet oxygen luminescence measurements using phenazine as a standard (for which $\phi = 0.83$ ^[122]). The quantum yield was calculated from the ratio of the slopes of plots of singlet oxygen emission intensity as a function of laser energy from solutions of phenazine and azine in acetonitrile. The plots are shown in figure 5.12. A correction factor corresponding to the ratio of the phenazine solution absorbance to the azine solution absorbance was applied to the slope of the azine plot to correct for slightly differing absorbances by the two solutions. This correction was considered valid since the difference in absorbances was less than 10%. The singlet oxygen quenching constant for the same dye in acetonitrile solution was determined also using singlet oxygen luminescence measurements, here the singlet oxygen lifetime as a function of azine concentration being the parameter of interest. The quenching constant was determined as $7.5\pm 0.5 \times 10^6 \text{ dm}^3 \text{ mol}^{-1} \text{ s}^{-1}$, the plot of singlet oxygen lifetime as a function of dye

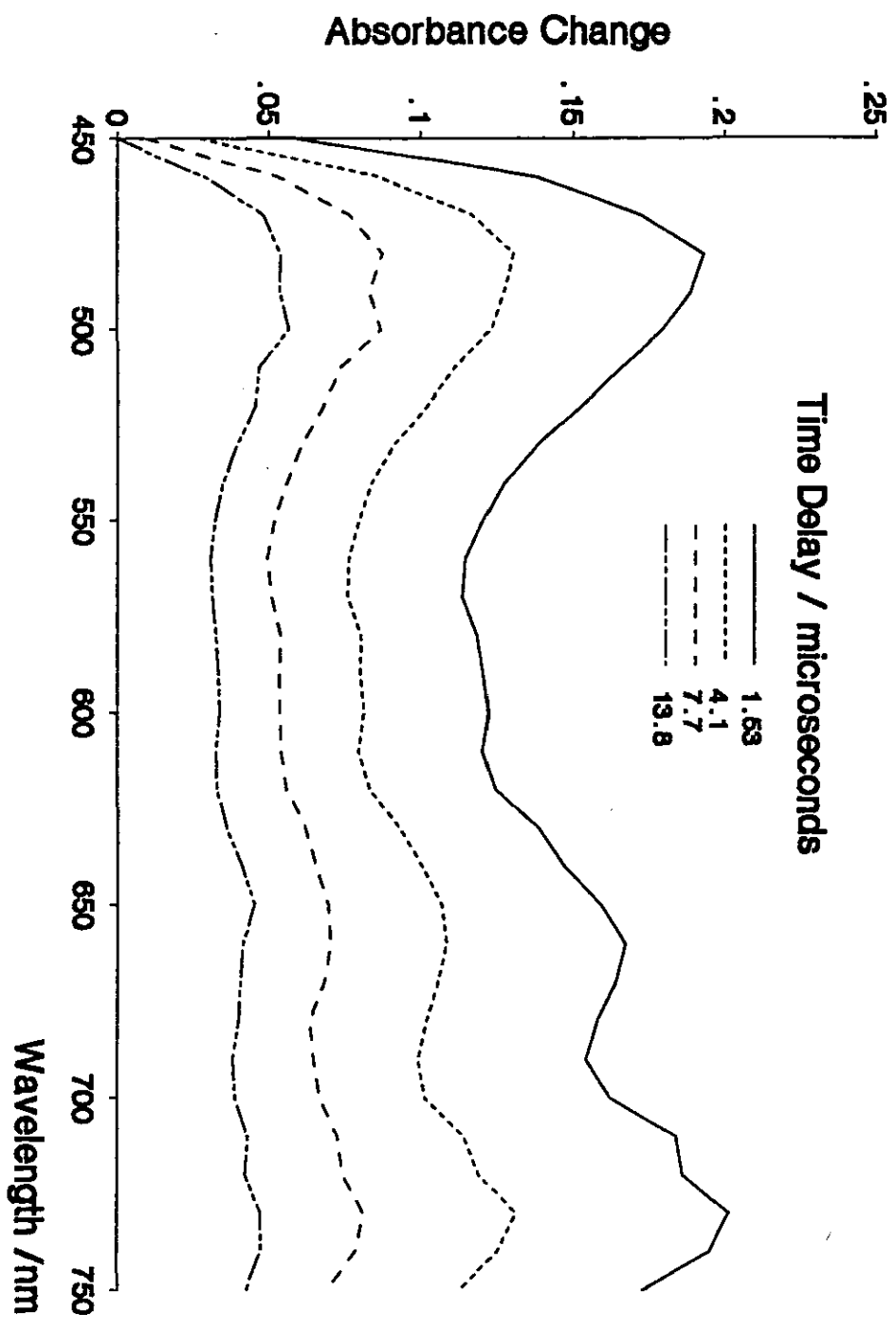


Figure 5.11: Transient difference spectrum of azine dye in acetonitrile solution following 354nm excitation

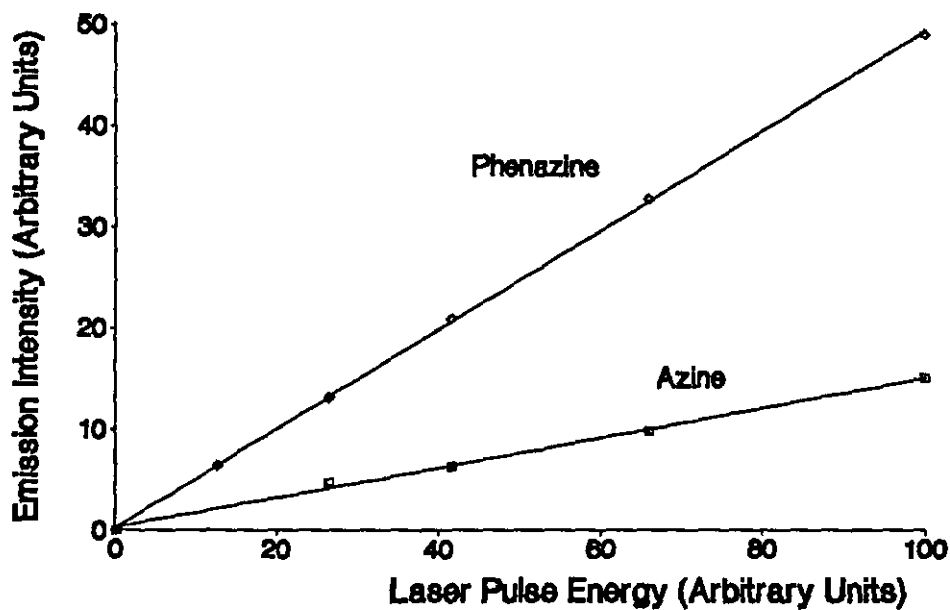


Figure 5.12: Singlet oxygen emission intensity as a function of laser intensity for solutions of phenazine and azine in acetonitrile

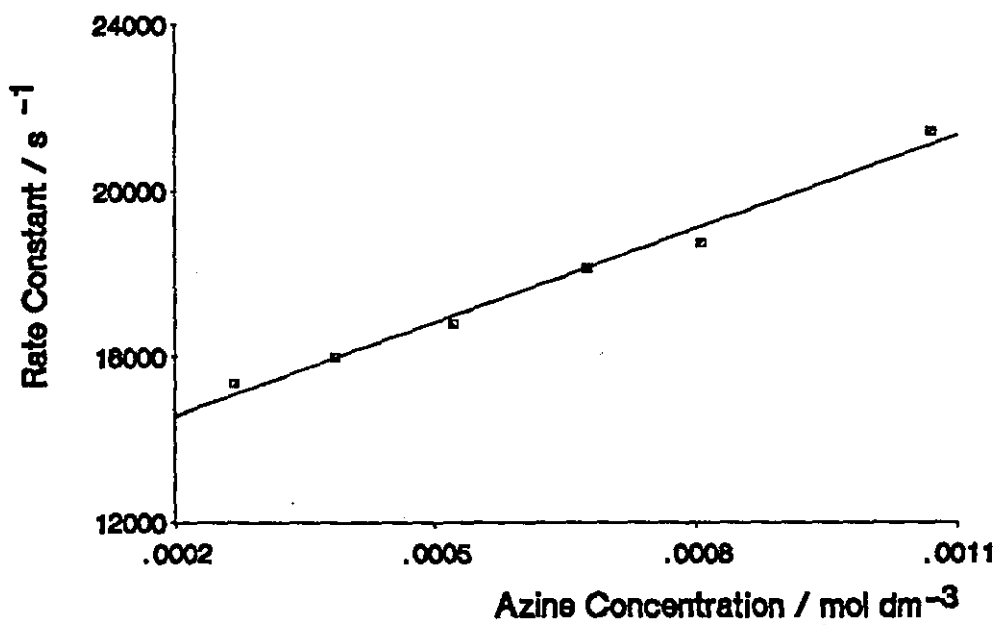


Figure 5.13: Singlet oxygen deactivation rate constant in acetonitrile solution as a function of azine concentration

concentration being reproduced in figure 5.13. From the good light stability of the azine in oxygenated solution it is inferred that physical quenching of singlet oxygen is the major relaxation mechanism, probably via a charge transfer process involving the tertiary amine group para to the azomethine nitrogen. This series of investigations involving a dye with structural similarities to the azomethine systems but without the flexibility in the dye skeleton illustrates very well the effect such flexibility can have on the photophysics of a molecule. In this instance the effects are to shorten considerably both singlet and triplet state lifetimes, and thereby to decrease both the fluorescence and intersystem crossing yields.

Chapter 6

Picosecond Flash Photolysis Studies

6 Picosecond pump-probe laser flash photolysis

6.1 Introduction

The advent of commercially available mode-locked laser systems as reliable sources of picosecond and, more recently, femtosecond light pulses has allowed photochemists access to events occurring on these timescales, and through the use of pump-probe laser flash photolysis (section 3.3.6) it has been possible to probe the time evolution of very short lived, non-emissive states. As such, picosecond pump-probe laser flash photolysis is an ideal tool with which to attempt to characterise the excited state behaviour of pyrazolotriazole azomethine dyes. Before describing the results obtained it is necessary to describe the possible events which could take place in such systems and the spectroscopic characteristics expected.

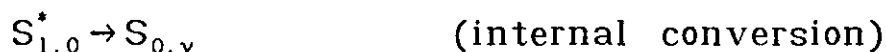
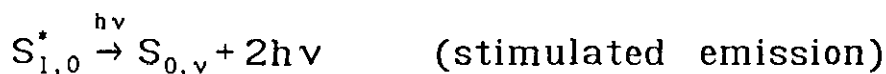
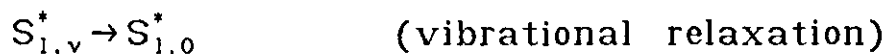
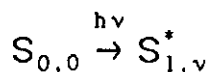
Vibrationally excited states in fluid solution at room temperature relax on timescales of a few picoseconds in many cases; for example in dyes such as the rhodamines, vibrational relaxation times have been measured to be from four to six picoseconds, with only a very small solvent viscosity dependence^[123]. This has been attributed to the vibrational relaxation in this dye class being an intermolecular process arising from coupling between the dye and the solvent; the mechanism of this coupling is thought to involve hydrogen bonding via the carboxylic groups on the rhodamine, vibrational energy being transferred into the modes of the hydrogen bond, or through it to the solvent molecules^[124]. Vibrational relaxation in the first excited states of azulene^[125] and coumarins^[126] are a little shorter than the rhodamines, being some one to two picoseconds. In rigid, non-polar molecules such as perylene, vibrational relaxation in the first excited singlet state occurs much more slowly over a period of around 30ps^[127]. In this

instance the solvent acts only as an energy sink and there is very little coupling between solvent and solute; thus the rate of internal conversion between the vibrational levels will depend only on the internal parameters of the molecule. In larger, flexible molecules containing functional groups, vibrational relaxation will take place via both inter- and intramolecular processes, via coupling with the solvent and through redistributing the vibrational energy through the degrees of freedom in the molecular skeleton^[128].

Vibrational relaxation may be probed principally by two means; for emissive S_1 states, the rise of population of the $S_{1,0}^*$ state following pulsed excitation to a state $S_{1,v}^*$ may be monitored as the gain in a probing beam of appropriate wavelength as a result of stimulated emission from the $S_{1,0}^*$ state. Where significant stimulated emission cannot be observed, vibrational relaxation may be probed by monitoring changes in the excited state absorption spectrum with time. Since following pulsed excitation the state $S_{1,v}^*$ evolves to $S_{1,0}^*$ by radiationless transitions, there is expected a change in the absorption spectrum of S_1^* since it will embody contributions from all of the intermediate states whose populations are time dependent. Such changes are often observed as shifts in and narrowing of the absorption bands in question. The general scheme for such a simple internal conversion process may be formulated as equations 6.1.

Polymethine dyes as a class of compound have received some attention from studies in the picosecond time domain^{[129]-[134]}, and if evolution of the transient absorption induced by excitation with picosecond pulses is monitored in a region of ground state absorption there is observed an initial bleaching which recovers to a

level somewhat higher than that prior to excitation. This increased absorption has a lifetime of the order of microseconds to milliseconds, dependent upon solvent



(equations 6.1)

properties. This long-lived species is assigned as being an isomeric form of the dye resulting from rotation about the carbon-carbon double bonds in the polymethine chain. The potential energy surface proposed to explain the photophysical behaviour of these dyes is illustrated in figure 6.1. The fast decay component to the transient absorption is assigned as deactivation of S_1

$$k_{\text{obs}} = k_{\text{ic}} + k_p \quad (6.2)$$

assuming k''_p and k'_p are very much greater than k_p . If both k''_p and k'_p are large there will be essentially instantaneous evolution to the isomeric conformations and a very small population of the "perp" ground state (i.e. with the ring systems disposed orthogonal to one another), and hence its evolution to the two possible isomeric forms will not be observed. Fluorescence lifetimes for polymethine dyes have been found to correlate well with the absorption recovery times, supporting the hypothesis that relaxation from the excited state surface is the rate limiting step^[129]. The absence

of any fluorescence from the less stable isomeric form of the dye following excitation of the ground state conformation indicates that isomerisation takes place from the vibrationally excited ground state and that the region of the excited state potential energy surface corresponding with the isomeric form is not populated.

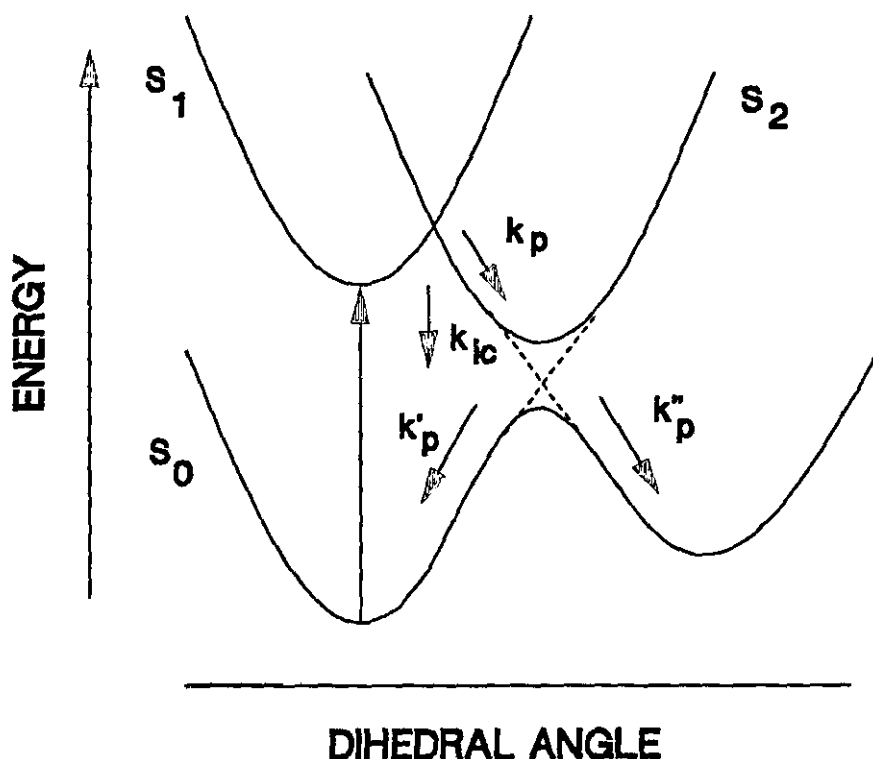


Figure 6.1: Potential energy surface for polymethine dyes

Radiationless relaxation of the first excited singlet state has been demonstrated for crystal violet in alcoholic solution to be mediated by conformational relaxation^[130], and hence some solvent dependency of the singlet state lifetimes are expected for flexible dye systems. This is indeed observed for the polymethine dyes, where fluorescence quantum yields increase significantly with increasing solvent viscosity. The maximum fluorescence quantum yields are observed in rigid low-temperature glasses, as is also the case in the azomethine dyes. The rate of internal conversion between the excited and ground states will depend in part on the

magnitude of the Franck-Condon factors describing the overlap of the vibrational states of the ground and excited states. These Franck-Condon factors decrease exponentially with increasing energy gap between ground and excited states^[131]; since this energy gap is determined by the dihedral angle between the ring systems, the rate of internal conversion will increase rapidly as the molecular conformation approaches a dihedral angle of 90 degrees, the precise manner in which the internal conversion rate varies being dependent upon the shapes of the potential surfaces (section 1.6).

In the polymethine dye DDEOCI, the recovery kinetics of the S_0 state are demonstrated to follow a three exponential decay scheme; two of the lifetimes are on picosecond timescales, and one on nanosecond. This is attributed to the dye in question existing as two isomeric forms in the ground state with overlapping absorption spectra. Excitation of both forms then takes place, the barrier heights from the singlet of each form to the perp conformation in the excited state being different giving rise to differing relaxation rates. The two picosecond components are then relaxation of the two singlet states to the perp conformation. Having reached this conformation, relaxation then follows immediately to either the cis or the trans isomeric form^[132]. Non-radiative transitions in many such dyes proceed principally via this twisted conformation^[133]. In some polymethine dyes, such as HITC, it has been demonstrated that the triplet state is populated from direct excitation, although in small yield^[134]. The triplet-triplet absorption spectrum of this dye lies in the 860nm to 960nm region, while the S_0 to S_1 absorption occurs at 700nm to 800nm. In contrast, the triplet state of for example DODCI cannot be populated by direct excitation.

In using picosecond pump-probe techniques, or indeed

emission techniques such as single photon timing or streak cameras having picosecond resolution (section 1.4.1), attention must be paid to rotational diffusion of the molecules being studied since this process occurs on timescales coincident with many of the kinetic processes being probed. The phenomenon arises since in general the excitation pulse and the probing pulse are linearly polarised. This polarised excitation pulse creates instantaneously a set of oriented excited state molecules, the time evolution of these excited states being the parameter of interest. If, however, these excited states are probed using a polarised pulse then there exists the possibility in such an experiment of probing not only the kinetics of evolution of the excited state, but also the rotational diffusion dynamics of the molecules. It is, however, possible to obtain transient kinetic data free from distortion by rotational diffusion provided the dynamics thereof are identical for the ground and excited state molecules by arranging the angle θ between the polarisations of the two beams such that

$$\tan^2 \theta = 2 \quad (6.3)$$

or $\theta = 54.7^\circ$ ^[135]. In flexible dye systems such as those studied here, however, although the instantaneously produced state will have the same conformation and hence diffusional characteristics as the ground state, there is very rapid conformational change from this state resulting in differing hydrodynamic radius and moment of inertia as compared with the ground state. Hence the above relation may not hold for this system and even working with so-called "magic angle" relative polarisations there may still be a contribution to the observed kinetics from rotational diffusion.

6.2 Kinetic Data

Detailed kinetic data at a limited range of wavelengths was collected for the 6-CO₂Et substituted Pt dye and dyes E1, A2, B1 and B2. The 6-CO₂Et substituted dye was investigated in detail at a range of wavelengths and in a range of solvent systems, as a consequence of its ground state absorbance spectrum being bathochromatically shifted relative to many PT azomethine dyes and therefore being very amenable to study using the range of pumping and probing wavelengths available at the Rutherford-Appleton laboratory. The other dyes were included in the studies to assess the effects of structural modifications on the lifetimes of the transients observed, and data was recorded in a much narrower range of wavelengths in these cases. Examples of the data traces recorded for the 6-CO₂Et substituted dye in di-n-butylphthalate solution are shown in figure 6.2, and further data is presented in figures 6.5 to 6.9. Some general points which should be made about the kinetic data are

(a) For all dye and solvent systems it was determined that the magnitude of the observed transient absorption was proportional to the laser pulse energy in the range of pump pulse energies used (3 to 10 μ J per pulse).

(b) Experiments involving changing the relative polarisation of the pumping and probing beams demonstrated that while the signal recorded with orthogonal polarisations was approximately 2/3 the size of that with parallel polarisations, the normalised traces were superimposable. All the data presented were recorded with pumping and probing beams oriented at 54.7° to one another to reduce any effects introduced by rotational diffusion, although there was no detectable difference between the shapes of the data traces recorded with this so-called "magic angle" arrangement and that with parallel or perpendicular relative polarisations.

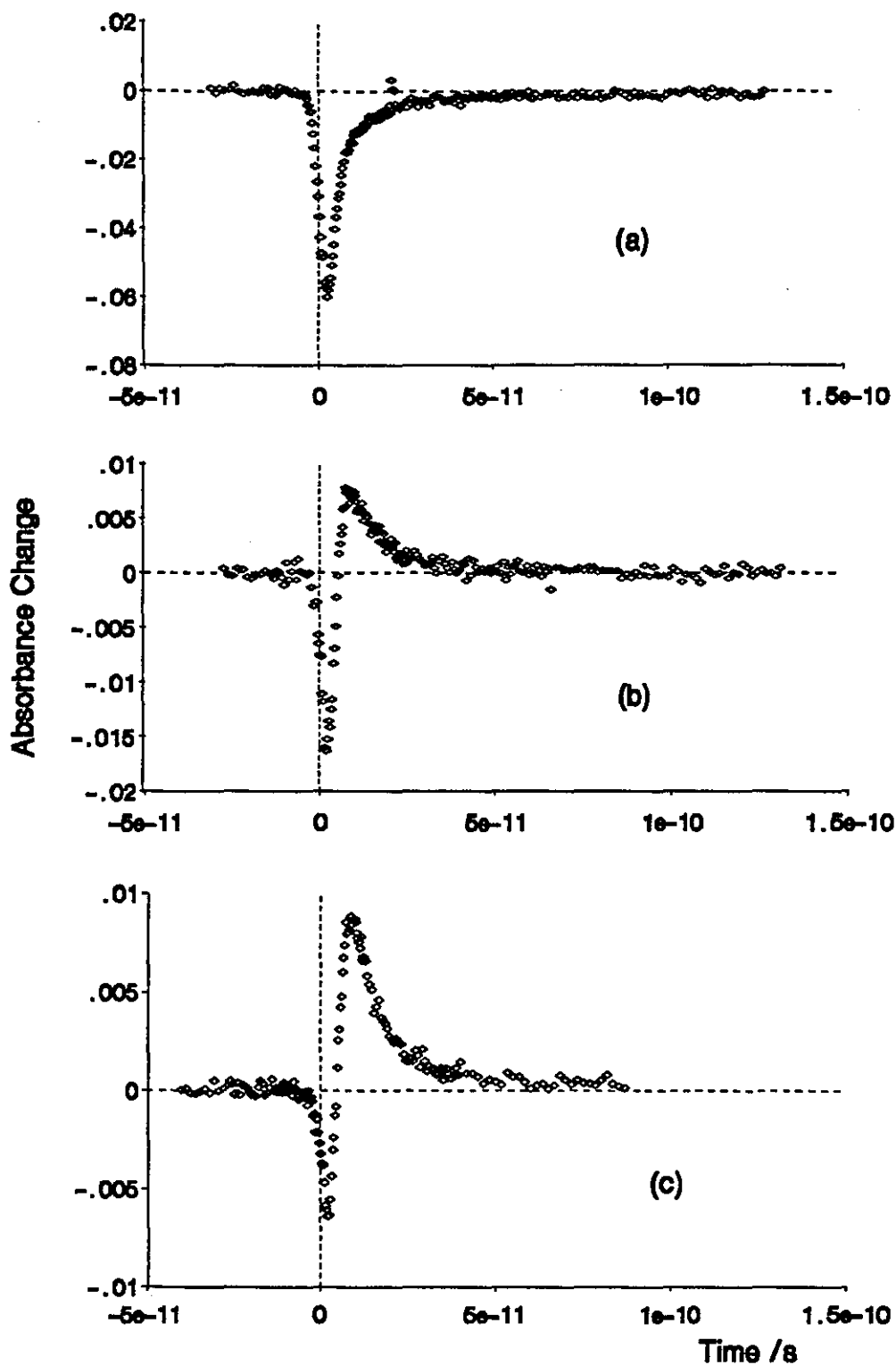


Figure 6.2: Transient difference data traces for the 6-CO₂Et substituted PT dye in di-n-butylphthalate solution probed at (a) 600nm (b) 640nm (c) 650nm

(c) Measurements of the absorbance spectra of the dyes in solution prior to and following the experiments revealed that no detectable sample degradation had occurred, except in the case of the 6-CO₂Et substituted dye in the hand coating. Here it was found that the coating suffered very rapid damage from laser irradiation, which is attributed to thermal breakdown of the coating structure. Although the absorbance of the coating as a whole was measured as 0.35 at the pumping wavelength (585nm), the absorbance of the individual dye-containing droplets within the coating is calculated as being in excess of 1, and hence a large amount of energy will be deposited into a very small (300 to 600nm diameter) oil droplet and the consequent thermal expansion will disrupt the coating structure. As a consequence, in order to record the data trace for the 6-CO₂Et dye in the coating presented in figure 6.10 the sample was changed every five data points. A possible way in which to overcome this problem would be to have a lower dye concentration in the droplets and a thicker coating, which would then give the same overall absorbance. However, as noted in chapter 7 changes such as these to the coating may have profound effects on the observed properties of the coatings, and as a consequence a system as close as possible to the real situation was used.

6.3 Kinetic Model

The kinetic model used as a basis for interpreting the picosecond pump-probe laser flash photolysis data obtained for pyrazolotriazole azomethine dyes is shown schematically as a one-dimensional potential energy surface in figure 6.3.

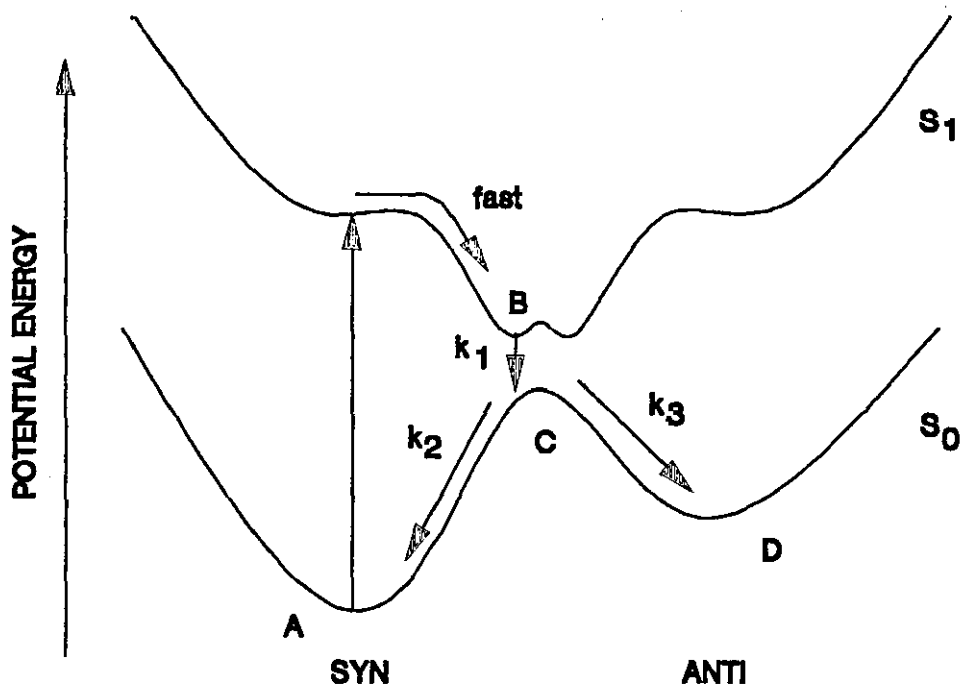


Figure 6.3: Potential energy surface for azomethine dyes

The assignments of levels A, B, C and D are discussed in the following sections. Drawing analogies with the polymethine dye systems, the effects of any steric hindrances at work may be expected to be minimised at the perp ground state conformation where the pyrazolo-triazole and phenylenediamine ring systems are disposed perpendicularly with respect to one another; however, this does not correspond with a potential minimum on the ground state potential surface due to loss of resonance stabilisation in such a configuration. Again by analogy with the polymethine dyes, in the excited state restrictions of resonance stabilisation are likely to be less and the potential barrier therein may be very small at room temperature^[136]. The red-shifted absorption spectrum of the anti isomer may be explained in terms of an increased ground state potential energy over that of the syn form, this increased energy not being reflected to such a large extent in the excited state surface. The

nature of the data obtained, displaying at some probe wavelengths an initial decrease in absorption followed by an increase over and above the ground state absorption level at that wavelength, requires the use of at least a four-level model. Representative kinetic traces are shown in figures 6.2 and 6.5 to 6.8. The question arises as to the nature of the initial absorbance decrease; this could be due to a depletion of ground state absorption due to pumping of population to excited states with lower molar decadic absorption coefficient than the ground state, or indeed zero molar decadic absorption coefficient, at the probe wavelength, or could be attributable to stimulated emission from the upper state to the ground state at the probe wavelength. Shortening of the lifetime of the first excited singlet state would result from such a process. However, the ratio of the magnitude of the absorbance depletion to the size of the absorbance increase observed at longer times is independent of probe intensity; if stimulated emission were a significant mechanism in depopulating the first state produced, then since the rate of stimulated emission is proportional to the magnitude of the stimulating flux (equation 1.32) the level of transmittance increase observed should increase, and that of transmittance decrease should be reduced, with increasing probe intensity. Hence stimulated emission, although possible as a contributory state depopulation mechanism, appears from the experimental data to not be a significant pathway; it is not possible, though, even invoking stimulated emission as a possible mechanism, to explain the observed results on the basis of a system containing less than four effective levels, since the superposition of an $S_x \leftarrow S_1$ transition with an induced $S_0 \leftarrow S_1$ fluorescence would result in the observed transmittance change having the same sign at all times^[137]. Inspection of the data reveals that this is

clearly not the case here. For the purposes of modelling this data, then, it is assumed that stimulated emission does not make a significant contribution to the excited states relaxation mechanism.

It is also necessary to consider the possibility of solvent dielectric relaxation being responsible for the observed fast relaxation process. Such a mechanism is considered unlikely on the grounds that data clearly demonstrating this component are obtained in solvents of widely differing dielectric constant. Also, dielectric relaxation in alcohols has been demonstrated to be composed of three dispersion regions, the shortest lifetime of which is 2.2ps in n-propanol at 298K^[138]. This is assigned as rotation of the -OH group, but accounts for only some 5% of the total dielectric relaxation. Since the second relaxation time, assigned as rotation of free alkyl chains, has a lifetime of 22ps under the same conditions and has no obvious influence on the data obtained, solvent dielectric relaxation is not considered to contribute significantly to the observed transient decay profile.

As mentioned, vibrational relaxation in the excited states may make a contribution to the observed transient decay kinetics on timescales of from 1 to 30 ps. This usually manifests itself as shifts in and narrowing of the absorption bands, but since significant spectral resolution was not available in these studies, such effects are difficult to detect. However, profound shifts in the absorption spectra of the excited state would have to take place in order for vibrational relaxation to explain the observed shapes of the transients. It is therefore considered more likely that the first component observed in the transient decay is a result of evolution of the excited state population toward the perp geometry rather than simply vibrational relaxation in the initially

formed state.

Having decided upon the potential surface model which will be used, then, it is necessary to derive the system of differential equations which will describe this model. In so doing, there are certain assumptions which have been made in order to simplify the model from the standpoint of fitting it to the experimental data. The important assumptions are

(a) There is no direct relaxation pathway back to the ground state from the point on the excited S_1 potential surface to which excitation occurs initially. This assumption is made to reduce the number of rate constants and quantum yields that need to be fitted in the final model, and should only affect the molar absorption coefficients determined for the states involved and not the lifetimes. This type of scheme has precedent in experiments with polymethine dyes, where at higher temperatures and low viscosity intramolecular twisting is postulated as the dominant non-radiative process for the excited singlet state^[139]. As will be demonstrated later, this assumption appears valid for these dyes also on the basis of the assignments of the states involved.

(b) Both the exciting and probing pulses are gaussian energy functions with respect to time, and both are the same width. The assumption that the pulse is gaussian is included to simplify the mathematical manipulation of the differential equations, although whether or not this is a totally accurate description of the pulse shape is not known and has not been determined for the picosecond laser system at the Rutherford-Appleton Laboratory. This is a consequence of the fact that the only diagnostic equipment on this laser system is a second harmonic generation autocorrelator, which cannot give information about the pulse shape (see section 3.3.3). In addition, the assumption that both pumping and probing pulses are

of the same width and temporal energy distribution may not be strictly valid, since the probe beam is generated via a non-linear process (section 3.3.4) and consequently some changes may be anticipated. However, since these differences have not been quantified the assumption is made that both pulses are the same rather than introducing an arbitrary difference between the pulses.

(c) There is no absorption by the excited states of the pump photons. This assumption is made given that there is no data available on the actual magnitudes of the molar absorption coefficients of the states involved, and that the populations of the states during the pumping pulse are sufficiently small that they will not absorb a significant quantity of the pumping pulse.

The equations which describe the potential surface model are shown as equations 6.4.

$$\begin{aligned}\frac{dA}{dt} &= -\frac{P}{\sigma\sqrt{2\pi}} e^{-\frac{(t-t_0)^2}{2\sigma^2}} (1 - 10^{-\epsilon A}) + k_2 C \\ \frac{dB}{dt} &= \frac{P}{\sigma\sqrt{2\pi}} e^{-\frac{(t-t_0)^2}{2\sigma^2}} (1 - 10^{-\epsilon A}) - k_1 B \\ \frac{dC}{dt} &= k_1 B - (k_2 + k_3) C \\ \frac{dD}{dt} &= k_3 C\end{aligned}\quad (\text{equations 6.4})$$

Level A is assigned as the syn isomer ground state, and level D as the corresponding state in the anti isomer. The assignment of the levels B and C as points on the potential surfaces is discussed in section 6.4. Here the rate of depletion of the syn isomer S_0 state is treated as the rate of absorption of photons by that state in $\text{mol dm}^{-3} \text{ s}^{-1}$. In the equations P is the total number of photons input in units of mol dm^{-3} , and σ is a parameter related to the pulse width; the full-width-half-maximum

(FWHM) of the pulse is equivalent to 2.355σ . Hence to obtain the number of photons absorbed in a time interval dt , we simply take the number of photons incident and multiply by the absorbance of the sample during that time (the absorbance of the sample is defined as $1 - (\text{transmittance of the sample})$, i.e. $1 - 10^{-\epsilon c l}$). In the rate equations all other parameters relating to the rate of change of population of a given state consist of a rate constant and a state population term. It is not necessary in this modelling to take account of the return of anti to syn isomer, since this process occurs so slowly that it proceeds to a negligible extent over the timescale investigated.

6.4 Modelling of data

The parameters used as input to the modelling of data obtained using picosecond pump-probe laser flash photolysis are derived in part from the nanosecond flash photolysis studies. The parameters which come from these studies are the molar decadic absorption coefficients of the isomer at the probe wavelength, calculated from the transient difference spectra obtained in the same solvent from nanosecond flash photolysis data as described in section 5.4, assuming no absorption by the anti form in the short wavelength edge of the syn isomer absorption band. Any absorption by the anti isomer at the pumping wavelength may be neglected since there is negligible population of the anti isomer during the length of the pumping pulse. In addition, the coherent coupling artefacts (section 3.3.5) have been deleted from the data sets so as not to interfere with the fitting; this procedure can be done since the coherent spike is simply an artefact and is not influenced by the photophysical processes which are occurring and as such provides no information about these processes. The molar decadic absorption coefficients of the syn isomeric form at the

pump and probe wavelengths are obtained from ground state spectra. The molar decadic absorption coefficients used in the modelling for the 6-CO₂Et substituted dye are shown below in tables 6.1 to 6.4. The relative errors on the quoted molar absorption coefficients for the syn and anti isomers are ±6% and ±15%, respectively. The isomer yields used in the modelling are given in table 6.5, and the dye concentrations which were used in gathering the data are as shown in table 6.6.

λ/nm	$\epsilon(\text{GS})$	$\epsilon(\text{anti isomer})$
700	1300	47850
650	14800	34500
640	25150	28600
610	70250	14700
600	69250	5250
585	54400	

Table 6.1: Molar decadic absorption coefficients for the syn and anti isomers of the 6-CO₂Et substituted PT dye in methanol solution

λ/nm	$\epsilon(\text{GS})$	$\epsilon(\text{anti isomer})$
650	16500	40000
640	30700	32300
630	51700	28100
610	85400	17800
600	82900	14700
585	66900	

Table 6.2: Molar decadic absorption coefficients for the syn and anti isomers of the 6-CO₂Et substituted PT dye in di-n-butylphthalate solution

λ/nm	$\epsilon(\text{GS})$	$\epsilon(\text{anti isomer})$
650	6500	40800
640	11700	37700
585	73000	

Table 6.3: Molar decadic absorption coefficients for the syn and anti isomers of the 6-CO₂Et substituted PT dye in benzene solution

λ/nm	$\epsilon(\text{GS})$	$\epsilon(\text{anti isomer})$
650	16900	46100
640	30600	37500
585	77000	

Table 6.4: Molar decadic absorption coefficients for the syn and anti isomers of the 6-CO₂Et substituted PT dye in acetonitrile solution

Dye	Solvent	Anti Isomer quantum Yield
6-CO ₂ Et	Methanol	0.0050
6-CO ₂ Et	Di-n-butylphthalate	0.0020
6-CO ₂ Et	Benzene	0.0021
6-CO ₂ Et	Acetonitrile	0.0140
6-CO ₂ Et	Ethyl Acetate	0.0100
6-CO ₂ Et	Hexane	0.0200
E1	Toluene	0.0200
B1	Toluene	0.0100
B2	Toluene	0.0100
B2	Acetonitrile	0.0100
A2	Acetonitrile	0.0100

Table 6.5: Isomerisation quantum yields used in data modelling

Dye	Solvent	Concentration /mol dm ⁻³
6-CO ₂ Et	Methanol	5.2×10^{-6}
6-CO ₂ Et	Di-n-butylphthalate	2×10^{-5}
6-CO ₂ Et	Benzene	6.8×10^{-6}
6-CO ₂ Et	Acetonitrile	5×10^{-6}
6-CO ₂ Et	Ethyl Acetate	7×10^{-6}
E1	Toluene	4×10^{-5}
B1	Toluene	4×10^{-5}
B2	Toluene	4×10^{-5}
B2	Acetonitrile	4×10^{-5}
A2	Acetonitrile	4×10^{-5}

Table 6.6: Dye concentrations used in the picosecond pump-probe flash photolysis experiments

It should be noted that there is a trade-off in the fitting between isomer molar decadic absorption coefficient and isomer yield; an increase in one may be offset by a decrease in the other. The strategy adopted,

therefore, has been for a given dye and solvent system to fix an isomerisation yield and to adjust the molar decadic absorption coefficients such that they fit the data. This isomerisation quantum yield has been calculated for the 6-CO₂Et substituted PT dye in benzene and acetonitrile solutions from computer simulations (section 5.5), while for other dyes and solvents it has been estimated on the basis of these calculations from nanosecond flash photolysis experiments.

Modelling of the data is performed by solving equations 6.4 numerically using fourth order Runge-Kutta integration (section 4.5), and using the concentration profiles as a function of time in conjunction with the molar absorption coefficients to generate a curve corresponding to absorbance as a function of time. The parameter measured in the experiments is the difference in absorbance between the sample before excitation and the sample a time t after excitation, and hence the absorbance of the sample prior to excitation is subtracted from each calculated point to yield a transient difference curve. However, the transient difference is probed by a pulse of a finite width, and hence it is necessary to convolve the probe pulse profile with the absorbance difference profile to yield a curve corresponding with what is actually measured during the experiments. The convolution integral is defined as^[140]

$$F(t) = \int_0^t G(t)P(t-t_0)dt \quad (6.5)$$

where $F(t)$ is the measured decay profile, $G(t)$ is the actual absorbance profile and $P(t)$ is the probe intensity profile. The integration is carried out using Simpson's rule with 13 ordinates, with the probe assumed to be a gaussian function as stated earlier. An example of a calculated absorbance profile with and without probe pulse

convolution is illustrated in figure 6.4. As would be expected, the convolution has the effect of "smearing out" the absorbance profile, and can lead to the evaluation of misleadingly long pulse widths and state lifetimes if not taken account of.

The results of the fitting of the picosecond flash photolysis data indicate that, perhaps not surprisingly, certain parameters in the model are coupled such that variation in one parameter may be compensated by variation in another, the net result being no significant change in the quality of the fit. The principle couplings of parameters identified are as follows (see tables 6.7 and 6.14 for examples).

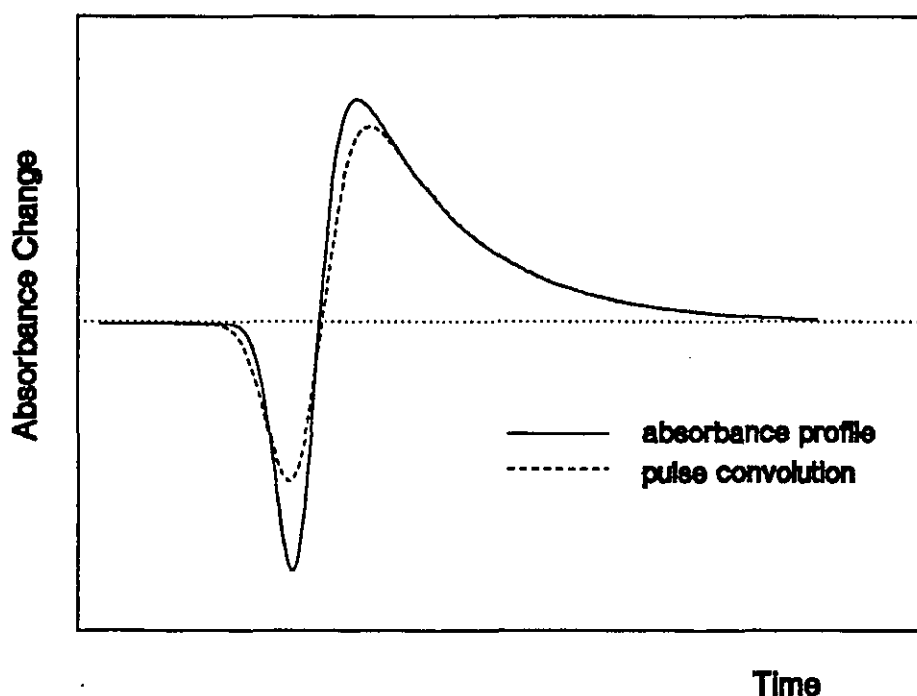


Figure 6.4: Shape of the absorbance profile with and without probe pulse convolution

(a) State B lifetime, absorption coefficient and pulse width

Increasing the lifetime of state B may be compensated by decreasing the pulse width and increasing the

absorption coefficient without significantly changing the quality of the fit. However, the relative change in pulse width required is less than that in the state B lifetime, so greater reliability may be placed on the former than the latter.

(b) State C lifetime and state C molar absorption coefficient

Increasing the lifetime of state C may be compensated by decreasing its molar absorption coefficient. However, the range of absorption coefficients and lifetimes which may be accommodated by the data is relatively small, being at the most $\pm 10\%$ on the lifetime and considerably less on the molar absorption coefficient.

It may be noticed, however, that there is considerable fluctuation in the determined isomer molar absorption coefficient from fitting of several traces recorded at the same wavelength, keeping the yield of isomer production constant in the model. This factor may be attributed to the uncertainty with which it is possible to determine the exact energy input to the sample. This uncertainty arises in part due to variations in the pump-probe overlap, i.e. if the probe beam does not quite go through the centre of the pumping beam, and also to the uncertainty in the energy distribution across the pumping beam. Hence the time- and space-averaged energy measured using a power meter at the sample may not be an accurate reflection of the energy input to the probed sample volume. Hence this uncertainty will prevail for each of the absorption coefficients determined, although the pulse width and lifetimes remain unaffected apart from the uncertainties therein described above.

The best fits to the data using the model described above are given in tables 6.7 to 6.15. Here, all absorption

coefficients have units of $\text{dm}^3 \text{mol}^{-1} \text{cm}^{-1}$. The full width half maximum (FWHM) refers to the pulse width used for both pumping and probing pulses.

λ/nm	ϵD	ϵB	$\tau B/\text{ps}$	ϵC	$\tau C/\text{ps}$	FWHM /ps
600	14000	63000	1.02	63800	5.96	3.67
610	57000	67000	1.01	69000	4.44	3.32
640 ²	29000	22000	1.17	26900	4.85	4.30
640 ¹	21000	19200	1.23	27300	4.38	2.63
640	18000	14900	1.24	28900	3.69	2.27
640	4000	19600	3.09	30900	3.64	3.13
640*	32000	22000	3.53	30600	2.70	3.38
640*	32000	19500	1.40	28500	3.06	4.06
640*	32000	18200	1.01	28000	3.26	4.11
650	29000	10300	1.91	19000	5.25	3.46

Table 6.7: Best fit parameters for the 6-CO₂Et PT dye in methanol solution (those marked * are fits to the same file from different starting points)

λ/nm	ϵD	ϵB	$\tau B/\text{ps}$	ϵC	$\tau C/\text{ps}$	FWHM /ps
600	14700	86200	1.15	79000	6.63	2.79
600	40000	78400	0.56	80000	5.59	4.13
610	86000	85500	0.96	85000	5.30	2.31
630	40000	45250	1.07	52100	11.1	7.17
650	30000	13500	1.04	17350	7.73	3.77

Table 6.8: Best fit parameters for the 6-CO₂Et PT dye in di-n-butylphthalate solution

λ/nm	ϵD	ϵB	$\tau B/\text{ps}$	ϵC	$\tau C/\text{ps}$	FWHM /ps
640	25000	10000	2.10	13200	7.41	4.74
650	49000	6000	1.17	9200	8.88	3.25

Table 6.9: Best fit parameters for the 6-CO₂Et PT dye in benzene solution

λ/nm	ϵD	ϵB	$\tau B/\text{ps}$	ϵC	$\tau C/\text{ps}$	FWHM /ps
630	28000	20700	0.68	31100	8.70	3.49
640	30000	15500	0.53	32500	9.57	3.61
650	20000	5100	0.55	20100	10.1	3.34

Table 6.10: Best fit parameters for the 6-CO₂Et PT dye in acetonitrile solution

Dye	ϵD	ϵB	τB /ps	ϵC	τC /ps	FWHM /ps
A2	1100	200	3.2	740	12.4	8.2
B2	1700	300	1.8	540	15.9	6.1

Table 6.11: Best fit parameters for PT dyes A2 and B2 in acetonitrile solution with 640nm probe

λ /nm	ϵD	ϵB	τB /ps	ϵC	τC /ps	FWHM /ps
630	3500	800	0.5	2000	4.72	2.46
640	3500	800	0.93	2050	4.71	2.46
650	1000	440	0.66	500	3.76	3.03

Table 6.12: Best fit parameters for dye E1 in Toluene solution

Dye	ϵD	ϵB	τB /ps	ϵC	τC /ps	FWHM /ps
B1	9000	330	0.8	1000	2.15	2.27
B2	3000	365	0.97	1200	2.62	2.37

Table 6.13: Best fit parameters for PT dyes B1 and B2 in toluene solution with 650nm probe

Solvent	ϵD	ϵB	τB /ps	ϵC	τC /ps	FWHM /ps
Hexane	8000	750	0.85	2750	6.67	1.01
Ethyl	22500*	18700	0.67	25900	5.66	3.36
Acetate	22500*	21800	1.26	25900	5.89	2.91

Table 6.14: Best fit parameters for the 6-CO₂Et PT dye with 630nm probe (those marked * are fits to the same file from different starting points)

λ /nm	ϵD	ϵB	τB /ps	ϵC	τC /ps	FWHM /ps
640	30700	500	5.3	34800	6.32	4.48

Table 6.15: Best fit parameters for 6-CO₂EtPT dye in a hand coating

Examples of fits to the data sets are shown in figures 6.5 to 6.10, with plots of residuals shown for each fitted trace. There are several points to note about the parameters fitted to the picosecond data, and these will be dealt with in turn. Firstly, however, it should be

pointed out that the values tabulated above are the actual numbers fitted to the data, but the number of significant figures quoted is not meant to imply that this is the precision with which the parameters are known, in part as a consequence of the coupling of several of the parameters as described above.

(a) Long lived component (state D)

Inspection of the data reveals the presence of a long lived component to the transient decay profile, which does not decay on the timescale accessible (approximately 1ns). This long lived component has lower molar absorption coefficient than the ground state at wavelengths shorter than about 630nm or 640nm, and greater absorption at longer wavelengths. These characteristics are identical with those observed for the anti isomer determined using nanosecond flash photolysis (figures 5.1 and 5.2). Anti isomer molar absorption coefficients for the 6-CO₂Et substituted PT dye in benzene and acetonitrile solution assuming no absorption by the anti isomer in the short wavelength edge of the syn isomer absorption band were determined in section 5.4 and presented in tables 5.3 and 5.4. It is worthwhile comparing the state D absorption coefficients in these two solvents calculated from the picosecond data on the basis of the quantum yields calculated in section 5.5 with these values. The values are shown tabulated for comparison in tables 6.16 and 6.17.

	$\epsilon/\text{dm}^3\text{mol}^{-1}\text{cm}^{-1}$	
λ/nm	State D	Anti isomer
640	25000	37700
650	49000	40800

Table 6.16: Molar decadic absorption coefficients for the 6-CO₂Et substituted PT dye anti isomer and state D in benzene solution

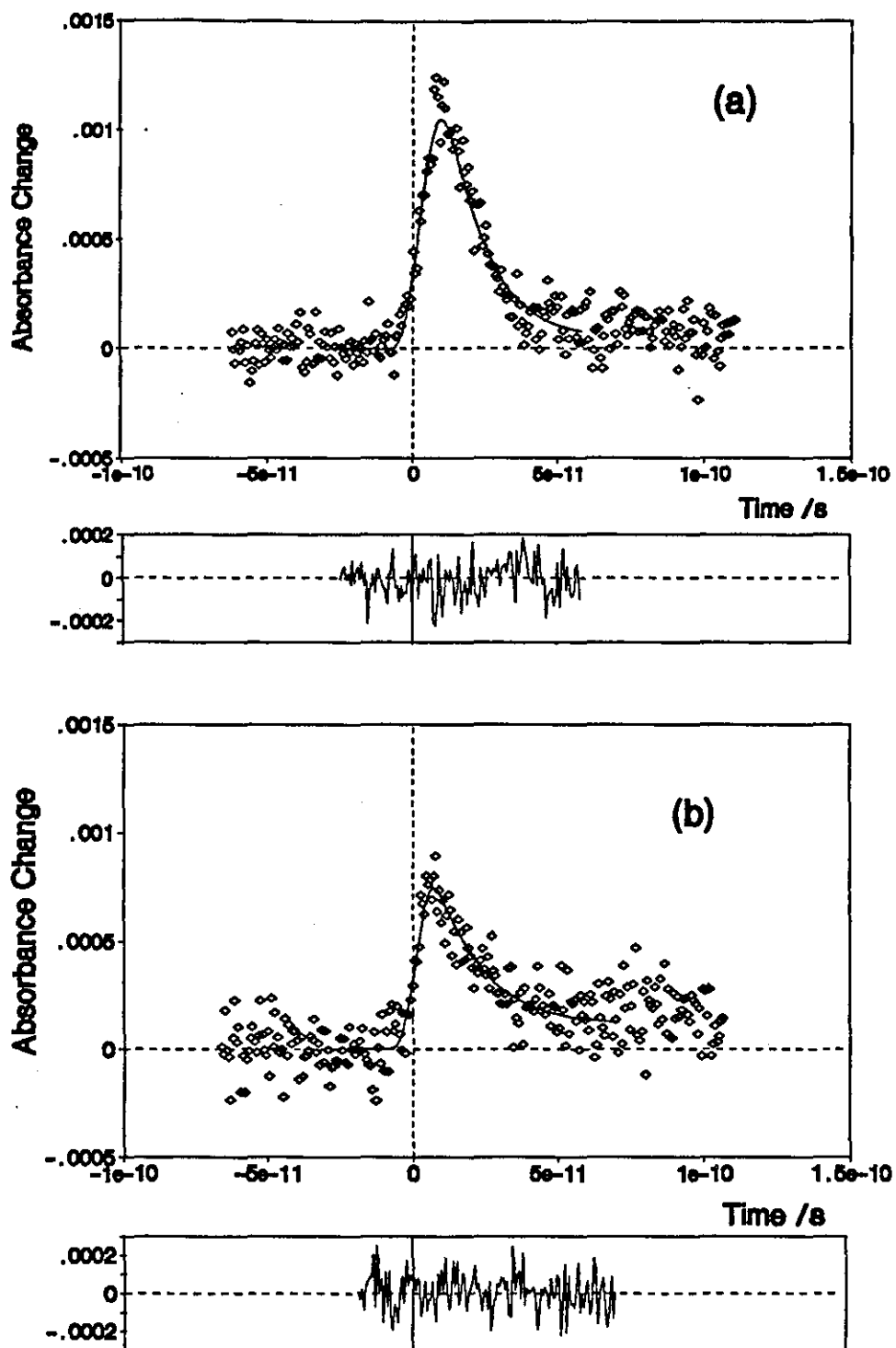


Figure 6.5: Best fits and residuals for (a) dye A2 in acetonitrile solution 640nm probe (b) dye B2 in acetonitrile 640nm probe (data from table 6.11)

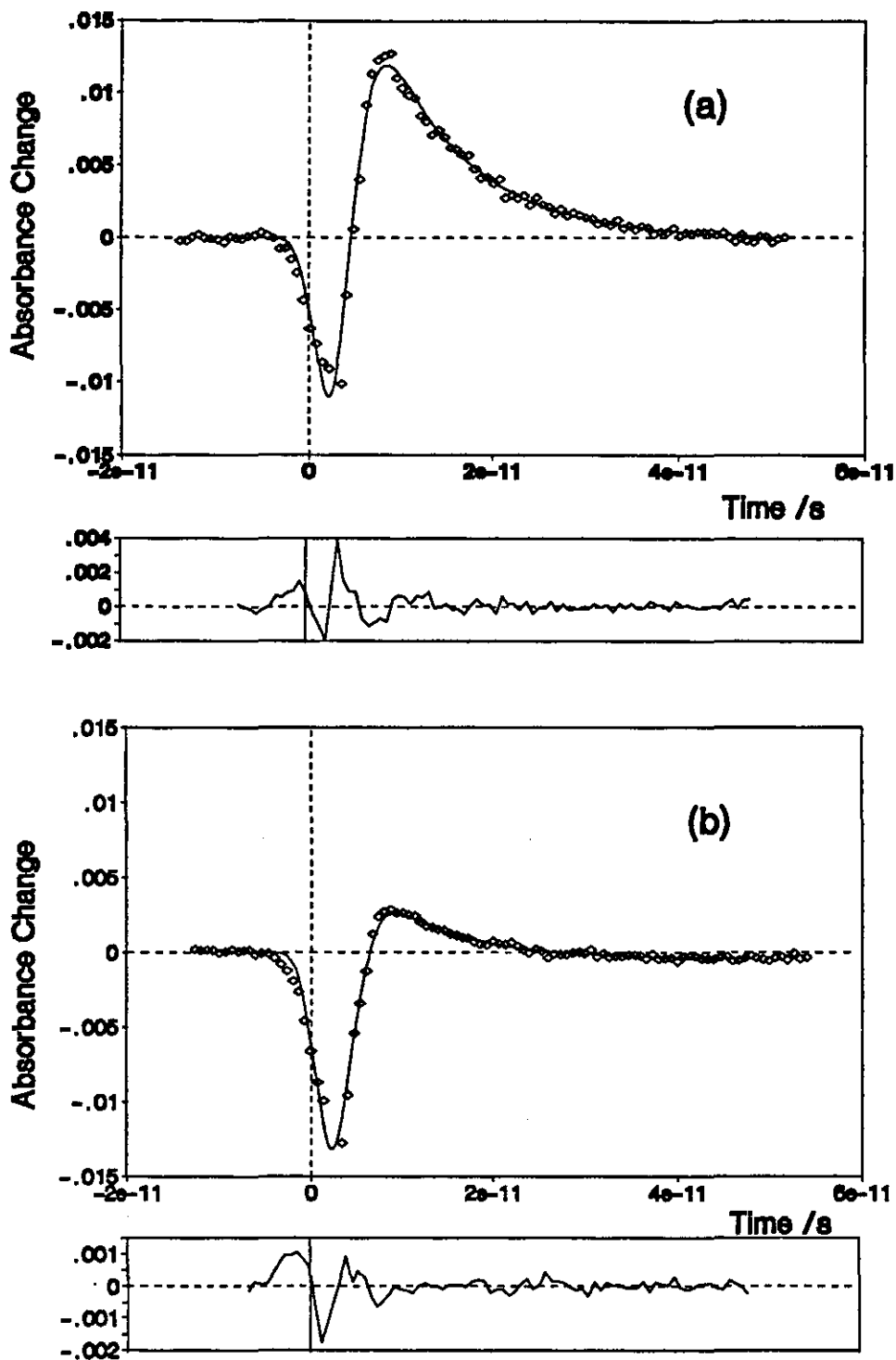


Figure 6.6: Best fits and residuals for (a) 6-CO₂Et PT in acetonitrile solution 640nm probe
 (b) 6-CO₂Et PT in acetonitrile solution 630nm probe (data from table 6.10)

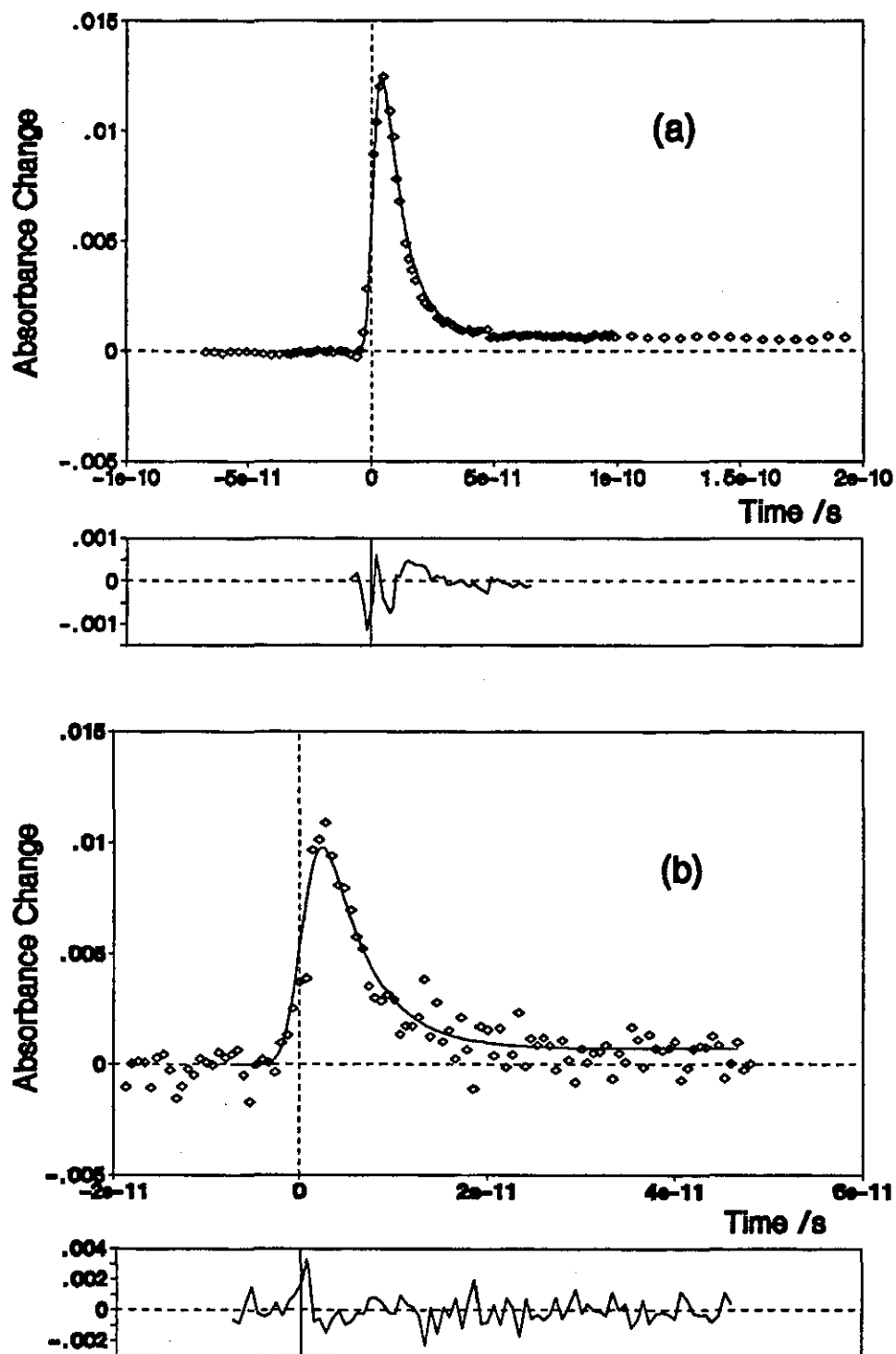


Figure 6.7: Best fits and residuals for (a) 6-CO₂Et PT in benzene solution 650nm probe (data from table 6.9) (b) E1 in toluene solution 650nm probe (data from table 6.12)

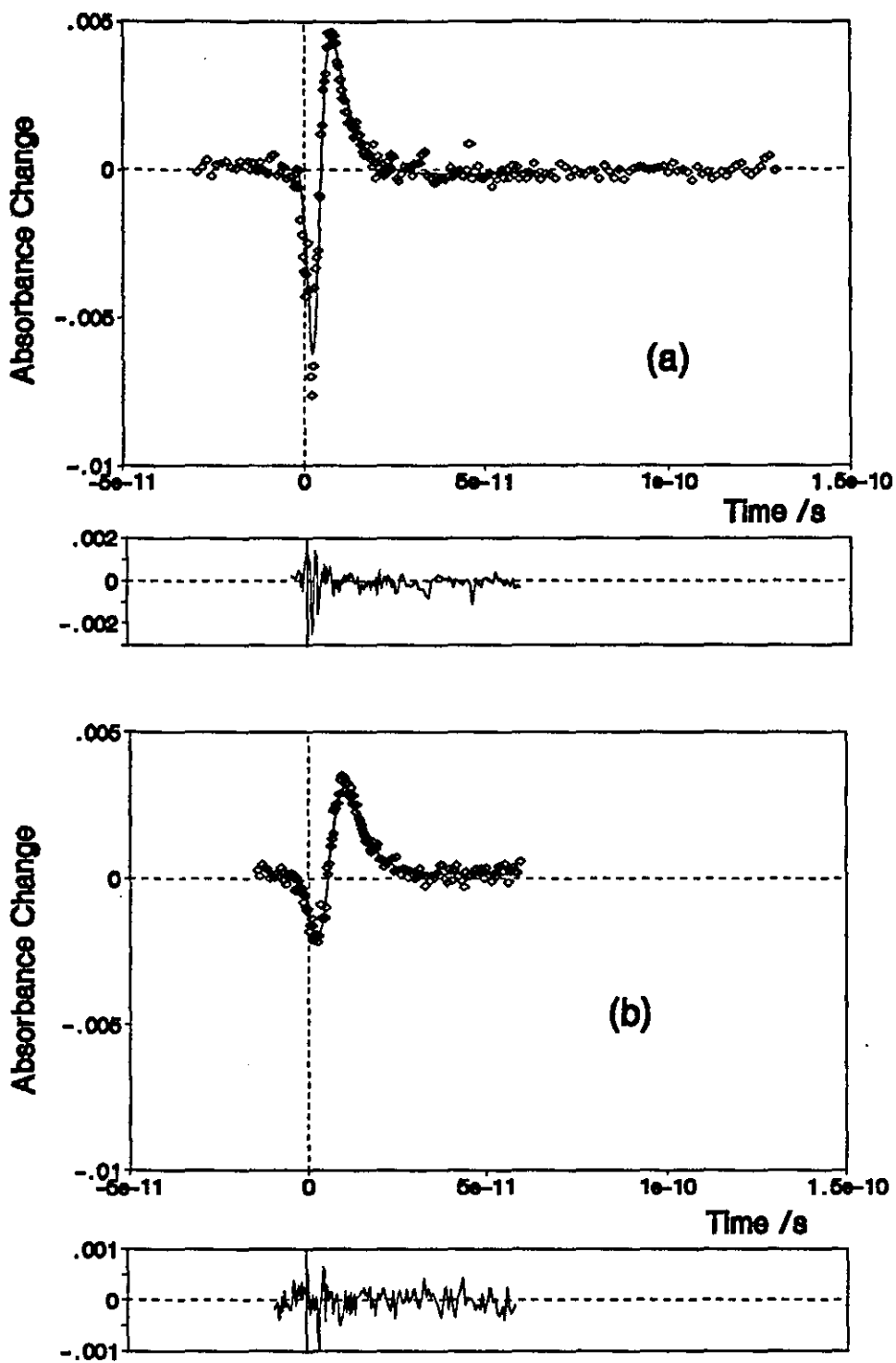


Figure 6.8: Best fits and residuals for 6-CO₂Et PT dye in methanol solution at 640nm probe, two different traces (1 and 2 respectively in table 6.7)

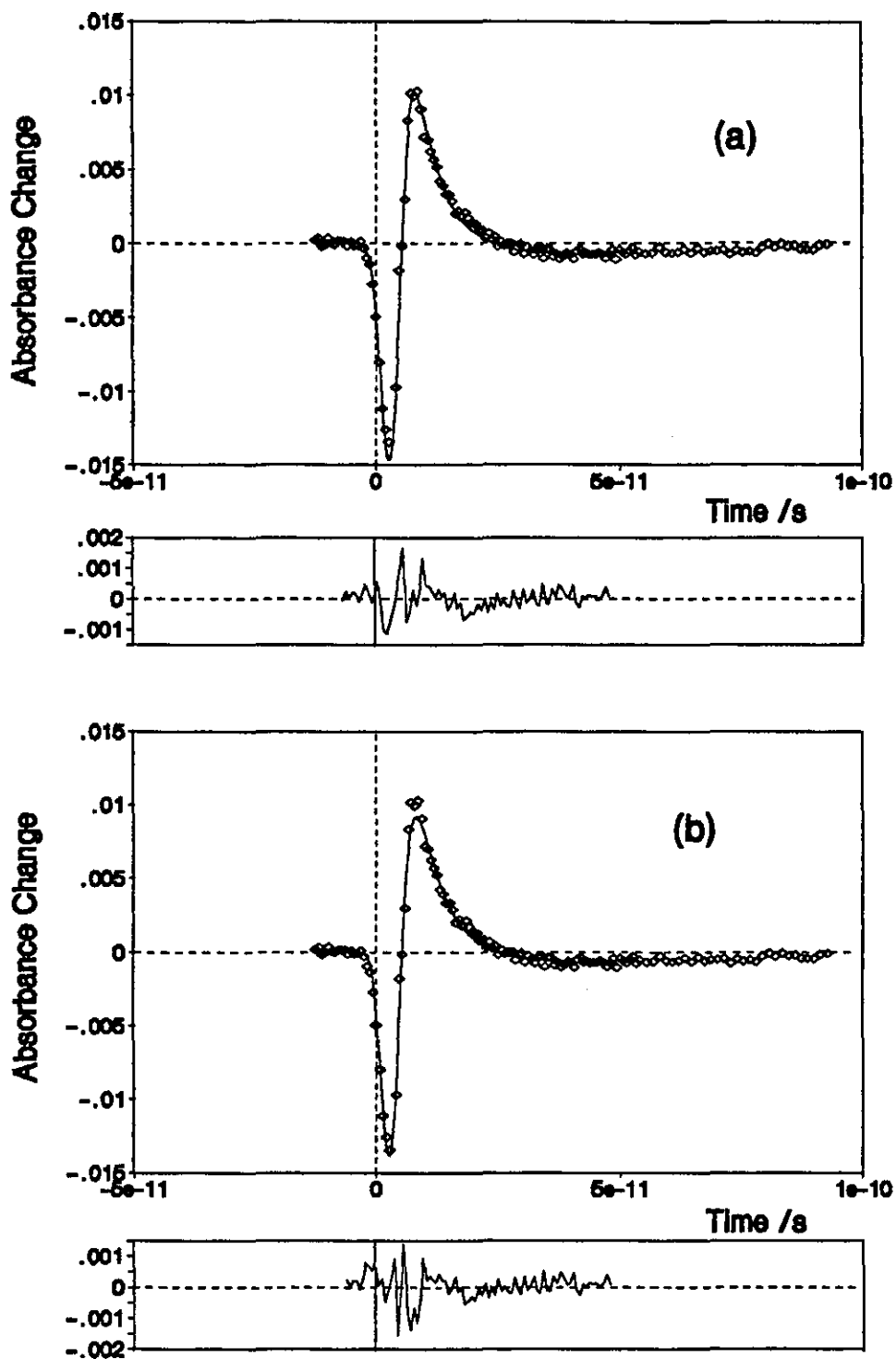


Figure 6.9: Best fits and residuals for 6-CO₂Et PT dye in ethyl acetate solution at 630nm probe, two fits to the same trace (data from table 6.14)

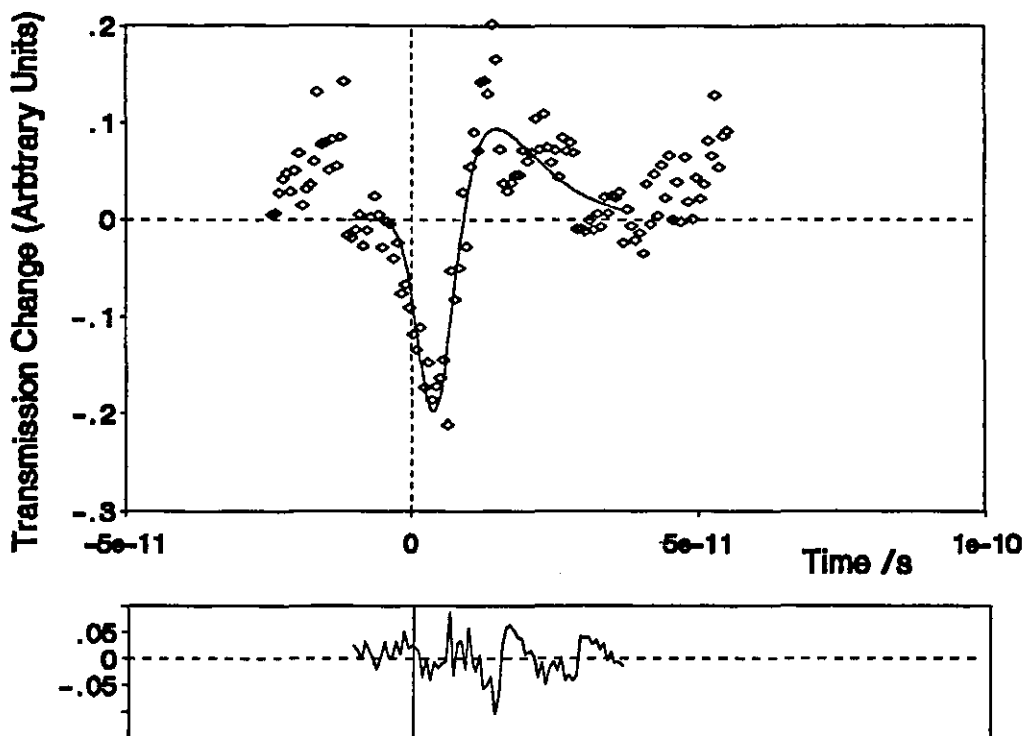


Figure 6.10: Best fit and residuals for 6-CO₂Et PT dye in a hand coating at 640nm probe

λ/nm	$\epsilon/\text{dm}^3\text{mol}^{-1}\text{cm}^{-1}$	
	State D	anti isomer
630	28000	29500
640	30000	37500
650	20000	46100

Table 6.17: Molar decadic absorption coefficients for the 6-CO₂Et substituted PT dye anti isomer in acetonitrile solution

With the exception of the value calculated for the dye in acetonitrile solution at 650nm probe, there is reasonable agreement between the molar absorption coefficients calculated from the two methods given the uncertainties involved in the calculations. Although only limited spectral resolution was possible owing to the nature of the picosecond laser system used, such data that is presented shows that both the magnitudes of the absorption coefficients and the shapes of the transient

spectra are consistent between picosecond and nanosecond data, supporting the hypothesis that the long lived component (state D) observed in the picosecond experiments is in fact the anti isomer observed in nanosecond flash photolysis experiments.

(b) First short-lived transient (state B)

All of the data traces for the 6-CO₂Et substituted dye in all solvents (except hexane where the syn isomer λ_{\max} is hypsochromically shifted) show an initial prompt bleaching which recovers in 0.5 to 3 picoseconds. As mentioned above, there is no evidence for stimulated emission from this state and hence it is not assigned as the fluorescent singlet state. The spectrum of this state follows largely that of the syn isomer ground state, and from the level of transmission increase observed it is clear that this state must have an appreciable molar absorption coefficient at the syn isomer λ_{\max} .

The data for dyes E1, B1, B2 and A2 do not show any initial bleaching by virtue of the very small absorption by the syn isomer ground state in the probed spectral region. On the basis of the data obtained for the 6-CO₂Et substituted dye, however, it was assumed that state B will be populated in these dyes also, and hence this step was included in the model. The characteristics of the state which are needed to fit the model to this data are similar to those required in the 6-CO₂Et data, i.e. state lifetimes in the 0.5 to 3 ps region with molar absorption coefficients of a similar magnitude the syn isomer ground state at the same wavelength.

Having assigned state B as not being the syn isomer fluorescent singlet state, there remains the possibility that it is in fact the twisted excited singlet state at the perpendicular conformation. Within experimental error, the lifetime of this state shows little solvent dependence, although there is evidence that this state

is slightly longer lived when the environment is that of the dye/di-n-butylphthalate droplet in the hand coating than in fluid di-n-butylphthalate solution. Changes in lifetime with solvent would, however, be very difficult to detect because of the coupling between the lifetime of this state, its molar absorption coefficient and the pulse width, as illustrated for the dye in ethyl acetate at 630nm probe in table 6.14; here both sets of parameters yielded perfectly acceptable fits (figure 6.9). It is proposed therefore that excitation takes place initially to the first excited singlet state of the syn isomer, and it is this which is the fluorescent singlet state. However, at the temperatures and low viscosities used throughout this work this state is very short lived and the population immediately evolves toward the perpendicular conformation. As a consequence, the steady state concentration of the fluorescent singlet state is very small and this explains the lack of stimulated emission. Hence what is termed here for simplicity as "state B" could in fact be thought of as being the excited state population as it evolves toward the perpendicular conformation, and will therefore have an "effective" absorption coefficient which varies with time since the absorption coefficient will undoubtedly vary with position on the excited singlet state surface. One may anticipate some solvent viscosity dependence of the rate of molecular twisting through viscous drag on the molecular motion; within experimental error, however, this is not observed in fluid solution and may be due to the effect being very small and masked by the coupling of the state lifetime, its absorption coefficient and the pulse width. Evolution to the perpendicular conformation is therefore postulated as very rapid, the rate limiting step in reaching the ground state surface in fluid solution being internal conversion from the perp conformation.

This may be relatively insensitive to solvent parameters provided the ground to excited state surface separation does not significantly change with changing solvent. Such changes may be expected to occur if there were significant charge separation in the perp geometry, and hence the suggestion is tentatively made that this is not the case and that isomerisation proceeds possibly via homolytic fission of the azomethine bond to yield the singlet biradical, followed by torsion about this bond. In the hand coating, the state B lifetime is seen to be longer than in fluid solution, and here evolution of the population to the twisted geometry is postulated as rate determining.

(c) Second, longer lived transient (state C)

Again taking the example of the data obtained with the 6-CO₂Et substituted dye first, it can be seen that the absorption coefficient of this state is somewhat less than that of the syn isomer ground state at wavelengths shorter than 630nm, but somewhat greater at longer wavelengths. The lifetime of the state also exhibits some solvent dependency, the mean lifetimes as a function of solvent being shown in table 6.18.

Solvent	τ /ps
Methanol	4.4 ± 0.9
di-n-butylphthalate	6.3 ± 1.1
Benzene	8.1 ± 1.0
Acetonitrile	9.5 ± 0.7

Table 6.18: State C lifetime as a function of solvent

It is clear from inspection of the solvent properties shown in table 5.10 that these lifetimes do not correlate with either solvent dielectric constant or viscosity. Interestingly, however, the order of solvents in which

the lifetime of state C increases is the same as that in which the lifetime of the anti isomer increases (table 5.8). This lends weight to the theory which naturally follows from the assignment of state B that C is a point (or points) on the ground state potential surface. The transient seen as state C may then be assigned as the evolution of the population along the ground state surface, and there will be a position dependent absorption coefficient on this surface and the transient seen will reflect the population in the ground state evolving toward the two isomeric forms. The precise reasons why there is no clear correlation between solvent properties and the measured state C lifetimes are not known, although several theories have been advanced for the lack of correlation of isomerisation rates in, for example, stilbenes with solvent viscosity^[141]. These may be summarised as

(i) The intramolecular potential surfaces exhibit a solvent dependence (specific solvent-solute interactions).

(ii) Macroscopic solvent viscosity is not an adequate measure of the friction felt by the isomerising molecule, possibly as a consequence of the molecular scale involved in the isomerisation process.

(iii) Other degrees of freedom than the isomerisation co-ordinate may contribute to the overall relaxation process.

It is felt that given the complexity of the dyes involved that probably all of the above make some contribution to the overall explanation, although given the small size of the moiety involved in the isomerisation process one may expect the failure of the macroscopic viscosity to adequately describe the prevailing friction to play a major role. This may explain the observation that the lifetime of state C in the hand coating, where the viscosity is very high, is of a similar order to that

seen in di-n-butylphthalate solution (tables 6.8 and 6.15). However, in the coating there is a considerable weight fraction of dye relative to solvent, and hence this will modify the environment considerably and direct comparisons between dilute, fluid solution and the coating environment must be made with caution. The data collected for dyes B1 and B2 in toluene solution demonstrate that these two dyes exhibit, to within the error of the fitting, identical properties (table 6.13). This suggests that steric hindrance in the 6-position is not an important factor in determining the state C lifetime (for dye structures see figure 3.8). Both dyes B1 and B2 have much shorter state C lifetimes than dye E1, the only difference between dyes E1 and B1 being the ballast group (figures 3.7 and 3.8). Precisely how this affects the state C lifetime is unknown, and without data in further solvent systems speculation is difficult. The lifetimes of state C in dye A2 appears slightly shorter than that in dye B2 (table 6.11), this factor being due to the difference in the N substitution pattern in the heterocyclic ring (figure 3.8). Dye B2, however, exhibits a marked effect of the lifetime of state C with solvent in going from toluene to acetonitrile solution (tables 6.11 and 6.13). The lifetime of state B appears independent of solvent, both of which factors support the data obtained for the 6-CO₂Et dye.

What should probably be pointed out at this juncture is that there is no direct evidence from the data that state B is a precursor of state C, and there exists the possibility that both states form simultaneously; the data is then simply the superposition of two transients. However, it is simple to rationalise the observed transients on the basis of a sequential model, so in the absence of evidence to the contrary such a model will be postulated.

Consequently the assignment of states B and C may be summarised as follows. State B is evolution of the excited state population to the twisted excited state conformation, which may have a short but finite lifetime. This explanation is favoured on account of the lack of stimulated emission observed, which can be explained if the population of the initially formed fluorescent state is vanishingly small. This is suggested to be a consequence of a very small potential barrier from the initially formed state and a very steep potential toward the perp conformation. There is little solvent dependency on the lifetime of this state, suggesting little interaction with the solvent. Such very fast decay times and little solvent dependency has been observed for the photoisomerisation of cis-stilbene, and has also been assigned as resulting from very little activation barrier in the excited state; however, following internal conversion to the ground state potential surface the molar absorption coefficient thereof is not observed to change significantly with time^[142]. It can be seen from the data in table 6.15 that the excited state lifetime even in the high concentration, high viscosity environment of the hand coating, although probably slightly longer than in fluid solution, is very short, which has implications for the interpretation of light fading experiments, of which more in chapter 7. In the case of the azomethine dyes state C is assigned as the population on the ground state surface evolving to the two isomeric forms, the absorption coefficient varying with position on the surface. The frequency of the motion on the ground state surface shows some solvent dependence, and this is the same dependence as seen for the thermal anti-syn isomerisation following population of the anti isomer. This picture was suggested by us as a possible explanation prior to gathering much of this data in a preliminary

publication on this work^[52]. Following this, data presented by Douglas et al^[99] has been rationalised in terms of a similar picture, although this work included different solvent systems to those presented here, and only a limited range, and as such comparisons are restricted. They did, however, succeed in detecting the fluorescent singlet state of the 6-CO₂Et substituted PT dye in a 96:4 v/v glycerol/methanol mixture at room temperature from stimulated emission measurements, this state having a lifetime of ≤ 2 ps. However, they could not detect such a state in pure ethanol solution, results which are in agreement with those presented here.

Chapter 7

Dye Fading in Photographic Coatings

7 Dye fading in photographic coatings

7.1 Introduction

With regard to photochemical image stability, the end use of the product will determine how important a feature this is. For instance, the light stability of colour negatives and cine film is often not of critical importance since the exposure to light of these media is usually very low. This is in contrast to professional colour enlargement prints, which may be exposed to direct sunlight in, for example, the entrance to a building, on a daily basis. The reactions involved in colour image degradation proceed very slowly, and as a consequence accelerated fading methods involving high intensity sources are used for their investigation. Such procedures reveal that the quantum efficiency of dye fade is not a single valued parameter, but depends upon both the wavelength and intensity of irradiation. Hence while in theory a five fold increase in light intensity should be met with a corresponding increase in dye destruction, this is rarely the case. As a consequence, it is important to take this so-called "reciprocity failure" into account when interpreting the results of accelerated fading tests and applying their findings to the real situation. The wavelength dependence of the fading efficiency also complicates the interpretation of the fade data. In a single dye layer coating, dye molecules in dispersion particles closest to the irradiated surface will absorb light mainly in the region of their principle absorption band, thus acting as a filter for the dye molecules in the lower reaches of the coating. As a consequence dye molecules in the bottom of the layer are irradiated with light relatively richer in blue light than green, and fading efficiencies will vary from top to bottom of the layer. Such problems are compounded in multilayer systems where dyes of different hue may reside in layers above

the one of interest. Thus the possibility exists that the principle mechanism(s) of fade in the multilayer product may be different from that elucidated on the basis of fading experiments involving a single layer model.

Dyes in the photographic product are not only subject to photochemical fade; heat, humidity and other factors may also lead to degradation, and these are the origin of the so-called dark fade. Hence under real conditions the observed fade will be a combination of light and dark fade, the extent to which each contributes depending upon the nature of the product and its storage conditions. A factor which must also be taken into account is that the fade rate may be radically altered by the build-up of products. These may have the effect of accelerating or inhibiting the fade rate by either interfering with the reaction pathways or introducing new ones. There are also other factors which need to be taken account of. For instance, in colour photographic products the couplers are "ballasted" with high molecular weight groups to immobilise them in their proper layer. This greatly simplifies processing, but as a result unreacted coupler is present in the layer in inverse proportion to the amount of dye formed. Therefore we must be concerned with possible colour forming reactions of the unreacted coupler, and also reactions between coupler and image dyes^[143].

To an extent, all colour photographic images are composed of dye deposits in the form of discrete droplets. This particulate structure arises from the nature of the coating itself, which at the simplest level of approximation may be regarded as composed of spheres of an oil phase, uniform in size and dye content, randomly distributed in a gelatin matrix which is essentially non-absorbing throughout the visible spectrum and

stabilised therein by a suitable surfactant. There are, of course, several inadequacies in this model as a description of the physical situation in a coating. For instance, larger dye particles (those greater than 300nm in diameter) will be deformed from a truly spherical shape by vertical compression of the gelatin as the coating is dried. The geometric form of the particles may then be adequately approximated as an oblate spheroid, with the minor axis normal to the image plane. In addition, real systems will be polydisperse rather than monodisperse, although it has been demonstrated that such systems may adequately be described in terms of optical properties by assuming a monodisperse system similar in all respects to the polydisperse system except possessing a suitable mean particle size. Although the macroscopic image may appear quite uniform, the colour purity and optical density of such an image will be strongly affected by the size and distribution of such particles. The effect will be composed in part of light scattering and refraction effects unless the refractive index of the gelatin matrix matches exactly that of the dye droplets. However, the major part the effect is simply a phenomenon of light absorption in such heterogeneous systems^[144]. In black and white photography it is well known that the structure of the silver deposit plays an important role in determining the capacity of the image to absorb light. A measure of this capacity is the photometric equivalent, p . This is the ratio of m , the quantity of silver per unit area in terms of grams per square decimetre, to the absorbance A of the image.

$$p = \frac{m}{A} = \frac{1}{C} \quad (7.1)$$

C, the reciprocal of the photometric equivalent, is termed the covering power. When dealing with heterogeneous colloidal systems such as the colour photographic dye image, it is convenient to consider a concept of covering power similar to that applied to a black and white image.

$$A = Cm \quad (7.2)$$

which has obvious similarities with the Beer-Lambert law, which may be formulated in this instance as

$$A_1 = \epsilon m \quad (7.3)$$

where A_1 is the limiting optical density, approached as the system approaches homogeneity. If in both expressions m is the number of moles per 1000cm^2 of area normal to the incident light then ϵ is the molar decadic absorption coefficient of the dye and C may be construed as the molar decadic absorption coefficient of the dye in the particular coating under investigation. Both ϵ and C are wavelength dependent, but C also depends upon droplet size and dye concentration. It can then easily be shown that

$$A = \left(\frac{C}{\epsilon} \right) A_1 \quad (7.4)$$

where C/ϵ is termed the covering power efficiency, relating the density of an heterogeneous image to the limiting maximum density of the same image as homogeneity is approached with diminishing particle size. The absorbance of a particulate image is a linear function of the image thickness but generally not of image dye concentration. With respect to concentration, the departure from the Beer-Lambert law increases with increasing heterogeneity.

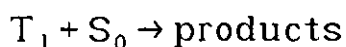
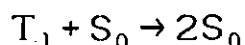
It should be noted that any effect which reduces the absorption efficiency of a particulate image such as covering power does so most effectively at absorption

maxima^[144]. As a consequence, the particulate structure of a photographic dye image can seriously affect its light absorbing properties. These manifest themselves as a loss of density in the spectral regions of maximum absorption, accompanied by a decrease in the sharpness of the absorption band. This decrease in band sharpness produces colours of low purity with apparent hue shifts relative to dilute, homogeneous solution.

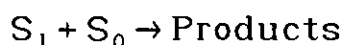
In addition to the light fading reactions which occur in the final colour print, there have been other degradation pathways identified involving the processing chemistry. For example, reactions with sulphite and thiosulphate ions used in the fixing stage of the development process can lead to degradation. The mechanism involves initial formation of a 1:1 adduct of the dye and bisulphite ion, hydrated with one molecule of water, which is then followed by further, reductive, reactions^[145]. Instability of pyrazolone azomethine dyes to fading under dark conditions has been demonstrated to involve nucleophilic attack of the enol form of the coupler on the dye molecule^[146]. Clearly the keto-enol tautomerism of the coupler involved in this reaction is not available to the pyrazolotriazole (PT) dyes and hence this degradation mechanism will not be active, possibly explaining in part the enhanced stability of the PT dyes.

Magenta pyrazolone azomethine dyes exhibit a characteristic in their fading that the fading efficiency passes through a minimum in the vicinity of 0.13m dye. Fading efficiencies are reasonably constant at constant dye molalities, regardless of the spread of dye and oil phase. High or low dye concentrations result in enhanced fading efficiencies relative to that observed at intermediate concentration. In addition, fading with blue light excitation is more efficient than fading with green light. The model proposed to explain the results^[147]

involves the use of four excited states; the two lowest excited singlet and two lowest excited triplet states. The longest wavelength absorption band has a high molar decadic absorption coefficient and shifts some 30nm on passing from polar to non-polar solvents, and hence S_1 is assigned as a π, π^* state, with significant charge transfer character. The assignment of T_1 as a π, π^* state is done on the basis of triplet-triplet energy transfer studies. Energy transfer from triplet violanthrene occurs at the limiting rate in benzene solution, placing the lowest triplet state at least some 100 kJ mol^{-1} below the lowest energy $S_1 \leftarrow S_0$ band. Such a large $S_1 - T_1$ split is characteristic of states with π, π^* but not n, π^* character^[148]. The changing of fading efficiency with increasing concentration may be explained on the basis of quenching of the dye excited states by ground state dye molecules providing an additional relaxation pathway. At low concentrations, the reactions



will dominate, while at higher concentrations the reaction



may become important. The wavelength dependence of the fading process may be explained on the basis of differing triplet yields from the first and second excited singlet states, and singlet-triplet radiationless transition selection rules may be of importance here (see section 1.2).

7.2 Results of fading experiments

Long term fading experiments involving both magenta pyrazolotriazole and pyrazolone dyes were carried out with the dyes contained within photographically formed coatings, made as detailed in section 3.4. Irradiation

of the coatings was carried out using the high intensity daylight (HID) source at Kodak Ltd.'s research laboratories in Harrow, the spectral radiance profile of which is shown in figure 3.6 in section 3.4.6. Such single dye layer coatings provide a simple model system in which to assess fading rates, since in the true three-layer product there are additional filters interspersed within the layers as well as the filtering effects of the dye layers themselves, which will obviously change as fading proceeds, making quantification of the processes involved more complex. The coatings are manufactured to reproduce as closely as possible the dye environment prevailing in the product, including conditions of coupler solvent properties, pH, covering power, particle size in the oil-in-gelatin dispersion, and dye concentration in the droplets.

The quantum yield of dye fade in these one-layer model systems can be estimated from the dye loss resulting from a given level of irradiation for a given time. The calculation of the fade quantum yield is then as follows. Consider a single strip of coating containing dye within oil droplets suspended in a gelatin matrix. If the absorbance of the coating due to the dye at the dye λ_{\max} is A_1 and the laydown of the dye, as measured by high performance liquid chromatography (HPLC), is L_1 mol m⁻², then it is possible to calculate an effective molar decadic absorption coefficient for the dye in this coating as

$$\epsilon_{\text{coating}} = \frac{A_1}{L_1} \text{ m}^2 \text{ mol}^{-1} \quad (7.5)$$

After exposing the strip to a source of known intensity for a given period of time, the OD due to the dye at the dye λ_{\max} is again measured, it being assumed that the decrease in absorption intensity is even across the absorption band; that is, any coloured products formed

from the fading either do not absorb in this spectral region significantly or are not present in sufficient quantity to have a significant effect. This assumption is not strictly correct since it is known that coloured products are formed during photodegradation of image dyes resulting in a shift of dye hue, and the quantum yield of fade calculated from the fading experiments will therefore be a minimum value. The dye coverage after fading L_2 is then determined using the molar decadic absorption coefficient calculated above as

$$L_2 = \frac{A_2}{\epsilon_{\text{coating}}} \text{ mol } \dot{m}^{-2} \quad (7.6)$$

where A_2 is the OD due to the dye at the dye λ_{max} after fading. The rate of absorption of incident photons by the dye in the coating is then calculated from the photon absorptivity integral (PAI) [149]

$$\text{PAI} = \frac{1}{hcL} \int_{\lambda_1}^{\lambda_2} E_{\lambda} T_{\lambda} I_{\lambda} \lambda \, d\lambda \quad \text{einstein } \text{cm}^{-2} \text{ s}^{-1} \quad (7.7)$$

where

$$I_{\lambda} = 1 - 10^{-A_{\lambda}} \quad (7.8)$$

Here, E_{λ} is the spectral radiance as a function of wavelength in $\text{W } \text{cm}^{-2}$, T_{λ} is the transmittance of any filters interposed between the source and the coating, and the factor $1/hcL$ serves to transform the integral from power absorbed in $\text{W } \text{cm}^{-2}$ to photons absorbed in $\text{einstein } \text{cm}^{-2} \text{ s}^{-1}$. The PAI is evaluated using Simpsons rule from the absorbance profile of the dye in the coating and the measured spectral radiance profile of the high intensity daylight (HID) source. Provided there is no

wavelength dependence on the fading efficiency, that is each photon absorbed causes fade with the same efficiency, the quantum yield of fade can be calculated from

$$\phi_{\text{fade,coating}} = \frac{L_1 - L_2}{10000 \text{ PAI}} \quad (7.9)$$

where the PAI used here is the mean of the integrals determined before and after fading, the factor of 10000 converting mol m⁻² to mol cm⁻². This assumes the fade rate remains constant throughout the irradiation time, i.e. that the amount of dye loss and formation of coloured products is low. Typically, about 10% of dye is lost and so the assumption is considered valid.

Data from the fading experiments for dyes E1 and K1 are shown in table 7.1. It must be borne in mind that such data may be distorted by the presence of coloured products, which will not only lead to the quantum yield evaluated being smaller than in reality has taken place, but may also themselves photodegrade with quantum yields substantially different to the parent dyes.

Dye	Initial A	Final A	Mean PAI /mol cm ⁻² s ⁻¹	Fade Time /h	ϕ_{fade}
K1 (strip 1)	1.37	1.28	3.90x10 ⁻⁸	168	7.71x10 ⁻⁸
K1 (strip 3)	1.06	1.01	3.66x10 ⁻⁸	168	4.73x10 ⁻⁸
E1 (strip 1)	1.66	1.46	4.38x10 ⁻⁸	24	1.53x10 ⁻⁶
E1 (strip 4)	1.04	0.99	3.76x10 ⁻⁸	24	4.04x10 ⁻⁷

Table 7.1: Quantum yields of dye fade calculated for dyes K1 and E1 on acetate base faded by irradiation with a high intensity daylight source.

Some explanatory notes regarding table 7.1 are in order. The initial and final absorbances recorded are those at the maximum of the absorption band in the coating. The assumption is made that the rate of fade remains constant throughout the fading experiment as a consequence of the

low level of dye loss; however, the existence of coloured products from photodegradation is established, and these could be a source of error. Indeed, reaction of dye E1 with benzophenone in degassed benzene solution following pulsed excitation of the benzophenone has been observed giving rise to products absorbing in a similar spectral region to the parent dye. This is attributed to reaction of the dye with the benzophenone ketyl radical rather than decomposition from the dye triplet state, since no reaction occurs in the corresponding experiment using anthracene as a sensitiser. Also assumed is that the degradation quantum yield and fade mechanism remain constant throughout the fade time. For pyrazolone dyes a wavelength dependence of fading efficiency has been established, and this may also be the case here. Consequently as pointed out earlier the fade mechanism may differ through the coating as a result of the filtering effect of the dye, so as the upper levels of dye in the coating fade, the wavelength distribution in the lower reaches of the coating will also change as possibly will the fading mechanism and quantum yield. The assumption is also made that oxygen availability remains constant throughout the irradiation, i.e. that no significant depletion of oxygen as a consequence of reaction occurs, which may again change the degradation mechanism.

The magenta coupler coatings on the acetate base were exposed using what is termed a granularity wedge, which is in fact a stepped neutral density filter. As a consequence, when the coatings are developed they consist of strips of differing dye density across the coating. To illustrate the phenomenon of changing quantum yield with different starting absorbance, two strips on the coating with differing initial absorbances were chosen for analysis. The mean PAI is the average value of the photon absorptivity integral determined before and after

fading. From the initial value of the absorbance and the dye laydown in each strip measured using HPLC, it is possible to calculate the absorbance which corresponds to a given dye laydown for the particular coating in question. From this and the final absorbance the change in dye laydown as a result of high intensity daylight (HID) fading may be calculated. This figure may then be used in conjunction with the PAI to calculate a quantum yield of fade. The results of the HPLC analysis of the dye laydown are shown in table 7.2.

Dye	Dye Laydown / mol m ⁻²
K1 (strip 1)	2.77x10 ⁻⁴
K1 (strip 3)	2.22x10 ⁻⁴
E1 (strip 1)	4.81x10 ⁻⁴
E1 (strip 4)	2.73x10 ⁻⁴

Table 7.2: Dye laydowns measured by HPLC for the coatings used in the HID fading experiments
An example calculation for strip 1 of the K1 dye coating is shown below.

Absorbance of K1 strip 1 0 hours fade	= 1.37
Dye laydown in K1 strip 1 0 hours fade	= 2.77x10 ⁻⁴ mol m ⁻²
"absorption coefficient" in K1 strip 1	= 4950 m ² mol ⁻¹
Absorbance of K1 strip 1 168 hours fade	= 1.28
Calculated dye laydown 168 hours fade	= 2.59x10 ⁻⁴ mol m ⁻²
Rate of fade	= 3.01x10 ⁻¹¹ mol m ⁻² s ⁻¹ = 3.01x10 ⁻¹⁵ mol cm ⁻² s ⁻¹
Photon absorptivity integral	= 3.90x10 ⁻⁸ mol cm ⁻² s ⁻¹
Quantum yield of fade ϕ_{fade}	= 7.71x10 ⁻⁸

Dye fading in fluid solution may be attributed to several possible mechanisms, which may broadly be classified as oxidative, reductive and hydrolytic. The oxidative mechanisms may involve production of singlet

oxygen from quenching of either the singlet or triplet state, and subsequent reaction of the singlet oxygen with the dye. In the very high viscosity regime of the photographic coating, where viscosity may be of the order of 10^5 centipoises^[150] rather than 0.3 to 1 centipoises as is the case in dilute fluid solution, the diffusion controlled kinetics will obviously be very slow and static quenching of the triplet state by oxygen may play a larger role. It is worthwhile at this stage mentioning the photochemical processes involved in the fading of azo dyes, since these show some similar properties to the azomethine systems. Among the different process of potential significance in the photofading process, self-sensitised oxidation via singlet oxygen has been considered particularly^[151]. Some of the oxidation reactions with singlet oxygen have been proposed to involve the hydrazone tautomer as an intermediate. Many azo dyes are not subject to azo-hydrazone tautomerism, however, and these in general show only slight reactivity toward singlet oxygen. Oxidative dealkylation may be an important fading process of non-tautomeric azo dyes containing dialkylamino groups, via a mechanism such as that in figure 7.1.

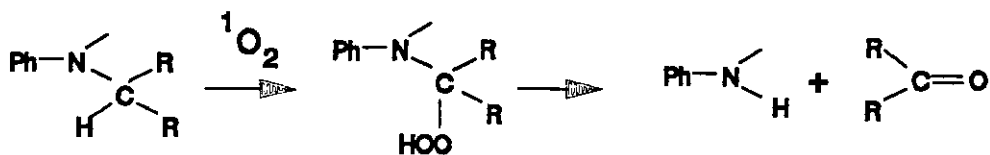


Figure 7.1: Oxidative dealkylation of azo dyes

Clearly from inspection of the structure of the azomethine dyes, such a mechanism may also operate as a consequence of the presence of the dialkylamino group para to the azomethine linkage, and indeed dealkylated products have been identified following photofading although the mechanism whereby these are produced has not been elucidated^[152]. For typical azo dyes there is a large disparity between the magnitudes of the physical and chemical singlet oxygen quenching constants. The chemical quenching constant k_{cq} (involving reaction with singlet oxygen) is of the order of $2 \times 10^4 \text{ dm}^3 \text{ mol}^{-1} \text{ s}^{-1}$, while that for physical quenching k_{pq} is around $2 \times 10^8 \text{ dm}^3 \text{ mol}^{-1} \text{ s}^{-1}$. Azo dyes in dilute, non-viscous fluid solution do not sensitise singlet oxygen in sufficient yield for it to be detected. In more viscous solvents such as di-n-butylphthalate, $\phi(^1\Delta_g)$ is found to be 0.002 to 0.03, depending on substitution pattern. Following UV irradiation of degassed solutions of azo dyes, the mechanism of fade involves reductive cleavage of the azo linkage to give the corresponding anilines. Irradiation of the same dyes with visible light results in no detectable fading reactions. Fading in aerated solution results in the production of less aniline, but products also appear which are the same as those resulting from e.g. methylene blue sensitised oxidative fade, such as benzene and anisole. This reaction is unlikely to involve direct interaction of a dye excited state with oxygen owing to the very short triplet lifetime, which is only some 10-20ns at low temperature^[153]. Rather, it is probably initiated by the same process as the photoreduction, i.e. H-atom abstraction from the solvent to give the dye hydrazyl radical. Oxygen then reacts with the hydrazyl radical yielding a peroxy radical which then either reverts to the starting azo derivative or undergoes further decomposition to the end products. Hence the data

interpreted as demonstrating the generality of the involvement of singlet oxygen in the photofading of azo dyes has been possibly overestimated, while radical pathways may play a much greater role than hitherto anticipated^[154]. This factor may not be very surprising considering the very poor characteristics of dialkylaminobenzenes as singlet oxygen sensitizers, a fact related to their very short triplet lifetimes, and their good physical and poor chemical singlet oxygen quenching characteristics. The consequences of these are that the self-sensitized photooxidation proceeds with a quantum yield of less than 10^{-9} . Hence similar considerations may also apply to the azomethine systems as a consequence of the very short singlet and triplet lifetimes, and the possibility exists of oxidative fade being initiated by a radical mechanism followed by subsequent reaction of the radicals with ground state oxygen. Hence both the reductive mechanism and oxidative mechanism may be initiated by the same radical formation step and the distinction between them is simply a function of oxygen availability and the relative reactivity of the radicals toward oxygen and ground state dye molecules. High viscosities will also have an effect on the degradation rate since geminate reactions may play an important role. Geminate reactions are those occurring between two species either (a) as a result of repeated collisions within a solvent cage (referred to as a primary encounter) or (b) which separate from a primary encounter and subsequently re-encounter (a secondary encounter)^[155]. In systems such as these which exhibit self-sensitized photooxygenation, when this proceeds via a singlet oxygen mechanism the reactive species is actually produced in a state of encounter with the sensitizer rather than encounter taking place via diffusional motion^{[156][157][158]}. Reactant molecules are therefore in close proximity to the dye

molecules rather than being randomly distributed and the system is heterogeneous on a microscopic scale. The efficiency of geminate reaction in fluid solution is independent of dye concentration and, owing to the short timescales involved for diffusion out of the solvent cage, of the singlet oxygen lifetime in the solvent in question. However, in the high viscosity regime of the dye droplets in the photographic coating, diffusion may be expected to be very slow and reaction or physical deactivation of singlet oxygen before cage escape may be the dominant processes. Diffusion apart and re-encounter (secondary reactions) may be expected to occur to only a small extent due to the timescales involved. Olefins react with singlet oxygen, but also quench singlet oxygen physically via an interaction with the C-H bonds, analogous to deactivation by solvents^[159]. Reaction of olefins with singlet oxygen results in the formation of hydroperoxyl groups and migration of the double bond, the mechanism being proposed to involve concerted cycloaddition of the singlet oxygen to the olefin^[160]. This is one class of photooxygenation reaction which is of interest synthetically as a method of introducing oxygen in a highly specific fashion to organic compounds. Another is the reaction of cyclic dienes, heterocycles and aromatic compounds to give cyclic peroxides, a fade mechanism which may again be operative here. It should be noted, however, that the formation of such peroxides does not necessarily proceed via a singlet oxygen mechanism in all cases, since radical formation (possibly initiated by H atom abstraction) followed by reaction with ground state oxygen may lead to the same products.

Azomethine dyes can be viewed as p-substituted anilines, and as such are expected to physically quench singlet oxygen. However, they are better singlet oxygen quenchers than is expected on the basis of them being

p-substituted anilines. Alkyl substitution ortho to the azomethine linkage increases the efficiency of the dye toward quenching singlet oxygen, while alkyl substituents ortho to the dialkylamino group have the opposite effect, which may be attributed as arising from steric hindrance of the dialkylamino group. This group is important in the quenching of singlet oxygen, as evidenced by the fact that the equivalent dyes lacking this group exhibit very little singlet oxygen quenching. Evidence suggests that azomethine dyes physically quench singlet oxygen by a mechanism involving both energy and charge transfer^[161]. Physical quenching is by far the dominant singlet oxygen quenching pathway for azomethine dyes. The physical quenching constant for dye K1 is determined by singlet oxygen luminescence measurements to be $2.5 \pm 0.2 \times 10^7 \text{ dm}^3 \text{ mol}^{-1} \text{ s}^{-1}$ in acetonitrile solution. The quenching constant was determined from a plot of reciprocal singlet oxygen lifetime as a function of dye concentration, the data being reproduced in figure 7.2. The chemical quenching constant for this same dye has been estimated as a factor of 10^3 less than this^[162]. The quenching constant determined by the same method in the same solvent for an azine dye (figure 5.10) is determined as $7.5 \times 10^6 \text{ dm}^3 \text{ mol}^{-1} \text{ s}^{-1}$, so clearly there are additional quenching factors associated with the azomethine dye K1. Whether this is as a result of some energy transfer quenching making a contribution or simply quenching by part of the additional functionality on the molecule is not clear.

It is probably appropriate here to consider some of the points regarding triplet state production in these dye made in chapter 5. As pointed out there and in chapter 6, there is no evidence from either picosecond or nanosecond flash photolysis studies of population of the triplet state as a result of direct excitation into the principle absorption band. To rationalise the data of

Herkstroeter^[53] and Douglas^[54] which suggested an oxygen effect on the isomerisation process in dilute solution, two proposals are advanced in this thesis namely (a) Excitation of the anti isomer may result in appreciable triplet state population and (b) Excitation into the higher energy absorption band may give access to the triplet state.

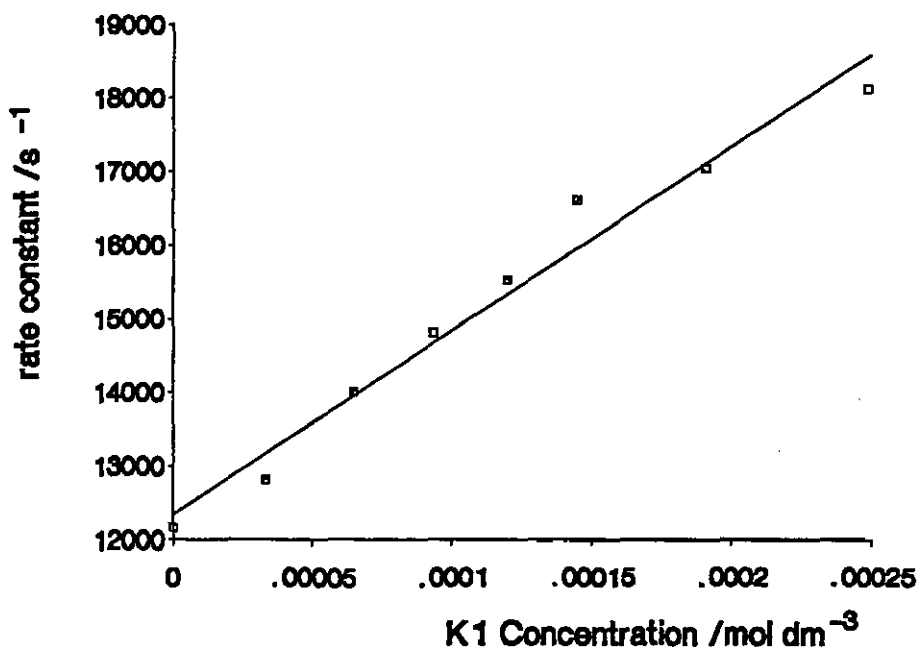


Figure 7.2: Plot of singlet oxygen deactivation rate constant against dye concentration for determining the singlet oxygen quenching constant of dye K1.

If the first explanation is correct, then given the very low quantum yield of isomer production it may be anticipated that from steady state irradiation the population of anti isomer will be vanishingly small and possibly the triplet state populated therefrom may not play a major role in the photodegradation. If the second explanation holds, however, this may in part explain the wavelength dependence of the fading efficiency. However, this would also lead to the conclusion that fading occurs from both singlet and triplet manifolds, since excitation

exclusively into the principle absorption band also results in an appreciable fade rate.

In summary, then, what has been observed in the past in fading experiments using steady state irradiation is that dye fade takes place in the presence and absence of oxygen, there being different product distributions in each case. This observation has been interpreted as resulting from the fading mechanism changing from a radical mechanism to one involving singlet oxygen production and subsequent reaction, mainly on the basis of bleaching of DPBF when this is incorporated within the coating. In the photographic coating, dye concentrations in the oil droplets are of the order of 2 to 3 molar, and hence from this consideration reaction of an excited dye molecule with a ground state dye molecule may be considered more likely than reaction with oxygen. Reaction with either ground state dye or ground state oxygen will necessarily be a static reaction owing to the very short excited states lifetimes and the very slow diffusion in such a high viscosity system. Short excited state lifetimes have been demonstrated using picosecond pump-probe laser flash photolysis to prevail in the coating as well as in fluid solution at room temperature (chapter 6). The singlet-triplet energy gap in magenta azomethine dyes is estimated to be in excess of 100 kJ mol^{-1} and consequently quenching of the singlet state by oxygen may give rise to singlet oxygen and the dye triplet state, which also has sufficient energy to sensitise singlet oxygen although it too has a very short lifetime in fluid solution. Given the very large difference between the physical and chemical singlet oxygen quenching constants, much of the singlet oxygen produced will immediately be deactivated without chemical reaction.

Consequently, the fading in the coating itself is probably composed of several mechanisms, which may be summarised as follows.

- (a) Radical production from direct photolysis of the dye, followed by reaction with ground state dye molecules
- (b) Radical production from direct photolysis followed by reaction with ground state oxygen
- (c) Radical production from direct photolysis followed by reaction with other components of the image
- (d) Quenching of the first excited singlet state by ground state molecular oxygen to produce singlet oxygen, followed by reaction of the singlet oxygen with the dye
- (e) Quenching of the first excited triplet state of the dye, produced from direct excitation or from process (d) above, to produce singlet oxygen which may then react with ground state dye.

This illustrates why improving light stability in the photographic product is not a trivial matter; excluding oxygen from the material or adding a singlet oxygen quencher will only cut off some of the degradation pathways, and consequently at best only reduce the fade rate. If the non-oxidative route is dominant, it may not even achieve a measurable reduction. Indeed, interception of the dye excited states by oxygen may in fact act to reduce reductive fade and excluding oxygen may in fact accelerate fading in some cases.

Appendix 1

Dye Ground State Absorbance Spectra

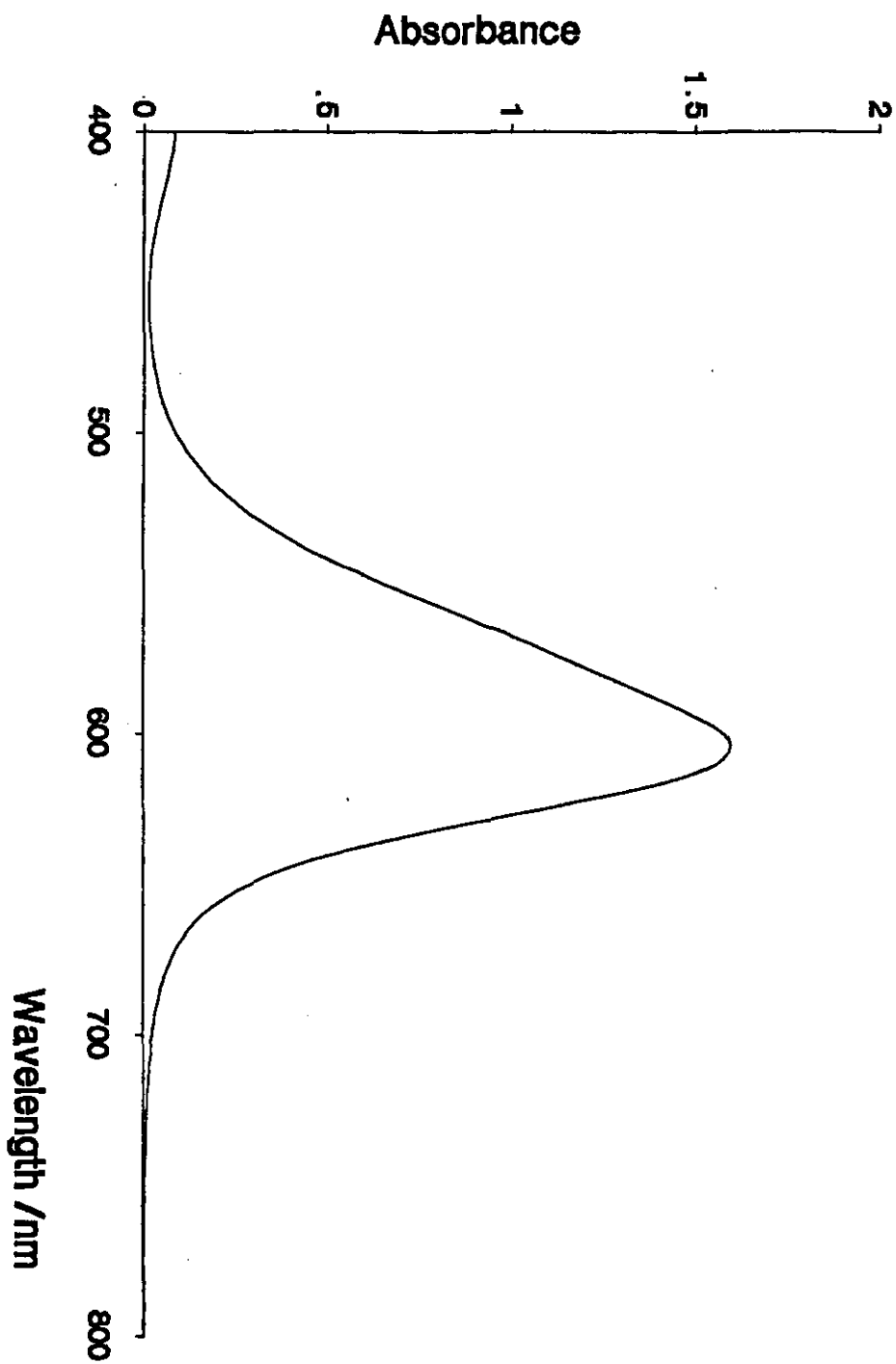


Figure A1: 6-CO₂Et substituted PT dye in acetonitrile solution. Concentration 1.68×10^{-5} mol dm^{-3} .

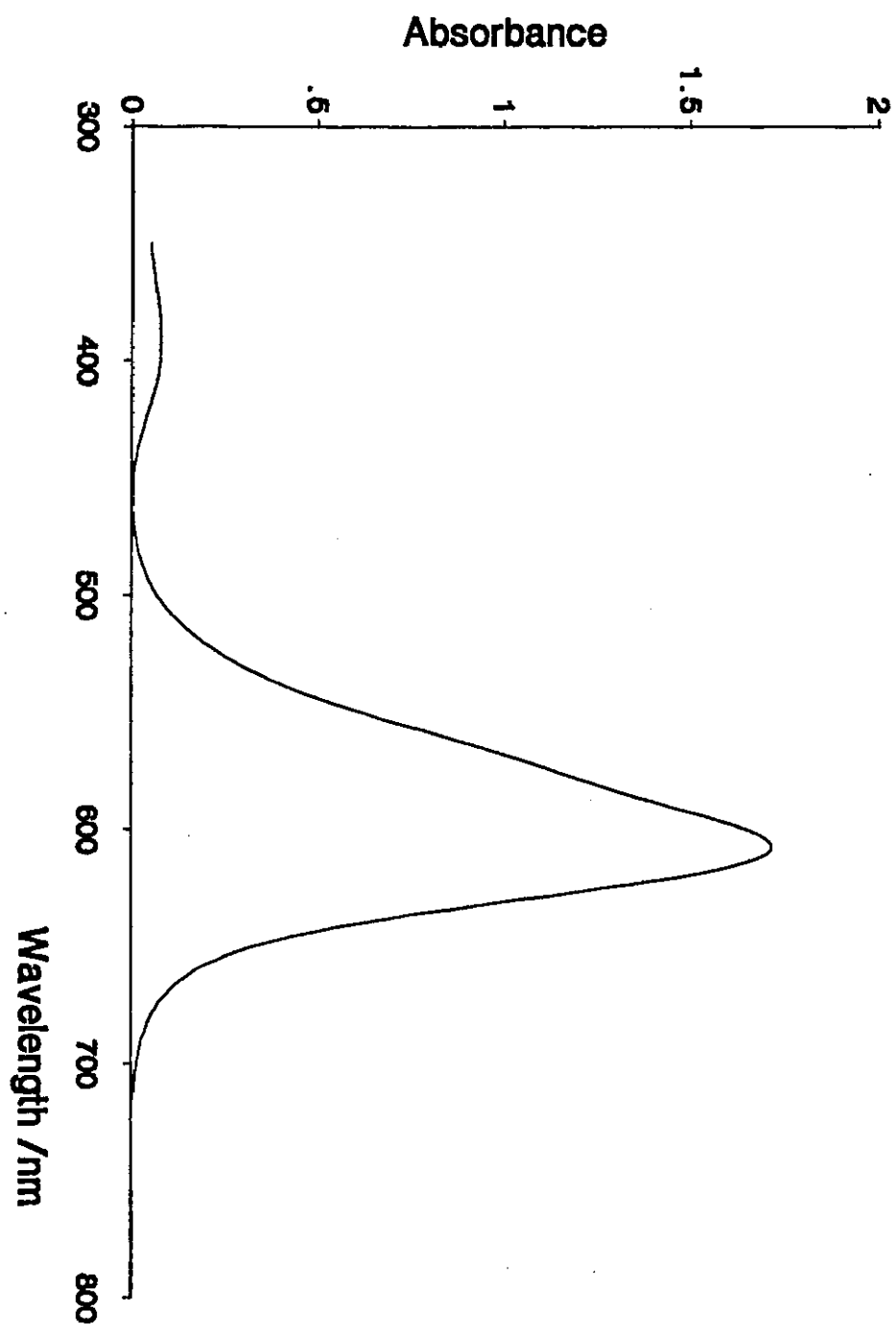


Figure A2: 6-CO₂Et substituted PT dye in di-n-butylphthalate solution. Concentration $2 \times 10^{-5} \text{ mol dm}^{-3}$.

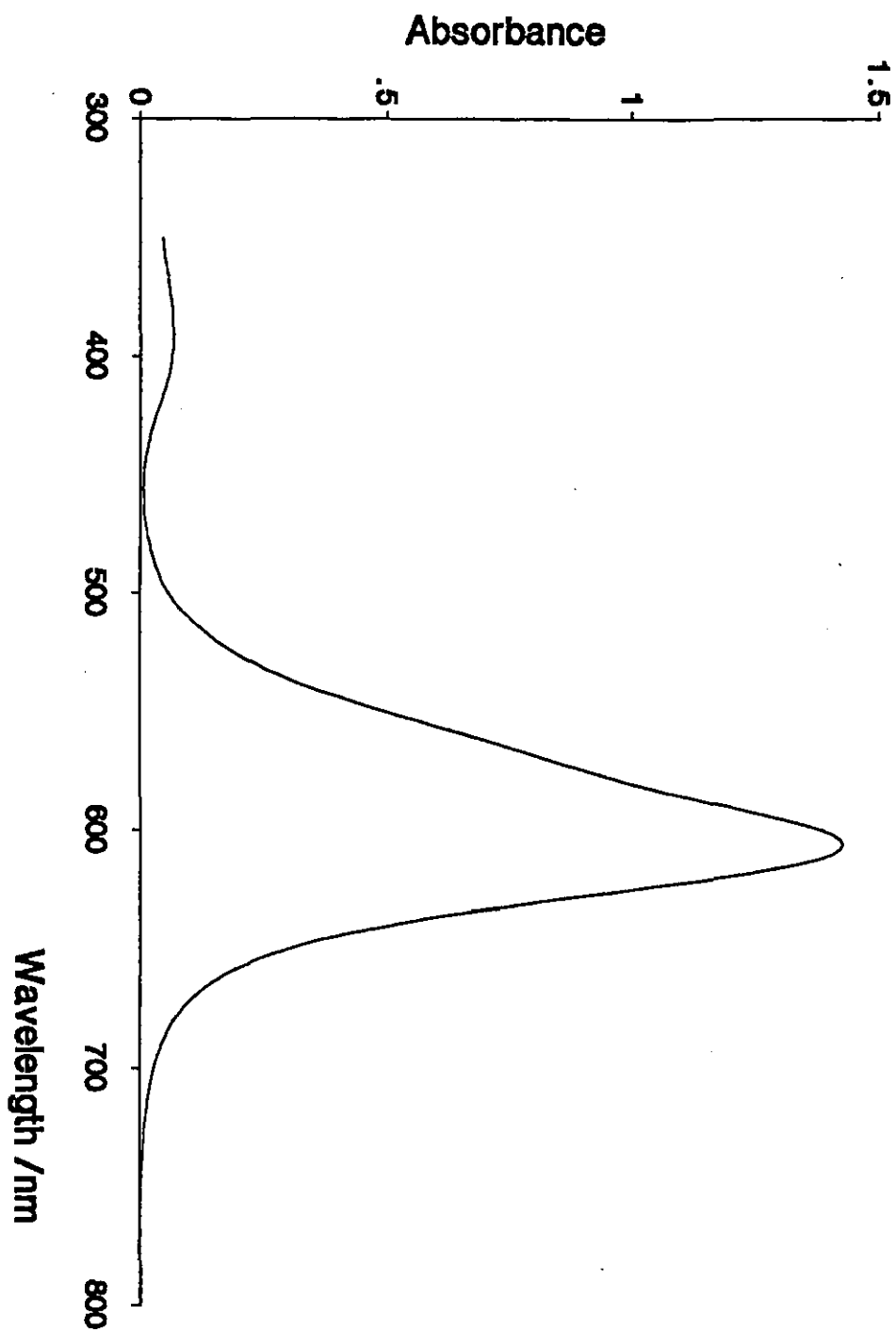


Figure A3: 6-CO₂Et substituted PT dye in methanol solution. Concentration $2 \times 10^{-5} \text{ mol dm}^{-3}$.

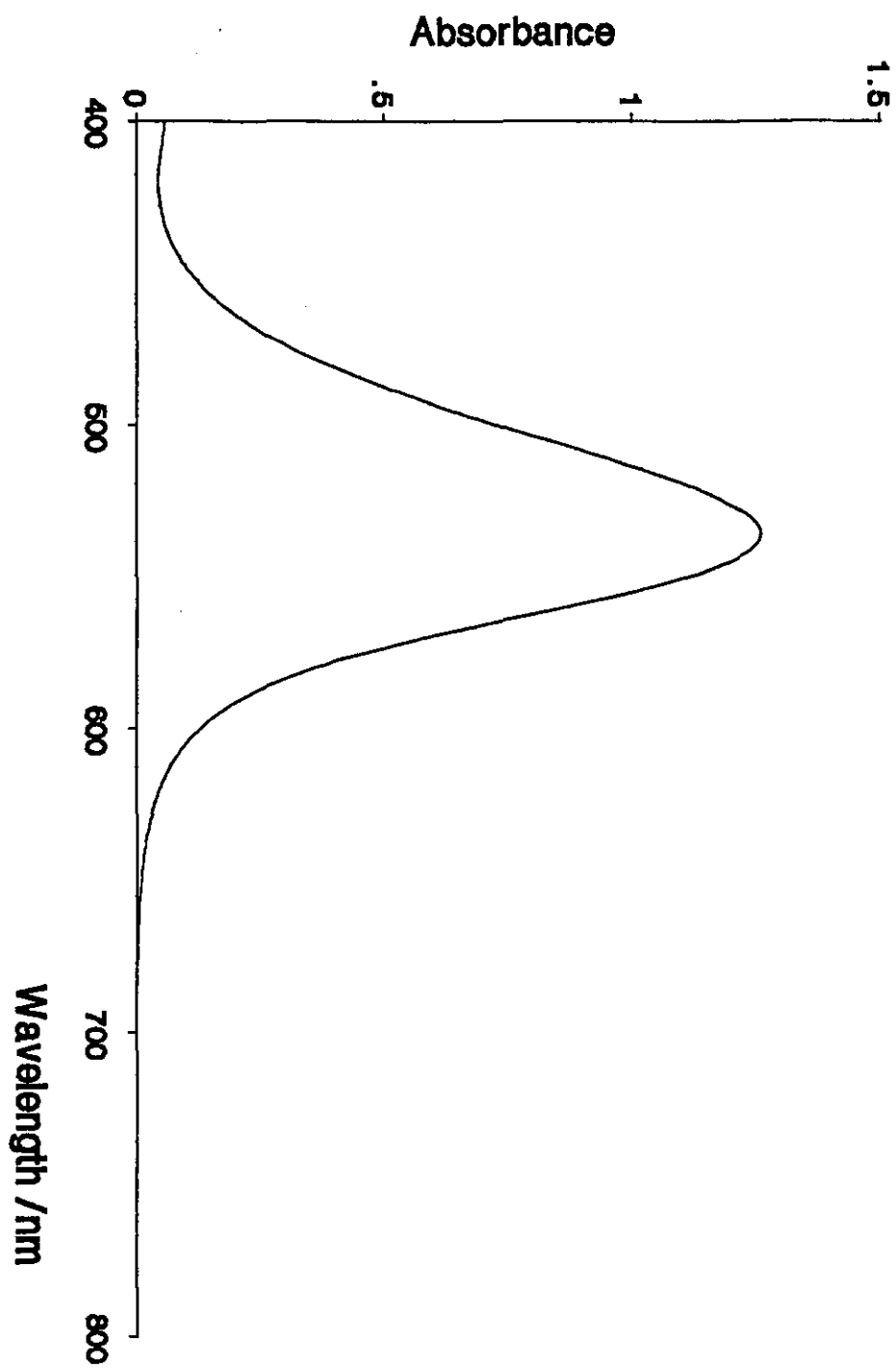


Figure A4: Dye B2 in acetonitrile solution. Concentration $4 \times 10^{-5} \text{ mol dm}^{-3}$.

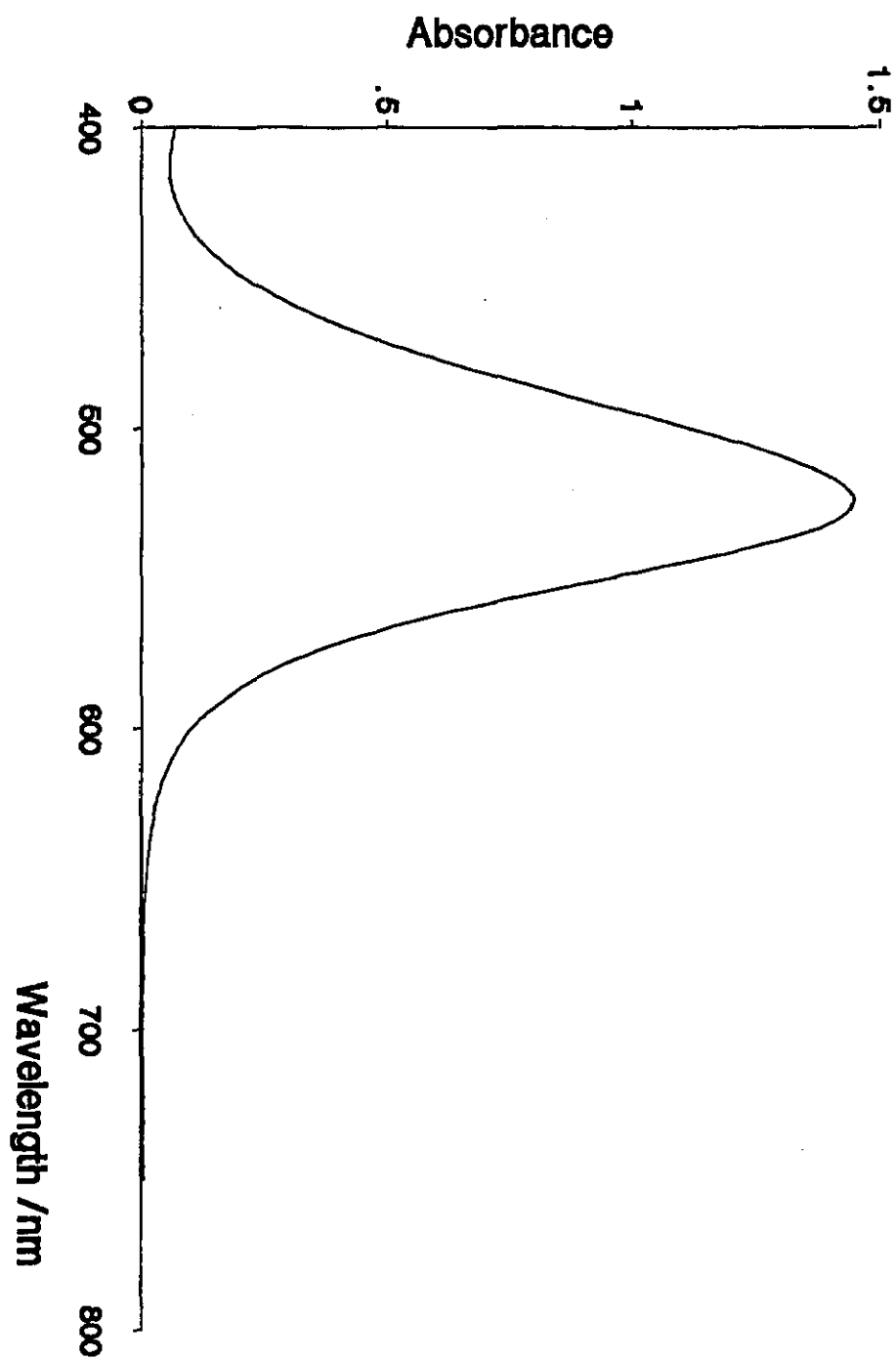


Figure A5: Dye A2 in acetonitrile solution. Concentration $4 \times 10^{-5} \text{ mol dm}^{-3}$.

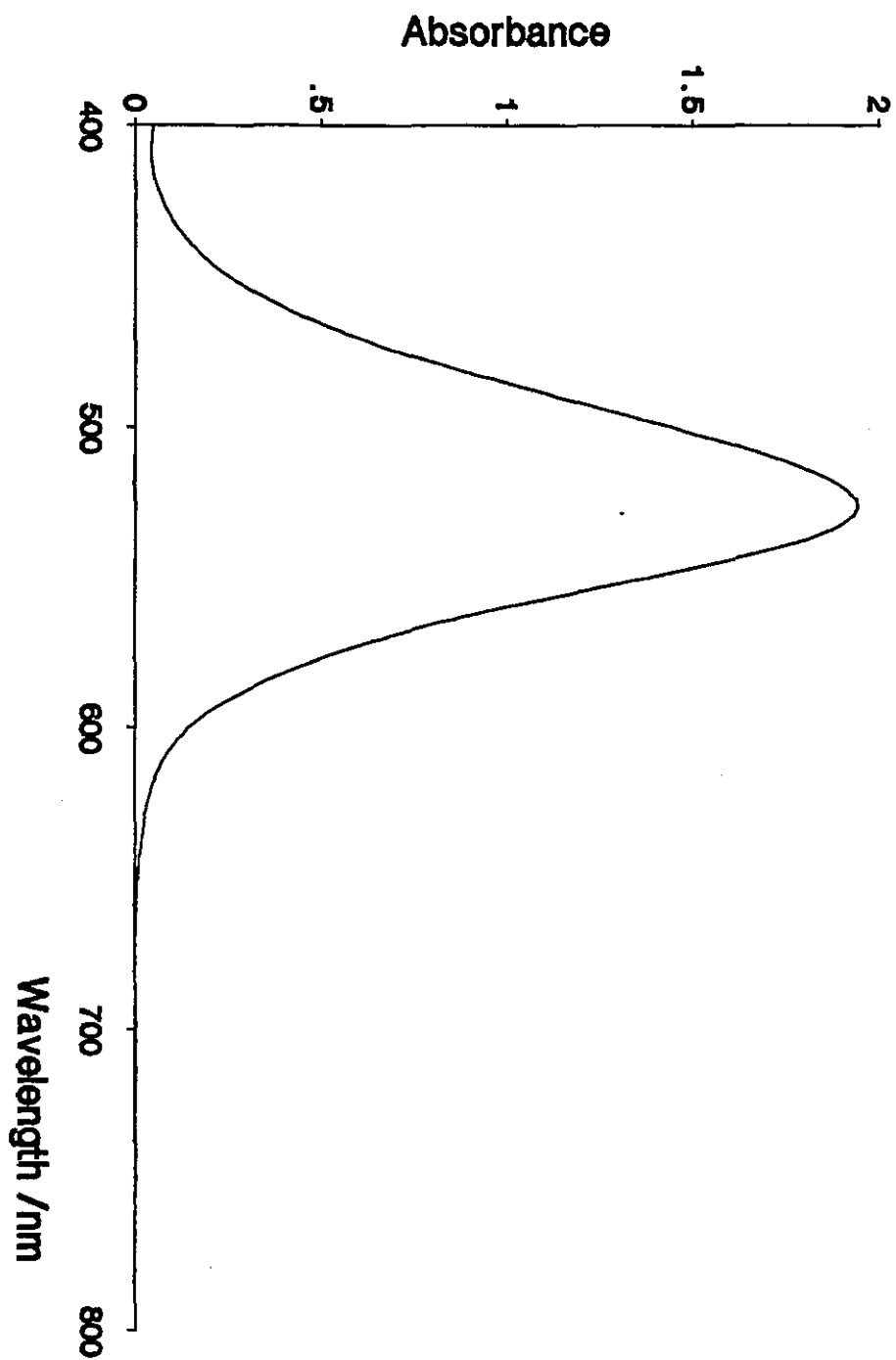


Figure A6: Dye E1 in acetonitrile solution. Concentration $4 \times 10^{-5} \text{ mol dm}^{-3}$.

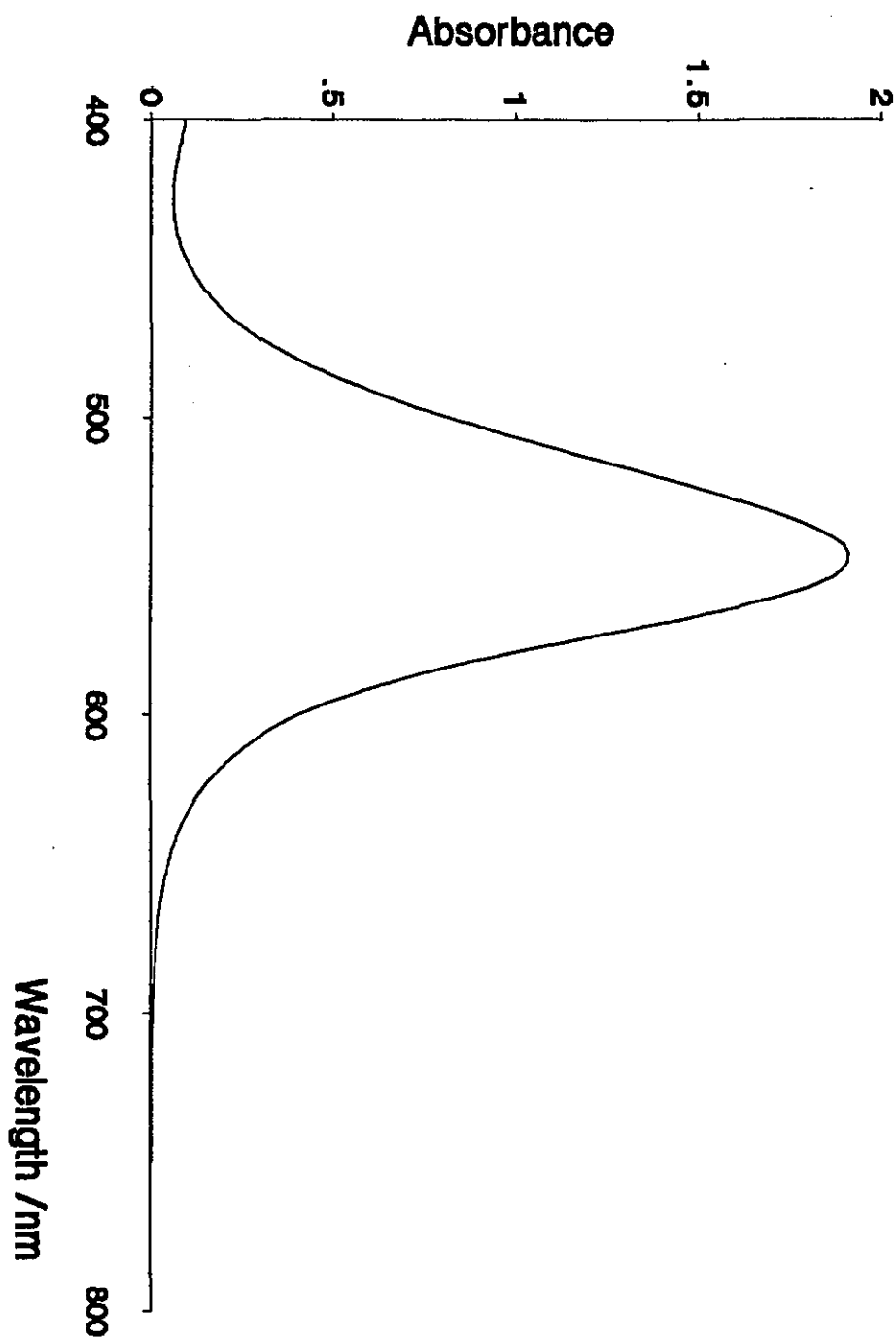


Figure A7: Dye B2 in methanol solution. Concentration $4 \times 10^{-5} \text{ mol dm}^{-3}$.

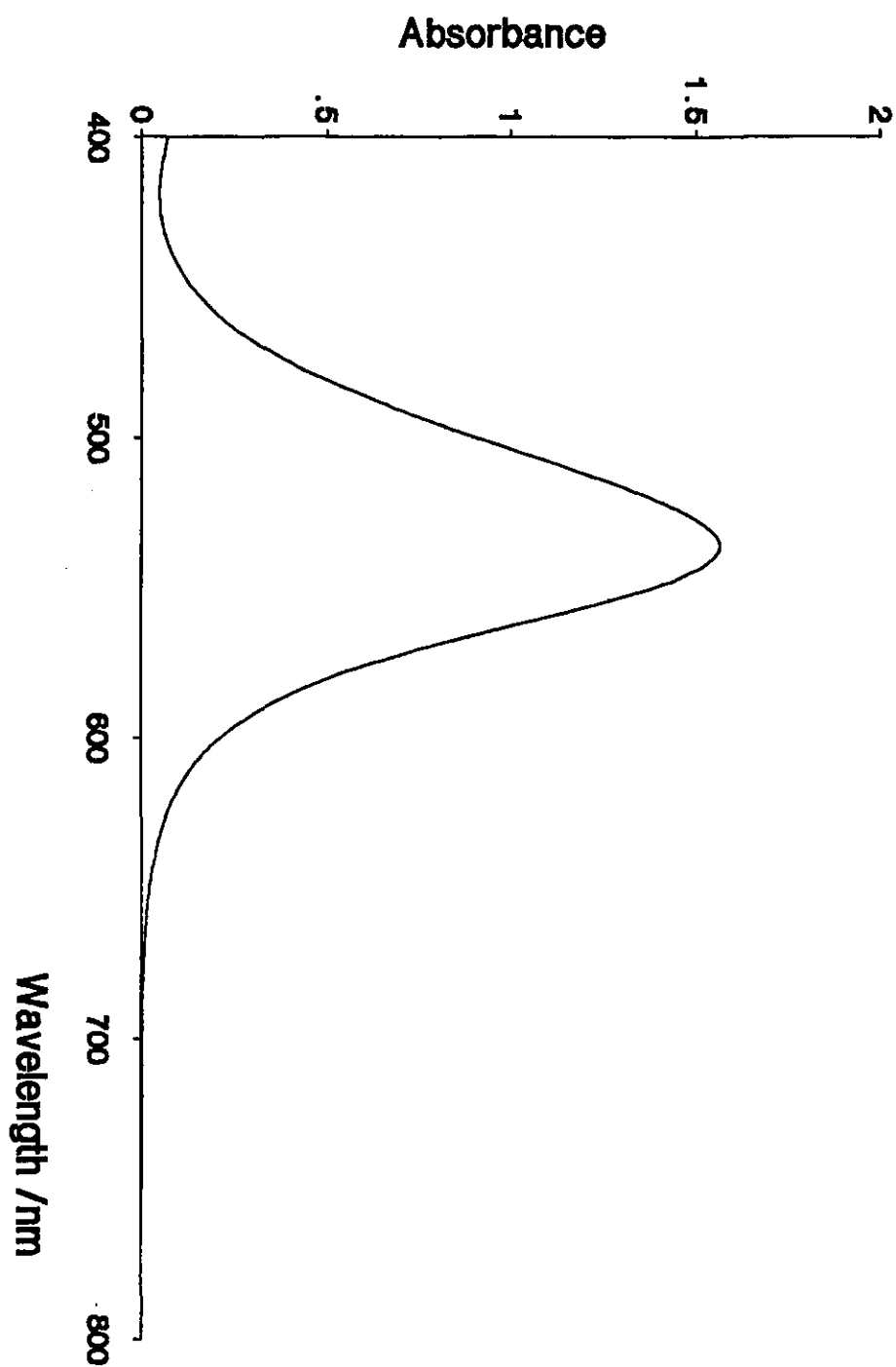


Figure A8: Dye A2 in methanol solution. Concentration $4 \times 10^{-5} \text{ mol dm}^{-3}$.

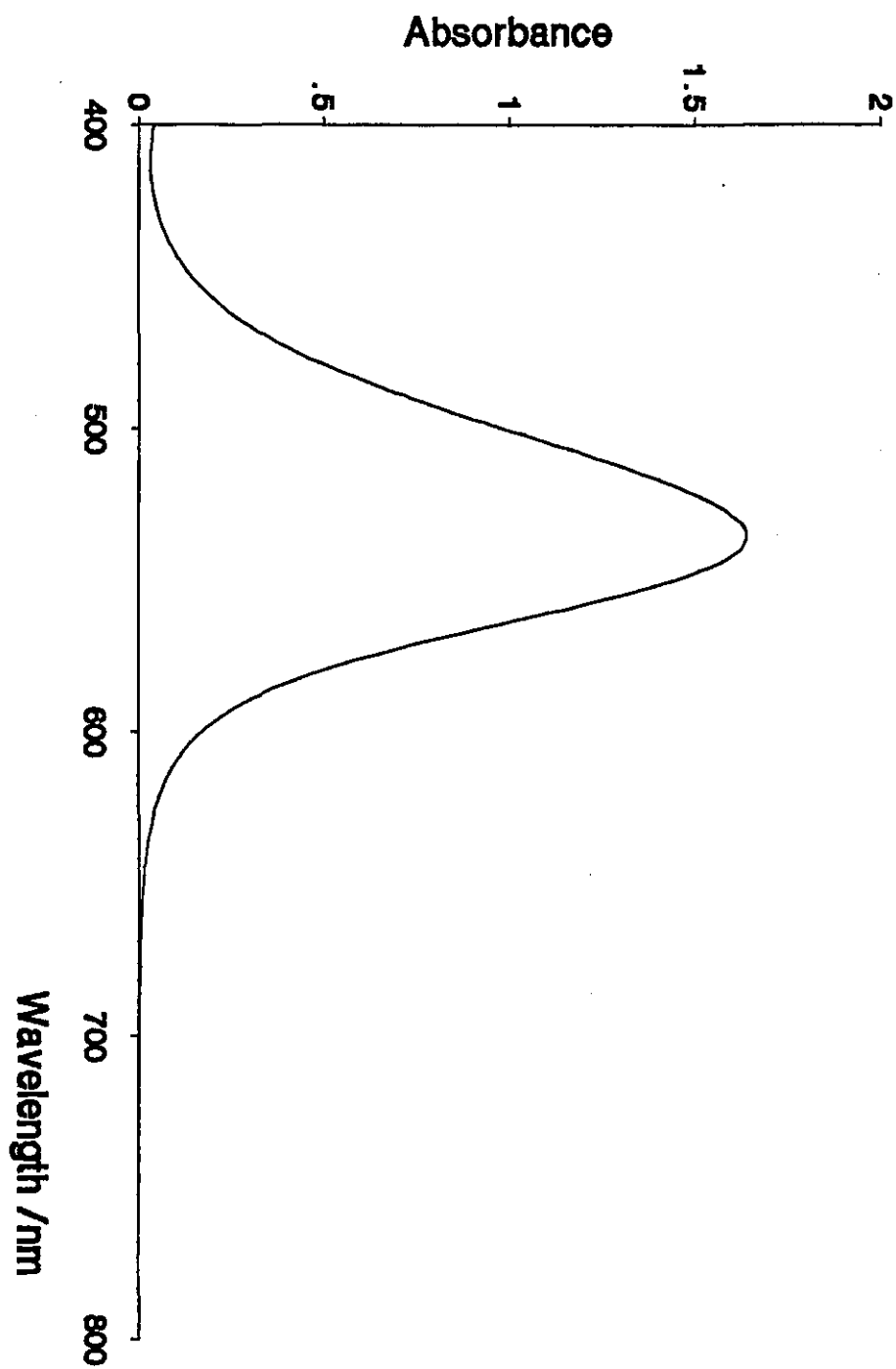


Figure A9: Dye E1 in methanol solution. Concentration $4 \times 10^{-5} \text{ mol dm}^{-3}$.

Acknowledgements

I would like to thank Frank Wilkinson for his encouragement and support throughout this project. Thanks are also due to following: to the research staff of Kodak Ltd., Harrow, for many interesting and useful discussions, particularly to Dr. Chris Winscom, Ruth Ratcliffe, Dr. Harry Adam and Dr. Gareth Evans; to the staff of the laser support facility at the Rutherford-Appleton laboratory for their assistance with the picosecond flash photolysis experiments, in particular to Dr. Andrew Langley and Dr. Roger Chittock; to Dr. J.C. Scaiano and Dr. R.W. Redmond, then at the National Research Council laboratory, Ottawa, Canada, for their assistance with the singlet oxygen luminescence work; and to Dr. Luis Filipe Vieira Ferreira of the Centro de Quimica Fisica Molecular at the Lisbon technical university in Portugal, for the use of his fluorimeter to measure fluorescence quantum yields. I should also like to acknowledge SERC and Kodak Ltd for providing financial support for this project through the CASE scheme, and Kodak Ltd. in particular for supplying all of the dyes and many of the other chemicals used in this work.

The rest of the Loughborough photochemistry research group, past and present, also deserve a mention, and I would like to thank Dr. Graeme Kelly, Phil Leicester, Andy Goodwin, Dave McGarvey, John Hobley, Dave Mandley and Sharon Gibbons, not least for keeping their sense of humour when I was losing mine. Also responsible for keeping me sane are too many old friends and colleagues to mention, and special thanks are due to them. The principle players have been Paul Love, Dave Vesey, Dave Ferriman, Alan Gould, Claire Thomas, Steve Allen, Mark Cooksey, Simon Cocks, Derek Palmer and Alan Davies. Finally, a special mention for Tracie Barker, for being Tracie.

Dave Worrall

14th February 1992

References

- 1 G. Herzberg, "Atomic spectra and atomic structure", 2nd Ed., Dover, New York (1944)
- 2 R. McWeeny, "Coulsons Valence", 3rd. Ed., Oxford University Press (1979)
- 3 N.J. Turro, "Modern Molecular Photochemistry", Benjamin/Cummings (1978)
- 4 M.W. Hanna, "Quantum Mechanics in Chemistry", 3rd Ed., Benjamin/Cummings (1981)
- 5 See, for example, M. W. Hanna, "Quantum Mechanics in Chemistry", 3rd. Ed., Benjamin/Cummings, p.69 (1981), and F. Pilar, "Elementary Quantum Chemistry", McGraw-Hill, p.249 (1968)
- 6 S.J. Strickler and R.A. Berg, J. Chem. Phys., 37, 814 (1962)
- 7 S.K. Lower and M.A. Al-Sayed, Chem. Rev., 66, 199 (1966)
- 8 G. Robinson and R. Frosch, J. Chem. Phys., 37, 1962 (1962)
- 9 G. Robinson and R. Frosch, J. Chem. Phys., 38, 1187 (1963)
- 10 D.L. Dexter, J. Chem. Phys., 21, 836 (1953)
- 11 N.J. Turro, "Modern Molecular Photochemistry", Benjamin/Cummings, p302 (1978), after Forster, T., "Fluoreszenz Organische Verbindungen", Gottingen: Vandenhoech and Ruprech (1951)
- 12 I.B. Berlman, Molec. Crystals, 4, 157 (1968)
- 13 R.D. Spencer and G. Weber, J. Chem. Phys., 52, 1654 (1970)
- 14 R. Norrish, Proc. Chem. Soc., 247 (1958)

- 15 G. Porter, Proc. Roy. Soc. (London), A200, 284 (1950)
- 16 D. Ramsay, J. Chem. Phys., 20, 1920 (1952)
- 17 G. Porter and M.R. Topp, Proc. Roy. Soc. Lond. A, 315, 163 (1970)
- 18 F.J. Blatt, "Principles of Physics", Allyn and Bacon (1983)
- 19 British Standard BS4803 part 1
- 20 G.R. Fleming, "Chemical Applications Of Ultrafast Spectroscopy", Oxford University Press (1986)
- 21 P.A. Franken, A.E. Hill, C.W. Peters and G. Weinreich, Phys. Rev. Lett., 7, 118 (1961)
- 22 A. Laubereau in W. Kaiser (Ed.), "Topics in Applied Physics Volume 60: Ultrashort Laser Pulses and Applications", Springer-Verlag, p.37 (1988)
- 23 B.A. Lengyel, "Introduction to Laser Physics", John Wiley and Sons, p.263 (1966)
- 24 I.R. Gould in J.C. Scaiano (Ed.), "CRC Handbook of Organic Photochemistry Volume I", CRC Press, p.161 (1989)
- 25 H.H. Wasserman and R.W. Murray, "Organic Chemistry Vol.40: Singlet Oxygen", Academic Press (1979)
- 26 J.R. Hurst, J.D. McDonald and G.B. Schuster, J. Am. Chem. Soc., 104, 2065 (1982)
- 27 K-K Iu and P. Ogilby, J. Phys. Chem., 91, 1611 (1987)
- 28 O. Stern and M. Volmer, Z. Physik., 20, 183 (1919)
- 29 K. Fuke, M. Ueda and M. Itoh, Chem. Phys. Lett., 76(2), 372 (1980)

- 30 G. Rossbroich, N.A. Garcia and S.E. Braslavsky, J. Photochem., 31, 37 (1985)
- 31 P.B. Merkel and D.R. Kearns, J. Am. Chem. Soc., 94, 7244 (1972)
- 32 D.R. Adams and F. Wilkinson, J. Chem. Soc., Faraday Trans. 2, 68, 586 (1972)
- 33 R.H. Young, D. Brauer and R.A. Keller, J. Am. Chem. Soc., 95, 375 (1973)
- 34 J-J. Liang, C-L. Gu, M.L. Kacher and C.S. Foote, J. Am. Chem. Soc., 105, 4717 (1983)
- 35 M.J. Thomas and C.S. Foote, Photochem. Photobiol., 27, 683 (1968)
- 36 I.B.C. Matheson and J. Lee, J. Am. Chem. Soc., 94(10), 3310 (1972)
- 37 B.M. Munroe, J. Phys. Chem., 81(19), 1861 (1977)
- 38 W.F. Smith, W.G. Herkstroeter and K.L. Eddy, J. Am. Chem. Soc., 97, 2764 (1975)
- 39 O.L.J. Gijzeman, F. Kaufman and G. Porter, J. Chem. Soc. Faraday Trans. II, 708 (1973)
- 40 A. Farmilo and F. Wilkinson, Photochem. Photobiol., 18, 447 (1973)
- 41 B. Bagchi, G.R. Fleming and P.W. Oxtoby, J. Chem. Phys., 78, 7375 (1983)
- 42 B. Bagchi, Chem. Phys. Lett., 115, 209 (1985)
- 43 E. Akesson, H. Bergstrom, V. Sundstrom and T. Gillbro, Chem. Phys. Lett., 126, 385 (1986)

- 44 C. Couture, personal communication
- 45 P.J.S. Pauwels, J. Am. Chem. Soc., 89, 580 (1967)
- 46 D.L. Smith and E.K. Barrett, Acta Crystallog. B., 27, 2043 (1971)
- 47 E.B. Knott and P.J.S. Pauwels, J. Org. Chem., 33(5), 2120 (1968)
- 48 H. Kessler, Angew. Chem., 82, 237 (1970)
- 49 M. Raban and E. Carlson, J. Am. Chem. Soc., 93, 685 (1971)
- 50 W.G. Herkstroeter, J. Am. Chem. Soc., 95(26), 330 (1976)
- 51 P. Sykes, "A Guidebook To Mechanism In Organic Chemistry", 5th Ed., Longman, p.345 (1981)
- 52 F. Wilkinson, D.R. Worrall and R.S. Chittock, Chem. Phys. Lett., 174(5), 416 (1990)
- 53 W.G. Herkstroeter, J. Am. Chem. Soc., 98(20), 6210 (1976)
- 54 P. Douglas, J. Phot. Sci., 36, 83 (1988)
- 55 W. R. Ware, J. Phys. Chem., 66, 455 (1962)
- 56 T.G. Truscott, E.J. Land and A. Sykes, Photochem. Photobiol., 17, 43 (1973)
- 57 D.L. MacAdam, J. Opt. Soc. Am., 32, 247 (1942)
- 58 T.H. James (Ed.), "The Theory of the Photographic Process", Fourth Ed., Collier-Macmillan (1988)
- 59 P. Glafkides, "Photographic Chemistry", Vols. 1 and 2, Fountain Press (1958)

- 60 R. Fischer and H. Siegrist, *Photogr. Korresp.*, 51, 18 (1912)
- 61 R.W. Gurney and N.F. Mott, *Proc. Roy. Soc. London Ser. A*, 164, 151 (1938)
- 62 L.K.J. Tong, M.C. Glesmann and C.A. Bishop, *Phot. Sci. Eng.*, 8, 326 (1964)
- 63 L.K.J. Tong and M.C. Glesmann, *J. Am. Chem. Soc.*, 79, 583 (1957) and *J. Am. Chem. Soc.*, 79, 592 (1957)
- 64 L.F. Vieira Ferreira, S.B. Costa and E.J. Pereira, *J. Photochem. Photobiol. A: Chem.*, 55, 361 (1991)
- 65 R.R. Alfonso, L.L. Hope and S.L. Shapiro, *Phys. Rev.*, A6, 433 (1972)
- 66 R.R. Alfonso and S.L. Shapiro, *Phys. Rev. Lett.*, 24, 584, 592, 1217 (1970)
- 67 H.P. Weber, *J. Appl. Phys.*, 38, 2231 (1967)
- 68 G.R. Fleming, "Chemical Applications of Ultrafast Spectroscopy", Oxford University Press, p.45 (1986)
- 69 U. Brackmann, "Lambdachrome Laser Dyes", 1st Ed., Lambda Physik GmbH (1986)
- 70 H. Masuhara, H. Miyasaka, A. Karen, T. Uemiya, N. Mataga, M. Koishi, A. Takeshima And Y. Tsuchiya, *Opt. Commun.*, 44, 426 (1983)
- 71 Y. Gauduel, S. Pommeret and A. Antonetti, *J. Phys.: Condens. Matter* 2, SA171 (1990)
- 72 Z. Vardeny and J. Tauc, *Opt. Commun.*, 39, 396 (1981)
- 73 H.J. Eichler, D. Langhans and F. Masserman, *Opt. Commun.*, 50, 117 (1984)

- 74 A.J. Taylor, D.J. Erskine, C.L. Tang, J. Opt. Soc. Am. B., 2, 663 (1985)
- 75 F. Wilkinson, D.R. Worrall, M. Naftaly, J. Hobley, D.J. McGarvey, A. Goodwin, A.J. Langley and W. Shaikh, Annual report to the laser facility committee, Rutherford-Appleton Laboratory, p.163 (1991)
- 76 T.F. Heinz, S.L. Palfrey and K.B. Eisenthal, Opt, Lett., 9, 359 (1984)
- 77 W. Kaiser (Ed.), "Ultrashort Laser Pulses", Springer-Verlag, p.83 (1988)
- 78 F.E. Lytle, R.M. Parrish and W.T. Barries, Appl. Spectrosc., 39, 444 (1985)
- 79 D. Waldech, A.J. Cross Jr., D.B. McDonald and G.R. Fleming, J. Chem. Phys., 74, 3381 (1981)
- 80 G.P. Kelly, P.A. Leicester, F. Wilkinson, D.R. Worrall, L.F. Vieira Ferreira, R.S. Chittock and W. Toner, Spectrochim. Acta., 46(A), 975 (1990)
- 81 M.P. Irvine, R.J. Harrison, M.A. Strahand and G.S. Beddard, Ber. Bunsenges. Phys. Chem., 89, 226 (1985)
- 82 H.J. Pollard and W. Zenith, J. Phys. E. Sci. Instrum., 18, 399 (1985)
- 83 M.A.J. Rodgers and P.T Snowden, J. Am. Chem. Soc., 104, 5541 (1982)
- 84 J.P. Keene, D. Kessel, E.J. Land, R.W Redmond and T.G. Truscott, Photochem. Photobiol., 43, 117 (1986)
- 85 K. Kobayashi, M. Morita and I. Uchida, Kokai Patent No. SHO 62[1987]-121451
- 86 L. Gaunt, "Film and Paper Processing", Focal Press, p.82 (1982)

- 87 M. Ezekiel and K.A. Fox, "Methods of Correlation and Regression Analysis", John Wiley and Sons, New York, Ch.5 (1970)
- 88 J.A. Nelder and R. Mead, *Comput. J.*, 7, 308 (1965)
- 89 W. Spendley, G.R. Hext, and F.R. Himsworth, *Technometrics*, 4, 441 (1962)
- 90 S.N. Deming and S.L. Morgan, *Anal. Chem.*, 45(3), 278A (1973)
- 91 J.N. Demas, "Excited State Lifetime Measurements", Academic Press (1983)
- 92 W.E. Wentworth, *J. Chem. Ed.*, 42(2), 96 (1965)
- 93 W.E. Wentworth, *J. Chem. Ed.*, 42(3), 162 (1965)
- 94 P.R. Bevington, "Data Reduction and Error Analysis for the Physical Sciences", McGraw-Hill, New York (1969)
- 95 D.F. Eaton, *Pure Appl. Chem.*, 62(8), 1631 (1990)
- 96 A. Grinvald and I.Z. Steinberg, *Anal. Biochem.*, 59, 583 (1974)
- 97 K. Jeffrey Johnson, "Numerical Methods in Chemistry", Marcel Dekker Inc., New York (1980)
- 98 J.P. Zeitlow, F.F. Cleveland and H.G. Meister, *J. Chem. Phys.*, 19, 1561 (1951)
- 99 P. Douglas, S.M. Townsend, P.J. Booth, B. Crystall, J.R. Durrant and D.R. Klug, *J. Chem. Soc. Faraday Trans.*, 87(21), 3479 (1991)
- 100 W.G. Herkstroeter, *J. Am. Chem. Soc.* 97, 3090 (1975)

- 101 W.G. Herkstroeter and G.S. Hammond, J. Am. Chem. Soc., 88, 4769 (1966)
- 102 P.J. Wagner and I. Kochevar, J. Am. Chem. Soc., 90(9), 2232 (1968)
- 103 N.J. Turro and T.J. Lee, J. Am. Chem. Soc., 96(6), 1936 (1974)
- 104 J.K. Roy and M.A. Al-Sayed, J. Chem. Phys., 40, 3442 (1964)
- 105 W.J. Moore, "Basic Physical Chemistry", Prentice-Hall (1983)
- 106 J. Saltiel and G.S. Hammond, J. Am. Chem. Soc. 85, 2516 (1963)
- 107 W.F. Smith, W.G. Herkstroeter and K.L. Eddy, J. Am. Chem. Soc., 97, 2764 (1975)
- 108 W.G. Herkstroeter, J. Am. Chem. Soc., 98(2), 330 (1976)
- 109 M.F. Mirbach, M.J. Mirbach, and A. Saus, Chem. Rev., 82, 59 (1982)
- 110 I. Carmichael and G.L. Hug in J.C. Scaiano (Ed.), "Handbook of Organic Photochemistry Volume I", CRC Press, p.378 (1989)
- 111 I. Carmichael, W. P. Helman and G.L. Hug, J. Phys. Chem. Ref. Data, 6, 239 (1987)
- 112 D.J. McGarvey, Ph.D. Thesis, Paisley College of Technology, Paisley (1988)
- 113 R.V. Bensasson, E.J. Land and T.G. Truscott, "Flash Photolysis and Pulse Radiolysis: Contributions to the Chemistry of Biology and Medicine", Pergamon, New York (1983)

114 R.W. Redmond, personal communication

115 Data obtained from "Handbook of Chemistry and Physics", 52nd Ed., CRC Press (1971) and E.W. Flick (Ed.), "Industrial Solvents Handbook", 3rd. Ed., Noyes data corporation (1985)

116 D.W. Green (Ed.), "Perry's Chemical Engineers Handbook", 6th Ed., McGraw-Hill, p.3-282 (1984)

117 J. Timmermans (Ed.), "Physical Properties Of Binary Systems In Concentrated Solutions", Vol. 2, Interscience Publishers (1959)

118 P. Douglas and D. Clarke, J. Chem. Soc. Perkin Trans. 2., 1363 (1991)

119 K. Mackenzie in J. Zabicky (Ed.), "Chemistry of the Alkenes", Interscience, Vol. 2, p.115 (1970)

120 C. Couture, poster presented at the XVth International Conference on Photochemistry, Paris, France (1991)

121 R.W. Redmond and S.E. Braslavsky, Chem. Phys. Lett., 148(6), 523 (1988)

122 M.D. Galanin and Z.A. Chizhikova, Bull. Acad. Sci. USSR, Phys. Ser. English Transl., 22, 1030 (1958)

123 D. Ricard, J. Chem. Phys., 63(9), 3841 (1975)

124 D. Ricard, W.H. Lowdermilk and J. Ducuing, Chem. Phys. Lett., 16(3), 617 (1972)

125 J.P. Heritage and A. Penzkofer, Chem. Phys. Lett., 44(1), 76 (1976)

126 A. Laubereau, A. Seilmeier and W. Kaiser, Chem. Phys. Lett., 36(2), 232 (1975)

127 C. Rulliere, A. Declamy and Ph. Kottis, Chem. Phys. Lett., 110(3), 308 (1984)

- 128 C.H. Brito-Cruz, R.L. Fork, W.H. Knox and C.V. Shank, Chem. Phys. Lett., 132, 341 (1986)
- 129 V. Sundstrom and T. Gillbro, J. Phys. Chem., 88, 1788 (1982)
- 130 T. Doust, Chem. Phys. Lett., 96(5), 522 (1983)
- 131 W. Siebrand and D.F. Williams, J. Chem. Phys., 49, 1860 (1968)
- 132 K-H. Feller, R. Gadonas and V. Krasauskas, Laser Chem., 8, 39 (1988)
- 133 C. Rulliere, Chem. Phys. Lett., 43(2), 303 (1976)
- 134 J.P. Fouassier, P.J. Lougnot and J. Faure, Chem. Phys. Lett., 35(2), 189 (1975)
- 135 H.E. Lessing and A. Von Jena, Chem. Phys. Lett., 42(2), 213 (1976)
- 136 C.J. Treadwell and C.M. Keary, Chem. Phys., 43, 307 (1979)
- 137 S.K. Rentsch, R.V. Danielius and A. Gadonas, Chem. Phys. Lett., 84(3), 450 (1981)
- 138 S.K. Garg and C.P. Smyth, J. Phys. Chem., 69(4), 1294 (1965)
- 139 S.P Velsko and G.R. Fleming, Chem. Phys., 65, 59 (1982)
- 140 D.F. Eaton, Pure & Appl. Chem., 62(8), 1631 (1990)
- 141 S.K. Kim and G.R. Fleming, J. Phys. Chem., 92, 2168 (1988) and references therein
- 142 S. Abrash, S. Repinec and R.M. Hochstrasser, J. Chem. Phys., 93(2), 1041 (1990)

- 143 R.J. Tuite, J. Appl. Phot. Eng., 5(4), 200 (1979)
- 144 R.J. Gledhill and D.B. Julian, J. Opt. Soc. Am., 53(2), 239 (1963)
- 145 T. Kurosaki, S. Itamura, S. Rokutunda, T. Teramoto and T. Miyagawa, J. Phot. Sci., 36, 79 (1988)
- 146 K. Sakanoue and N. Furutachi, J. Phot. Sci., 36, 64 (1988)
- 147 W.F. Smith, W.G. Herkstroeter and K.L. Eddy, Phot. Sci. Eng., 20(3), 140 (1976)
- 148 G. Porter and P. Suppan, Trans. Faraday Soc., 61, 1644 (1965)
- 149 W.F. Smith, W.G. Herkstroeter and K.L. Eddy, Phot. Sci. Eng., 20(3), 140 (1976)
- 150 C.J. Winscom, personal communication
- 151 A. Albin, E. Fasani and S. Pietra, J. Chem. Soc. Perkin Trans. 2., 1021 (1983)
- 152 R. Ratcliffe, personal communication
- 153 H. Gorner, H. Gruen and D. Schulte Frohlinde, J. Phys. Chem., 84, 3031 (1980)
- 154 A. Albin, E. Fasani, S. Pietra and A. Sulpico, J. Chem. Soc. Perkin Trans. 2, 1689 (1984)
- 155 R.M. Noyes, J. Am. Chem. Soc., 77, 2042 (1955)
- 156 P.B. Merkel and W.F. Smith Jr., J. Phys. Chem., 83(22), 2834 (1979)
- 157 A. Mozumber, J. Chem. Phys., 76(10), 5107 (1982)

158 H-D. Brauer, A. Acs and R. Schmidt, Ber. Bunsenges. Phys. Chem., 91, 1337 (1987)

159 C. Tanielian and R. Mechin, J. Photochem. Photobiol., 48(1), 43 (1989)

160 C.S. Foote, Acc. Chem. Res., 1, 104 (1968)

161 W.F. Smith, W.G. Herkstroeter and K.L. Eddy, J. Am. Chem. Soc., 97(10), 2764 (1975)

162 R. Ratcliffe, personal communication

